CRANFIELD UNIVERSITY

TAIHIRET ALHASHAN

Experimental Investigation of Bubble Activity at an Early Stage Using the Acoustic Emission Technique in Two-Phase Flow Systems

School of Engineering
Energy Centre

PhD Thesis
Academic Year: 2017 - 2018

Supervisor: Dr. Abdulmajid Addali

Supervisor: Dr. Joao Amaral Teixeira

January 2018

CRANFIELD UNIVERSITY

School of Energy
Energy Centre

PhD Thesis

Academic Year 2017 - 2018

Taihiret Alhashan

Experimental Investigation of Bubble Activity at an Early Stage Using the Acoustic Emission Technique in Two-Phase Flow Systems

Supervisor: Dr. Abdulmajid Addali

Supervisor: Dr. Joao Amaral Teixeira

January 2018

This thesis is submitted in partial fulfilment of the requirements for the degree of PhD

ABSTRACT

This thesis presents an experimental investigation and identifies the feasibility of the use of AE technology to detect and monitor both early stage bubble occurrence and throughout the boiling process. The research programme also included monitoring of bubble formation/collapse phenomena in ball and globe valves using AE techniques. It was demonstrated that an AE piezoelectric sensor can detect pressure pulses associated with bubble occurrence during pool boiling and cavitation in flow through valves.

For the pool boiling test, a dedicated test-rig was used to diagnose and monitor bubble formation. It was concluded that bubble occurrence is detectable with AE techniques and there is a clear relationship between increasing AE levels and bubble formation during the boiling process. For the valve tests, a purpose-built test-rig was used to monitor and detect cavitation phenomena with various flow rates and different valve opening percentages. It was shown that AE will detect incipient cavitation and that there is a clear correlation between AE signal levels and the flow rate through the ball and globe valves at a constant opening percentage.

This investigation successfully demonstrated that AE monitoring is capable of early diagnosis and monitoring of bubble formation phenomena in boiling processes and valves. This research developed a methodology and prototype framework for using the AE technique for detection and diagnosis of early bubble formation and collapse, allowing cavitation development to be tracked, and maintenance activity to be planned to maximise equipment life and minimise downtime.

Keywords*:* Acoustic emission, bubble occurrence, pool boiling, valves.

ACKNOWLEDGEMENTS

I would like to offer my deep and sincere gratitude to my supervisors Dr Abdulmajid Addali and Dr Joao Amaral Teixeira, for their guidance and support throughout this research programme. Their comprehensive knowledge, experience, helpful suggestions and comments have all contributed significantly to the success of this research work.

I would like to give thanks my country-Libya generally, and specifically the Libyan embassy for sponsorship during this period of study.

To my brothers and sisters, you have always supported me and have given me so much guidance throughout the years. I couldn't thank you more for helping me through this tough time.

Sincere thanks to my father, Eribe Alhashan who motivated me to be involved in academia, and to aim as high as possible in my career, and to my mother, Gadera Zriba; my lovely wife Areg Suliman, and my beautiful children, Awab, Yusuf, and Gana, for their prayers and support.

Also, to my friend, Heather Woodfield-your support was invaluable and I am indebted to you for always being there when needed. Your advice throughout helped me substantially, and you provided guidance when I felt like giving up, so thank you.

Lastly, heartfelt appreciation goes to my colleagues for their support and creative guidance throughout this project. You enabled me to overcome the many obstacles I faced and provided academic help when needed. Thank you for your motivation and patience.

TABLE OF CONTENTS

LIST OF FIGURES

LIST OF TABLES

NOMENCLATURE

Symbol	Denotes
AE	Acoustic emission
f_o	Resonance frequency of the bubble
d	The bubble diameter
γ	Polytropic index of the gas inside the bubble
ρ	Liquid density
P_o	Hydrostatic pressure
FB	Buoyancy force
FC	Surface tension force
FD	Dynamic force
σ	Cavitation index
P_1	Upstream pressure
P_2	Downstream pressure
C_v	Flow coefficient
ΔP	Pressure drop across the valve
GS	Specific gravity of the fluid
Cd	Discharge coefficient
Q	Flow rate
V	Liquid velocity
K_i	Loss coefficient
K_v	Flow factor
C_p	Pressure coefficient
$P_{0,stat}$	Static pressure
$P_{\min}$	Minimum pressure
Ω_b^{scat}	Ratio of the time-averaged power scattered by bubbles from a plane wave to the intensity of that plane wave

R_o	Bubble radius
W_o	Radial frequency of bubble resonance
W_1	Resonating frequency
B_{tot}	Parameter associated with the damping of bubbles
ΔT_{excess}	Excess temperature.
T_s	Surface temperature of the heater
T_{sat}	Saturation temperature of the liquid
$q''_{boiling}$	Boiling heat flux
μ_l	Viscosity of the liquid
h_{fg}	Enthalpy of vaporization
g	Gravitational acceleration
ρ_l	Density of the liquid
ρ_v	Density of the vapour
σ	Surface tension of the liquid
C_{pl}	Specific heat of the liquid
C_{sf}	Experimental constant - depending on surface-fluid combination
P_{rl}	Prandtl Number of the liquid for a given state, and *n* is the experimental constant that depends on the liquid
n	Experimental constant that depends on the liquid

Chapter 1 Introduction

1.1 Introduction

This research starts with the definition of bubble occurrence and a brief statement of the problem that led to the selection of this research topic. It is followed by a brief introduction to problems associated with bubble and cavitation phenomena and the suitability of AE techniques for diagnosis and monitoring of bubble formation in the early stages of pool boiling and cavitation in valves. Following this, is the identification of the research topic based on available published work and, lastly, the aims and objectives identified for the research approach.

1.1.1 Definition of bubble occurrence

In this research work, the term bubble occurrence includes bubble formation, expansion and bursting in pool boiling of a liquid [1][2]. It is also used to refer to any movement of the bubble, such as oscillation and coalescence [1]. In addition, it can refer to bubble formation and collapses due to cavitation in valves.

1.1.2 Problem statement

The bubble/cavitation phenomenon involves bubble formation and collapse inside a liquid when at ambient temperature the local pressure falls, under both static or dynamic conditions [3]. It causes high levels of noise and vibration and a decrease in equipment efficiency and working life. Importantly, cavitation causes damage to the inner surfaces of liquid-carrying components, such as centrifugal pumps by removing material from the surface, as well as creating bearing damage and early failure of seals [3][4]. The growth and collapse of bubbles during cavitation can lead to the erosion or pitting of metal surfaces [5] and is recognised as the principal reason for the damage occurring to hydro machine surfaces in conditions where friction and corrosion have little effect [2]. Cavitation damages occur for all kinds of metals and solids, brittle or ductile, hard and soft [6][7][8][9].

Studying cavitation phenomena using bubble formation performed under laboratory conditions is a good way to understand bubble behaviour: formation,

oscillation, coalescence, collapse and burst. The occurrence of bubbles in a liquid during pool boiling, and in valves, is a source of Acoustic Emission (AE), which will be demonstrated during this research.

To decrease the damage caused by cavitation, bubble occurrence in valves and rotating machines such as centrifugal pumps should be diagnosed and monitored [10]. AE is a physical phenomenon that occurs where passing high-frequency elastic waves are emitted by a sudden release of energy from local sources within the body of a solid or liquid, such as might occur in turbulent flow or with cavitation [11][12].

There is a wide range of possible AE applications in the monitoring of industrial processes. However, the use of AE for the detection of boiling is less common than other AE applications [13]. AE is a sensitive, reliable and robust method for the detection of bubble formation and its bursting at the free surface of the water during the boiling process [14][15][16][17].

Application of AE is not limited to diagnosis and monitoring of cavitation in hydraulic systems such as centrifugal pumps and valves; and is used for detection and observation in different industries such as gas-liquid pumps in petroleum engineering [18], bearings and gearbox faults in mechanical processes [19], and chemical processing stations [20].

Here, the AE technique is applied to the diagnosis and monitoring of bubble occurrence during pool boiling and in valves while the bubbles are still in their early stages of development [15][16]. To date, published work shows few attempts to apply the AE technique to the diagnosis and monitoring of bubble formation in pool boiling [13][16]. There are many different ways of monitoring and detecting bubble formation in boiling processes, valves and pumps, including vibration, and AE is a useful technique because its frequency range is about 100 kHz to 1 MHz [17][21], above most environmentally generated noise and above the limit of human hearing.

Most of the published reports on bubble formation and collapse that made use of AE methods were to observe cavitation in centrifugal pumps. This research

assesses the feasibility of the use of the AE technique for monitoring of the early stages of bubble formation in boiling processes and valves. Bubble formation is an important phenomenon in heat transfer in so-called boilers as used in many industries such as chemical, manufacturing and power plants. The capability for early detection and monitoring of bubble formation during the boiling process can identify such phenomena as overheating and will be relevant to nuclear safety and many another industrial processes [16][22].

1.1.3 Research scope

Bubble occurrence is a phenomenon in which cavities appear in the liquid medium during important industrial processes, as described above, and it is necessary to establish a monitoring system for problem detection. Possible indicators that could detect the occurrence of cavitation and bubbles are vibration, noise, and reduction of operation efficiency. This research will examine the novel application of AE as a method for detection of bubble formation in the early stages, providing an early warning of reduced efficiency, necessary maintenance, incipient failure and increased costs.

1.1.4 Research aim and objectives

This work aims to show the experimental application of AE technique to monitor bubble formation during pool boiling and cavitation in valves.

In support of the aim of this study the following objectives are proposed:

- Carry out an intensive literature review of previous work in this area.
- Experimentally monitor bubble formation and bursts during the boiling process using the AE technique.
- Investigate the effect of different liquid types, different electric power-supplies (kW), free surface water level, and AE sensor position on AE signals measured during the pool boiling process.
- Study of AE parameters in time and frequency domains to determine which is better for diagnosis and monitoring of bubble formation, bursts, and collapse.

- Explore the effect of threshold levels (dB) on AE energy levels measured for pool boiling and valves.
- Explore the possibility of using AE techniques for the diagnosis and detection of bubble formation and collapse in valves.
- Investigate the influence of flow rate, temperature, pressure and different liquid types on bubble formation and collapse (cavitation development) through valves at various opening percentages using an AE technique.

It is believed that the results of this study will make a significant contribution towards the progress of AE technique as a detection tool for bubble formation, burst and collapse, the discovery of cavitation phenomena and flow monitoring in two-phase (gas/liquid) systems.

1.1.5 Main contributions of the present work

Bubble occurrence and flashing phenomena are considered common causes of reduced efficiency, increased costs and even failure in process systems. Therefore, the early diagnosis and monitoring of bubble formation and collapse during fluid transportation in pipes, valves and centrifugal pumps are necessary. A condition monitoring system that can pick up early signs of bubble formation can be used to provide a warning signal for control purpose to avoid the consequent bubble collapse (cavitation). However, a review of published work to date has shown that there have been few attempts of the applications of the AE technique for monitoring and detection of bubble formation and collapse [14][15][16].

Therefore, bubble formation and collapse in valves either as cavitation or flashing phenomena are investigated experimentally. This will offer the opportunity to characterise and differentiate between bubble formation and collapse under different flow conditions, such as flow rate, liquid type, temperature, pressure and valve opening percentages.

In addition, this investigation addresses the possibility of AE techniques to monitor the effect of: liquid properties, liquid levels and electric power-supplies (kW) on such bubble formation characteristics as bubble size, bubble generation rate, and detachment of bubbles during pool boiling. In fact, the boiling process

offers a good opportunity to study bubble formation due to increase of liquid temperature.

Finally, this research will provide a new reference on the use of AE techniques for monitoring bubble activities in process systems.

Below is a list of publications that are outcomes of this investigation and demonstrate its contribution to knowledge.

1.1.6 Publications

Obtained results have been published in different international journals and presented at conferences:

Journals:

- Taihiret Alhashan, Mohamed Elforjani, Abdulmajid Addali and Joao Amaral Teixeira. ‘’Monitoring of Bubble Formation During the Boiling Process Using Acoustic Emission Signals", Int. J. Engineering Research & Science, 2016; 2(4): 66–72.

- Taihiret Alhashan, Abdulmajid Addali and Joao Amaral Teixeira ‘’Exploration of the Possibility of the Acoustic Emission Technique for Detection and Diagnosis of Bubble Formation and Collapse in Valves’’, J. Mechanical and Civil Engineering (IOSR-JMCE). 2016; 13(6): 32-40.

- Taihiret Alhashan and Abdulmajid Addali ‘’The Effect of Salt Water on Bubble Formation during Pool Boiling Using Acoustic Emission Technique’’, J. Mechanical and Civil Engineering, 2016; 13(5): 51-56.

- Taihiret Alhashan, Abdulmajid Addali and Joao Amaral Teixeira ‘’Experimental Investigation of the Influences of Different Liquid Types on the AE Energy Levels During the Bubble Formation Process’’, Int. J. Energy and Environmental Engineering (IJEE-D-17-00110R2). 08 September 2017; (Springer).

- Taihiret Alhashan, Abdulmajid Addali and Joao Amaral Teixeira ‘’Identifying Bubble Occurrence During Pool Boiling Employing Acoustic Emission Technique’’, Accepted 7 November 2017 in Journal of Applied Acoustic (10.1016/j.apacoust.2017.11.006) (Elsevier).

- Taihiret Alhashan, Abdulmajid Addali, Joao Amaral Teixeira, ‘’Identification of the Influence of Flow Rate on Bubble Formation and Collapse in Ball Valves at Various Opening Percentages Using an AE Technique’’, Accepted in Journal of Insight.

Conferences:

- Taihiret Alhashan, Abdulmajid Addali, Joao Amaral Teixeira, ‘’Effect of electric power-supplies on acoustic emission signal during pool boiling using tap water’’ Libyan International Conference on Electrical Engineering and Technology (LICEET 2018).

1.1.7 Thesis Structure

This thesis is divided into seven chapters. Chapter 2 reviews relevant literature, including bubble occurrence and formation, and cavitation, and introduces boiling. Existing condition monitoring techniques and their relevance to detecting and monitoring bubble generation in pool boiling, and bubble occurrence in valves are discussed. In Chapter 3, AE is considered in greater detail. Chapter 4 presents the research methodology with details of the test procedures; the test rigs for the boiling and valve experiments. Chapter 5 introduces possible AE parameters for use in detecting and diagnosing the initial stages of bubble formation in pool boiling. The main purpose of this chapter is to investigate how competent the AE parameters were for detecting and monitoring detachment of bubbles from the heating surface in open pool boiling. Experimental results are presented for discussion. In Chapter 6 the procedure was replicated for detection of the formation of bubbles, and their subsequent collapse (cavitation), in valves.

Finally, in Chapter 7 conclusions and recommendations for future work are presented.

Chapter 2 Literature review

2.1 Bubble characteristics

This chapter commences with a summary of bubble generation, collapse and burst, then by a general review of boiling and, finally, bubble occurrence and flashing in control valves. Bubble manifestation is important in numerous process industries because it can cause such undesirable phenomena as slug flow, cavitation and flashing, generated due to sudden falls in pressure within the liquid flow [23][24][25].

The most important sources of sound that occur naturally in liquids are due to bubble formation and burst. The sound generated by the formation and/or collapse of bubbles in two-phase gas/liquids is used in many applications to detect and monitor of formation and collapse of the bubbles. The pressure wave generated by the bubbles can be used to determine time of bubble formation and bubble detachment, the size of the bubble, bubble collapse and bubble burst at a free surface.

The five stages of occurrence of bubble phenomena with pool boiling are: 1) bubbles form on the heated surface at the base of the boiler, 2) bubbles detach from the heated surface and start to float upwards in the liquid being heated, 3) separate bubbles coalesce into a single bubble, 4) single bubbles split into two or more bubbles, and 5) bubbles reach the free surface and burst [16][17][26][27]. The magnitude of the pressure waves generated at each of these stages depend primarily on the dimensions of the bubble and the properties of the liquid. The duration of the pulses generated by bubble formation, collapse and burst are all very short [14][28].

2.1.1 Bubble formation

Leighton, et al., [29] observed that running brooks are sources of sound emitted by the transient pressure waves caused by gas bubble pulsations within the water. Earlier, Minnaert, et al., [30] observed that pressure waves were formed from volumetric bubble oscillations during bubble occurrence. The bubbles are subjected to initial oscillations, which produce an acoustic pressure wave, before

reaching an equilibrium state. Pumphrey, et al., [31] studied the effect of liquid drops on a free surface using a high-speed camera, and found that the majority of the acoustic noise created was due to volume pulsations of the bubble, which generated audible sound inside the liquid. Leighton, et al., [32] concluded that the sources of many sounds emitted from oceans were caused by pressure waves generated by bubble occurrence inside the liquid. Strasberg, et al., [33] found that the noise occured only when the bubble is in volume pulsation, and that smaller bubbles, with a lower surface area, radiate less energy for a given volume rate of bubble formation.

Bubble formation and bubble collapse generate pressure waves which can be detected within a wide frequency band. Furthermore, bubble size can be determined using Equation (2-1), derived by Minneart [30], for the natural frequency of oscillation of the bubble.

$$f_0 = \frac{1}{\pi d}\sqrt{\frac{3\gamma P_0}{\rho}} \qquad (2\text{-}1)$$

Where f_0 the resonance frequency of the bubble, d is the bubble diameter, γ is the polytropic constant of the gas in the bubble, P_0 is the hydrostatic pressure and ρ is the density of the liquid surrounding the bubble.

Strasberg [33] took high-speed photographs of bubble formation at an underwater nozzle with an oscillograph of the noise produced, see Figure 2-1. The oscillograph indicates that greatest acoustic pressure happened at the moment of bubble departed from the nozzle. Later studies by Deane and Czerski [34] and Manasseh, et al., [35] investigated the sound signals from incipient bubbles using a high-speed camera, recording bubble formation and break away from a nozzle tip and found its pressure amplitude signal was as shown in Figure 2-2.

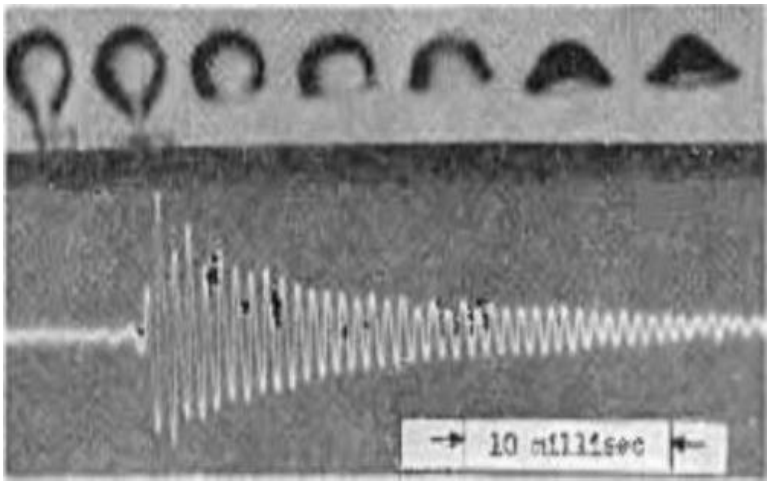

Figure 2-1 Acoustic pulses produced by a single air bubble forming and breaking away from an underwater nozzle [33].

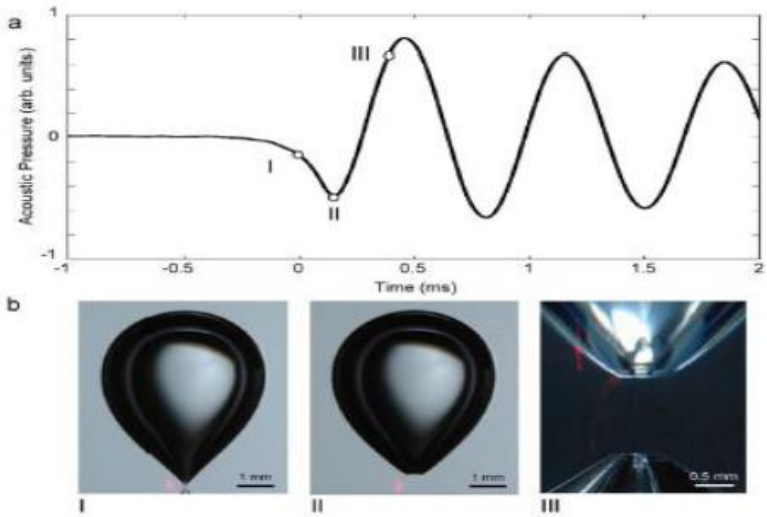

Figure 2-2: Acoustic emission caused by bubble formation at a nozzle tip underwater [34].

Figures 2-1 and 2-2 presents the sound pressure emission from bubble formation and break away from the nozzle. This event and the movement of bubbles during generation are very different from the bubble burst that occurs at the free surface, where the bubble burst appears more violent, but the energy which is transferred to the liquid is less than during bubble formation at a nozzle. Manasseh, et al., [35] used acoustic techniques for monitoring bubble size, and found nonlinear relationships between bubble size, rate of production of bubbles and peak frequency produced. However, a measure of spectral frequency could be related to the radius of the bubble on its formation, see Equation (2-1) above.

Longuet-Higgins [36] suggested that there are two general mechanisms by which the energy causing an initial acoustic turbulence could be transported to the bubble: 1) Laplace pressure difference at bubble formation; and 2) change of the volume of the bubble by nonlinear inter-actions of shape modes [37][38]. Longuet-Higgins [39] also noted that bubble formation at an orifice could generate sound. Movement of bubbles in water or other liquids can generate large sound pressures. In addition, the oscillatory motion of the bubble wall causes sound inside the liquid [33]. For bubble generation in water, the surface tension is the main factor determining bubble formation. With turbulent flow, viscosity will be an important factor, but surface tension is still important.

2.1.2 Bubble collapse and burst at free surface

Bubble collapse within a liquid causes high pressure shock waves, local high temperatures, and local high velocities in the form of micro-jets; if this happens near a metal surface the surface will be subject to vibration and surface pitting. The bubbles that occur in cavitating flow are not usually spherical, but assuming spherical symmetry predicts maximum possible pressure, temperature, vibration and damage resulting from bubble collapse. Tomita, et al., [40] studied the influence of a convex solid wall on bubble collapse. They found that when a bubble collapses close to a convex boundary, the micro-jet velocity is dramatically higher than that of the flat boundary case.

When small bubbles combine to create a large bubble the collapse, when it comes, will start at this maximum radius and can be caused by tiny increases in local pressure. In typical cavitation flow, the final bubble radius may be of the order of 100 times the original nuclei size. When the bubble contains non-condensable gas, or when the temperature of the liquid increases, the pressure within the bubble is not constant. However, when there is condensable gas inside the bubble, the bubble collapses more slowly than an empty bubble. The importance of liquid compressibility is not its influence on the bubble's movement, but the role it plays in the production of shock waves in the rebound stage that follows the bubble collapse. Hickling, et al., [41] used numerical solutions of the compressible flow equations to study the creation of the pressure wave during

the rebound stage. Figure 2-3 gives a good example of distributions of the pressure in the liquid before and after the moment of the creation of the smallest bubbles. Hickling and Plesset showed that the pressure pulse presents an approximate linear attenuation (r^{-1}) with distance from the bubble. Where: P_b is a pressure inside the bubble, P_∞ is an external pressure in the liquid, r is a radial distance from the centre of the bubble, and R_M is a measure of bubble radius at the moment of collapse.

Ivany, et al., [42] confirmed that the liquid properties such as viscosity, density and surface tension have an effect on small bubble formation and collapse, where the viscosity acts to increase the liquid pressure at the bubble wall during the collapse. Bubble collapse phenomena due to pressure increases, create sound and release energy into the water [33]. Of course, viscosity is more important than surface tension in determining e.g. the time bubbles take to float to the surface. Viscosity is also important for bubble bursts at the surface. Viscosity will also play an important role in determining oscillation frequencies of the bubbles.

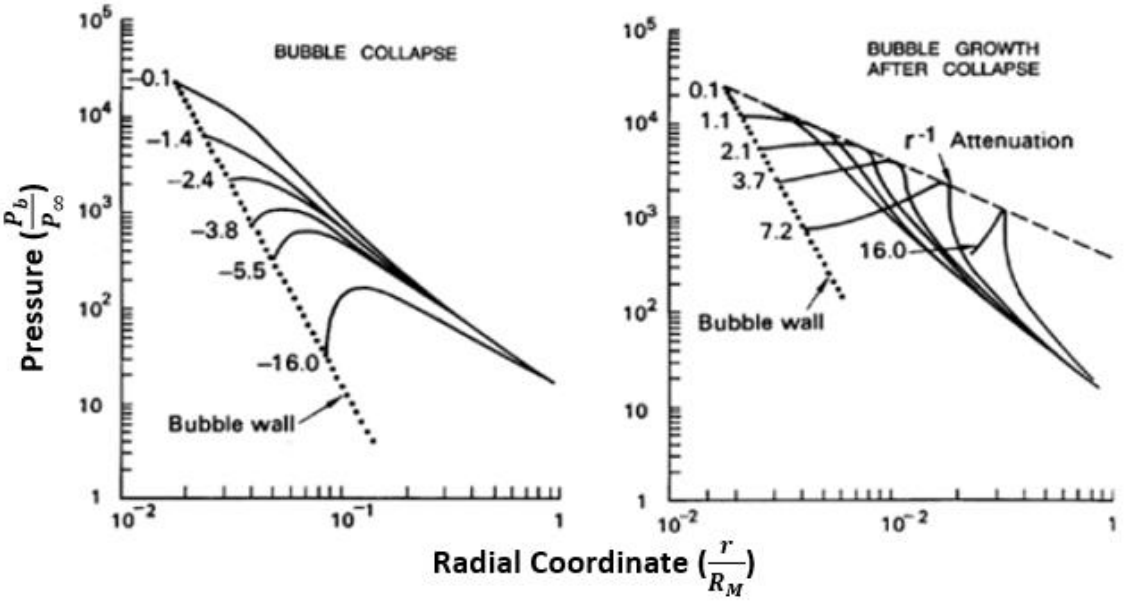

Figure 2-3: Shows distribution of the pressure in water immediately prior to bubble collapse and after collapse [41].

The phenomena associated with cavitation collapse depend on the number and size of the bubbles. Small bubbles generate higher-frequency noise and vibration, while large bubbles produce lower-frequency noise and vibration, see Equation (2-1) [43][44]. A bubble of order of 6 μm diameter will produce a signal with peak frequency of about 500 kHz, and 10 μm diameter yields 300 kHz, as shown in Figure 2-4, which tends to confirm Equation (2.1) that the peak frequency of the pulse is inversely proportional to the bubble diameter [16].

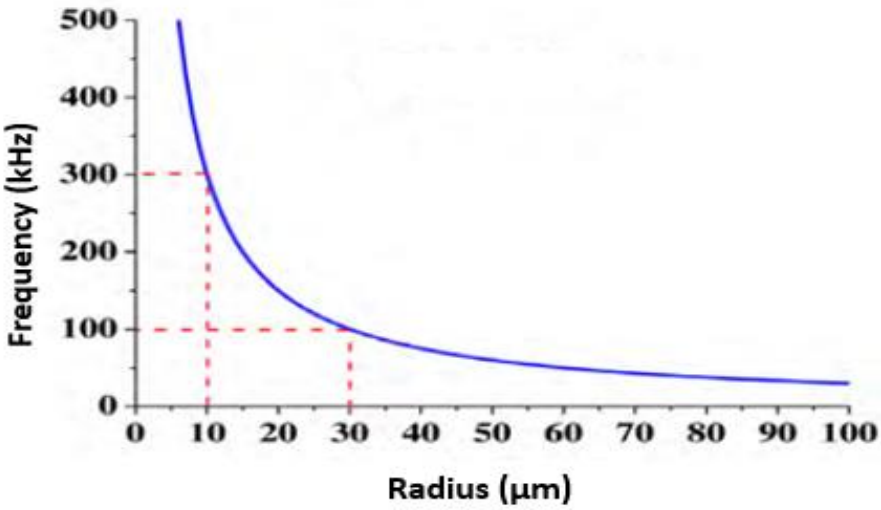

Figure 2-4: Relation between frequency and bubble size [16].

A bursting bubble at the free surface is the last stage in the life of the bubble in two-phase gas/liquid. This is evident in a manufacturing reactor or heated tank that contains different phases of gases and liquids. The energy emitted from a burst bubble should be related to bubble size and properties of the liquid. When the bubble bursts at a free surface, it creates two jets moving in opposite directions. The first jet moves downwards crossing the bubble internally, as in Figure 2-5 towards the body of the liquid, and an inverse jet out of the free surface. However, the jet out of the free surface is more violent than jet inwards and its velocity can as high as 110 m/s [4][45].

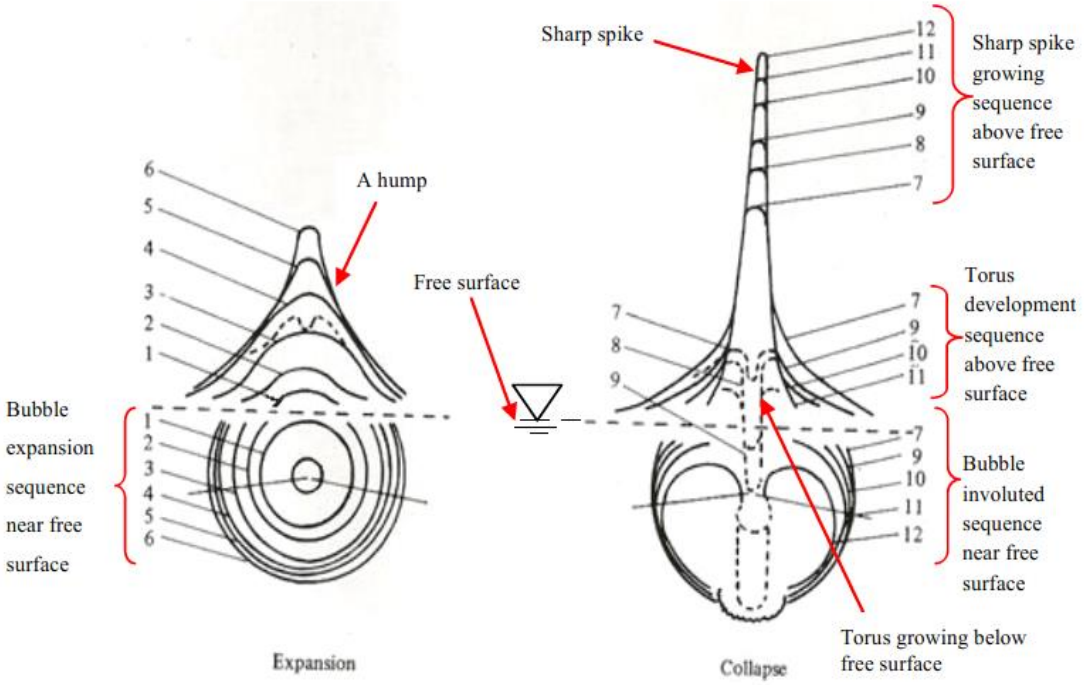

Figure 2-5: Bubble collapse close to the free surface; showing the opposite directions of the jets created - a micro-jet crosses the bubble in a downward direction and a counter-jet out of the free surface [45].

Pressure sensors have been used to demonstrate that pressure changes occur the moment a bubble collapses and prove that pressure shockwaves are associated with bubble collapse [46]. Figure 2-5 shows the dynamic of bubble collapse close to a free surface. There is an extension of the bubble along the axis of symmetry, which causes a deformation of the free surface where there is a hump. This hump increases, and starts to form a spike as the bubble approaches burst. The numbering in Figure 2-5 is a series showing how the bubble increases in size and then collapses close to the free surface. The spike continues to grow along the axis of symmetry, then collapses as a micro-jet. The growth of this spike is consistent with the shrinkage of the bubble until the bubble reaches its smallest size, at which point a micro-jet is created, that moves with high speed along the axis of symmetry in the opposite direction to the free surface spike. The presence of a gas inside the bubble will play a significant role in bubble

collapse and formation of micro-jets, and help store the kinetic energy of the suddenly collapsing bubble [1].

Bubbles do not collapse to zero radius, they collapse to a minimal radius of between 2% and 10% of their original, maximum radius. Also, when a bubble collapses the micro-jets and shock waves generated can lead to the formation of small bubbles. Figure 2-6 shows the temporal progress of the radius of a bubble having finite gas content. Figure 2-7 shows the growth and the collapse of an empty bubble. There are two different types of bubbles, gas bubble and vapour bubble (cavitation bubble). The only difference is the content inside the bubble: either vapour or gas. Vapour bubbles grow and collapse much more than gas bubbles because the gas content provides damping during the collapse of the bubble and helps cause problems such as pitting and surface erosion [47][48].

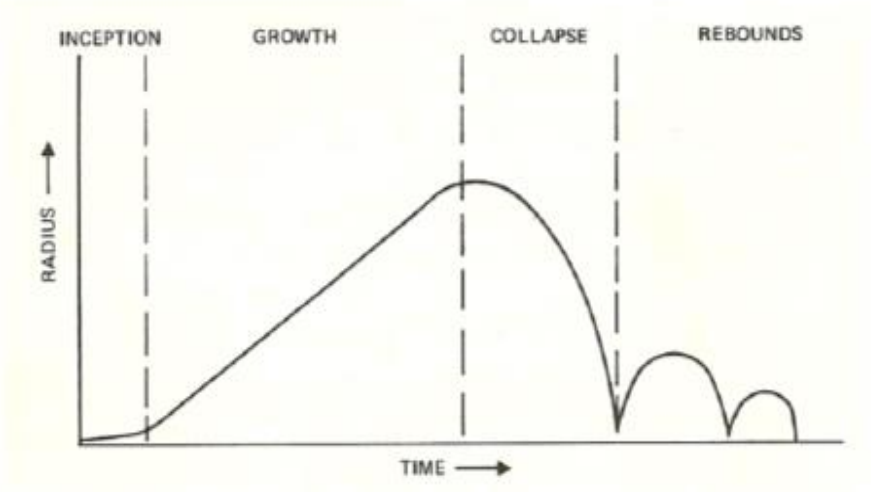

Figure 2-6: Growth and collapse of bubble having finite gas content [48].

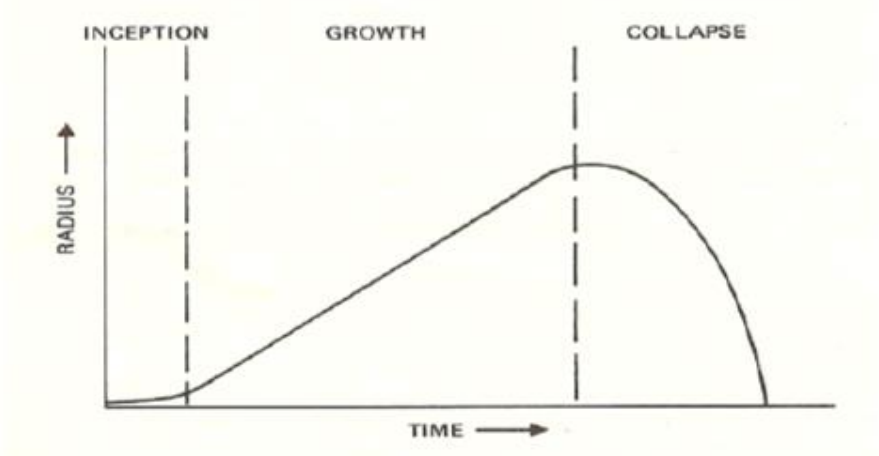

Figure 2-7: Typical growth and collapse of empty bubble in an incompressible liquid [48].

When a high pressure pulse is created by bubble collapse, it causes compression of the liquid, resulting in shockwaves. It has been found by Shangguan, et al., [49] that from about 10% to 15% of the bubble energy is used in generating the shockwave, and the duration of the stress pulse for a single bubble collapse is about 1 μs. The emitted shockwave can be detected by underwater pressure sensors such as hydrophones, microphones and AE sensors [48][49].

Pandit, et al., [50] observed that gas bubbles inside water or other liquids could generate large sound-pressure pulses when stimulated by an external pressure source. In addition, bubble coalescence has been shown to be associated with pressure pulses [33][51][52]. Leighton, et al., [53] concluded that the sound from an oscillating bubble is controlled by the pulsating zero-order mode, while oscillations of shape with a fixed gas bubble volume gave rise to a lower frequency sound pressures.

2.1.3 Bubble breakup and coalescence

The size of the largest stable bubble is controlled by surface tension forces and hydrodynamic pressure [54]. Walter and Blanch [55] demonstrated that bubble breakup is determined by the hydrodynamic stresses in the vicinity of the bubble. For laminar flows bubble breakup is controlled by the stretching of the bubble

surface by viscous shear forces. In turbulent flow, impacts of turbulence eddies on the surface of the bubble cause it to breakup.

When bubbles divide or coalesce, as with bubble formation, a rapidly decaying pressure pulse is emitted. Here, volume pulsations are generated by the difference between the equilibrium pressures inside small and large bubbles. The pressure difference is because the internal pressure is less than for smaller bubbles [33].

Hinze investigated, experimentally, air flow through an underwater needle into a tank of water and the formation of bubbles on the tip of the needle. For a low, steady flow rate of air, the bubbles detached one at a time with very little sound generated. Once the flow rate reached a certain value two bubbles were generated, in rapid succession, see Figure 2-8 [51].

When two bubbles coalesce, see Figure 2-8, a short but high level sound pulse is generated [51]. As the size (radii) of the bubbles increase the amplitude of the acoustic pressure pulse also increased. The maximum level of the pressure pulse occurred at the moment when the pressures in the coalescing bubbles were equal. The duration of the sound pulse was about 5 ms, but this would be expected to vary with the diameters of the bubbles. It was noted that sound level generated at pinch-off of the primary bubble was an order of magnitude lower than the amplitude of the sound generated on coalescence [51].

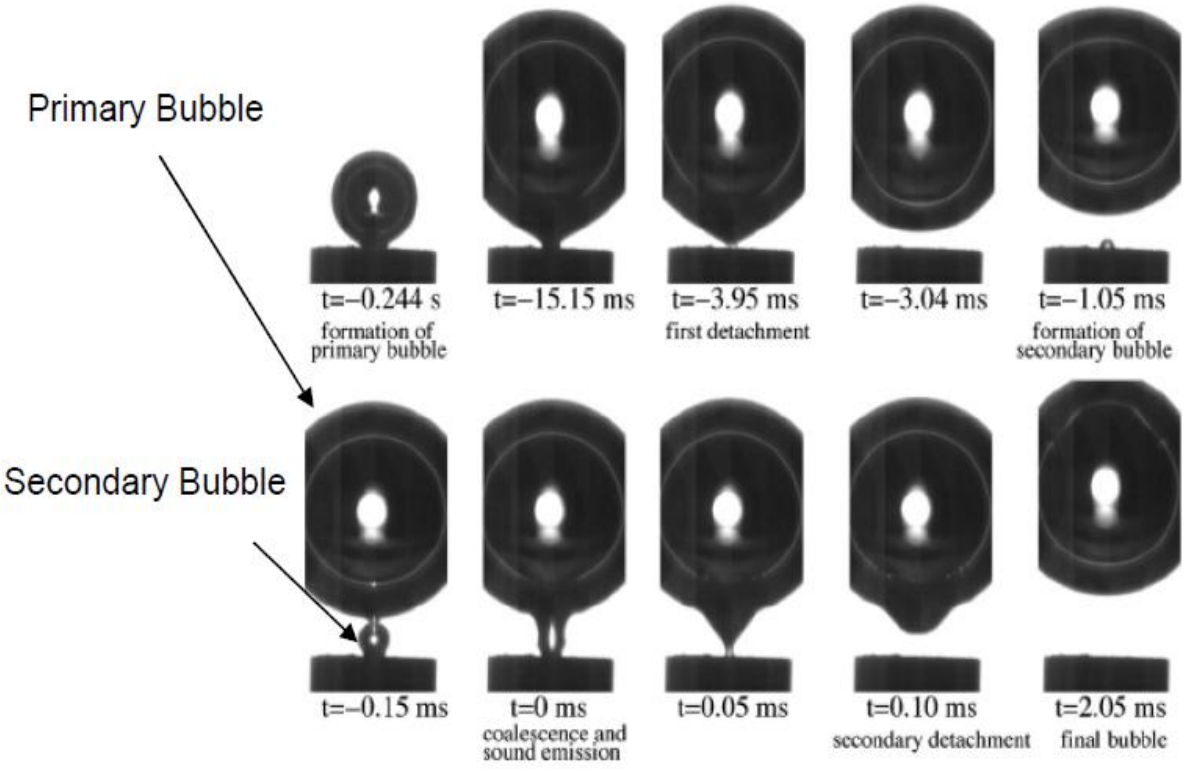

Figure 2-8: High-speed video of bubble phenomena and coalescence – the air bubbles are white, and the black background is the water into which the bubbles are being injected [51][52].

2.1.4 Factors affecting bubble formation

The process of bubble formation depends on many operating parameters such as gas flow rate through the orifice, liquid temperature and the properties of the liquid. The main forces affecting bubble movement are buoyancy, drag, surface tension, dynamic forces, pressure contact force and viscous forces, as shown in Figure 2-9 [56].

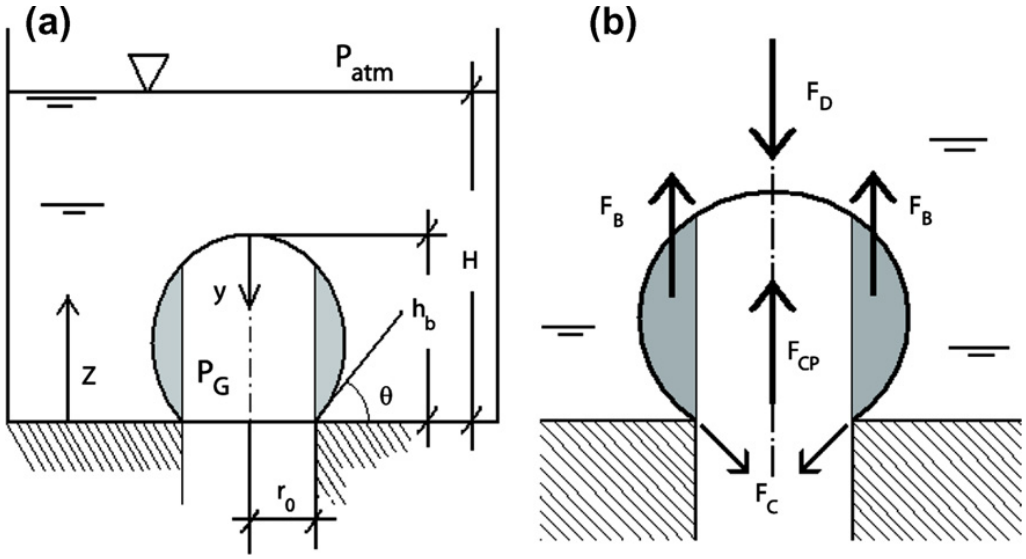

Figure 2-9: Force acting on bubble growth [57].

$$F_B = \rho g V_B \quad (2\text{-}2)$$

$$F_C = 2\pi r_0 S \sin\theta \quad (2\text{-}3)$$

$$F_{CP} = \pi r_0^2 (P_g - P_L) \quad (2\text{-}4)$$

Where F_B is the buoyancy force, F_C is the surface tension force, F_D is the dynamic force, F_{CP} is the contact pressure force, V_B is the volume of the bubble, P_L is the liquid pressure value at the bubble tip, r_o is the contact radius, g is the gravity vector, S is the liquid surface tension and θ is the contact angle at the triple contact line.

Bubble growth in the dynamic region is dominated by the interplay of inertial, viscous, surface tension and buoyancy forces [58].

2.1.5 Effect of different liquids on bubble formation process

In a container filled with fresh water, a great many bubbles appeared and disappeared in a short time. With salt water, there were no significant individual bubbles; only small bubbles were created and continued in the container for a very long time, much longer than in the fresh water. While the mechanism of bubble formation is the same in salt water and fresh water, there is an obvious

difference in the size of the bubbles, and small bubbles play a significant role in incipient cavitation [59]. Blanchard, et al., [60] noted that bubbles coalesce in tap water more than in sea water. Abe [61] found that sea water foams more than fresh water. Ceccio, et al., [44] concluded that there is a significant difference between bubble occurrence in salt water and pure water. Additionally, they noted that small bubbles create higher acoustic emission compared to large bubbles. Bubbles of similar size generated similar acoustic emission regardless whether they are in salt water or fresh water, and the chemical difference of the water does not appear to influence the acoustics directly.

Surface tension is a major factor in bubble formation. In fact, bubble formation with no flow depends almost entirely on surface tension. However, the bubble formation in turbulent flows depends on viscosity as a factor alongside surface tension because viscosity is a an important factor in determining the turbulence levels of the flow and the turbulence can give rise to local pressure variations which can be significantly lower than the mean pressure in the flow. Viscosity is also important with bubbles rising to the surface and in bubble bursts at the surface. It can be a major factor in bubble collapse [6][62].

The less the surface tension, the less energy is required for a bubble to form, so a liquid with lower surface tension should allow more and larger bubbles to form and this in turn will mean there are more and bigger bubbles to collapse and to generate cavitation pressure pulses. The liquid with lower surface tension and lower viscosity is more likely to experience cavitation. The surface tension of the liquid is also an important factor in determining the rate and nature of the collapse of cavitation bubbles, and causing such damaging cavitation processes as the erosion of solid surfaces and pitting [63][62].

2.2 Boiling phenomenon

One objective of this research programme was to investigate the AE energy emitted from bubble occurrence to detect bubble formation during pool boiling.

Boiling is a process change from liquid-to-vapour. The boiling phenomenon is characterized by the fast formation of bubbles at the heating surface, then the bubbles start to detach from the surface as their size increases and rise to the free surface of the liquid. Boiling is a complicated process because of the large number of variables involved and the complex liquid motion patterns caused by the bubble occurrence [64].

The boiling point of liquid depends on the surrounding environment such as atmospheric pressure. Boiling occurs when the vapour pressure of the water is equal to the external pressure (atmospheric pressure). When the local vapour pressure of the water is more than the local atmospheric pressure, bubbles start to form inside the water. Invariably, water has some air dissolved in it, which act as nuclei for bubble formation.

There are two types of bubbles formed in the process of boiling a kettle of water. First, when the liquid begins to get hot, bubbles will form on the heated surface, usually at the bottom of the kettle. These bubbles are dissolved air.

Second, as the boiling point of water reaches (100^0C), water vapour bubbles start to form in the water. At its boiling point, water is at equilibrium with its vapour; all molecule in the system have nearly the same “willingness” to be in the vapour phase. For this reason, bubbles are formed inside the liquid very readily. Figure 2-10 shows how to bubbles start in boiling water. The vapour pressure depends on temperature and as the temperature increases, the vapour pressure increases as well, and the kinetic energy of the molecules increases so they can more readily move to the gas phase. The bubbles are created at the bottom, on the heated surface of the container, and they move up under buoyancy forces [65]. The position of the energy source means the bottom of the container is hotter than the top.

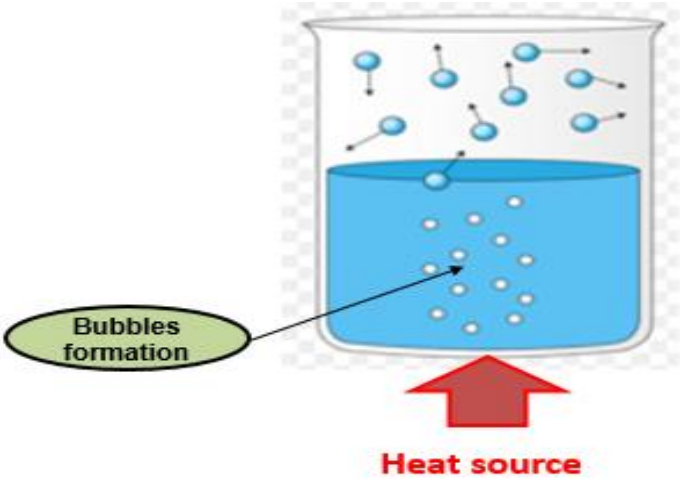

Figure 2-10: Vapour bubbles forming inside heated water.

Water boils and turns into vapour at 100 ^{o}C at an atmospheric pressure of 1 bar (10^5 Pa). The boiling point of water decreases when the related pressure decreases, and vice versa. This helps explain why water boils and turns to vapour in a control valve at normal temperatures; it is due to the drop in the local pressure. When any liquid becomes a vapour, cavities or bubbles form in the low-pressure fields, and then they collapse when the fluid flow moves them to an area where the pressure recovers. This phenomenon is called bubble occurrence and typically takes place over a short time [66].

A boiler is often a closed vessel in which liquids are heated. The heated or vaporised liquid exits the boiler for use in different processes or heating applications, including water heating and power generation [67][68]. Boiler explosions are catastrophic failures. Generally explosions can be divided into two types. The first is a failure usually connected with the generation of steam and the high pressures associated with it. There are many different reasons for this, failure of the safety valve, corrosion of parts of the boiler due to bubble activity. The second type is a fuel/air explosion in the oven, known as a firebox explosion, and is still a potential hazard in gas or oil-fired boilers [69]. The fundamental causes of explosions are reduced strength of the shell or other parts of the boiler probably due to original defects, or bad workmanship, or deterioration from use, or mismanagement [70]. For this reason monitoring of bubble formation during the boiler is necessary.

2.3 Boiling heat transfer

2.3.1 Classification of boiling

Figure 2-11 below shows a classification of boiling:

1) Pool boiling occurs in the absence of volumetric flow rate. Any movement of the liquid is due to natural convection and the bubbles rise under the influence of buoyancy.
2) Flow boiling (forced boiling) happens in the presence of a volumetric flow rate. In flow boiling the liquid is forced to travel in a heated pipe by an external force such as a pump.

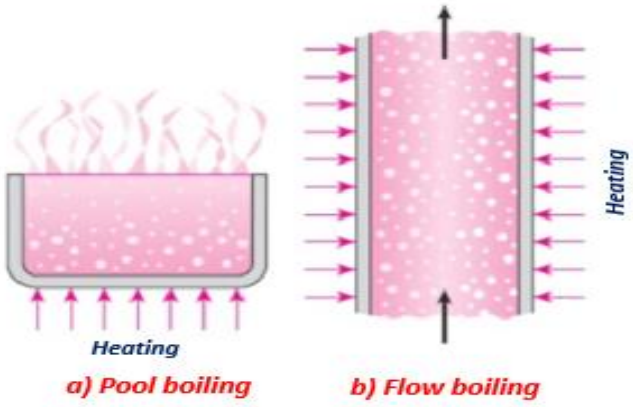

Figure 2-11: Classification of boiling process [64].

2.3.2 Boiling regimes and the boiling curve

Boiling phenomenon is possibly the most familiar form of heat transfer, yet it remains the least understood. The macroscopic boiling process is well known and defined since the first discovery of the boiling curve by Nukiyama [71]. This classification is divided into two categories; subcooled, which occurs when the temperature of the liquid is lower than the saturation temperature, and superheated boiling (saturated boiling), which occurs when the temperature of the liquid is identical to the saturation temperature, as shown in Figure 2-12 below.

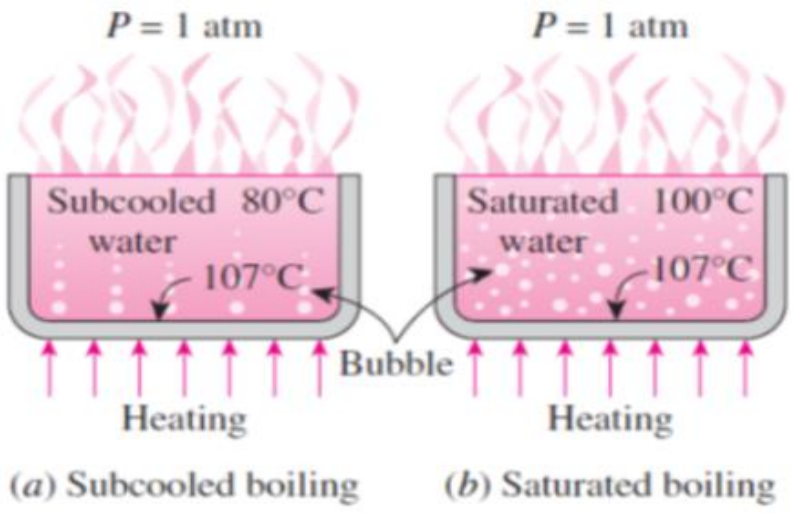

Figure 2-12: Shows categories of boiling process [64].

A boiling curve relates the boiling heat flux (this is the heat supplied by the heater, W/m^2) to excess temperatures (ΔT_{excess} ^{0}C), which is the difference between the temperature of the boiling surface and saturation temperature of the water. The following section describes the physics of pool boiling which applies to the experiments described in this work. There are four different boiling regimes, as shown in Figure 2-13 [16]. Note that the bulk temperature of the water is constant at 100^{0}C.

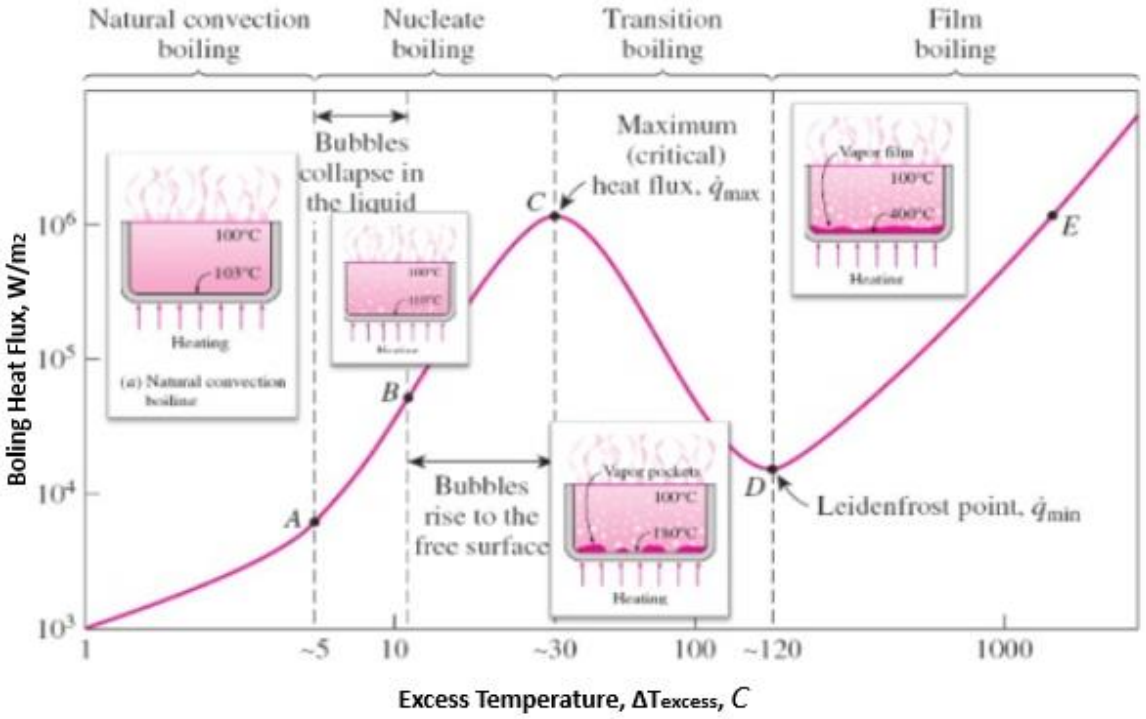

Figure 2-13: Different four regimes during boiling curve for water [64].

In Natural Convection Boiling (up to point A on the boiling curve), which comprises stage I, the bubbles do not form on the heating element and heat is transferred from the heating surface to the water by natural convection.

The two stages between points A and C are jointly known as Nucleate Boiling. Stage II lies between points A and B, when the value of ΔT_{excess} increases and bubbles are formed on the bottom, heated surface of the boiler vessel. These bubbles rise towards the surface, but collapse within the liquid. Rising bubbles carry some liquid along with them, which is known as liquid entrainment. The disturbance caused by liquid entrainment in the water increases the heat transfer coefficient and the heat flux is increased. It is believed that the initial stage of boiling nucleation involves bubble formation and departure separately from the heating surface [16]. In Stage III, from B to C, the value of ΔT_{excess} increases further, and the bubbles form at a faster rate. These vapour bubbles move upwards and merge to form a continuous column of vapour in the liquid. The bubbles in the column reach the free surface where they burst and release

vapour. At point C the boiling heat flux attains its maximum value, known as the critical heat flux.

Stage IV between C and D is known Transition Boiling. The value of ΔT_{excess} increases but the heat flux decreases because a significant section of the heated surface of the pool becomes covered with a vapour film which acts as an insulating layer and decreases thermal conductivity. In this regime, both nucleate and film boiling occur. For water, transition boiling occurs in the excess temperature range from about 30^0C to about 120^0C.

The final stage (film boiling) is between D and E, during this stage, the ΔT_{excess} increases and the heating surface is completely covered by a continuous layer of vapour film. Radiation heat transfer is now the dominant heat transfer mechanism between the heated surface and the water. The presence of the film reduces the heat transfer rate but as the temperature of the radiating surface increases so does the boiling heat flux [64].

The equations for excess temperature, boiling heat flux, maximum and minimum value of heat flux are given by the equations below [64].

$$\Delta T_{excess} = T_s - T_{sat} \tag{2-5}$$

$$q^{\bullet}_{boiling} = \mu_l h_{fg}\left[\frac{g(\rho_l - \rho_v)}{S}\right]^{1/2}\left[\frac{C_{pl}(T_s - T_{sat})}{C_{sf} h_{fg} P_{rl}{}^{n}}\right]^3 \tag{2-6}$$

$$q^{\bullet}{}_{\max} = C_{cr} h_{fg}[\sigma g \rho_v{}^2(\rho_l - \rho_v)]^{1/4} \tag{2-7}$$

$$q^{\bullet}_{\min} = 0.09\rho_v h_{fg}\left[\frac{\sigma g(\rho_l - \rho_v)}{(\rho_l + \rho_v)^2}\right]^{1/4} \tag{2-8}$$

Where:

ΔT_{excess} is the excess temperature; T_S is the surface temperature of the heater, ^{0}C; T_{sat} is the saturation temperature of the liquid, ^{0}C; $q^{\bullet}_{boiling}$ is the boiling heat flux, Wm^{-2}; μ_1 is the viscosity of the liquid, $kgm^{-1}s^{-1}$; h_{fg} is the enthalpy of vaporization,

Jkg^{-1}; g is the gravitational acceleration, ms^{-2}; ρ_l is the density of the liquid, kgm^3; ρ_v is the density of the vapour, kgm^{-3}; S is the surface tension of the liquid, N/m; C_{pl} is the specific heat of the liquid, $Jkg^{-1}\,{}^0C^{-1}$; C_{sf} is an experimental constant depending on the surface-fluid combination; P_{rl} is the Prandtl Number of the liquid for a given state, and n is an experimental constant that depends on the liquid.

The boiling process produces acoustic pressure waves of frequency above 50 kHz in the different stages due to bubble initiation, growth, departure from the heated surface, bubble collapse in the body of the liquid, natural oscillations of bubbles and bubbles bursting on the water surface. Thus, it can be assumed that the boiling process will involves sequences of pulses, whose amplitudes, durations and time intervals between them vary randomly. Thus, AE techniques have a good potential for revealing and distinguishing between the different boiling regimes represented on the boiling curve.

2.4 Types of nucleation

There are two kinds of nucleation; homogeneous and heterogeneous.

2.4.1 Homogeneous nucleation

The thermal motions inside the liquid can form temporary, microscopic cavities that constitute the nuclei necessary for rupture and growth to micro bubbles. In pure water, surface tension is a macroscopic manifestation of the intermolecular forces that bind molecules together. When the pressure falls below the vapour pressure, a bubble starts to form which overcomes the tensile strength of the liquid (where the tensile strength = $2S/R$). Assuming a spherical bubble, with an internal pressure P_b, the differential pressure between the two boundaries of the bubble is calculated by the Young-Laplace equation (2-9) [72]:

$$P_b = P_\infty + \frac{2S}{d} \qquad (2\text{-}9)$$

Where P_b and P_∞ are the pressure inside the bubble and external pressure in the liquid, respectively, S is the surface tension, d is the radius of the bubble.

If the temperature is uniform and the bubble contains only vapour, then the internal pressure will be the saturated vapour pressure at the given temperature. But the external liquid pressure, will have to be less than that to produce equilibrium conditions. When the external liquid pressure remains constant, at just slightly less than (P_V - 2S/d), the bubble will grow, d will increase, the excess pressure causing growth will rise, and the bubble will rupture [6].

2.4.2 Heterogeneous nucleation

In heterogeneous nucleation, the weaknesses happen on the boundary between the liquid and the hard surface of the boiler, or between the liquid and nuclei suspended in the liquid.

Figure 2-14 shows different cases of heterogeneous nucleation. When the pressure of the liquid (P), is reduced below the critical value (P_V - 2S/R), the microscopic gaps increase, causing rupture.

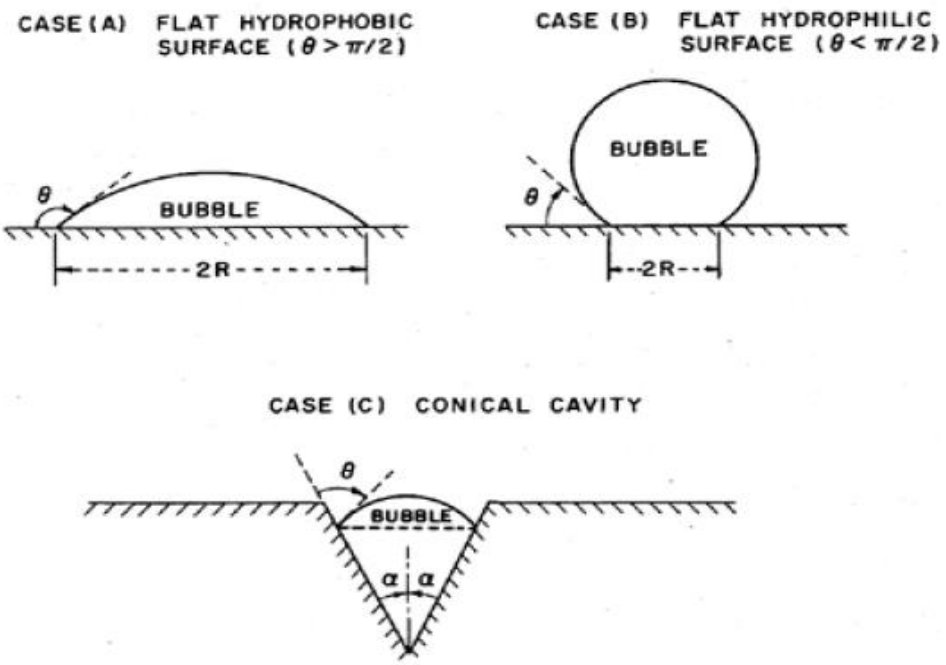

Figure 2-14: Different types of heterogeneous nucleation [6].

The contact angle at the liquid/vapour/solid intersection is indicated by θ, see Figure 2-14. It follows that the tensile strength for the flat hydrophobic surface is

2sinθ / R, where *R* is radius of the area of contact between bubble and surface. In theory, the tensile strength could be equal to zero within this range, as $\theta \to \pi$. Otherwise, the tensile strength for a hydrophilic surface is comparable with that for homogeneous nucleation of the maximum dimensions of the gaps. It was concluded that the presence of a hydrophobic surface would cause heterogeneous nucleation and greatly reduced tensile strength. At the microscopic scale where the surfaces are not flat, the effects of local surface geometries should be considered. The conic cavity of case (*C*) is commonly studied in other conditions affected by surface geometry [6]. The half angle at the vertex of this cavity is indicated by α, then it is clear that zero tensile strength happens at $\theta = \alpha + \pi/2$ rather than $\theta \to \pi$. Furthermore, if $\theta > \alpha + \pi/2$ it is clear that the vapour bubble would grow to fill the cavity at a pressure above the vapour pressure [6].

2.5 Cavitation phenomena

2.5.1 Background of cavitation

Cavitation is the localised formation and subsequent collapse of bubbles into micro-jets in a liquid. The collapse of these bubbles not only produces structural vibration and resulting noise but also creates localised stresses in the pipe walls and valve body and can cause severe pitting and damage to valves [73][66].

Gaitan [74], reported that the cavitation phenomenon was detected by Leonhard Euler in 1754 when he proposed that passive pressures can be produced when the local velocity of a liquid is high enough to break the liquid. This phenomenon was termed cavitation by Froude in 1895 and used to explain the occurrence of space and bubble clouds around propellers and pumps. Since then, the term cavitation phenomena has been used to describe the bubble formation that appears when a liquid is subjected to sudden internal pressure drops, for example in pumps and hydraulic systems [59]. Vokurka and Rydberg have confirmed that cavitation comes from the occurrence of bubble due to the pressure decreases caused by changes in the flow rate of a liquid [75][76]. Baker, et al., [61] argued

that cavitation phenomena can be used to explain any bubble occurrence within the body of a liquid, including formation and collapse.

2.5.2 Definition of cavitation

Cavitation is the occurrence of bubbles in a liquid, usually water, when the local pressure drops below its SVP (saturated vapour pressure) [66]. When a liquid, in a container such as a boiler, is heated, the SVP increases until it becomes equal to atmospheric pressure when bubbles commence forming, invariably on the hot surface [77]. The bubble moves with the liquid flow and if the local pressure rises or the local temperature falls the bubble collapses, it is this collapse of the bubble which generates pressure pulses of high amplitude that is termed “cavitation”.

Cavitation occurs in a large number of industrial processes. If bubble collapse occurs close to the wall of the contained the micro-jets formed in the bubble’s collapse, cause noise and vibration, and surface erosion and pitting, reducing working life [4][75]. Weninger, et al., [78] showed that bubble collapse into micro-jets generates a shockwave containing significant energy. Forming, cavitating and bursting bubbles all generate AE signals which can be used to define certain of the liquid’s properties [79].

Five conditions are necessary to generate cavitation in, say, a globe valve.

1. The liquid must remain as a liquid in both the downstream and upstream directions.

2. When the liquid enters the valve it should be saturated. Otherwise the pressure difference across, say, the globe valve will generate an ongoing vapour trail downstream from the valve.

3. The pressure at the vena contracta must be lower than the SVP.

4. The outlet pressure of the valve needs to be larger than the SVP of the liquid.

5. The liquid must contain impurities or entrained gases to act as nuclei for bubble formation [77].

.

2.6 Cavitation occurrence in valves

Cavitation phenomena commonly occurs in valves and rotating machines such as a centrifugal pumps. This study will investigate the detection and monitoring of bubble formation and collapse (bubble occurrence) in two such valves.

In industrial processes, controlling and monitoring the flow rate or achieving a certain decrease in pressure is important for the operation of, e.g., water plant. This is often attained by using different valve types to control the flow rather than changing the input to the pump or the compressor. There are many different types of throttling valves used in the industry today, such as ball and globe valves.

Cavitation in valves can generate levels of severe noise and vibration with the intensity of the cavitation increasing with upstream pressure and valve size, at a constant value of the cavitation index (σ), which is closely related to the differential pressure ratio across the valve. Using σ it is possible at the design stage to determine a likely level of cavitation, see Section 2.7. The higher the value of σ the less likely it is that cavitation will occur which means a decrease in both incipient and choking cavitation for butterfly valves, with less damage to the valve [80].

Ball and globe valves play a significant role in industry, including the control of water, gas and oil flow in pipelines and nuclear power plants. When the valves fail consequent problems that occur can include environmental pollution, waste of resources, decrease in the working life of equipment and increase in maintenance costs [81][82]. The literature review revealed that a main type of valve failure is liquid leakage caused by sealing surface failure [83]. Techniques such as the shock pulse method, ultrasonic leak detection, vibration measurement and AE have been used to detect and identify leakage in valves [5]. The application of the AE technique to monitor and detect leakage without dismantling valves is a very active area of research [5][84]. In this study, background theory and a literature review are provided to improve understanding of the causes of bubble formation and flow phenomena which increase the likelihood of the occurrence of cavitation.

Figure 2-15 shows the appearance of bubbles in a globe valve. When the liquid accelerates through the throttling element at the vena contracta, the pressure drops below the vapour pressure of the liquid. This causes vapour bubbles to start to form. There are two possible scenarios for this region. The first, is where the vena contracta pressure is greater than the vapour pressure, and there will be no bubble formation (no cavitation). The second, is where the flow conditions through the vena contracta are such that the local pressure is less than the vapour pressure, and there will be bubble formation. In the given example the pressure then recovers and increases to a level above the vapour pressure, and the bubbles collapse into micro-jets (cavitation). However, if the pressure increase that occurs after the vena contractor is not sufficient, and remains less than the vapour pressure, flashing occurs [77][85].

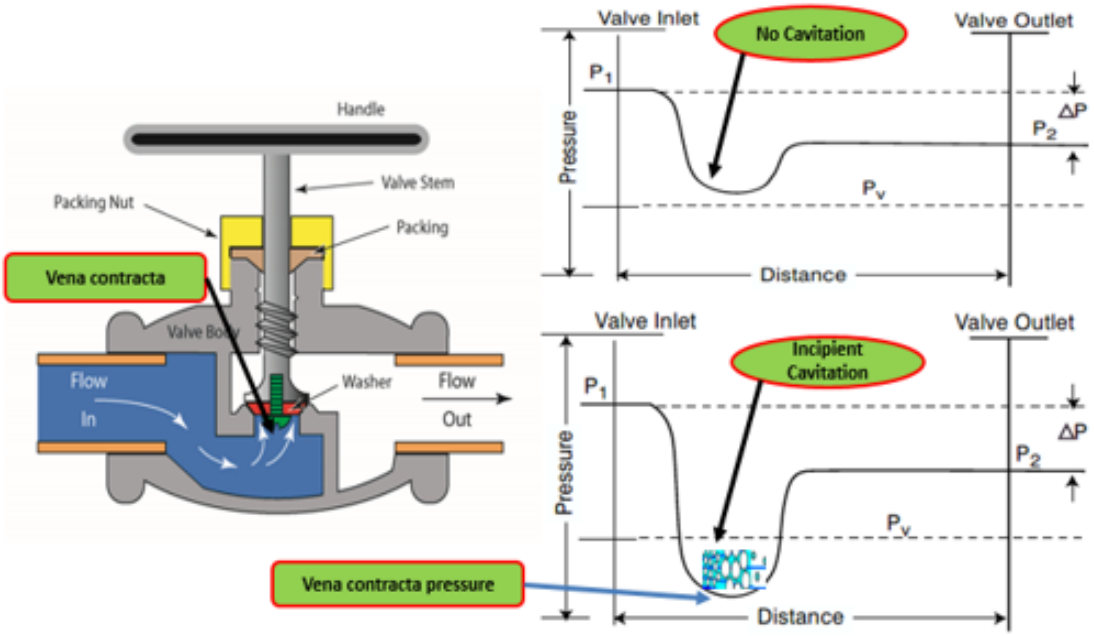

Figure 2-15: Pressure distribution in globe valve [85].

The globe valve is the most commonly used type of valve in the industry [86], thus if cavitation occurs in this type of valve the problem will be widespread. Cavitation occurs in a globe valve when the opening percentage is lower than 12%, and can be detected by analysing the high-frequency vibration signal from incipient

cavitation [66][86]. Figure 2-16 shows average AE count as a function of differential pressure ratio (*K*) for a ball valve 60^0 open (8.3% open) [66].

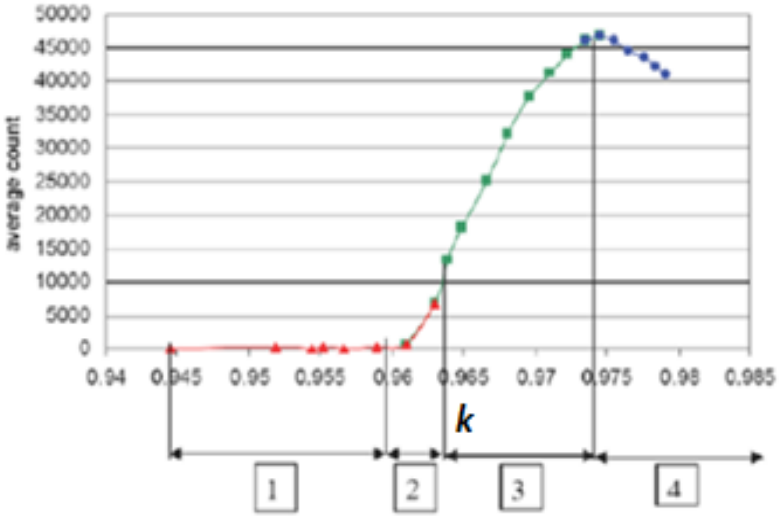

Figure 2-16: Plot of AE counts against differential pressure ratio (K) for tap water for globe valve opening of 60^0 [86].

Four regions can be seen in Figure 2-16. The first region has no cavitation and the vibration due to flow turbulence is negligible. In the second region, there is incipient cavitation and vibration increases. In the third stage, the bubble occurrence increases quickly to reach to the fully developed point. In the last stage, the downstream pressure is less than the saturated vapour pressure. As a result, the bubbles do not collapse when they move downstream, and flashing occurs [86].

2.7 Cavitation parameters

To carry out experiments on the test-rig valve with cavitation, it was necessary to know the fluid design parameters used to quantify cavitation susceptibility. The cavitation initiation in the valve can be predicted by many parameters such as cavitation index [80][87]. There are many parameters related to cavitation, some of which are:

- **The cavitation index (σ)**

Cavitation index has been used to relate performance data to predict the likelihood of cavitation occurring and to improve design of hydraulic systems. The

cavitation index (σ), was developed and is still applied to quantify likelihood of cavitation in valves. σ shows the ratio of the potential to resist cavitation formation to the likelihood of causing cavitation. This cavitation index is defined and calculated by Equation (2-10) [80][87].

$$\sigma = \frac{P_1 - P_v}{P_1 - P_2} \qquad (2\text{-}10)$$

Where:

P_1: Upstream pressure

P_2: Downstream pressure

P_v: Vapour pressure of the liquid

Laboratory and field tests have determined an emprical relation between σ and the likelihood of cavitation (and its related choking, noise, and damage) occurring. For typical globe valve operating conditions:

$\sigma \geq 2$	No cavitation is likely to occur
$1.7 < \sigma < 2$	Some cavitation might occur
$1.5 < \sigma < 1.7$	Onset of cavitation
$1 < \sigma < 1.5$	Severe cavitation
$\sigma \leq 1$	Flashing is occurring

- **Flow coefficient, C_v**

The flow coefficient is a suitable measure to gauge the efficiency of equipment in allowing liquid flow. It describes the correlation between the pressure drop in the orifice, valve and the flow rate [88]. The flow coefficient is defined as [88]:

$$C_v = Q\sqrt{\frac{\rho_1 / \rho_0}{\Delta P}} \qquad (2\text{-}11)$$

$$C_v = \frac{Q}{\sqrt{\frac{\Delta P}{SG}}} \qquad (2\text{-}12)$$

Where:

Q = volumetric flow rate (m^3/min)

ΔP = pressure drop across the valve (kP_a, or bar)

ρ_1 = density of the working fluid flowing through the valve (kg/m^3) (this will invariably be water)

ρ_0 = density of pure water (kg/m^3)

$SG = \rho_1 / \rho_0$ = specific gravity of the fluid (dimensionless)

$$SG = \frac{\rho}{\rho_0} = \frac{\rho}{999.25} \qquad (2\text{-}13)$$

The *SG* of a liquid is its density relative to the density of water at 15.5^0C (60^0F). For most working fluids their density is very close to, or equal to the density of water, so SG is often taken to be = 1.

- **Discharge coefficient, C_d**

In a valve or other throttling device, the discharge coefficient is the ratio of the actual discharge to the theoretic discharge; the ratio of the flow rate at the end of discharge of the valve to that of a typical valve which expands a similar working liquid from the same conditions to the same exit pressures [88]. The discharge coefficient is defined as [88]:

$$C_d = \frac{V}{\sqrt{2\Delta P / \rho + V^2}} \qquad (2\text{-}14)$$

Where: C_d is the discharge coefficient, V (=Q/A) is the averaged flow velocity, A is valve inlet area, Q is flow rate, ΔP is differential pressure across valve, and ρ is the density of the liquid. The relationship between C_v and C_d can be expressed as [88]:

$$C_v = 38AC_d \qquad (2\text{-}15)$$

Loss coefficient, K_i

The loss coefficient is defined as the local pressure losses through the valves and fittings in the hydraulic networks and is represented by the following equation [89]:

$$K_i = \frac{2\Delta P}{\rho V^2} \qquad (2\text{-}16)$$

Where:

ΔP : Differential pressure across valve, kPa

ρ : Density of the water, kg/m^3

V : Liquid velocity, m/s

The relationship between C_v and K can be expressed as [89]:

$$C_v = 0.04634 \frac{D^2}{\sqrt{K}} \qquad (2\text{-}17)$$

- **Flow factor, K_v**

Flow factor is the water flow with temperature ranging between 5 and 30 ^{0}C through a valve in cubic meters per hour (m^3/h) when the pressure difference is 1 bar. The following equation can be used to find the relationship between C_v and K_v [89]:

$$C_v = 1.156\ K_V \qquad (2\text{-}18)$$

2.8 Cavitation physics

Figure 2-17 below shows the cavitation in a nozzle. The temperature of the liquid in the four stages varies from T_1 to T_4 with the corresponding relative vapour pressures P_{v1} to P_{v4}. In the first stage, $P_{min} > P_{v1}$ (T_1), the vapour pressure is not reached, and no evaporation occurs. During the second stage, $P_{min} \leq P_{v2}$ (T_2) initial vapour bubbles develop. At the third stage, $P_{min} \leq P_{v3}$ (T_3) a large cavity occurs which influences the flow in the channel. During the fourth stage, the

pressure recovery in the diffuser is smaller than $P_{v4} - P_{min}$, so that the vapour generated does not condense and two-phase flow is maintained over the length of the entire channel downstream of the diffuser. Due to pressure loss and the thermodynamic equilibrium, some fluid evaporates with increasing pipe length. Such a process is called expansion evaporation or flashing [90]. Only a fraction of the flowing fluid mass evaporates.

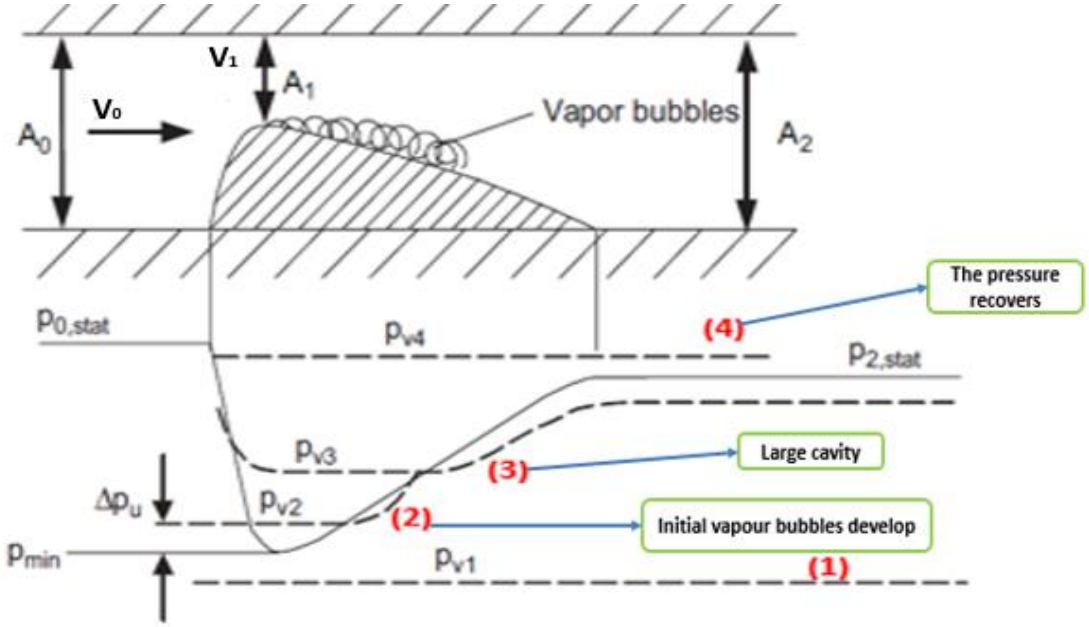

Figure 2-17: Cavitation in a nozzle [90].

When the pressure recovers such that P (the pressure inside the bubble) > P_v, the size of bubbles also increases, and they ultimately collapse into micro-jets. The heat transport requires a finite temperature difference ΔT_u. This temperature difference corresponds to a pressure difference ΔP_u between the pressure in the bubble and the vapour pressure, as shown in Figure 2-17.

$$P_{0,stat} - P_{\min} = \frac{\rho}{2}(V_1^2 - V_0^2) + \Delta P_u \qquad (2\text{-}19)$$

Where: the $P_{0,stat}$ is a static pressure, P_{min} is the minimum pressure of the liquid, ρ is the density of the liquid, V_0 and V_1 velocity of the liquid in the two sections respectively and ΔP_u is the pressure difference between the pressure in the bubble and vapour pressure.

2.9 Cavitation nuclei

Cavitation can occur when a liquid contains dissolved gases or tiny particulates which act as bubble nuclei. Experience has shown that the probability of this being the case in most process liquids used in industrial systems is very high so the probability that vapour bubbles will form is also high [90].Theoretically if a liquid was free of such nuclei cavitation would not occur, though such a situation is practically impossible [77]. The dissolved gases (including water vapour) can exist as bubbles so small they can be seen only with a microscope, with diameters being in the range of 1 to 100 microns [90]. Experiments have demonstrated the existence of these bubbles which are spherical due to the domination of surface tension forces [91].

Bubbles of gas in a non-saturated liquid will slowly dissolve in the liquid, although the nuclei can be stable in a non-saturated fluid as explained by the theory that the gas molecules are absorbed on non-wetting particles.

Free nuclei (in the body of the liquid, away from any wall) will, due to buoyance forces, tend to rise. The nuclei present in a liquid will, by a process of diffusion, exchange gases between themselves. Typical mass diffusion times for this process are one second, while it takes only microseconds for bubble collapse [91].

Liquid flow in a pipeline is complicated multi-phase turbulent flow. Turbulence, if sufficiently intense, can rupture the liquid, causing cavitation [7]. Turbulent flow can also cause bubbles to coalesce which contributes to increased bubble size. The bigger the size of the bubble, the greater the potential energy contained [45][46][92]. Commonly, the bubble occurrence generated as a result of the flow turbulence is classified as a temporary cavity and usually exists for less than one cycle of bubble formation before collapsing violently [93]. Six types of flow regimes have been characterized in two-phase flow in a horizontal pipe; stratified, wavy, bubble slug, dispersed, bubble flow, and annular. The flow patterns are dependent on the phase flow rates, see Figure 2-18 [23].

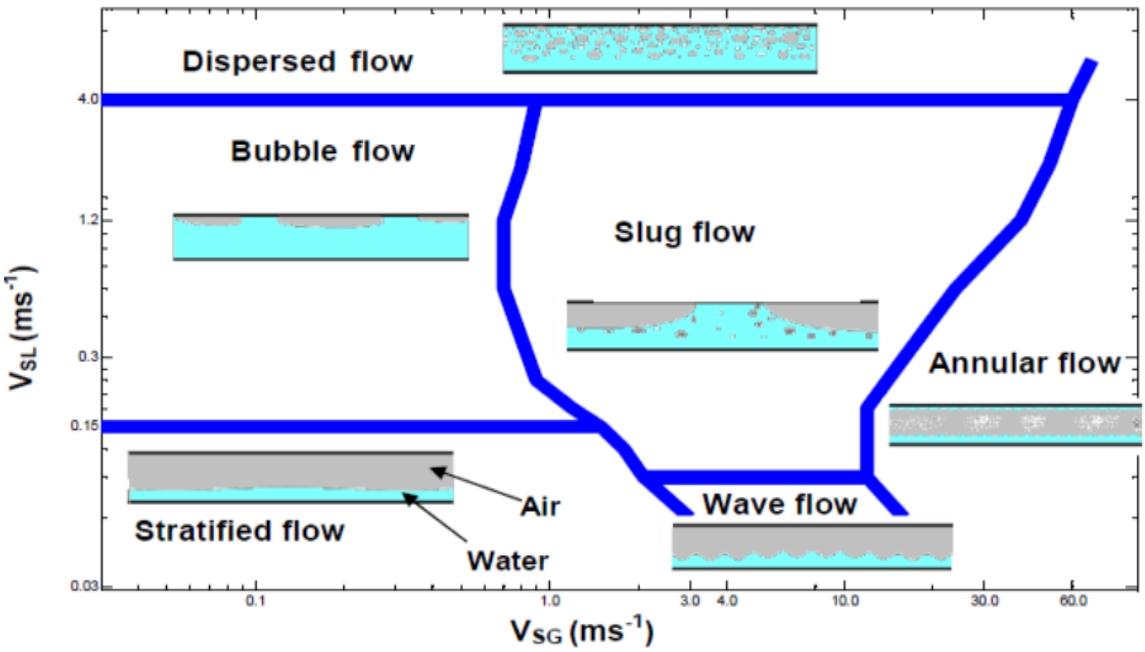

Figure 2-18: Flow regimes in horizontal pipe shown as a function of the relative speeds of the two phases, liquid and gas [23][94].

2.10 Vapour pressure and cavitation

Usually, cavitation phenomenon depend on two main factors, pressure and temperature. Figure 2-19 shows the vapour pressure curve for water. The red line is called the vaporisation line. It separates the liquid and vapour phases. When the ambient pressure decreases, the boiling point of water also decreases. There are two ways to boil water. The first is to increase the temperature while keeping the pressure constant until the temperature is high enough to produce vapour bubbles. The second way is lower the pressure while keeping the temperature constant, at a sufficiently low pressure the liquid will boil [95].

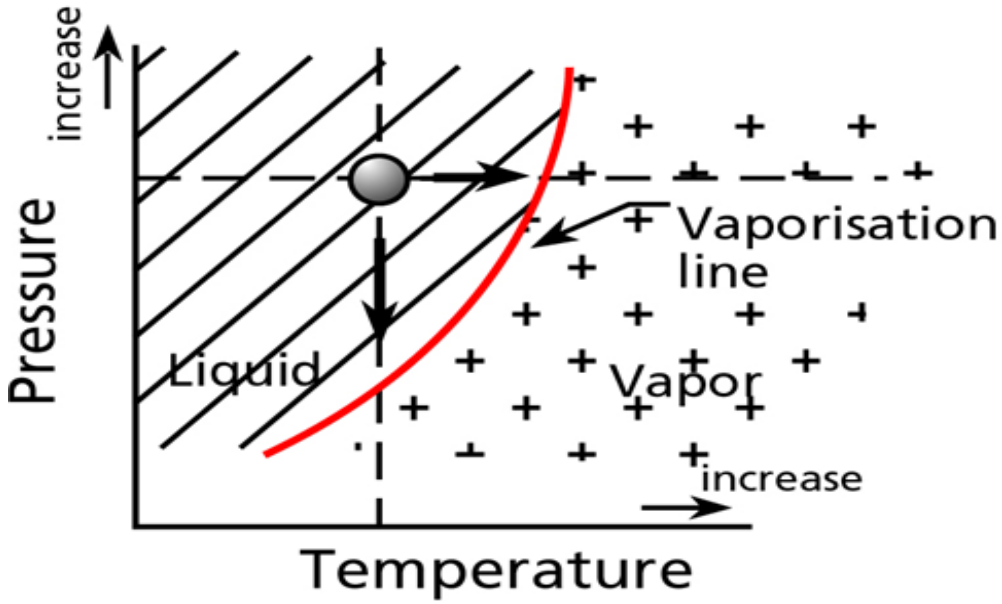

Figure 2-19: Vapour pressure vs. temperature [95].

For example, at atmospheric pressure the boiling point of water is 100^0C. However, when the pressure is decreased to about 0.5 bars, the boiling point of water drops to approximately 80^0C. That's what happens at the pump inlet when the pressure becomes lower than vapour pressure. Consequently, if the fluid's temperature is high and the pressure drops as the fluid enters the pump, the conditions are such as to increase the likelihood of cavitation [96].

2.11 Velocity and pressure profile through control valves

Figure 2-20 shows the velocity and pressure distributions through a globe valve. When the liquid passes through a control valve, at the 'vena contract' (point of narrowest flow restriction), the velocity of liquid increases because the cross-sectional of the flow at this point is less than for the rest of the flow path. The increase in velocity at the vena contracta results in lower pressure where the bubbles can start to form. When the liquid leaves this high-velocity area, the pressure gradually increases, causing bubble collapse [87].

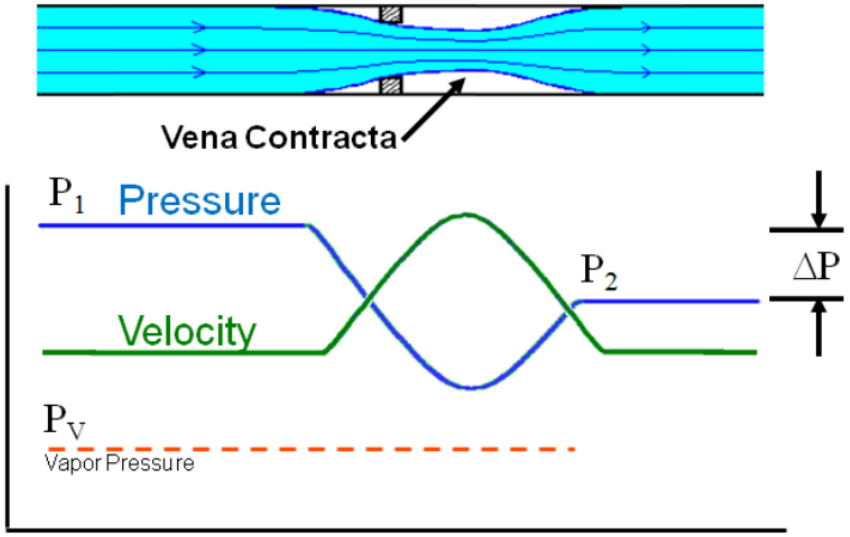

Figure 2-20: Typical velocity and pressure profiles in a control valve [97].

2.12 Flashing phenomenon

In liquid systems, if the outlet pressure from the valve is equal to or less than the vapour pressure, the bubbles that started to form at the vena contracta do not collapse into micro-jets. This phenomenon is known as flashing. Some of the bubbles escape downstream without collapsing, as shown in Figure 2-21. When flashing occurs, the liquid downstream is a mixture of vapour bubbles and liquid at high velocity, which causes erosion and pitting in both the valve and the downstream piping [98][77][87].

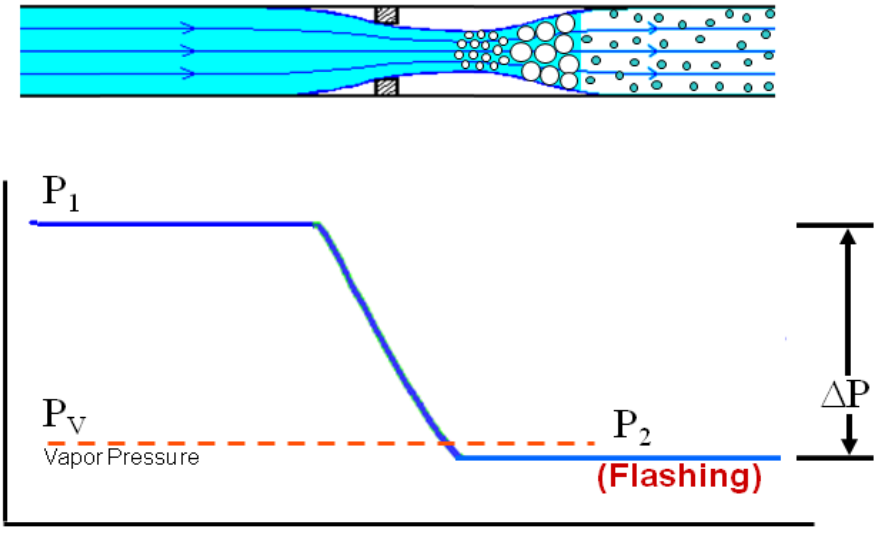

Figure 2-21: Pressure profile for flashing [97].

2.12.1 Controlling flashing

To eliminate flashing, the system must be modified to either increase the outlet pressure or decrease the vapour pressure. However, not all systems are easily changed. When flashing happens, no solution can be designed into the valve except to the hard trim material where flashing occurs [77][97]. On the other hand, re-locating the valve could be one way of eliminating this problem. If the valve empties the flow into a big container or tank the valve could be positioned close to the vessel such that the flow contraction takes place in the large volume of the container and away from any critical surfaces.

2.12.2 Difference between cavitation and flashing phenomena

Cavitation is a two-stage phenomenon. The first stage is the bubble formation, invariably due to a drop in pressure. The second stage is the bubble collapse into micro-jets as happens when the vena contracta pressure recovers and increases to a level above the vapour pressure. When the bubbles collapse into micro-jets, all their energy is concentrated into a very small volume. This creates tremendous pressure, generating minute shock waves, causing fatigue and wear of e.g. the metal forming the pipe.

Flashing is a one-stage phenomenon. If the inlet pressure is increased sufficiently to raise the outlet pressure above the liquid vapour pressure, the bubbles will collapse into micro-jets, producing cavitation. It is easy to visualise why high-recovery valves tend to be more susceptible to cavitation since the downstream pressure is more likely to rise above the vapour pressure [77][99], see Figure 2-22.

Millions of micro bubbles collapsing near the valve’s solid surfaces can gradually wear away the material, causing severe damage to the valve body or its internal components. It is usually apparent when a valve is cavitating, because a noise much like gravel flowing through the valve will be audible. Areas damaged by cavitation appear rough and irregular. Flashing can also damage valves, but it will produce areas that appear smooth and shiny since flashing damage is mostly

erosion. The most significant flashing damage tends to occur at the point of highest velocity [98][99].

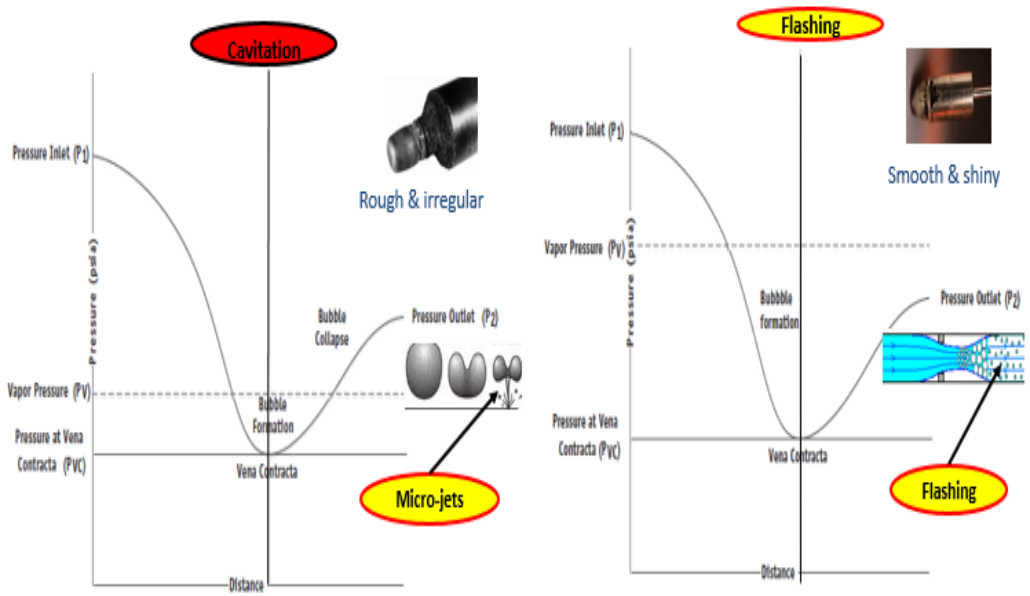

Figure 2-22: Cavitation and flashing phenomena [99].

2.12.3 General features of control valve cavitation

Valves play a critical role in industry, and especially, in the engineering, manufacturing and scientific communities. The primary purpose of valves is system control. Valves are used to start, stop, or throttle the flow to ensure safe operation of the process. Different kinds of valves are used in various industrial plants. In mechanical devices, such as pipelines, they regulate the flow rate of the liquid system; in chemical plants, they regulate the process pressure. Hence, the development of industrial control valves is crucial for high-quality operation of both current and future technologies.

Cavitation in control valves is a severe liquid-mechanical problem that can occur in all valves, with all types of liquids and over a wide range of pressures and temperatures. Figure 2-23 shows typical data extracted from many reports and experiments for cavitation in different kinds of valves. When the flow rate Q increases, the differential pressure ΔP also increases when keeping the upstream pressure and valve opening unchanged [88]. The relationship between Q and ΔP , is as shown in the equation below [88].

$$Q = C_d A\sqrt{2\Delta P / \rho + V^2} \qquad (2\text{-}20)$$

Where: C_d is discharge coefficient, A is valve inlet area, V (=Q/A) is the averaged flow velocity, and ρ is the liquid density. The discharge coefficient is calculated using Equation (2-14).

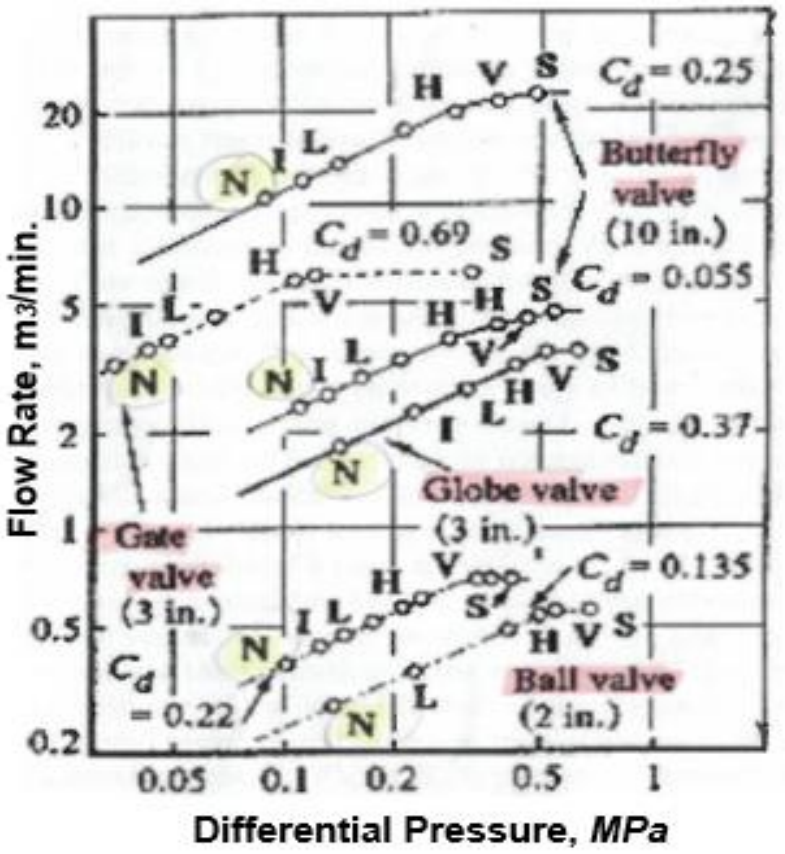

Figure 2-23: Flow rate vs differential pressure for four valves showing presence of cavitation [88].

It is noted in Figure 2-23 that the curve for each valve shows a steady increase in flow rate with increase in differential pressure until the cavitation is “very heavy”, as shown by the letters V and S. During this stage, the gradient of the discharge curve decreases slowly until it is horizontal, with constant flow rate. Here a slight decrease in the outlet pressure does not increase the flow rate. This situation, with super-cavitation on the downstream side of the valve, is usually called choking cavitation, and the crossing of the straight line is expressed by Equation 2-20.

Choking cavitation is the last step in cavitation development. This condition should be avoided in normal control operations because it causes heavy vibration, rapid pitting and cavitation erosion in the downstream pipework. As shown by the letters on each curve in Figure 2-23, cavitation phenomena start and develop at values of the differential pressure much lower than the choking value. It was observed that in the early stage of the development the volume change of the liquid was only slight and cavitation was hard to detect [88][100].

2.13 Types of cavitation

Initial cavitation describes cavitation that is only just detectable. There is a specific hysteresis effect with the beginning and disappearance of cavitation. The pressure conditions for incipient cavitation are not the same conditions for cavitation to disappear. Usually an increase in pressure above that at which the cavitation appears is required for the disappearance of the cavitation. Van der Meulen [101] has suggested the term “desinent cavitation” for the latter condition. Here cavitation is classified into travelling cavitation, fixed cavitation, vortex cavitation, or vibratory cavitation.

- Travelling cavitation: in this type the bubbles appear inside the liquid, and then move within the liquid until they collapse. Usually, the bubbles appear within the region of liquid at points of low pressure generated by turbulent flow or at solid boundaries [102].
- Fixed cavitation: in this type a submerged solid body is present in the flowing liquid, and as the flow disconnects from the body, cavitation becomes attached to the boundary. Herbich [103] has defined such fixed cavitation as constant in a nearly steady sense.
- Vortex cavitation: occurs when the turbulence flow starts caused by vortices contained in a region of high shear. Such cavitation can appear as travelling or stable [10][102].
- Vibratory cavitation: is a special case and happens when the flow velocity is so low that recirculation occurs in centrifugal pumps, valves and elements of the liquid experience many cavitation cycles [104].

2.14 Cavitation damage

2.14.1 Principles of cavitation damage

The most widely recognised effect of the bubble activity phenomenon is known as cavitation erosion. Cavitation erosion is the removal of metal from the surface of centrifugal pumps and valves caused by stresses associated with the burst and collapse of bubbles in the liquid. All types of metallic solid whether hard or soft metal, brittle or ductile are susceptible to damage by cavitation erosion. While every effort should be made to design and apply centrifugal pumps and valves so as to avoid cavitation, it is not always possible to do so, particularly in cases where the capacities being handled by a pump are less than its rated capacity [105]. There are four fundamental principles for cavitation harm (cavitation damage):

- Cavitation phenomenon depends on liquid properties, such as viscosity where the low liquid viscosity causes the liquid to penetrate into the surface of the metal. For example, water can penetrate more deeply into the surface of metal than heavy oil.
- The greater the pressure, the more the liquid penetrates into pores in the material increasing cavitation damage.
- The smaller the area of the orifice the greater the pressure generated when bubbles burst and collapse.
- The higher the frequency of vibration, the more severe the destruction of the surface layer of metals.

Operating a pump affected by cavitation for long periods can cause serious damage, especially to the impeller. It can cause pitting of the suction vane edge, discharge vane edge, impeller blade shroud and the pump casing. Severe cavitation can wear holes in the impeller and damage the blades to such a degree that the impeller becomes ineffective. Figures (2-24) and (2-25) show an example of the damage that cavitation can cause to different impeller types. In addition to the physical damage, there is damage to the pump‘s performance and efficiency, which increases with the degree of cavitation [106].

Figure 2-24: Damage caused by cavitation to a closed impeller [6].

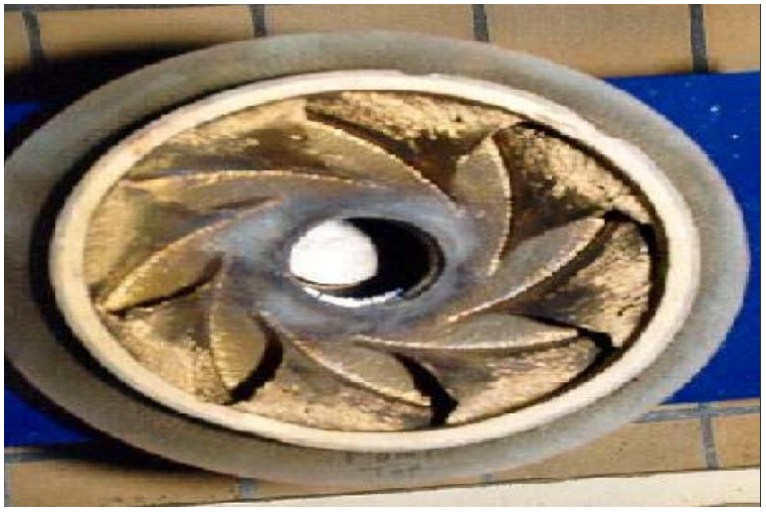

Figure 2-25: Damage caused by cavitation phenomena to semi-open impeller [107].

Figure 2-26 shows photos of bubble collapse along with the corresponding pressure trace. The moment of the minimum volume is between frames 6 and 7, and the evidence apparently shows the peak pressure occurs at that moment. When linked with Schlieren photos showing a spherical shock being generated at this moment, this seemed to relegate the micro-jets to a secondary role.

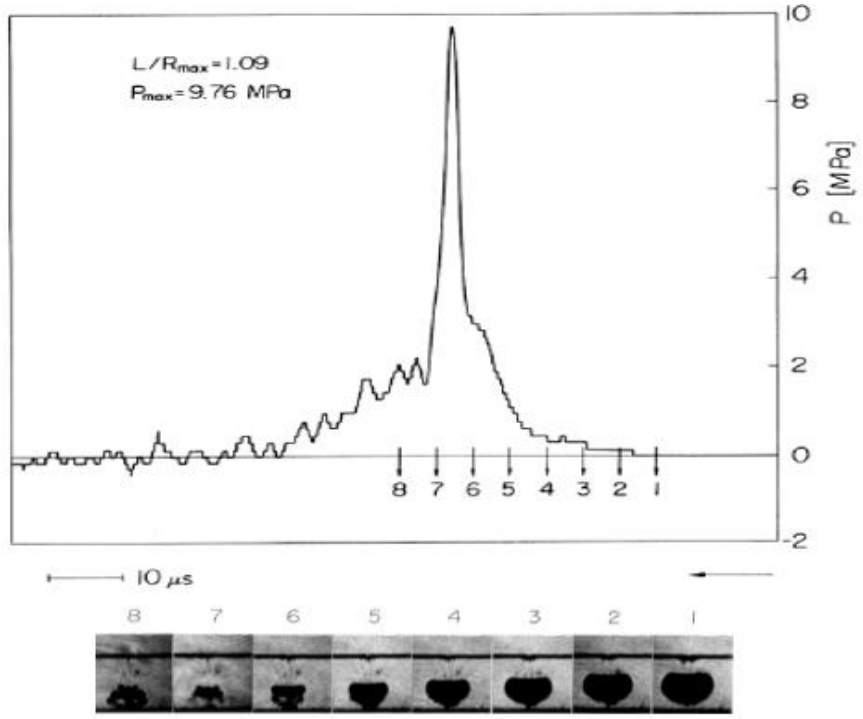

Figure 2-26: Sequence of photos of a cavitation bubble collapsing near a wall with wall pressure trace [6].

2.15 Mechanisms of damage caused by cavitation

Cavitation erosion occurs when the bubble collapse takes place near to a solid surface and can be identified by the particular marks it leaves on the surface. There are two possible mechanisms [108].

2.15.1 The collapse of the main bubble

Plesset, et al., [109] studied the simulated shape of a bubble at several stages of collapse using numerical techniques. They assumed a pure vapour bubble, incompressible fluid, and constant ambient temperature and vapour pressure. The investigations were performed using a differential pressure to water density ratio of 1 atmosphere to 1000 kg/l for two cases. For the first case, the bubble was initially touching a solid wall. In the second case, the distance from the centre of the bubble to the solid wall was 1.5 R. Figure 2-27 shows the changes in the bubble shape as it collapses for the first case.

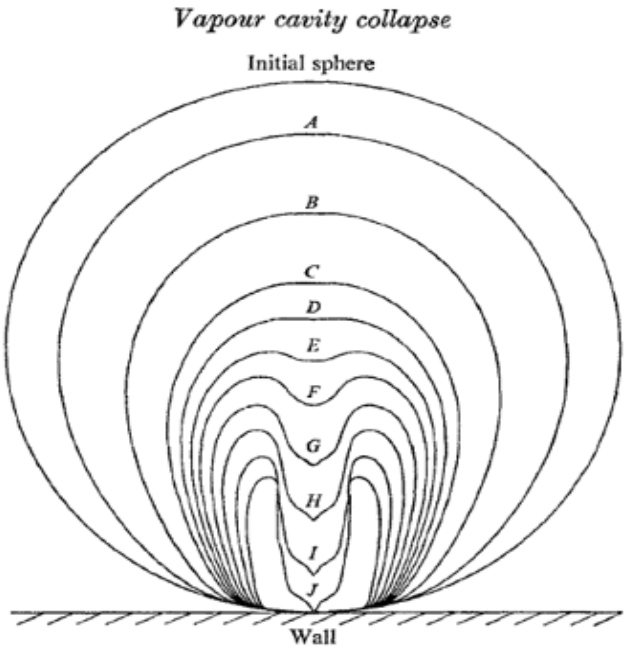

Figure 2-27: Numerical study of bubble collapse for an initially spherical bubble touching a solid wall [109].

The results of these time stepped simulations showed that in the final stage of the collapse, velocities as high 130 m/s and 170 m/s could be reached in the first and second cases respectively. The water hammer effect of these jets for a bubble 1 mm in size can cause stresses as high as 2000 atm with a duration in the order of 10^{-7} seconds where the stagnation pressure in the first case was as high as 800 atmospheres and a duration in the order of 10^{-6} seconds which is most likely the damaging mechanism.

This numerical study was subsequently validated by an experimental investigation performed by Lauterborn, et al., [110]. In this experiment, two ruby laser beams were used and converged to create a bubble, and the collapse of the bubble was observed. This study showed velocities as high as 120 m/s. Previously Plesset, et al., [109] had shown simulated velocities as high as 170 m/s. It is unclear whether velocities as high as 170 m/s did occur and were not detected due to the state of the technology at the time or such high velocities were not present. Given the imaging rate of 300,000 frames per second, technically it was possible to measure velocities even higher than 170 m/s, but this study does not give any reasons why the numerical study and the

experimental study did not agree when it comes to maximum velocity reached near the boundary. (see Figure 2-28).

Collapsing bubbles may be unstable regarding shape when the collapse happens near a solid surface. It was observed that the developing spherical asymmetry took the form of a rapidly accelerating liquid jet, entering the bubble at 6 and 7, from the side farthest from the wall as illustrated in Figure 2-26.

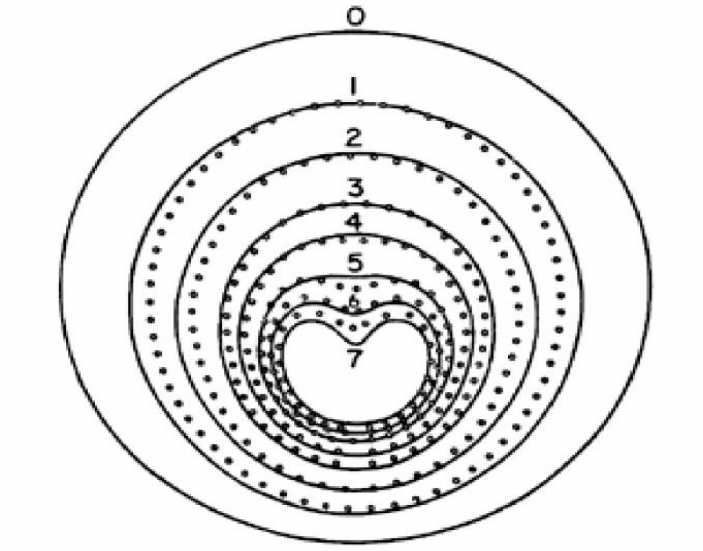

Figure 2-28: Comparison of numerical and experimental bubble shape in different stages of bubble collapse, solid lines represent numerical predictions, and open circles represent the experimental data [6][109][110].

The micro-jet are very high speed and when the jet impact on the other side of the bubble it can generate a shock wave and a highly localised pressure, affecting the surface of the near wall [6][108].

2.15.2 Bubble cloud

Figure 2-29 shows a cloud of cavitation bubbles, consisting of numerous small bubbles often with a foamy appearance. The result is called "cloud cavitation". The dynamics of these clouds produce a process of collapse which can generate much greater damage than the same number of similar isolated bubbles. This mechanism generates great disturbance when the microjet is disruption, the cloud of bubbles collapses to its minimum gas or vapour volume. This mechanism

generates another shock wave that effects nearby solid surfaces. When this mechanism occurs many times on the same surface, there is unacceptable damage due to the action of the micro-jet mechanism on the surface.

There are many factors effecting the degree of cavitation erosion, such as the geometry of flow paths, pressure distribution in the system and the properties of the liquid. The existence of solid material alone does not affect the occurrence of cavitation. However, it can increase the incipient cavitation in centrifugal pumps and valves where cavitation is already present [108]. In many types of equipment, cavitation damage is observed to occur in quite localised areas, for example, on a pump impeller, often as the result of the collapse of a cloud of cavitation bubbles.

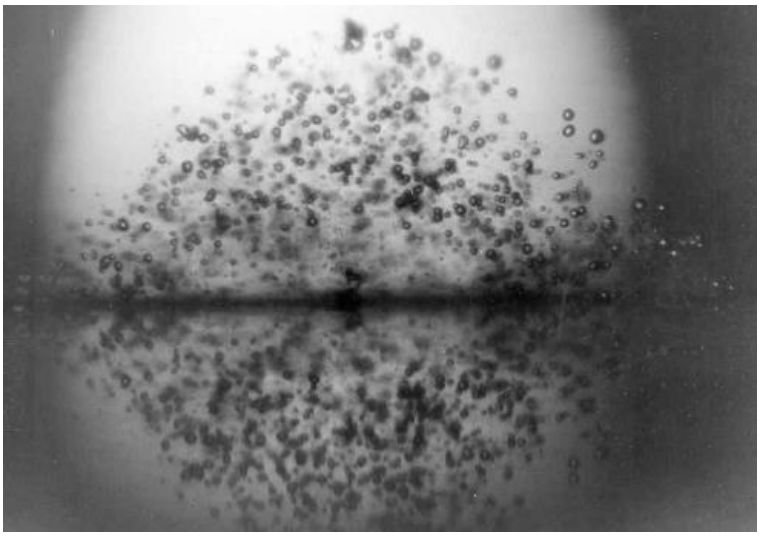

Figure 2-29: Photograph of a transient cloud of cavitation bubbles [111].

2.15.3 Cavitation erosion of valves

Figure 2-30 below shows cavitation erosion of a valve with time. The cavitation index has been suggested [77] as the primary parameter determining whether pitting of the valve trim will be significant and to establish a criterion for selecting valve type, material and lifetime. However, erosion cavitation will depend not only on this simple parameter but also on the positioning of the valve.

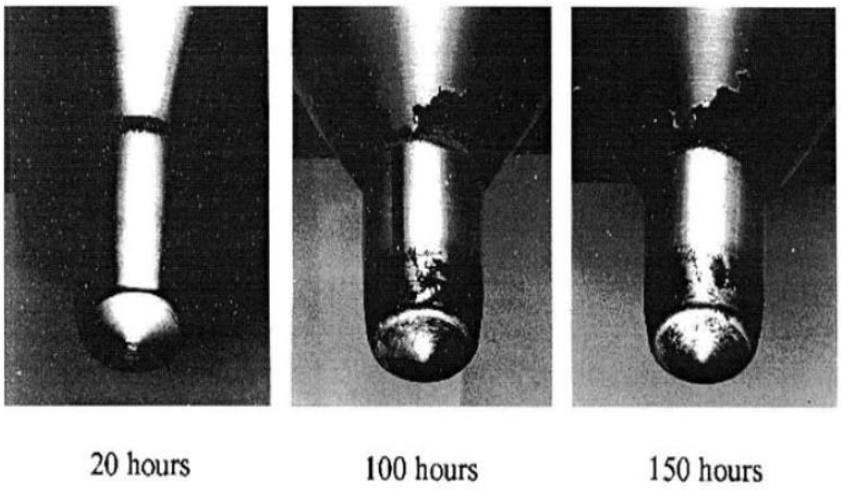

Figure 2-30: Cavitation erosion of a valve developed over time at a high upstream pressure of 20 Mpa [77].

2.15.4 Cavitation damage in valves

Figure 2-31 shows damage to a butterfly valve when the operating conditions were [95]:

- Upstream pressure between 1.2 to 1.4 bar.
- Downstream pressure about 0.1 bar.
- Flow velocity around 2.3 m/s.
- The operational duration about 24 months.
- The degree of the opening of valve approximately 30^0.

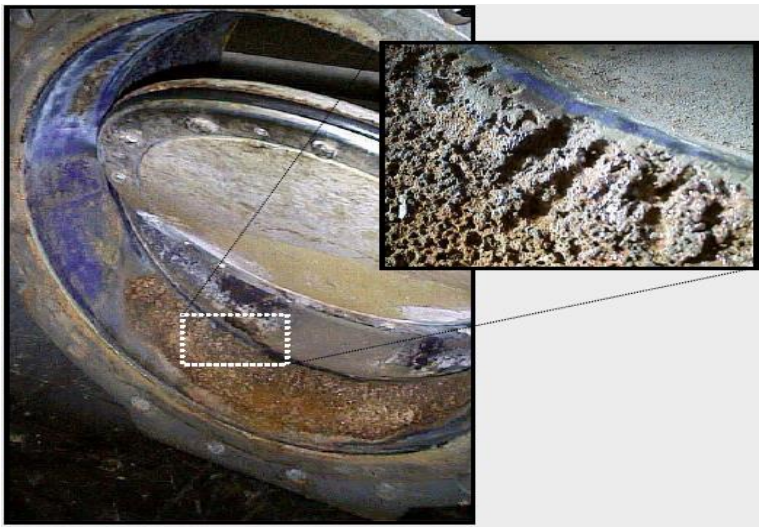

Figure 2-31: Cavitation damage to a butterfly valve [95].

Figure 2-32 shows cavitation damage to a partly closed gate valve. After three months operation, the body of the valve was severely damaged [112][113][114] [115].

Figure 2-32: Cavitation damage to a gate valve [95].

2.16 Conclusions

Bubble occurrence is undesirable in process systems. It occurs in boiling processes, valves, pipes and rotating machines such as a centrifugal pumps. The bubble formation, burst, collapse, coalescence and break-up occur when the pressure drops below the liquid's saturated vapour pressure in multi-phase (gas/liquid) processes. Energy release from this processes depends on mechanisms of liquid properties, such as surface tension, viscosity and hydrodynamic forces, will create bubble oscillations and pressure waves, which produce acoustic waves. This chapter has reviewed and explained the mechanism of AE generation due to bubble occurrence during multi-phase gas/liquid flow. The mechanisms discussed included; bubble formation, collapse, break-up, burst at a free surface, bubble coalescence, incipient cavitation and developed cavitation. The next chapter will provide a brief background for condition monitoring and acoustic emission.

Chapter 3 Condition Monitoring Technologies

This chapter gives a brief introduction to Acoustic Emission (AE) and its possible applications. It starts by defining AE, and giving a description of useful AE signal measurements. After this it provides information on the principles of AE technology, AE signals, AE measurements and AE generated by gas bubbles in liquids. The chapter ends by considering AE signal processing, and the feasibility of applying AE technique for the detection and monitoring of cavitation in two-phase flow.

Condition monitoring (CM) can be defined as the processes of detecting and monitoring physical parameters related to hydraulic systems including machinery such as centrifugal pumps and valves, for the purpose of identifying machine integrity. The costs of the component parts of industrial processes that might be damaged by cavitation are high and, thus, preventing equipment failure and minimizing costly stoppages due to unscheduled servicing and maintenance are priorities that can be achieved using CM. CM of rotating machinery not only maintains machine performance at a high level but can prevent failure of one component damaging adjacent parts which would be more costly than replacing the faulty part.
This section, will present CM technologies, which are may be viable for use with bubble occurrence, outlining both their capabilities and limitations [14][116]:-

- **Vibration analysis:**

Vibration is the technique most commonly used in industry. The monitored vibration signals can be displacement, velocity, or acceleration, though with modern equipment acceleration is the preferred measure. The most basic vibration monitoring technology is to measure the RMS value of the overall vibration level, to trend this measure against time as an indicator of deteriorating machine condition and when it reaches a pre-defined value take remedial action. This method is not so accurate due to the high levels of intrusive noise in industrial environments. The sensor is selected based on the frequency range relevant for the diagnostic applications [108][117][118].

- **Acoustic emission:**

AE is a non-destructive detection method that is suitable for continuous monitoring and may be used for detecting cavitation in two-phase flow with a high degree of accuracy. AE measurements may be divided into two types: active - where the measured excitation is generated externally; and passive - where the measured excitation is generated within the component. Typical frequencies ranges for AE measurements are in the range of from about 20 kHz to higher than 3 MHz [108][119][120]. The sensors commonly used are resonance type piezoelectric transducers that are attached to test surface using an appropriate couplant [121][122][123].

AE has the potential to monitor acoustic cavitation through the detection of the acoustic signals generated by bubble formation, oscillation, collapse and burst. The spectrum detected contains much information about the dynamics of the cavitation process. In the case when the initial cavitation starts under the influence of a high ultrasound field in a liquid, the cavitation bubbles become a secondary source of sound generating a broadband AE signal that can be detected using sensors such as the hydrophone [124] and the fibreoptic hydrophone [124]. An example of a broadband acoustic emission spectrum generated by cavitation bubbles and detected by the B&K 8103 hydrophone produced by a 40 kHz transducer is shown in Figure 3-1.

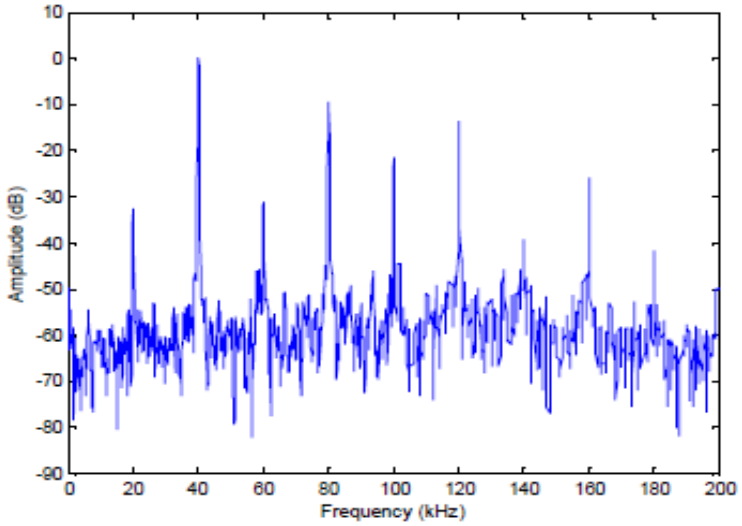

Figure 3-1: Acoustic emission spectrum measured by the B&K 8103 hydrophone. AE transducer produces a signal at 40 kHz and 30 W.

The AE spectrum contains the broadband noise signal generated by shock waves due to bubble collapse which contain information on the cavitation phenomenon. Many articles describe AE as a method for detection and monitoring of cavitation events [125][126] such as occur in hydraulic turbines and pumps where cavitation is a source of damage and degrades the machine. Induced vibration and pressure are used to identify and analyse the cavitation activity.

Wolff, et al., [126] investigated how bubble collapse in the liquid causes AE. It was reported that the AE signal generated was linked with high amplitude pressure pulses in the hydraulic system. It is believed this process will allow monitoring of incipient cavitation. Their work showed increasing AE RMS voltage levels with increasing pressure and cavitation. The cavitation activity as acquired by hydrophone detectors, provided a broadband AE spectrum revealing the high-frequency range of the emission spectrum. The intensity of cavitation activity as determined by broadband integrated energy from the AE spectrum has been presented by Hodnett [125].

- **Airborne acoustic signals**:

Cavitation produces high levels of sound which may, thus, be a useful way of detecting its onset. Microphones, which are relative easy to install, can be used to pick up these sound signals. Microphones may be positioned remotely, and non-intrusively. This makes acoustic monitoring an attractive option for on-line CM. The biggest single problem with monitoring of airborne sound is usually the contamination of the signals because other similar machines in the vicinity of a valve (e.g. motors, generator and cooling fans), will also generate airborne noise. Other adverse effects include interference from reflecting surfaces [108].

3.1 Definition of acoustic emission (AE)

AE is a physical phenomenon that occurs where high-frequency elastic waves are emitted by a rapid release of energy from local sources within the body of a solid or liquid, such as might occur in turbulent flow or with cavitation [11][12][127]. Stresses generated by dynamic processes in a material can produce internal changes such as cracks and plastic deformation which are

accompanied by the creation of pressure waves. These waves contain information on the internal behaviour of the material and can be detected by use of a suitable sensor that converts mechanical deformation into electric signals. These signals are detected and processed by suitable AE instruments, see Figure 3-2 [21]. The range of frequency for AE sensors starts above the limit of the human hearing, above 20 kHz and extends to about 2 MHz [14][128].

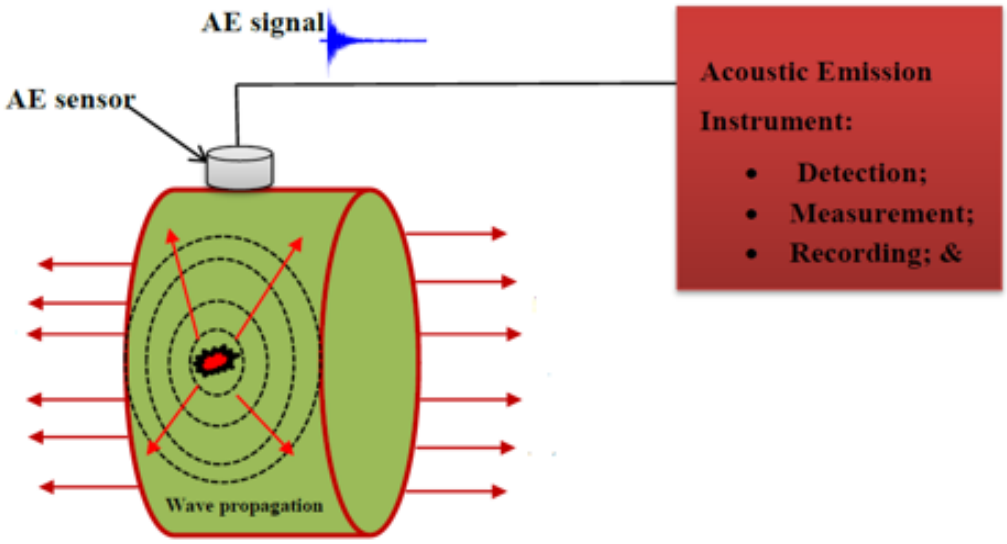

Figure 3-2: Principle of Acoustic Emission [11].

3.2 AE applications

Applications of AE technology can be found in:

- Diagnosis and monitoring bubble formation at early stages of the boiling process [17].
- Monitoring of bubble formation and collapse (cavitation) in valves and centrifugal pumps.
- Pressure equipment: AE methods are used to detect, corrosion, erosion and leakage in tanks, pressure containers, piping systems and steam boilers.
- Petrochemical and chemical: storage tanks, nuclear reactor containers, drill pipes, pipeline leakage.
- Civil engineering: bridges, dams, cable suspension bridges, concrete structures fixed by composites.

- Research and development: AE is a useful technique to monitor and investigation the reasons for damage in equipment such as pumps and valves caused by cavitation.
- Wind turbine: blade damage [122][129].

3.3 AE signals

There are two types of AE signals, as shown in Figures (3-3) and (3-4).

3.3.1 Burst signals

An AE burst signal is a signal emitted from a single event, see Figure 3-3. For a given process, such signals tend to occur randomly. These signals have a definite start and a definite end, features which distinguish them from continuous signals [11][130].

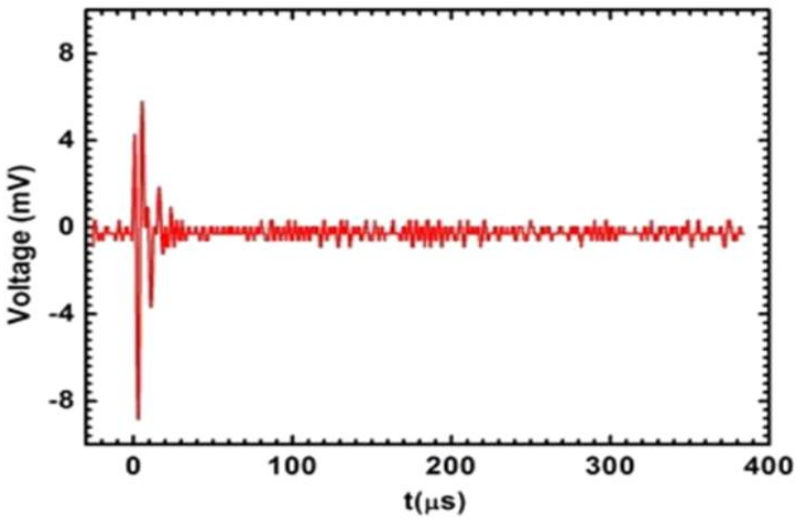

Figure 3-3: AE burst signal [11].

3.3.2 Continuous signals

The figure below shows this type of signal; it is a continuous wave that contains different frequencies and amplitudes. A continuous signal is a sequence of burst signals combined to produce the appearance of continuity [11][130].

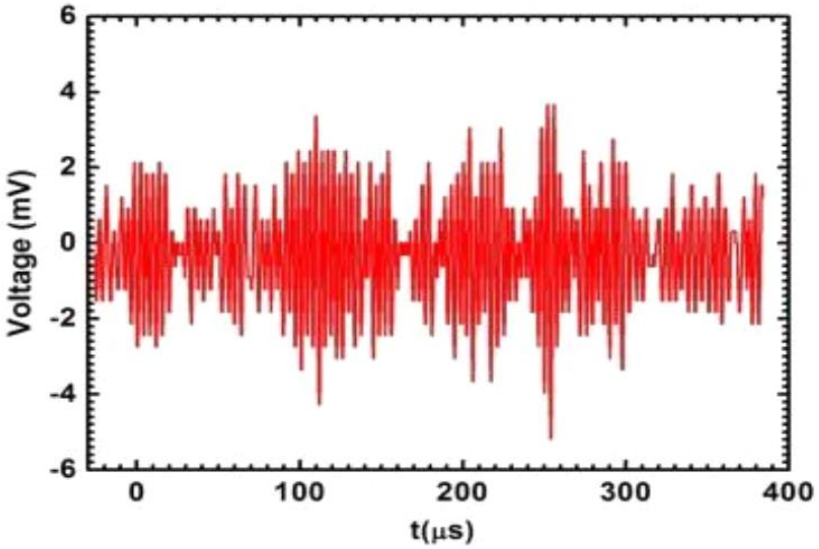

Figure 3-4: AE continuous signal [11].

3.4 AE measurements

Data obtained using AE systems can provide useful information, but this will usually require one or other signal processing technique. The most useful approaches have been found to be: hit driven data measurement and time driven data measurement. These are described below.

3.4.1 Hit driven data measurement

Figure 3-5 shows the most common AE signal parameter measures. Only those signals which exceed a pre-set voltage threshold are considered. This is to avoid background noise contamination of the signals.

- Threshold: is a voltage level that the AE signal must exceed to be counted as an AE event [12][128].
- Arrival time: is the time of the first crossing of the threshold level, and can be used to identify signal source locations.
- Rise time: is the time duration between peak amplitude and the first signal crossing of the threshold [12].

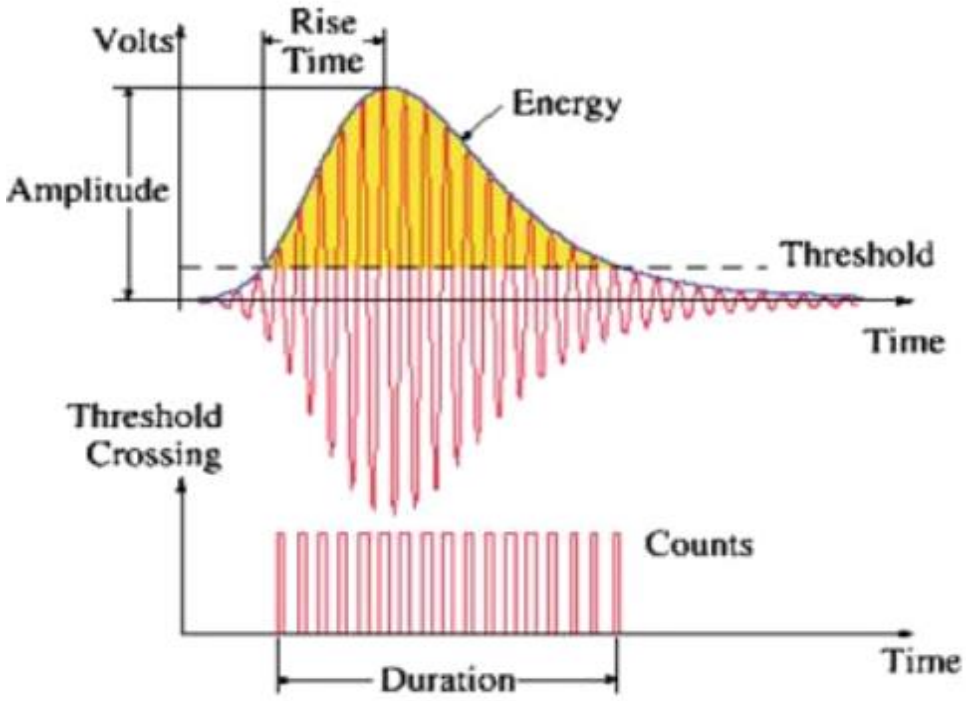

Figure 3-5: AE signals measurement parameters [128].

- Amplitude: is the peak signal level that occurs within the duration of the signal event, see Figure 3-5.
- Duration: is the time period between first and last crossing of the threshold by the AE signal [12][131].
- Counts: are the number of times the AE signal crosses the detection threshold. Also known as ring down counts or threshold crossing counts [12].
- Energy: is the value of an integrated measurement of the square of the voltage signal correlation time [12].
- Frequency: the number of cycles occurring in unit time [12].
- AE-Hit: is the process of detecting and measuring an AE signal's levels through a channel [127][12].

3.4.2 Time driven data measurement

Typical time domain waveforms are shown in Figure 3-6. With this method of measurement a continuous record of the AE analogue waveform as detected by AE sensor which is subsequently sampled and digitised after which it is stored.

Modern measurement systems have the capacity to continuously digitise the measured AE time domain waveforms at different sampling rates. The data collected can then be analysed to identify and specific characteristics in order to identify the sources of the signal.

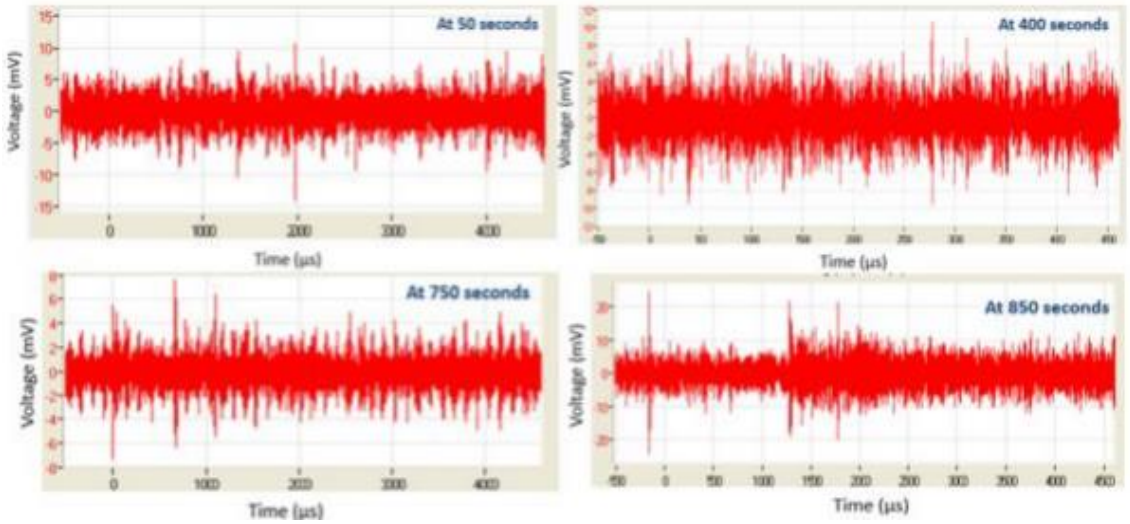

Figure 3-6: AE waveforms generated by pool boiling process [15].

3.5 AE mechanisms

AE is a technique for the continuous real-time monitoring of dynamic processes. Traditionally, AE was applied to solid materials and thus this chapter opens with a short description of AE signals produced by a material that is loaded and stressed.

3.5.1 Kaiser effect

Some twenty years ago, Wilhelm Kaiser demonstrated that for relatively low loads, AE occurs in a loaded material only after any prior maximum load had been exceeded. For example, consider Figure 3-7, as the applied load become greater, from A to B in the figure, an AE signal is generated. However, if the applied load falls, from B to C and is then increased again, from C to B, there is no AE until after point B is reached, when AE starts again [11].

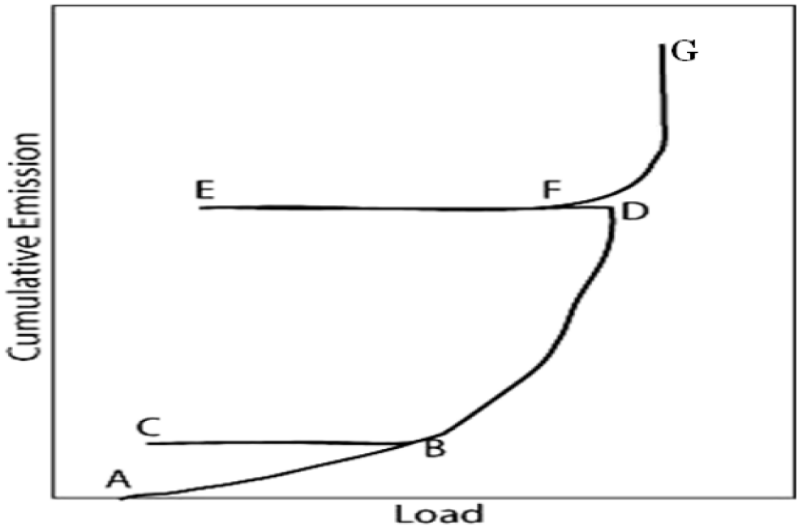

Figure 3-7: Kaiser and Felicity Effects [11].

3.5.2 Felicity effect

It can be seen from Figure 3-7 that if the load is decreased (e.g. from D to E), there is no emission. If the load is subsequently increased, from E towards D, no emission takes place until point F is reached. The load at F is a lower than at point D [11].

3.6 AE Detection and measurement system

Usually any AE detection system contains sensors, amplifiers and data acquisition board. As below:

3.6.1 AE sensors

AE sensors are instruments that convert elastic deformations into electrical signals. There are many kinds of AE sensors but today the piezoelectric transducer is the most popular [17][131]. The piezoelectric sensor normally has a base of piezoelectric material in the form of a thin disk that converts mechanical deformation into an electrical signal. These piezoelectric materials are mainly piezoelectric ceramic made from crystals such as titanates and zirconates [11] [127].

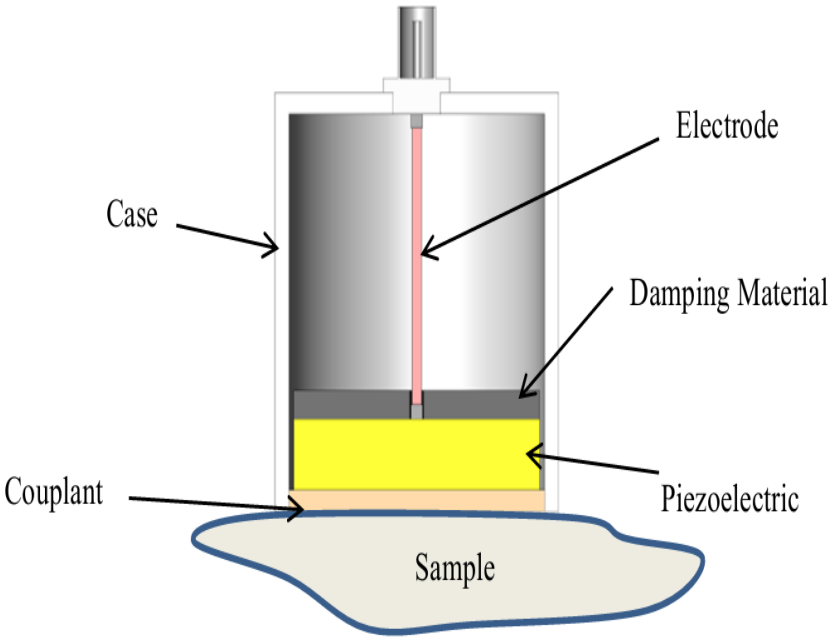

Figure 3-8: Elements of the piezoelectric sensor [11].

Figure 3-8 shows the components of the piezoelectric sensor. The selection of sensor depends on the application, sensitivity required and local environment. Sensors can be classified as passive or active: active sensors have an integral preamplifier; passive sensors are without integral preamplifiers [11][132].

3.6.2 Sensor couplant

AE sensors must be coupled with the medium which carries the AE signal. With solids, the sensor must be connected in a manner which maximises signal transmission across the interface between material and sensor. This can be enhanced by adding a thin layer of commercially available couplant between transducer and the material's surface [133][134]. The couplant serves two functions (i) to prevent the presence of air between sensor and sample surface and (ii) to better match the impedance of the surface to the sensor and so reduce signal attenuation as it crosses the interface [11][135]. Couplant has little strength or adhesive qualities and is not recommended for attaching the sensor to a surface.

When the source of AE is within, say, two-phase flow the sensor can be immersed, to a greater or lesser extent, in the liquid. However, if the sensor is attached to the outside wall of the container then the above comments of coupling apply.

3.6.3 Amplifiers for AE

The amplifier is used to increase the amplitude of the AE signal, but can also be used to improve signal quality. It is also be used to match the impedance of the sensor to the impedance of the following circuitry to maximise signal transmission and minimise signal distortion.

3.6.4 Data Acquisition (DAQ) board

The heart the AE-Data Acquisition System (DAQ) was the six-channel DAQ card (see Figure 3-9) which samples the analogue voltage signal at a rate of 5 MHz, and transforms it to a digital signal with 18-bit precision giving a dynamic range of more than 85 dB. The six channels were linked to the PC using the PCI bus (PCI-2 Based AE System with six channels). The PCI-2 was chosen because of its relatively low cost and superior low noise system [12]. Each of the six channels was attached to an AE-sensor via a preamplifier. For signals of sufficient magnitude, i.e. greater than the threshold, the DAQ card collected the signal data and converted them into digital signals which were analysed in terms of arrival time, AE-Count, AE-Rise time, AE-Amplitude, AE-Duration and AE-RMS, as required [11][12]. The A-D converter card contained anti-aliasing filters that are tuneable (i.e. variable band pass filter) directly by the software.

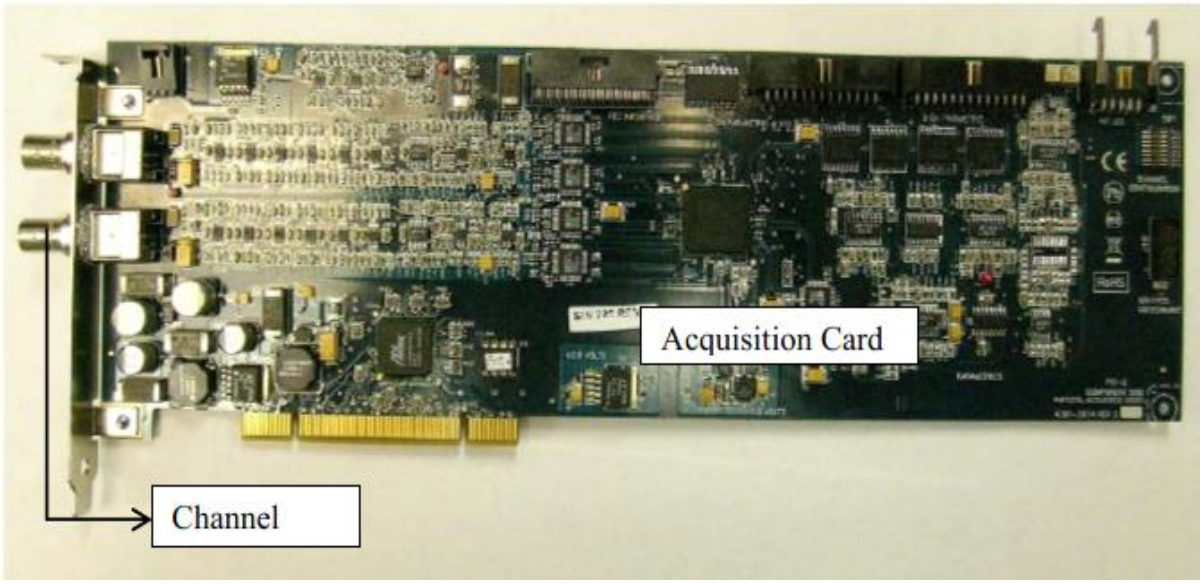

Figure 3-9: Six channel AE data acquisition board [12].

3.7 Advantages and disadvantage of AE technique

3.7.1 Advantages of AE technique:

There are many benefits associated with the AE technique:

- AE is more sensitive than other technique for detection of defects at an early stage.
- It can be used for both pre-service and in-service testing.
- AE is a good technique for locating the source of defects [11][116].

3.7.2 Disadvantage of AE technique:

Limitation of the AE technique are:

- Sensitive to ultrasound sources.
- Low signal amplitude, thus amplifier is required.
- AE cannot be repeated because every loading is different and has its own signal stress signature.
- It requires skill and experience for the signal processing [11][116].

3.8 Sources of AE and sound emitted from fluid flow processes

In most industrial processes, AE sources can be divided into two types: mechanical or hydraulic.

Mechanical sources in machinery will include impacts and/or frictional rubbing between moving parts, such as occurs in bearings, gears, pumps and valves. Mechanical sources within solid materials include dislocations, crack formation and growth, fatigue and fractures [4][129][136][137].

Hydraulic sources are the AE sources of major interest in this thesis. The following is a list of AE hydraulic sources [4][137][138].

1. Cavitation and flashing phenomena, bubble activity, bubble formation, burst and collapse [139][140].

2. Turbulence flow noise generated by flow vortices [6].

3. Liquid-mixture interaction in multiphase flows, two-phase gas/liquid systems [141].

4. Flow branches in piping systems causing pressure drop in a liquid [142].

5. High flow velocities causing turbulence flow noise [142].

7. Liquid drops on a liquid free surface (rain fall) [31][143].

8. Leakage from hydraulic systems such as valves and pipes [144].

9. Bubble activities caused by chemical reactions [145].

11. Oceanic noise caused by the breaking and pressure of waves due to bubbles of air inside the liquids: e.g. sea foam [139][146][147][148].

AE from bubble formation, collapse and burst are important areas for research due to their industrial significance.

3.9 Acoustic cavitation

Acoustic cavitation can be the result of bubble activity caused by high power ultrasound in a liquid medium. It is the process of formation, growth and subsequent collapse of the bubbles formed, and leads to mechanical and chemical phenomena. The cavitation bubbles will oscillate, stimulated by the high power ultrasound before they subsequently collapse and produce a shock-wave. Figure 3-10 shows a schematic of the generation, expansion and collapse of such bubbles [149].

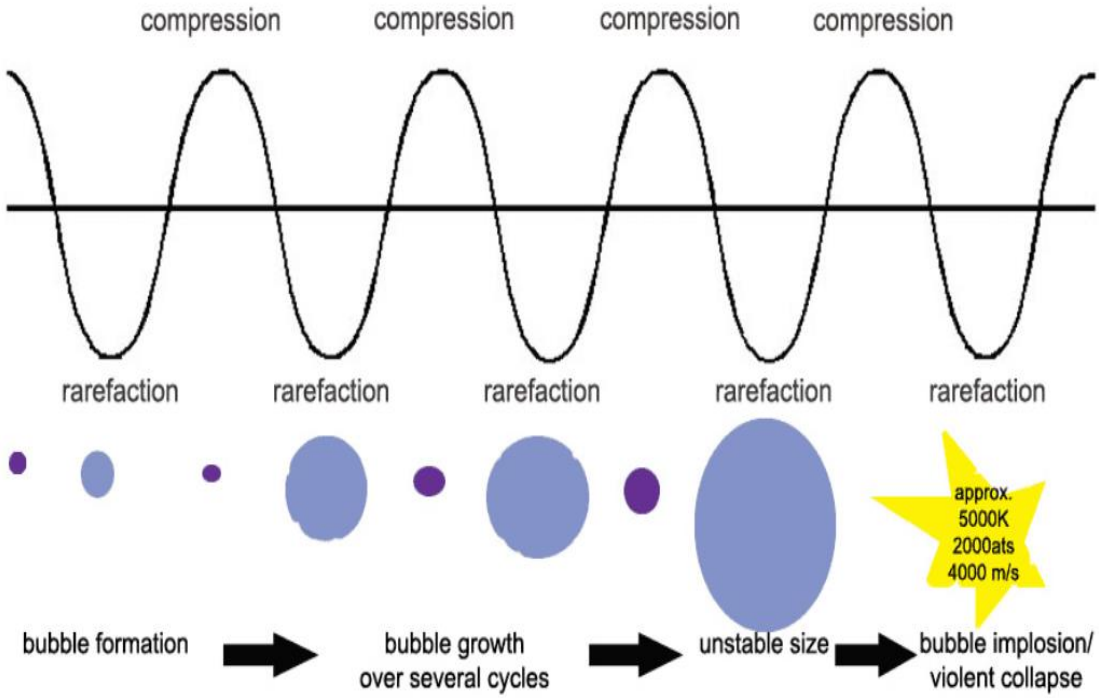

Figure 3-10: The schematic illustration of the expansion and collapse of bubbles [150].

Stable cavitation describes the expansion of gas bubbles under equilibrium conditions. Inertial cavitation is defined as the process of oscillation and collapse of bubbles. During the collapse process, a bubble is capable of causing high pressure in the liquid medium, which in turn causes high fluid velocity and the micro-jetting phenomena. That creates the cavitation effect that produces high local temperatures, approaching 5000^0C and extremely high pressure in a liquid medium, and a high local velocity C_i, which can be calculated from Rayleigh's equations, (Equation 3-1) [90][112].

$$C_i = \sqrt{\left[\frac{2}{3}.\frac{P - P_B}{\rho}.(\frac{R_0^3}{R_e^3} - 1)\right]} \qquad (3\text{-}1)$$

Where:

P: The pressure in the surrounding liquid.

P_B: The pressure inside the bubble at the start of the collapse.

R_o: The bubble radius at the start of the collapse.

R_e: The bubble radius at the end of the collapse.

ρ : The water density.

3.10 The mechanisms of acoustic emission created from bubbles

Minnaert [30] reported that the peak frequency of the sound generated by a bubble formed underwater at a nozzle was a function of the liquid, the gas used to "blow" the bubble and the physical dimensions of the nozzle. Strasberg [33] investigated the pulsation oscillations of bubbles as a function of their sizes and modes of oscillation. He concluded it was the oscillatory motion of the bubble wall that generated the acoustic signals. Figure 3-11 illustrates four different oscillation modes.

The zeroth mode is represented by a sphere subject to simple volume pulsation. The 1st mode is represented by a sphere of fixed volume subject to lateral simple harmonic oscillations about a fixed point. In the 2nd and 3rd modes, the bubble volume remains constant but the bubble experiences oscillatory changes in shape. For the zeroth oscillation mode, Strasberg [33] found the natural frequency was given by Equation (3-2). The natural frequencies of the other three oscillatory modes shown in Figure 3-11 can be determined according to Lamb's [151] model, see Equation (3-3).

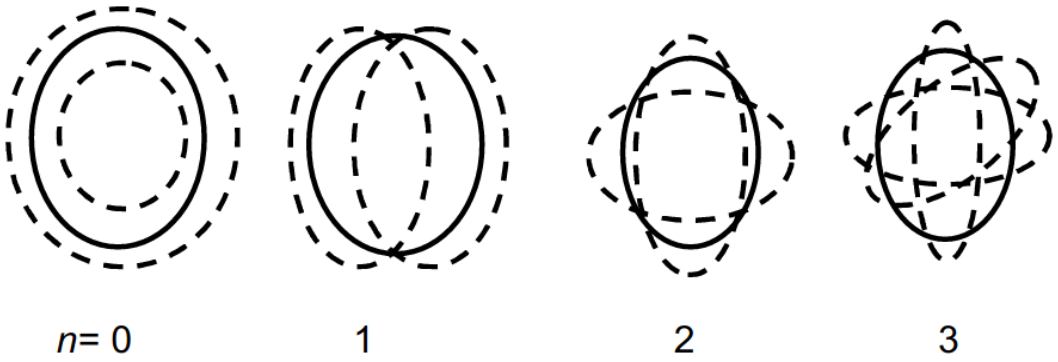

Figure 3-11: First four modes of oscillation of a globular bubble [33].

$$f_o = \frac{[3\gamma P_o / \rho]^{1/2}}{2\pi R_o} \tag{3-2}$$

$$f_n = \frac{[(n^2-1)(n+2)T / \rho R_o]^{1/2}}{2\pi R_o} \tag{3-3}$$

Where, according to Strasberg [33]:

" f_0 : The natural oscillation frequency for the volume pulsation during zeroth mode.

f_n : The frequency for the n^{th} mode.

P_0 : The static pressure.

γ : The specific heat of the gas in the bubble.

R_0 : The mean radius of bubble.

ρ : Density of the liquid.

T : The surface tension of surrounding liquid."

3.11 Signal Processing Techniques

To successfully detect and monitor the formation of bubble requires the extraction of useful information identifying their formation from AE signals which themselves will be corrupted by background noise. Thus the AE measures (and sampling rates) chosen to identify within the signal those characteristics corresponding to bubble formation will be important.

Time domain signals, AE for example, are analysed using statistical parameters to identify characteristics of interest. These often include, signal peak amplitude, root mean square (RMS), crest factor and kurtosis. This section discusses the likely usefulness of the different statistical parameters and reviews literature describing how these parameters were used to detect bubble formation.

- **Root Mean Square (RMS)**

RMS gives an average measure of the continuously varying AE amplitude; defined as the square root of the average of the rectified time averaged signal, typically it will be recorded in volts or decibels [12][122][152]. RMS is calculated as:

$$RMS = \sqrt{\frac{X_1^2 + X_2^2 + ... + X_N^2}{N}} \qquad (3\text{-}4)$$

Where, X_1, X_2 …….X_N are sampled values of the voltage, and N is the total number of samples.

- **Energy (E)**

Energy, E, is defined as the integral of the square of the voltage signal (α) over the test duration (T) and determine by using the Equation (3-5) [12][122][131].

$$E = \int_0^T \alpha^2(t)dt \qquad (3\text{-}5)$$

- **Kurtosis (KU)**

Kurtosis is a measure of the magnitude and frequency of peaks present in a signal, see Equation (3-6). Kurtosis is a measure that has been used relatively successfully to detect incipient faults in gears and in the occurrence of bubbles in

two phase flo [15][153]. The numerical value of the kurtosis for a Gaussian, or Normal, distribution is 3, and this is assumed to be measure for a healthy bearing. When a defect or fault starts to form it will produce a distinct peak in the AE signal which will give a clear increase in the kurtosis, but as the defect advances the kurtosis decreases until it reaches the value for an undamaged bearing [119][122].

The kurtosis can be found using Equation (3-6):

$$UK = \frac{1}{N}\sum_{i=1}^{N}\left(\frac{S_i - \mu}{\sigma}\right)^4 \quad (3\text{-}6)$$

Where:

Si: Signal data points.

μ: Signal mean.

σ: Standard deviation.

N: Number of data points.

- **Skewness (SK)**

The value of skewness is determined by Equation (3-7):

$$SK = \frac{1}{N}\sum_{i=1}^{N}\left(\frac{S_i - \mu}{\sigma}\right)^3 \quad (3\text{-}7)$$

Skewness is a measure of the extent to which a curve is skewed to the right or left of the Gaussian curve. Symmetrical distributions have $S_k = 0$. Negative values of S_k show that the distribution is asymmetric, whose tail extends in the direction of lower values. Positive S_k show that the distribution is asymmetric and whose tail extends into higher values. However, skewness is not a good indicator under all conditions of speed, load and fault deterioration [122][154].

- **Crest Factor (CF)**

The Crest Factor (CF) is given by Equation (3-8). The CF is the ratio of the measured peak amplitude of the signal divided by the RMS value. It is well known and widely used as a measure of how defective a bearing is. The smoother the signal the less likely the presence of a defect, the more spiky a signal the more likely the presence of a defect. [122].

$$CF = \frac{PeakValue}{RMS} \qquad (3\text{-}8)$$

- **Energy Index (EI)**

The AE Energy Index (EI) was used to identify bubble formation during the test period with different rates of electric power-supply to the plate heater. The Energy Index (EI) is defined as the square of the ratio of root mean square of a defined segment ($RMS_{segment}$) of a given signal to the root mean square of the entire signal ($RMS_{overall}$). This measure has been successfully applied to experimental data from gears, bearings, and bubble activity [15][155]. For this particular research investigation, every AE waveform recorded throughout the tests was divided into 1650 segments and EI was calculated using Equation (3-9).

$$EI = \left(\frac{RMS_{segment}}{RMS_{overall}} \right)^2 \qquad (3\text{-}9)$$

The Fourier transform is well-known and widely-used method for transforming time-domain signals into the frequency-domain. One serious weakness of the Fourier transform is that the frequency spectrum produced is the average of the input signal over the entire sampling period. That means it does not show how the spectrum of a signal changes with time. Such transforms are extremely useful when the time domain signal contains periodic events. Today, the Fourier Transform is no longer determined by analogue methods because signals are digitally sampled. The Discrete Fourier Transform (DFT) is computed and a development of this is the Fast Fourier Transform (FFT) which carries out the same transformation process

but much more quickly [122][156]. The FFT is now commercially available as a sub-routine contained in, e.g., Matlab, or as a stand-alone app.

For rotating machines where bearings are the most frequent sources of faults, spectral analysis of the measured vibration signals is by-far the most common method for fault detection [115][157].

However, information can be lost when the frequency spectrum is derived from the time-domain signal. The frequency spectrum is derived on the assumption has that the time domain signal is stationary, and a rectangular window is imposed on the time-domain which itself introduces “leakage” which makes weak signals harder to detect. Attempts to resolve the leakage problem by using more suitable window functions have been attempted, but any success has reduced frequency resolution [122][158].

Another problem is associated with data length. Notwithstanding, a high SNR (signal-to-noise ratio) the achievable resolution decreases as the data length is reduced [122][158].

3.12 Previous work

3.12.1 AE and sound generated from bubble formation process.

According to Shuib et al. [27] AE is an useful technique for detection and monitoring of AE signals caused by bubble formation and burst. It was observed that the velocity of acoustic wave inside the liquid can be measured by using the AE technique. In addition, they note that bubble formation and burst at the surface of the water causes AE signal amplitude when the bubble size increases, and bubble size can be determined using AE signals. Carmi et al., [16] used AE in the detection of bubble transitions during flow boiling. It was observed that the capability of using AE in the diagnosis and detection of the bubbles at an early stages during boiling process was good. Baek et al., [159] found that bubble density increases with the increase of liquid temperature. Furthermore, they identified a relation between the water boiling phenomenon and the AE signals in a transparent glass cell at 1 bar. Alhashan et al., [15] used AE to monitor bubble

occurrence during the pool boiling. They establish that there is a relationship between an increase in AE signal levels and bubble formation rate within the boiler vessel. Benes and Uher [13] note that overheating is correlated with the AE signal parameters. It was confirmed that the AE technique can be used to predict the boiling phenomena.

It has been known for some time that the pressure pulses associated with the bubble formation and burst at the surface of the liquid also act as sources of AE [6][160]. Husin, et al., [161] used AE technique to explore sound in the frequency range 100 kHz -1 MHz from gas bubble formation and bursts. Experimentally, they found that AE energy and amplitude are directly correlated to the bubble at its inception and burst. AE is a good technique for diagnosing and monitoring of bubble formation and their detachment from the heating surface to the surrounding water. Furthermore, it was established that the AE RMS parameter is sensitive, reliable and robust for monitoring bubble formation and the propagation to the surface of the liquid during the boiling process [162]. Husin et al., [94][163] used AE to detect bubble inception and burst, and they have confirmed that the source of AE activity in two phase flow comes from bubble occurrence. Furthermore, this study again demonstrated that AE sensors are sensitive enough to catch the emission from single bubble activities, as at bubble formation, burst and collapse. With pool boiling the bubbles generate the highest level of acoustic emission when they detach from the heating surface [15][17]. The AE of a bubble burst at free surface is correlated to the bubble's size [27].

3.12.2 AE and sound generated from two-phase air/liquid flow.

AE is a good technique for observing and checking the presence of gas bubbles in two-phase flow. Addali [21][24] used AE to measure the gas void fraction having found a direct relationship between the gas void fraction and the measured AE energy. Addali also found measured AE energy levels could be used to determine superficial gas and liquid velocities. Al-lababidi et al., [164] established a correlation between AE energy, gas void fractions and slug flow velocities in two-phase air/water flows. Alssayah et al., [18] confimed not only that AE can be used to detect and measure slug velocity but also to differentiate

between two phase gas/liquid flow regimes in pipes. All studies reviewed confirmed the viability of AE for detecting bubble activity and for monitoring flow patterns of gas-liquid two-phase flow.

3.12.3 AE and sound generated from cavitation phenomena.

Neill et al., [4] found that the energy density associated with bubble formation and its break away from the nozzle generated an associated pressure shock wave in the surrounding liquid [165] which was identified by an AE sensor. They also used AE techniques for monitoring cavitation phenomena in centrifugal pumps and got more accurate results than with a vibration signal. Alfayez et al., [116] found the AE method to be a useful technique for detection of cavitation using the RMS value of the AE signal, with a high possibility of determining the best efficiency point of a centrifugal pump or hydraulic system. Jaubert et al., [166] noted that AE is a good method for the detection of early stage cavitation phenomena in pumps and valves, which makes it possible to study incipient cavitation. Bezn [167] and Joon-Hyun Lee et al., [168] reported that AE parametres such as RMS may be used to identify the opening percentages of valves, such as safety valves, and also to indicate damage and degradation of check valves in nuclear reactors. Jazi et al., [66] used two methods, characteristic diagrams and acoustic analysis, in the detection of cavitation phenomena in globe valves, with acceptable levels of accuracy and agreement between the two techniques.

Osterman et al., [169] proposed a visualisation method for the detection of initial cavitation, and made a comparison with pressure oscillations measured by a hydrophone technique for different percentage openings of the valve. They showed that the visualisation technique was more accurate than hydrophone measurement.

Rahmeyer [80] considered the cavitation index (σ) as a means to calculate the design flow conditions at which cavitation would occur, and extended the concept to butterfly valves based on the analysis of experimental data. Using the experimental data he set cavitation indices (or limits) for initial, critical, early damage, and choking cavitation. The main emphasis of his paper was to suggest a design index limit for cavitation noise, and to that end the paper provided tables

of data and scaling exponents so the proposed design limits could include consideration of upstream pressure and valve size. Kaewwaewnoi et al., [170] used the AE technique to monitor valve leakage, and established a high correlation between AE parameters such as signal level (ASL) and AE root mean square (AE-RMS) and leakage rates of different valve sizes and inlet pressures. It was found that the AE activities increased with the leakage rate and inlet pressure but diminished with valve size.

Alhashmi [108] made some significant new contributions to the field of CM of cavitation in centrifugal pumps, including detection and diagnosis of cavitation by using instantaneous angular speed and low frequency (0-1 KHz) vibration for the monitoring of cavitation in such a pump. Chan et al., [171] used the minimum net positive suction head (NPSH) method to show that a centrifugal pump can work without risk of erosion. They recognised that cavitation erosion could only be induced when the collapse of bubbles occurs near a working surface. The results of the experiments, carried out on a centrifugal impeller in a closed circuit, demonstrated that below the critical NPSH the erosion rate first rises, then declines, and finally rises for a decreasing NPSH. Furthermore, 3 % head excess above the calculated value ensured no cavitation. Tan Lei et al., [172] simulated cavitation occuring in centrifugal pumps at a low flow rate. They found good agreement between results obtained by calculating the values of net positive suction head available (NPSHa) and the experimental results. Lee et al., [173] found that the inception of cavitation caused the efficiency of the primary pump to be reduced significantly, and for it to generate vibration and noise. To avoid this phenomenon, the inlet of the pump was fitted with a mechanical device, a single rotor called an inducer, which was used to increase the operating pressure sufficiently to overcome cavitation. The cavitation modes were analysed by using cross-spectral density of fluctuating pressures at the inducer inlet.

3.13 Conclusion

The AE technique is very sensitive, it can detect and monitor high frequencies above the frequency range of human hearing between 20 kHz and 3 MHz. One

of its important advantages over other technologies is that AE technique offers a passive and non-destructive technique which provides a practical means of detection particularly for the monitoring of two-phase gas-liquid systems such as cavitation and liquid flow in pumps, valves, pipelines and columns where the bubble occurrence phenomena cannot be avoided.

This chapter has presented a brief description of AE systems, AE parameters, sources, propagation and signal characteristics. The advantages and disadvantages of using AE to detect and measure cavitation have also been presented. This chapter concluded by reviewing previous work describing AE applied to monitor bubble formation, burst and collapse, including monitoring gas void fraction and single bubble characteristics in multi-phase flow in horizontal pipes and a liquid filled column.

However, to date no one has investigated bubble formation and collapse at an early stage in ball and globe valves with two phase (gas/water) flow in horizontal pipes. Similarly with the monitoring of bubble formation during pool boiling. On the basis of the literature review this study will focus on investigating the capability of AE for detecting bubble activity at an early stage for both valves (ball/globe) and pool boiling. The study will also monitor and diagnose bubble occurrence during pool boiling and cavitation in ball/globe valves using AE methods. The next chapter will show the research methods used to obtain early detection and monitoring of bubble formation during pool boiling; and similarly for early stage cavitation phenomena in ball and globe valves.

Chapter 4 Research methodology

The aim of this chapter is to demonstrate the possibility of using AE techniques to obtain early detection and subsequent monitoring of bubble formation during pool boiling; and similarly for early stage cavitation phenomena in ball and globe valves. The research methodology is divided into three different sets of experiments; attenuation tests, boiling tests and valve tests, as shown in Figure 4-1.

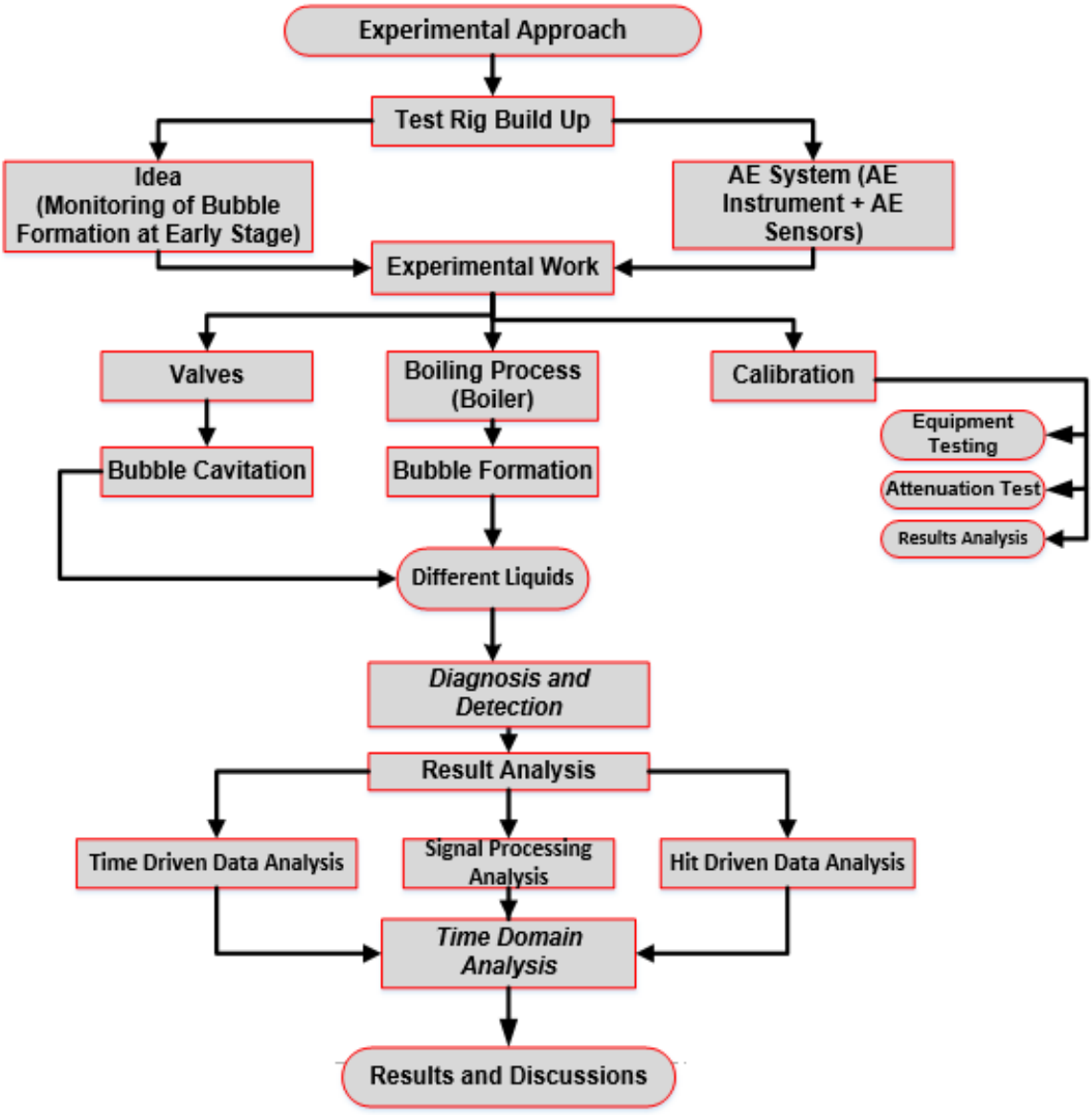

Figure 4-1: Schematic of the steps in the early detection and subsequent monitoring of bubble formation and cavitation from basic design to the interpretation of results.

Figure 4-1 summarises the procedure followed in this research. Details of boiler test rig design, valve test rig design, and laboratory experiments. This chapter also describes the experimental work of detecting and monitoring bubble formation and incipient cavitation phenomena using AE techniques. The experiments were divided into two main parts: pool boiling tests and valve tests.

4.1 Experimental setup and procedures for pool boiling tests

This study depends on previous work carried out in this area [13][15]. In these tests, a vertical cylindrical boiler vessel was used to separate between different bubble activities region, such as bubble formation and burst. Three different liquid types, two different electric power-supplies and three different levels of liquid were used during the pool boiling experiments, as shown in Table 4-1.

Table 4-1: Experimental procedures of boiler test.

Water Type	Power rating of heater (W)	Water Level above heated surface (mm)
Tap water	2500-3000	100-200-350
Demineralized Water		
Water with Different Salt Concentrations (5 g/litre, 15 g/litre and 20 g/litre)		

Figures 4-2 and 4-3 show the pool boiling test-rig, where the boiling tests were carried out. It consisted of a stainless steel water boiler with 270 mm inner diameter, 440 mm in height, and 2.5 mm wall thickness. The capacity of the boiler is 25 litre. It is integral with a heater, located at the boiler bottom, and used to heat the water inside the boiler. The circular heater had an external diameter of 150 mm. Constant electrical power of 2.5 kW was fed to the boiler vessel throughout the experiments.

Two piezoelectric sensors (Physical Acoustic Corporation type “PICO”) were used in this investigation. The operating range of these sensors was between 20

kHz –750 kHz. The sensors were attached to the external surface of the boiler using superglue, as shown in Figure 4-2. The AE sensors were 200 mm apart, the one vertically above the other. Sensor 1 was attached 100 mm above the bottom of the boiler, to detect and monitor the bubble formation. Sensor 2 was located 200 mm above Sensor 1, and 100 mm below the top of the boiler, to monitor bubble formation, and bursts and oscillations when the bubbles are at the free water surface. Water temperatures were measured every second by using a thermocouple (T-type) that was fixed inside the boiler vessel 5 mm above the heating surface, see Figure 4-2. The AE sensors were connected to a data acquisition system by a preamplifier set at 40 dB gain. It continuously acquired AE waveforms from the system at a sampling rate of 2 MHz. The software (signal processing package “AEWIN”) is integrated within the PC to detect and monitor AE parameters, such as AE-Energy, AE-ASL and AE-RMS.

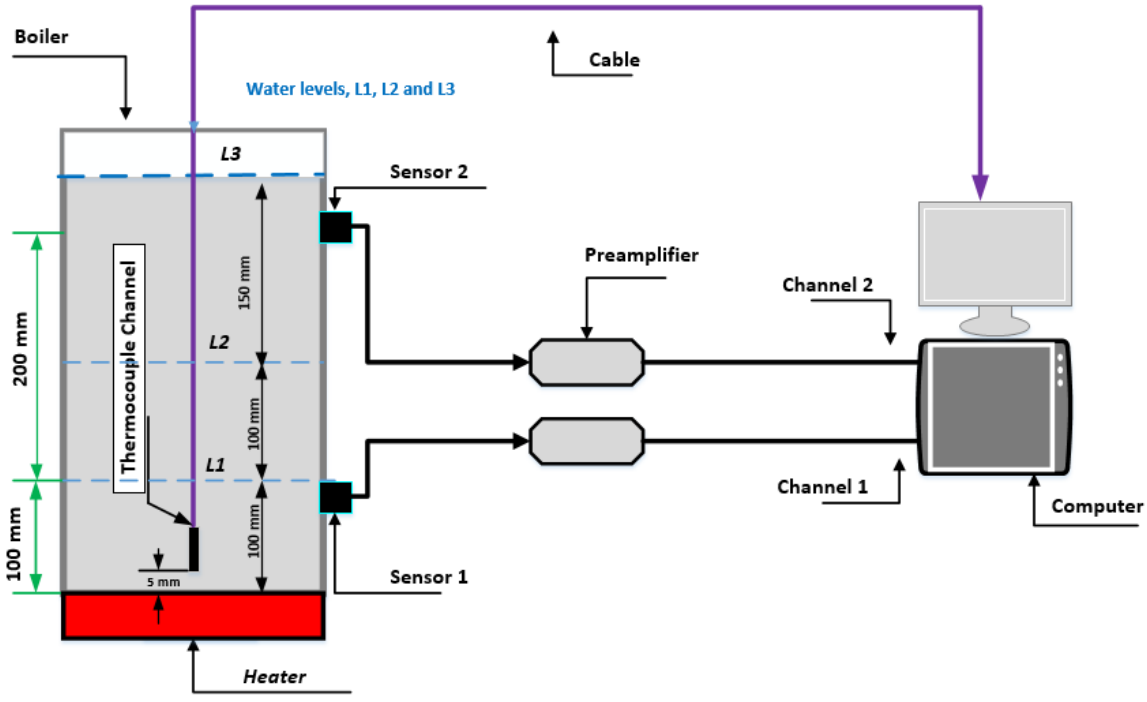

Figure 4-2: Schematic diagram of pool boiling test setup.

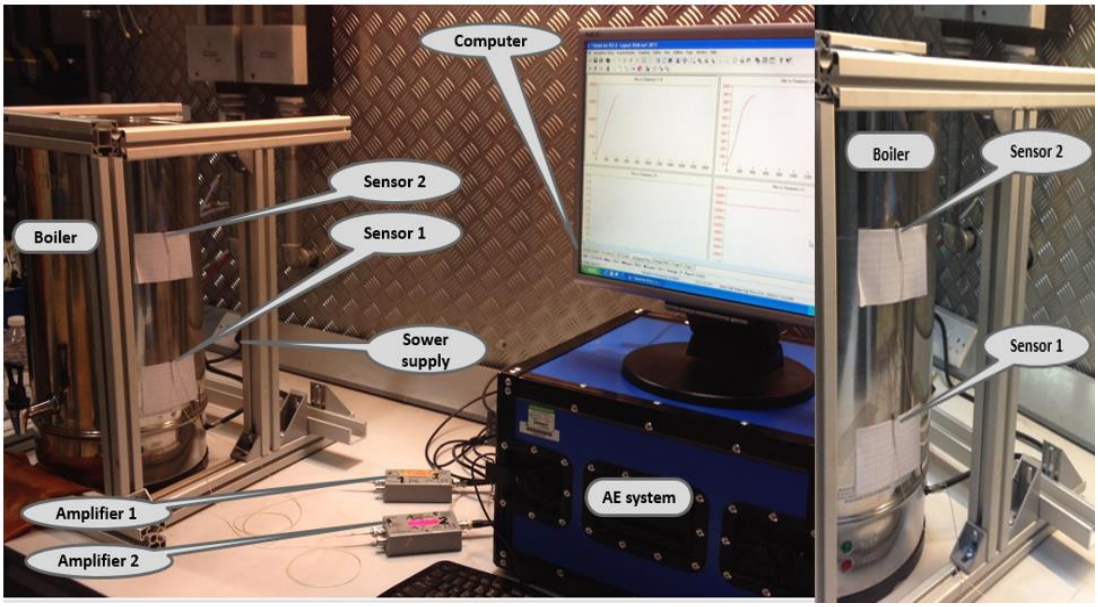

Figure 4-3: Pool boiling test-rig.

The author chose a threshold level of 36 dB, after observing that the AE sensors still recorded some background noise when the level was set between 28 and 32 dB. AE-hits detected for just background noise for a range of five threshold levels are plotted in Figure 4-4. At 34 dB, zero noise was recorded, but the threshold value was set at 36 dB to ensure consistent results throughout the tests.

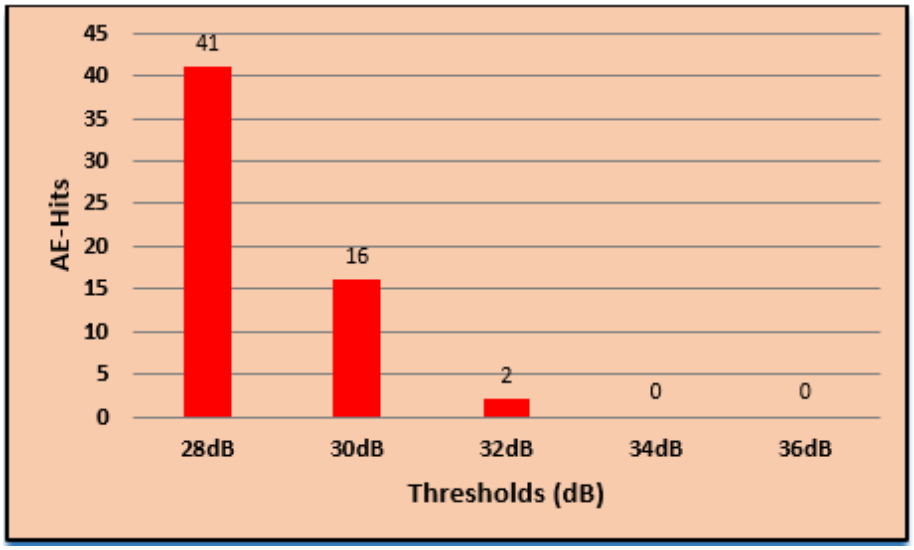

Figure 4-4: AE-Threshold levels of background noise for boiling tests.

Two Physical Acoustics Pico AE sensors, see Figure 4-5, each having an operating range of between 20 kHz and 750 kHz, were used for the AE tests.

These sensors are suitable for diagnosis and monitoring of bubble occurrence during pool boiling and valves, where small size and sensitivity is important. These sensors have an integral 0.5 m coaxial cable, which exits from the side of the AE sensor, as shown in Figure 4-5. For AE sensors calibration certificate see Appendix (A), Figures A-1 and A-2.

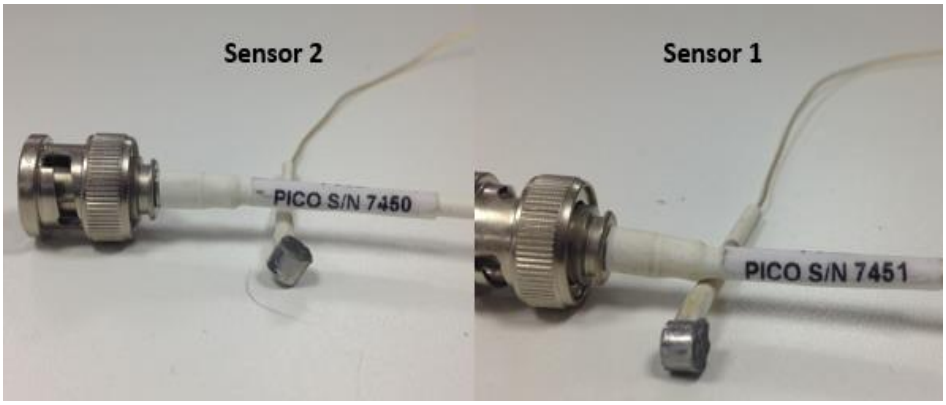

Figure 4-5: AE Pico Sensor.

Figure 4-6 shows AE sensors with an acquisition system. The AE experiments used type 2/4/6 pre-amplifiers to provide initial amplification of AE signals and decrease background noise.

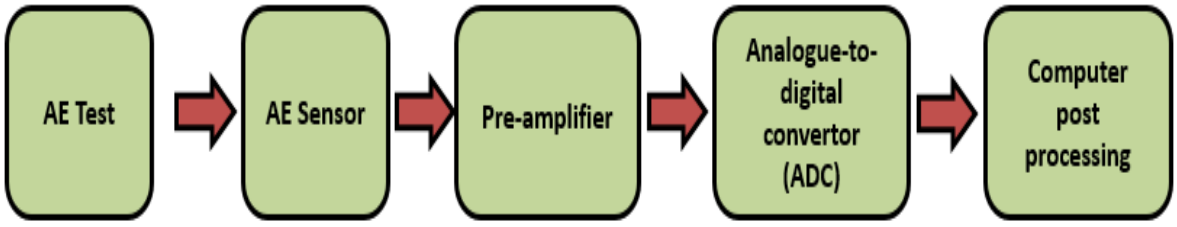

Figure 4-6: Schematic diagram of acquisition system.

These pre-amplifiers, see Figure 4-7, have a selectable gain of 20, 40, or 60 dB. These pre-amplifiers show better temperature performance than could be achieved with an integral pre-amplifier. They also contain a filter which reduces low-frequency noise.

Figure 4-7: Pre-amplifier.

For these experiments, to avoid unwanted background noise and give a better SNR, the pre-amplifiers were set at a 40 dB gain. Co-axial cables less than 1 m long, to avoid electromagnetic and background noise, connected the AE sensors with the pre-amplifiers. As explained in Section 3.6.2, the pre-amplifiers were connected to the DAQ card within the Pentium host PC.

4.2 Experimental setup and procedures for valves tests

Ball and globe valves are popularly used in many different industrial processes and hydraulic systems because of their light weight and simple structure. However, they are susceptible to cavitation phenomena and the growth and collapse of the bubbles formed leads to erosion and pitting of the metal surfaces. This investigation presents the detection and monitoring of bubble formation at an early stage, in both ball and globe valves using AE. It was shown that AE will detect incipient cavitation and that there is a clear correlation between AE signal levels and the flow rate through ball and globe valves at a constant opening percentage.

This study was built on previous work on ball and globe valves [66]. For these experiments, a purpose built test rig was used to monitor early stage bubble

formation and subsequent bubble collapse employing AE techniques. This work will investigate cavitation in different liquid types at 20 ^{0}C, as shown in Table 4-2.

Table 4-2: Experimental procedures of valves test.

Liquid types	Flow rate (m^3/h)	Opening percentage (%)
Tap water	0.55, 0.66, 0.77, 0.88, 0.99, 1.05, 1.09, 1.15, 1.20 and 1.25	15^0,16^0 ,17^0,18^0, and 20^0
Demineralized water	0.55, 0.66, 0.77, 0.88, 0.99, 1.05, 1.09, 1.15, 1.20 and 1.25	15^0,16^0 ,17^0,18^0, and 20^0
Water with different salt concentration (5 g/litre, 15 g/litre and 20 g/litre)	0.55, 0.66, 0.77, 0.88, 0.99, 1.05, 1.09, 1.15, 1.20 and 1.25	15^0,16^0 ,17^0,18^0, and 20^0

Each test was carried out three times, this was done to improve accuracy and reduce the likelihood of anomalous results. Each set of data recordings was one minute. It was considered that at a sampling rate of 5 MHz, a duration of one minute provided a sufficiently large sample to confirm the accuracy of the results. In each test run of the ball and globe valves, a file containing the waveform data was saved to the computer. These waveforms are transformed by FFT into frequency and power spectrums. The main characteristics of the waveforms are count, RMS, amplitude, frequency, rise time and energy.

According to the IEC 60534 standard [32] [175], the differential pressure ratio, *K*, across the valve is calculated by Equation (4-1):

$$K = \frac{P_1 - P_2}{P_1 - P_v} \qquad (4\text{-}1)$$

Where P_1 and P_2 are the pressures at upstream and downstream locations respectively. P_v is is the vapour pressure of the liquid at the operating temperature.

The cavitation index (σ) is calculated using Equation (2-10), and is a measure of possibilty of cavity formation [175]. The results of laboratory and field tests have demonstrated that it is acceptable to use σ for assessing the possibility of cavitation, (and related choking, noise, and damage) [175].

The rig for the ball and globe valves tests is shown in Figures 4-8 and 4-9. The valve was a commercially available, straight through, lever handle valve with one inch (25.4 mm) bore manufactured by BSS BOSS products. The system contained two piezoelectric sensors (Physical Acoustic Corporation type “PICO”) to detect and monitor any early stage cavitation that occured. One sensor was placed immediately upstream, and the other immediately downstream of the valve, such that the two sensors were 70 mm apart, see Figures 4-10 and 4-11. Both sensors were attached to the external surface of the valves using superglue. The AE sensors were connected to the data acquisition system via preamplifiers, set at 40 dB gain. The system was set to continuously sample the AE waveforms at a rate of 5 MHz.

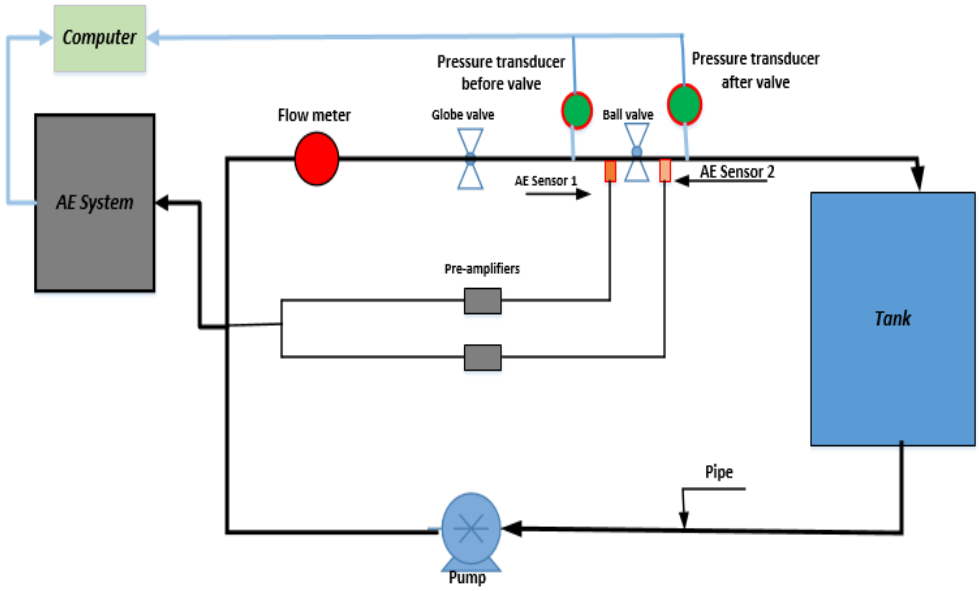

Figure 4-8: Schematic diagram of the cavitation test setup.

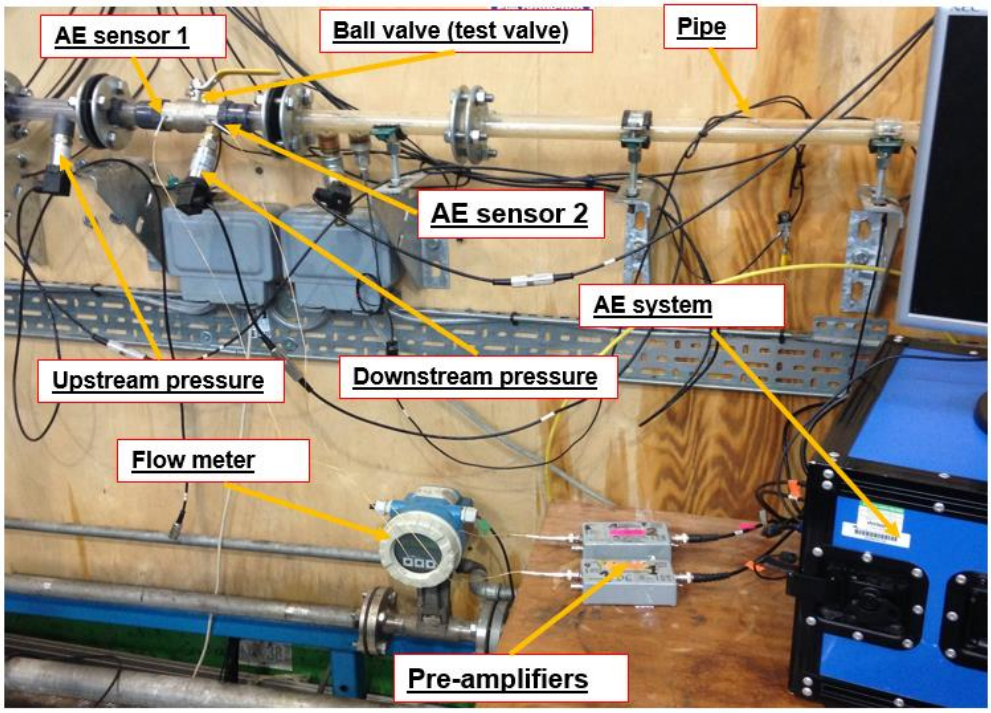

Figure 4-9: Ball and globe valves test-rig.

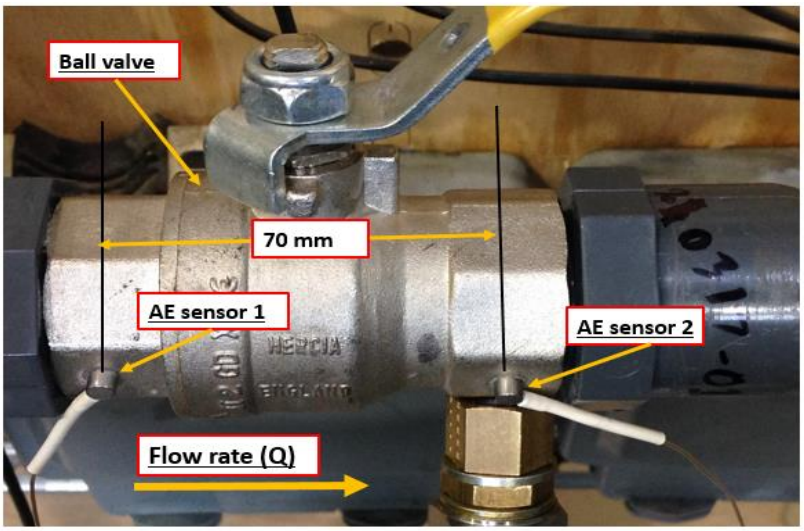

Figure 4-10: Close-up of ball valve showing positions of both AE sensors.

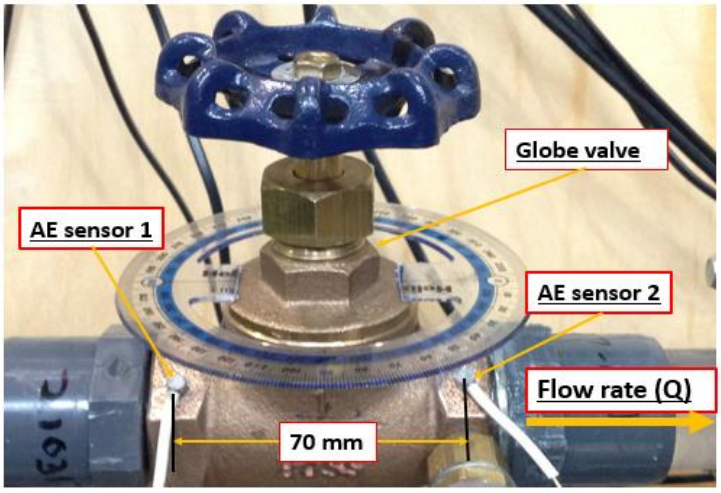

Figure 4-11: Close up of globe valve showing locations of both AE sensors and protractor arrangement for measuring angle of opening.

The pump drives water through horizontal, clear plastic tubing of 1 in (25.4 mm) diameter to the test valve, see Figure 4-9. Plastic tubing is used to attenuate vibration that could be transmitted to the sensors. The pump was situated within a wooden box to avoid the possibility that pump noise could contaminate the AE data. The upstream and downstream pressures of the water flow through the test valve were measured by pressure transducers (PMP 1400), and measured data transferred to the computer where it was stored. Simultaneously, flow rate data were measured using a flowmeter and stored in the computer. The experimental data from the AE sensors were also stored on the computer for later analysis.

For these experiments, the chosen threshold for the AE signal was 26 dB because it was observed that the AE sensors still measured some background noise when the threshold was set between 20 and 24 dB. At 25 dB, zero noise was recorded, but the threshold value was set at 1 dB above operational background noise, to ensure consistent experimental results throughout the tests. These experiments related to a preamplifier gain of 40 dB. AE-counts for four threshold levels are shown in Figure 4-12.

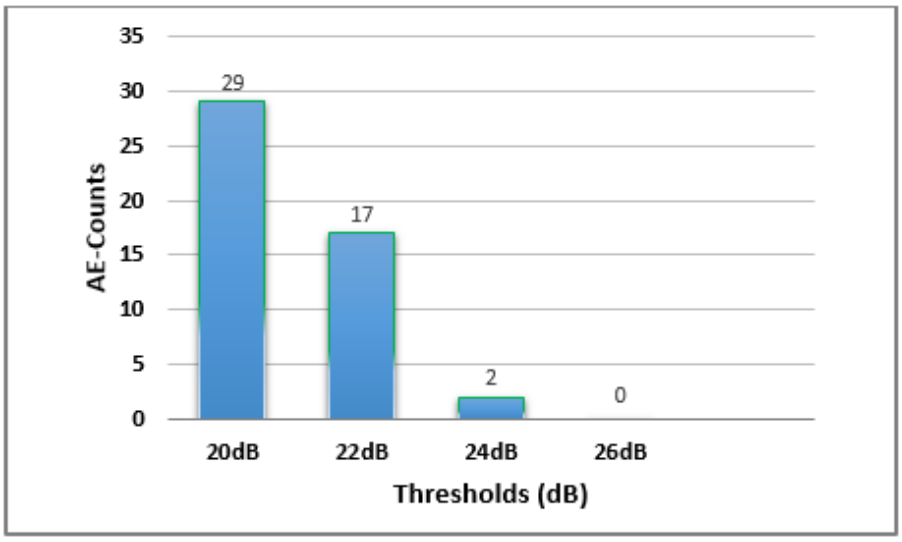

Figure 4-12: Threshold level tests for operation background noise for valve tests.

For the initial tests, tap water was used because large volumes were required. Tests were also carried out using demineralized water and salt water. Table 4-3 presents the viscosity, density and surface tension of the liquids used for a temperature of 20^0C. The viscosity of these liquids was measured using a precision torque meter, the rotational BROOKFIELD, DV-I Prime Viscometer, see Figure 4-13, which rotates at specific speeds. The resistance to the rotation of the spindle is a measure of the viscosity. The density of these liquids were measured using measurement device of density, see Appendix A (Figure A-9).

Table 4-3: Liquid properties at 20^0C [14][176][177].

Properties / Liquids	Demineralized water	Tap water	Salt water (5g/L)
Viscosity	0.809 mm^2/s	1.002 mm^2/s	1.019 mm^2/s
Density	0.941 g/cm^3	0.998 g/cm^3	1.025 g/cm^3
Surface tension	68 mN/m (Literature)	72 mN/m (Literature)	75 mN/m (Literature)

Figure 4-13: BROOKFIELD, DV-I Prime viscometer

4.3 Calibration of AE transducers by using Hsu-Nielsen method

The European Standards (EN1330-9:2000) AE transducer calibration method is the easy and simple Hsu-Nielsen (H-N) test [178] which requires snapping a 2H pencil lead of given length and diameter. The H-N test can be used to verify the existence of a good acoustic connection between each of the AE sensors and the outside surface of the device or container being used [122].

A H-N test, see Figure 4-14, was carried out before taking any AE measurements [122][178]. A 2H graphite pencil lead (3 mm long and 0.5 mm diameter) was pressed against the surface of interest until the lead snapped. This break in the pencil lead is taken to simulate an AE event. In fact the signal generated really is very similar to many AE sources found naturally [122][179].

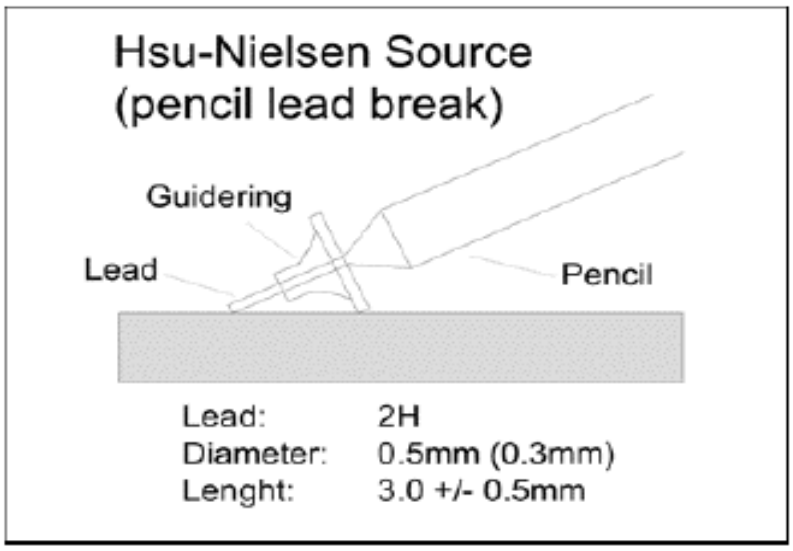

Figure 4-14: Hsu-Nielsen source.

4.3.1 AE sensor calibration

The calibration test was undertaken to quantify the attenuation properties of the boiler vessel material. Attenuation is any reduction (or loss) in the strength of the AE signal, and it is usually expressed in decibels (dB's) [21][122][179]. With the discovery threshold set at 36 dB the pencil lead break test was performed at heights of 50 mm, 100 mm, 150 mm and 200 mm above Sensor 1. Break tests were also performed at 50 mm, 100 mm, 150 mm and 200 mm below Sensor 2, giving a degree of symmetry to the two sets of tests, see Figure 4-15. Furthermore, The pencil break tests were carried out in the same vertical line sensors. The an average value of the maximum signal amplitude of five pencil breaks from each location was calculated. In all cases the water level was constant at 350 mm. Signal amplitude and relative attenuation were computed using Equation (4-2) [12][122]:

$$Attenuation(dB) = 20 * Log_{10}\left(\frac{V_s}{V_d}\right) \qquad (4\text{-}2)$$

Where V_s and V_d are the signal voltages at the signal source location and at the signal destination location respectively. As expected, measurements revealed

that the AE signals generated on the surface of the boiler are attenuated with increasing distance from the source, see Figure 4-15.

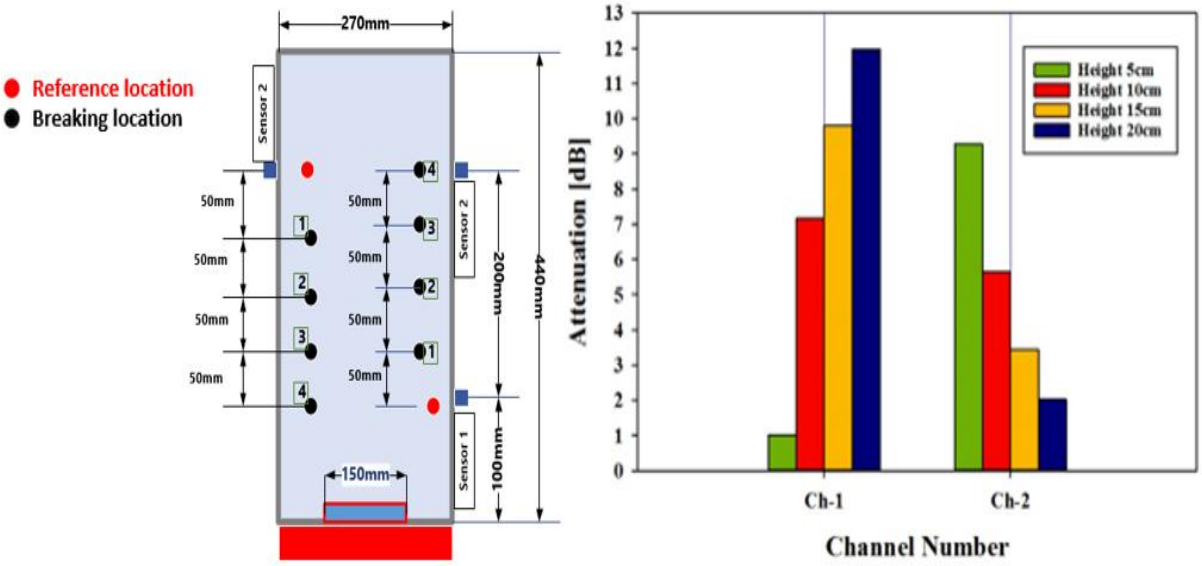

Figure 4-15: Relative attenuation at four different heights.

4.4 Conclusion

In this investigation, two different test-rigs were used. First, a pool boiling test-rig, which provided bubble formation for different liquids of a given depth, under atmospheric pressure and increasing liquid temperature. Second, the valve test-rig to monitor incipient cavitation phenomena under different flow rate conditions, where AE sensors were used to detect bubble activity. Two types of valve and three different liquids were used to investigate the effect of pressure difference and opening percentage of valves on the AE signal from bubble occurrence. In addition, sensors calibration tests, pressure transducer calibration and thermocouple calibration test have been reported in this chapter. The next chapter will provide results obtained from an experimental investigation of the possibility of AE technique for diagnosis and monitoring bubble formation and burst caused by water temperature increases during pool boiling.

Chapter 5 Results, observations and discussion for pool boiling experiments

Obtained results from a series of pool boiling experiments are presented in this chapter. Analysis of the results will use statistical analysis of the AE output parameters: AE RMS, AE amplitude, AE absolute energy, AE-Rise time, AE-Count, Energy index and AE-Hits. Signal processing of AE waveforms using the FFT is also presented.

5.1 Pool boiling tests

5.1.1 Monitoring of bubble formation using tap water

In this investigation, tests were undertaken for three levels of water, at 100 mm (level with sensor 1), 200 mm (a level midway between sensor 1 and sensor 2), and 350 mm (a level 50 mm above sensor 2). For this particular study, one experimental test is presented, with measurements made three times for each of the three levels. Tests were terminated once the water temperature reached the boiling point of 100^0C. The initial water temperature for all tests was set at 20^0C.

Figures 5-1, 5-2 and 5-4 show the value of the AE-RMS signal for each of the two channels during pool boiling when the water levels were 100 mm, 200 mm and 350 mm deep. In these Figures, it was noted that the three AE sensors had the same trend. The value of AE signal in Channel 1 was higher than that of Channel 2 because it was closer to the bubble formation source. In this work, the value of AE signal in Channel 1 will be used for all analyses.

The bubbles start to detach from heating surface at around 220 s for a water level of 100 mm, as shown in Figure 5-1. While, for a water level of 200 mm the bubble detached from heating element at 245 s, see Figure 5-2. For a water level of 350 mm, the bubbles begin to detach from the heating surface at 400 s, see Figure 5-4. It was observed that when the water level increases during pool boiling, the detachment of bubbles from heating wall take longer time. Because a larger volume of water takes longer to heat up.

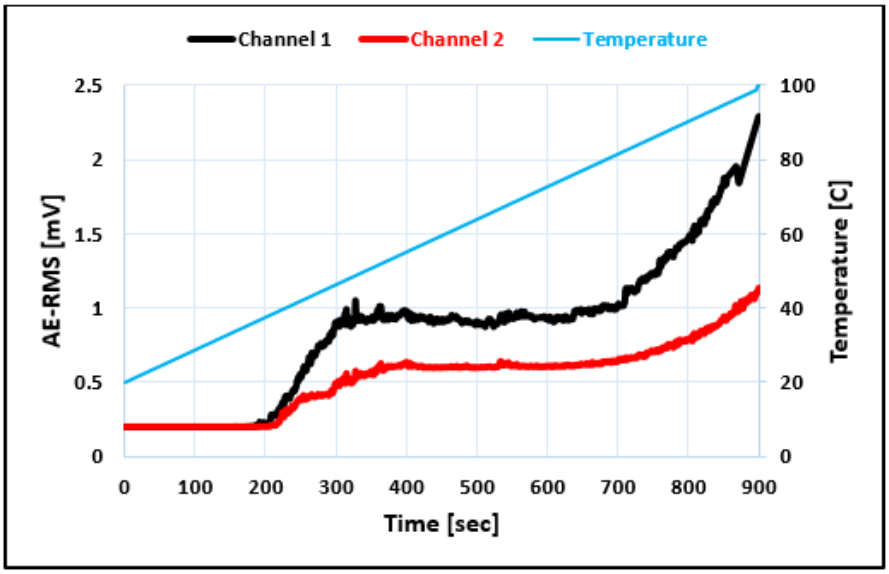

Figure 5-1: Measured temperature and AE-RMS signals for both sensors for boiling test using tap water (water level 100 mm).

Continuous observations were made of AE-RMS (mV) and temperature (^{0}C) with time (sec), and the trends associated with each sensor identified. Results for the boiler filled with water up to a depth of 200 mm, are presented in Figure 5-2. Note, the water surface level was 100 mm below sensor 2.

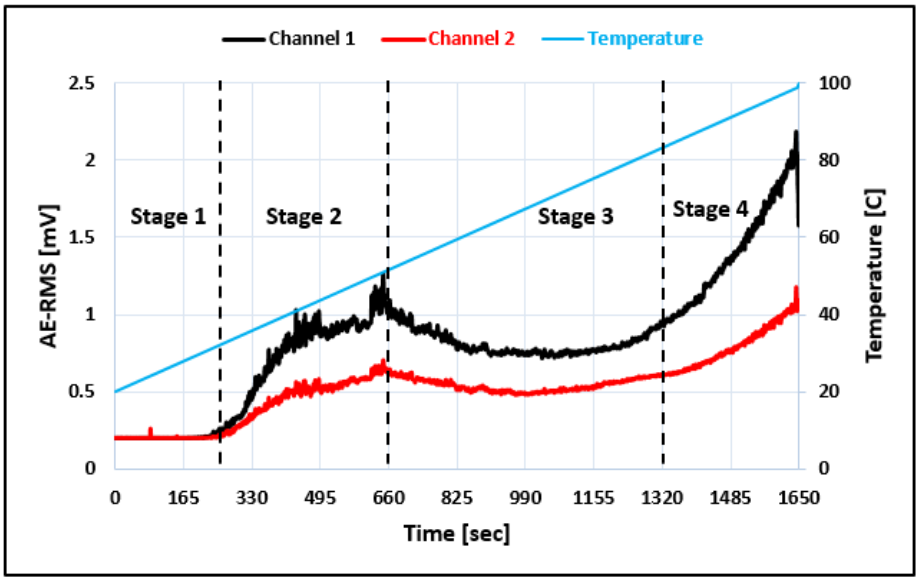

Figure 5-2: Measured temperature and AE-RMS signals for both sensors for boiling test using tap water (water level 200 mm).

Figure 5-2 above is divided into four different stages. During the first stage, which is between 0 and around 245 s, the heat transfer mechanism is natural convection and few bubbles form on the heated surface. The measured water temperature rose from its initial value of 20^0C to about 35^0C. At the second stage, between 245 and 660 s, isolated vapour bubbles form at about 40^0C on the heated surface, break away and rise through the water bursting when they reach the surface. In this stage, there is a substantial increase in measured AE-RMS in both channels. The value of the AE signal in channel 1 is higher than that of channel 2, (1.3 and 0.7 mV respectively), because the position of sensor 2 is 100 mm above the water surface and so does not receive direct AE transmission through the water. In addition, for tap water, gas voids appear on the boundaries between the water and the small particles suspended in the water; a phenomenon called heterogeneous nucleation - the process by which bubbles form on nucleation sites, which may be a scratch on a surface or small particles within the system [6].

As the bubbles begin to form, and then collide with each other, some combine to produce larger bubbles. Buoyancy forces cause the bubbles to rise and as they do so the water pressure surrounding them decreases and they grow so that the buoyancy force increases and they accelerate upwards [64].

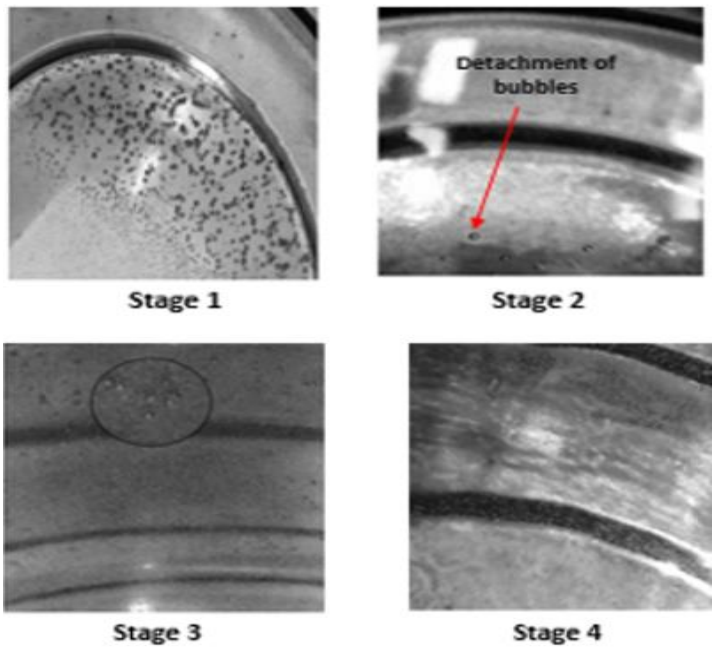

Figure 5-3: Bubble mechanisms in different stages for water level of 200 mm.

During the third stage, between 660 and around 1150 s, the value of measured AE-RMS for both channels start to decrease. Not all the bubbles detach from heated surface to the surrounding water, some combine with adjacent bubbles and stick to the heated surface, the beginnings of an insulating layer as shown in Figure 5-3. This layer is responsible for attenuation of AE-signals [116][180]. At about 1100 s, between 75 and 83^0C, the value of AE-RMS is a minimum in both channels. After this both measured AE-RMS levels begin to increase as the heat supplied to the water is experienced not as sensible heat but as latent heat, i.e. the heat supply produces vapour bubbles rather than raising the temperature of the water.

Finally, in stage four, as the water approaches the boiling stage between 83 and 100^0C, there is a gradual but quite steep increase in the value of AE level from 0.8 mV to approximately 2.2 mV in channel 1, due to the increase in bubble formation because of heat gained by the water due to the increase in the radiant component of the heat transfer. The number of bubbles reaching the top surface of the water increases, and large bubbles with higher internal energy levels start to burst on the water surface.

Figure 5-4 shows the continuous monitoring of bubble formation in a boiling test with water level 350 mm. In this particular test, a significant increase in the value of AE-RMS in both channels was noted during the period between 300 and 900 s, and from 30 to 50^0C. The AE-RMS levels reached a value of 1 mV in both channels, due to the departure of small bubbles from the heating surface of the boiler to the surface of the water. After this stage, the value of AE-RMS decreased gradually for both channels, as shown in Figure 5-4, because the bubbles stick to the inner surface of the boiler, and an insulating layer is being created by the new bubble formation on the internal surface of the boiler. It was observed that for water levels of 350 mm, the value of AE signal in channel 2 is similar to that of channel 1 because the position of channel 2 is below the water level. It was concluded that the AE signal showed the same behaviour in both channels for all levels, but with slightly different values.

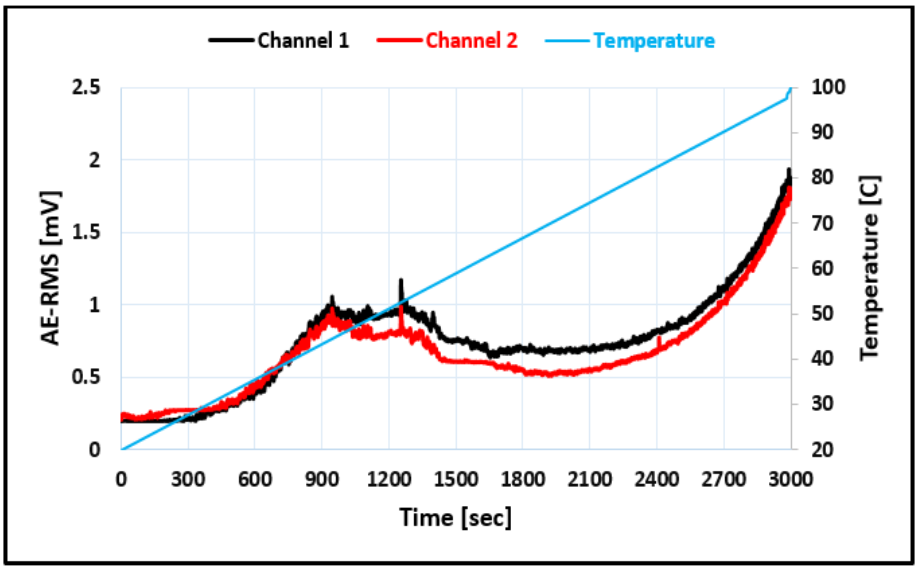

Figure 5-4: Measured temperature and AE-RMS for both sensors for boiling test with tap water (water level 350 mm).

As the water approached the boiling phase, approximately 3000 s into testing, the AE levels in both channels increased relatively rapidly. The reason for the increased AE level was the increased bubble formation, caused by the bubbles colliding with each other and combining to create new bubbles, which were larger, and had higher internal energy.

5.1.2 Waveforms analysis of AE amplitude using tap water

The AE waveforms measured by sensor 1, when the water level was 200 mm, showed different characteristics depending on the stage. Typical AE waveforms are shown in Figure 5-5. During stage 1, at 100 s, between 20 and 30^0C, there is virtually no AE signal because only a few bubbles start to form but generally do not detach from the bottom surface of the boiler into the surrounding water. During the second stage, it was observed that the value of peak AE-Amplitude increased to as high as 6 mV at 495 s. At this stage, more bubbles are formed and detach from the heating surface, some collide with others and combine to produce larger bubbles.

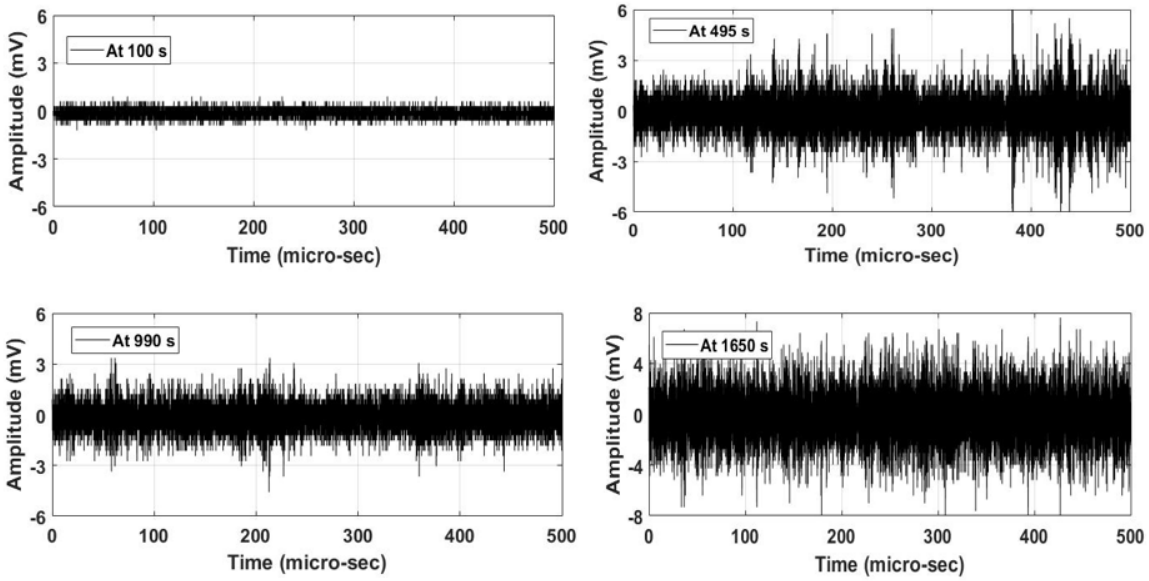

Figure 5-5: AE waveforms associated with the tap water level of 200 mm for channel 1.

At stage 3, the value of AE-Amplitude dropped to 3 mV at 990 s. During this period, some bubbles combined with adjacent bubbles and adhered to the heated surface causing attenuation of the AE signals. During stage 4, the value of peak AE-Amplitude increased until it reached about 8 mV; the temperature of the water increased, and large bubbles began to burst on the water surface and this continued until the end of the test. As the size of bubbles increased so did their internal energy.

5.1.3 Observation of the influence of the level of the tap water on AE signals

Figure 5-6 shows the relationship between the AE-Energy (atto-joule) measured by sensor 2 with water temperature (^{0}C) measured by the thermocouple, for a tap water surface level of 100 mm, some 200 mm below sensor 2. The AE-Energy was only 200 atto-joules for a water temperature of 100^{0}C, this was because sensor 2 was 200 mm above the water surface and the AE signal was transmitted to the sensor only via the wall of the container.

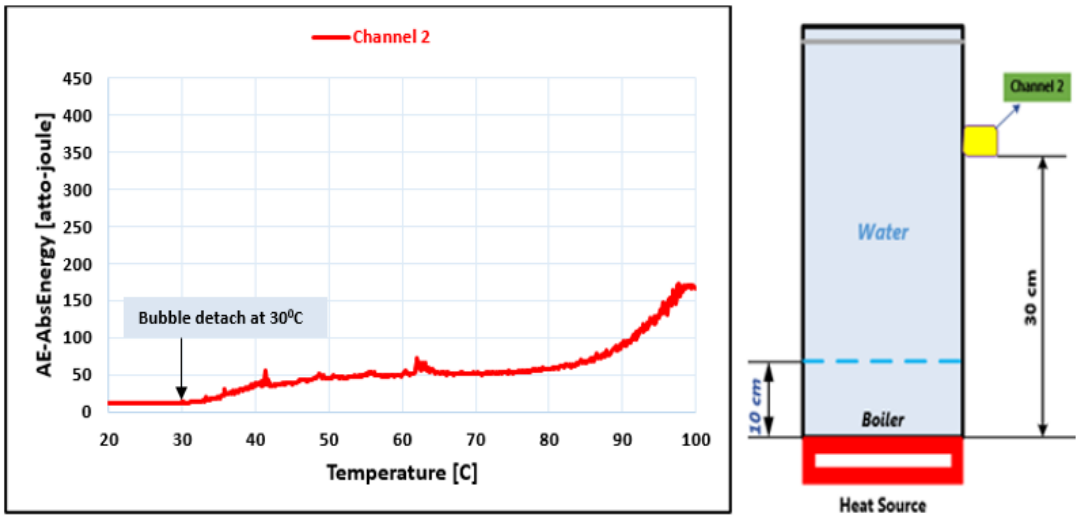

Figure 5-6: AE-Energy measured at sensor 2 with tap water level of 100 mm above the bottom of the boiler.

Figure 5-7, shows the same process but with the water surface level at 200 mm, only 100 mm below the sensor. The value of AE-Energy signal increased to approximately 250 atto-joules for a water temperature of 100^0C, this small increase was due to the water level being closer to the sensor and the AE signal not having to travel so far through the wall of the container.

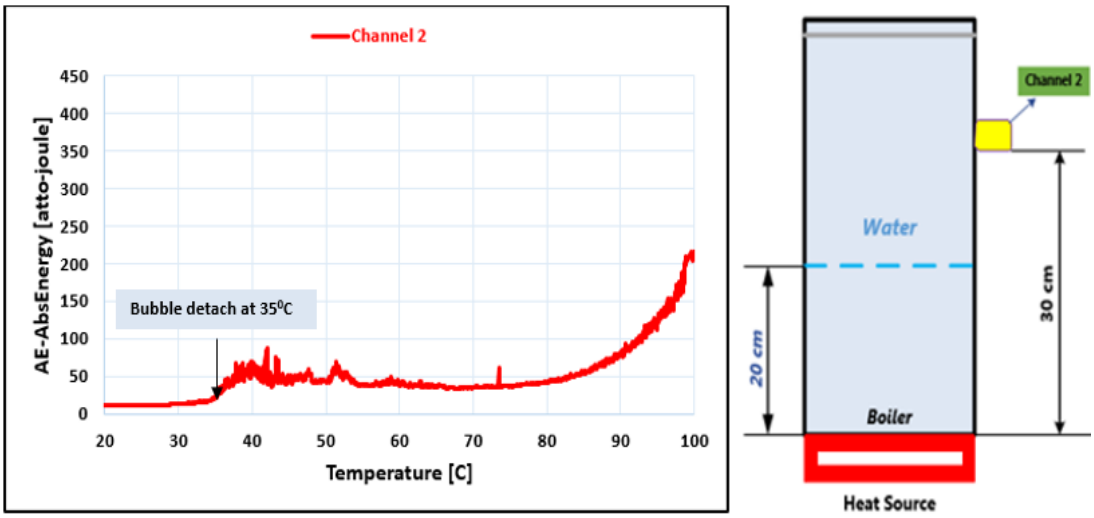

Figure 5-7: AE-Energy measured at sensor 2 with tap water level of 200 mm above the bottom of the boiler.

Figure 5-8 again shows the same process but now the water depth is 350 mm which is 50 mm above sensor 2. There is a substantial increase in the measured

AE-Energy, to about 425 atto-joules when the water approached the boiling phase.

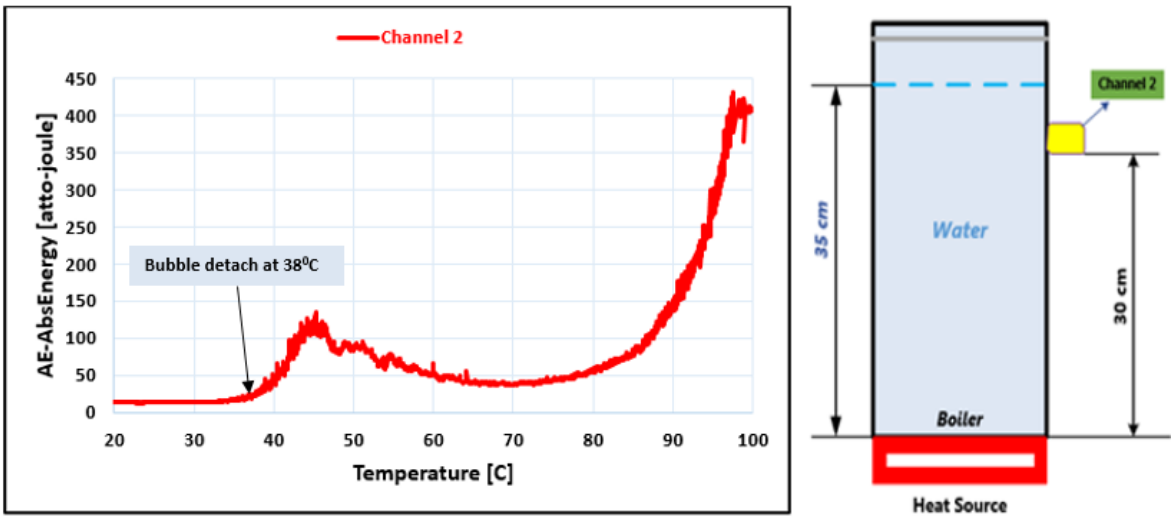

Figure 5-8: AE-Energy measured at sensor 2 with tap water level of 350 mm above the bottom of the boiler.

Obviously, the water level has a substantial effect on the measured level of AE energy with pool boiling, using sensor 2. When the water level is below the level of the sensor direct transmission from water to the sensor is not present and the measured signal is only that transmitted through the wall of the container. Thus, as expected, there is a marked drop in amplitude of the signal when the water level falls below that of the sensor. The maximum value of AE-Energy is recorded between 90 and 100^{0}C for all levels because more bubbles form at these temperatures and their energy increases.

Figure 5-9 summarize the outcome of the effect of water levels of the tap water on the level of AE-Abs Energy signal.

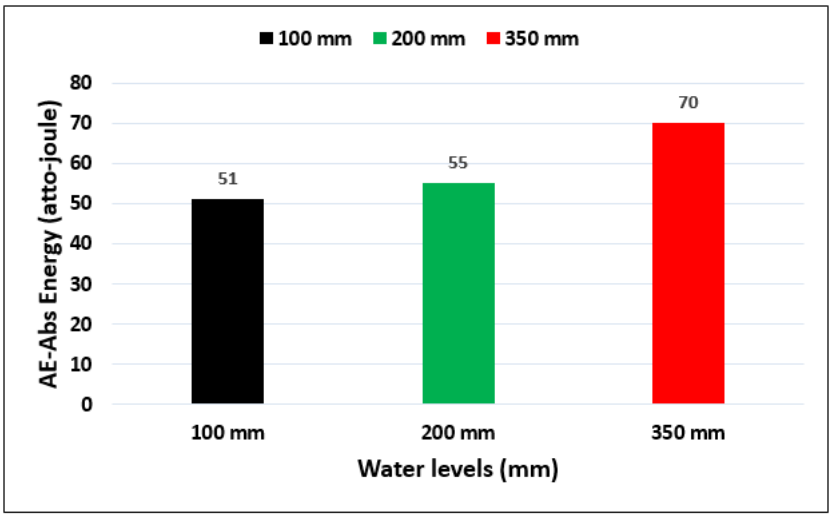

Figure 5-9: AE-Abs Energy measured at sensor 2 with different levels of tap water.

5.1.4 Observation of the effect of salt water (5g/L) concentration on AE signals

Tests were undertaken for two levels of salt water: 200 mm and 350 mm. Each test was repeated three times for both water levels. As previously, tests were terminated once the water temperature reached 100^0C (boiling temperature). Regarding water levels of 100 mm, see Appendix B, Figure B-4. The onset water temperature condition for all tests was 20 ^{0}C. Figure 5-10 below shows the relation between AE-RMS (mV), time (s) and temperature (^{0}C) at the salt water (5g/L) with water level of 200 mm.

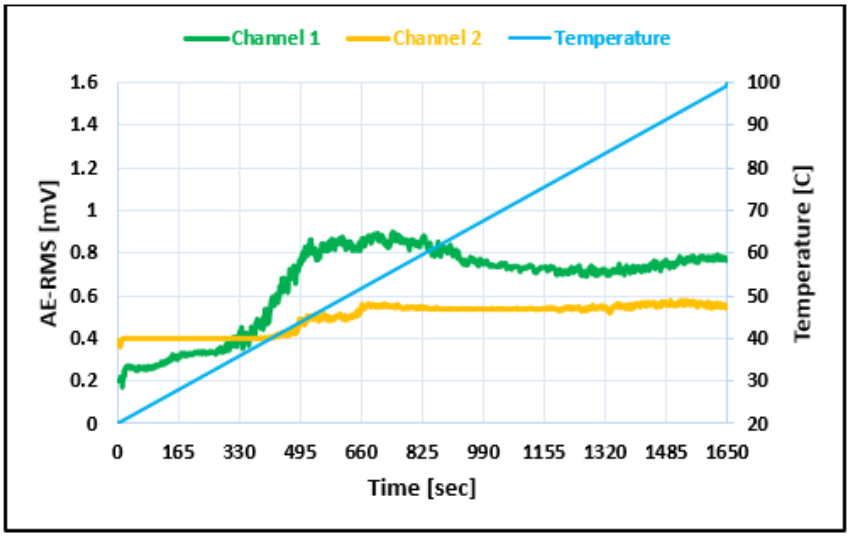

Figure 5-10: Measured temperature and AE-RMS for both sensors for boiling test with salt water (5g/L) (water level 200 mm).

At the beginning of the process, the initiation of bubble formation is on the bottom wall of the pool boiling. Moreover, the bubbles form at cavities, scratches and grooves on the heated surface of the boiler. This process is also heterogeneous nucleation. Then the bubbles detach from the heating surface to rise to the surface of the water at an early stage, at about 22^0C. Bubbling happens on the boundary between the salt water and the solid wall of the boiler vessel. Additionally, bubbles also occur on the small particles of salt suspended in the water. For this reason, the bubbles detach from heating element at an early stage.

The value of AE-RMS ranked the highest for both channels, occurs between 495 and 825 s. In this stage, the water temperature increases and the bubbles start to form at a faster rate. Then the bubbles grow and depart to the top of the boiler, where they burst at the free surface and release vapour. As a result, the heat flux attains its maximum value. However, as expected, the value of AE signal in channel 1 is higher than that of channel 2, with 9 and 5 mV respectively, because the position of channel 2 is above the water surface. After that, the value of AE signal decreases slowly to approximately 7 mV in channel 1, between 60 and 75 ^{0}C. During this period, more bubbles form, rise and burst on reaching the water surface. As can be seen from Figure 5-10, the signal from channel 2 attains a more or less steady level, between 55 and 95 ^{0}C, again this is because the position of channel 2 is above the water surface. When the salt water (5g/L) approaches the boiling stage between 90 and 100 ^{0}C, the value of AE increases in both channels, as shown in Figure 5-10, with the increase in channel 1 greater than the increase in channel 2. There is an increase in the heat flux, and more bubbles form with a greater size and increased internal energy, they rise to the free surface, where they burst.

Figure 5-11 shows the continuous monitoring of bubble formation for salt water (5g/L) in the boiling test with water level of 350 mm.

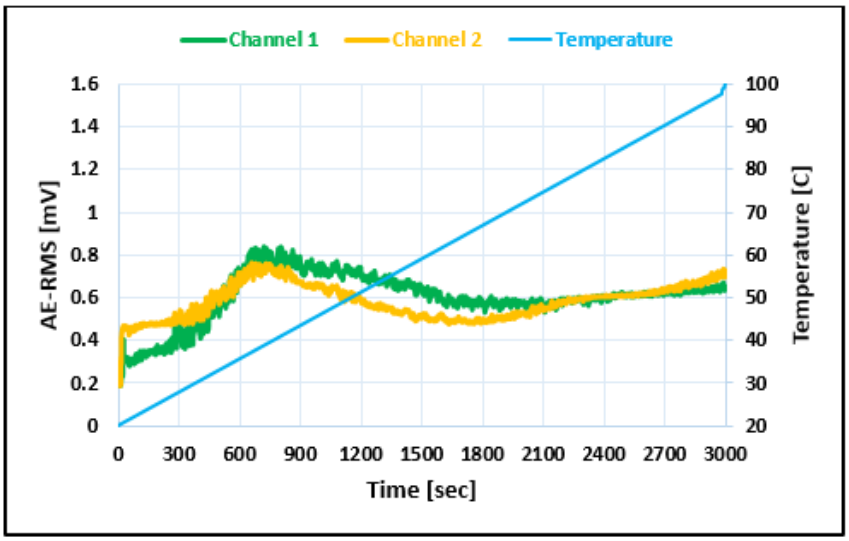

Figure 5-11: Measured temperature and AE-RMS for both sensors for boiling test with salt water (5g/L) (water level 350 mm).

The value and behaviour of the AE-RMS signal in channel 1 was similar to that of channel 2 throughout the test, because the position of channel 2 was below the water surface. Interestingly, the level of the signal from channel 1 was not consistently higher than for channel 2, possibly because of bubble bursts on the surface.

5.1.5 Observation of the effect of demineralized water on AE signals

Figure 5-12 below shows the relationship between AE-RMS [mV], time [sec] and temperature [^{0}C] for demineralized water, where the red line presents AE signal in channel 1, and the yellow line shows the AE signal from channel 2. This figure shows the value of AE-RMS signal for each of the two channels, when the water level was 200 mm deep. Results for water levels of depths 100 mm and 350 mm are presented in Figures B-5 and B-6 respectively, see Appendix B.

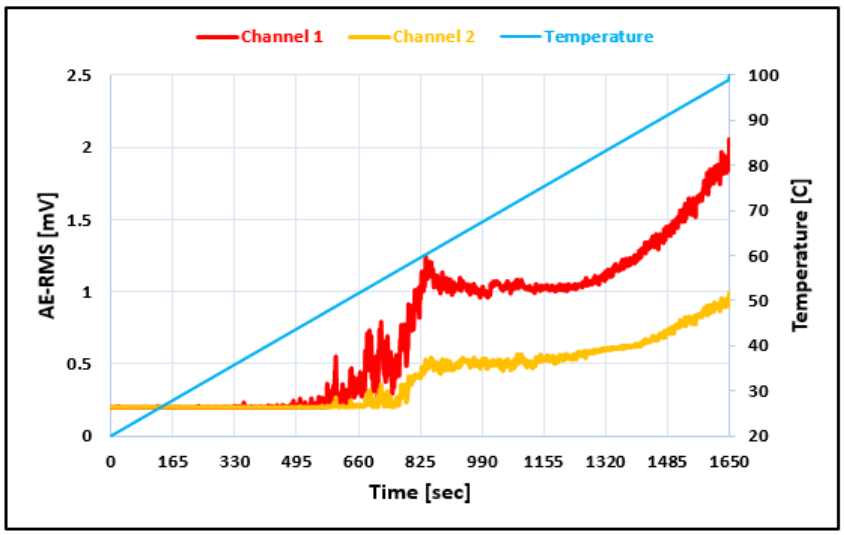

Figure 5-12: Measured temperature and AE-RMS for both sensors for boiling test with demineralized water, water level 200 mm.

For demineralised water it can be seen that, for channel 1, the AE signal is stable from 0 to around 660 s, when bubbles start to form on the bottom surface of the boiler vessel but then stick to the heating surface between 20^0C and 52^0C. After 660 s, between 52^0C and 60^0C, the bubbles begin to detach from the heating wall of the boiler and rise through the water. It is suggested that the reason for the relative delay in the process of bubble formation is that in demineralized water there are far fewer small particles in the liquid on which heterogeneous nucleation can occur [6]. However, once of sufficient magnitude, the thermal motion of the demineralized water formed temporary, microscopic voids which by themselves can produce the nuclear cavitation necessary for formation and growth of micro-bubbles. An increase in water temperature meant the local saturation vapour pressure became greater than the surrounding water pressure and bubbles formed.

Once again, the value of the AE-RMS in channel 1 is higher than that of channel 2, (1.4 and 0.5 mV respectively), at 825 s, because the position of sensor 2 is 100 mm above the water surface and does not receive an AE signal directly from the demineralized water. Following this, the value of AE signal slowly decreased to approximately 1.0 mV, between 990 and 1320 s. During this stage, not all the bubbles detach from heating surface to the surrounding demineralized water,

some combine with adjacent bubbles and stick to the heating wall of the boiler vessel, forming an insulating layer. This layer is responsible for attenuation of the AE-RMS level.

At 1320 s, between 82^0C and 100^0C, a slightly increase in the value of AE signal in both channels, was observed as shown Figure 5-12. This increase can be attributed to the heat that was gained by the demineralized water. This heat caused more bubbles to form and depart towards the water surface where, finally, at the end of the test, large bubbles started to burst with increased internal energy.

5.1.6 Observation of the influence of different liquid types on AE signal levels

Figure 5-13 below shows the AE-RMS (mV), time (sec) and temperature (^{0}C) for sensor 1, where the black line represents tap water, the red line demineralized water, and the green line salt water (5g/L). The signals from both channels for tap water, demineralised water and salt water have been described individually, above.

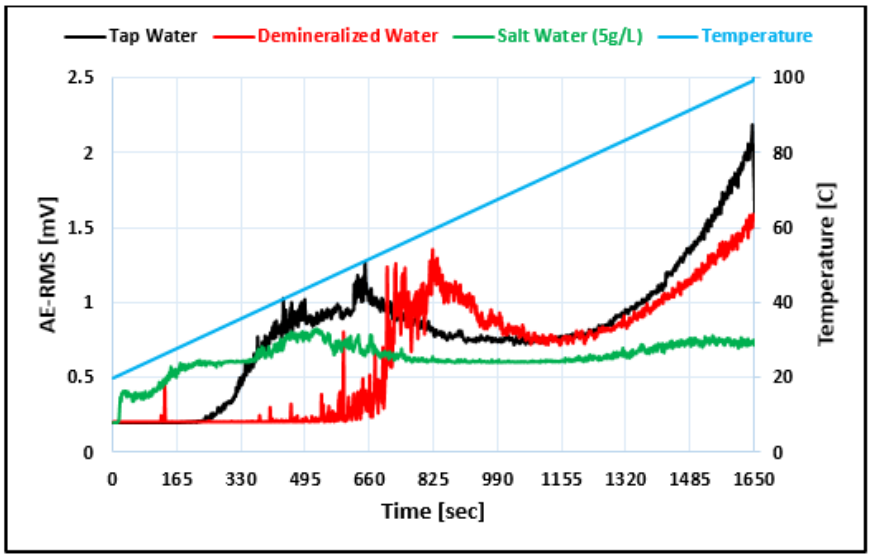

Figure 5-13: Comparison of temperature and AE-RMS results obtained from channel 1 for tap water, demineralized water and salt water (5g/L) (water level 200 mm).

From Figure 5-13 it can be seen that bubbles detach from the heated surface to the water surface in the salt water faster than for either tap water or demineralized water. With salt water (5g/L), bubbles start to detach from the heated surface into the surrounding water at a very early stage, from about 22^0C. This is due to the surface tension of salt water (5g/L) being higher than that of the other two liquids. Additionally, bubble voids appear on the boundary between the liquid and small salt particles suspended in the liquid, which is responsible for formation and growth of micro-bubbles, providing what is called a hydrophilic surface [6].

It can be seen that the detachment of bubbles from the heated surface with both tap water and salt water is faster than for demineralized water because in demineralized water, there is a much lower concentration of mineral ions and other small particles [6][181].

5.1.7 Frequency domain analysis of bubble formation using tap water

The FFT was used to derive the power spectrum and identify frequency characteristics of the signal from channel 1 for bubble activity in tap water with a water level of 200 mm, the results are shown in Figure 5-14. The spectrum obtained from the FFT was used to monitor bubble formation during pool boiling. During stage 1 there was a small peak at about 2300 kHz, indicating the presence of only a few bubbles forming on the heating surface. These tended to stick to the heated surface where the temperature was still relatively low. During this stage the heat transfer from the heated surface to the water was by natural convection.

At stage 2, the value of AE amplitude at the peak frequency at about 2300 kHz increased substantially to approximately 0.2 mV. In this stage, the temperature increased, the heat flux increased, and bubbles started to form at a faster rate and to detach from the heated surface. There is a small peak at 1250 kHz which suggests the presence of larger bubbles contributing to the AE signal, these might be surface bursts. At stage 3, the peak value of AE amplitude level decreased gradually to approximately 0.1 mV. The peak at 1250 kHz also decreased in magnitude. During this stage, some bubbles combined with others and stuck to

the heated surface to form an insulating layer. This layer reduced the levels of the AE signals. The AE signal grew substantially during stage 4, reaching its highest level of 0.3 mV at 2300 kHz. The smaller peak at 1250 kHz also increased in magnitude. During this stage, there was a lot more bubble activity. Additionally, this stage presents liquid entrainment, a phenomenon that occurs with nucleate boiling when the bubbles rise to the water's free surface and carry with them hot water which helps increase the overall water temperature. The bubbles grow and rise to the water's free surface under the influence of buoyancy. Then the bubbles burst and release the contained vapour. As a result, the heat flux reaches its maximum value.

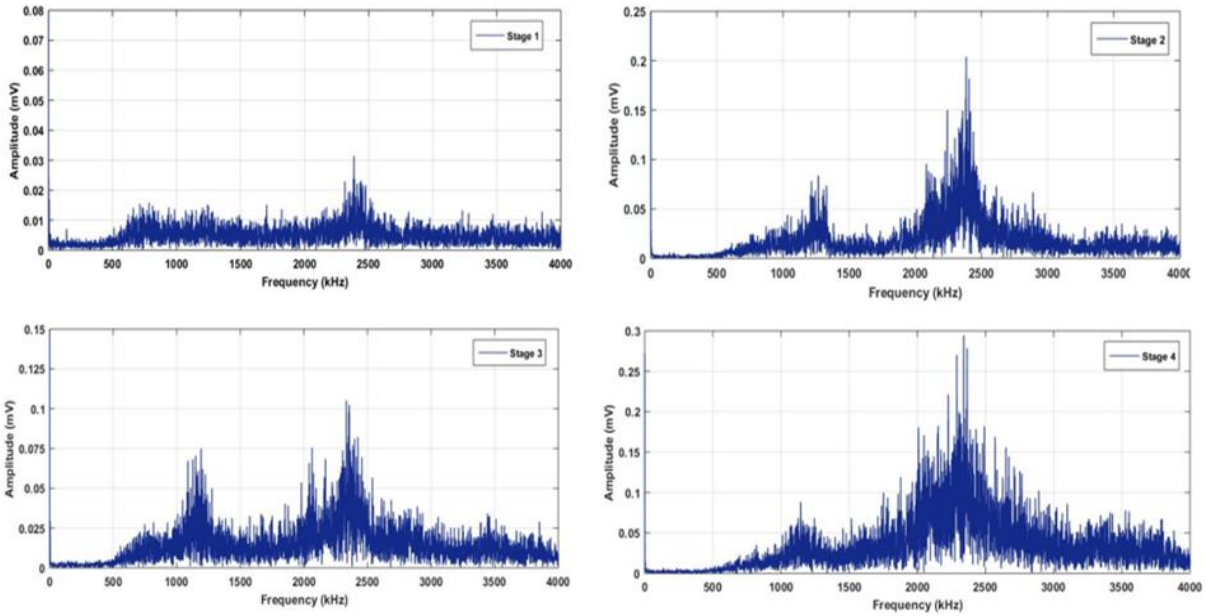

Figure 5-14: Plot of bubble activity frequency at (stages 1, 2, 3 and 4) tap water, for a water level of 200 mm.

Observations from the spectra of the AE signal note the presence of more bubble formation at a faster rate, as shown in Figure 5-14, stage 4. Typically, AE signals associated with bubble activity increased throughout the boiling test.

5.1.8 Statistical analysis of AE parameters of bubble formation during pool boiling with different liquid types

Bubble formation during pool boiling depends on liquid properties such as viscosity, density and surface tension. The AE signals corresponding to bubble formation were statistically analysed to determine a critical AE parameter indicator for bubble activity detection. Table 5-1 shows average values for comparison between AE Amplitude, AE Rise time, AE Count and AE Energy obtained from sensor 1 (for bubble formation, time interval was 0 - 1650 s).These statistical parameters were obtained directly from the AE system (AEWin).

Table 5-1: Comparison of averaged AE parameters for bubble formation with different liquid types for water level of 200 mm and time interval 0 - 1650 s.

Liquid Types	AE Parameters			
	AE Amplitude (dB)	AE Rise Time (µs)	AE Count	AE Energy (atto-joule)
Tap Water	38	701	29	5
Demineralized Water	38	1133	75	8
Salt Water (5g/L)	37	27	4	0.33

The AE signals presented in Table 5-1 were the average of 9 tests based on the raw data from the AE system. One recommendation could be the use of waveform analysis for the transient signal instead of taking data from the whole waveform (statistical AE parameters from the AE system). A comparison of AE measures (Rise Time, Count and Energy) for bubble formation in tap water, demineralized water and salt water (5g/L), are shown in Figures 5-15, 5-16, and 5-17.

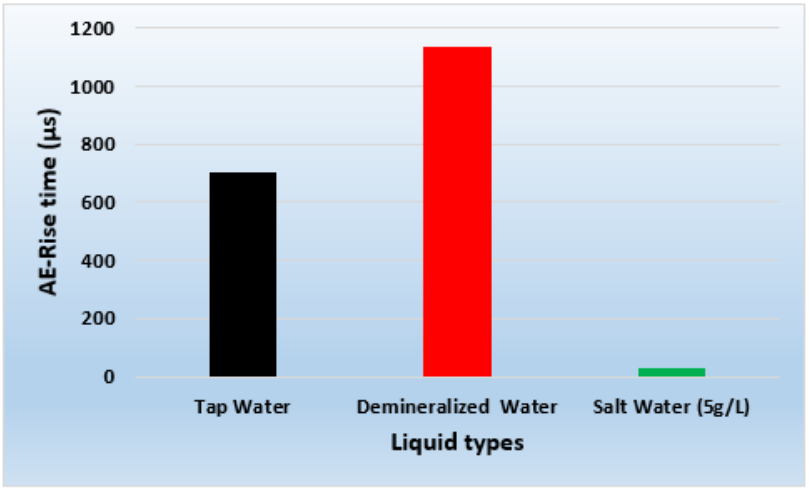

Figure 5-15: AE Rise time for bubble formation as a function of liquid type.

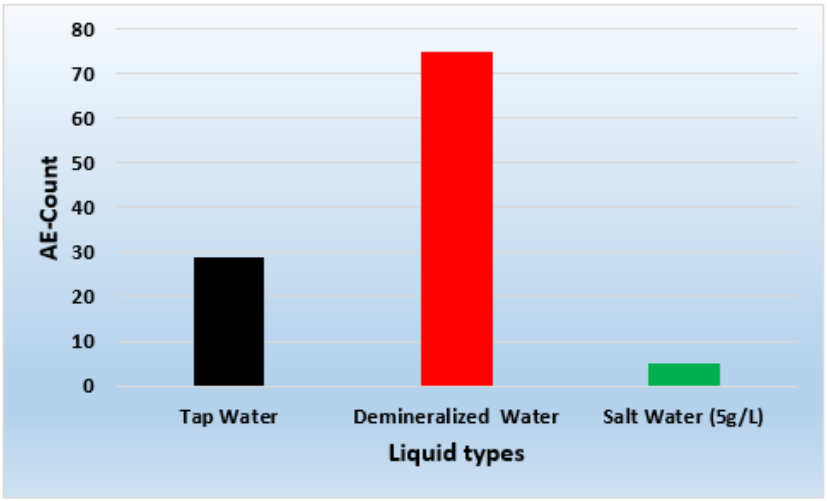

Figure 5-16: AE Count for bubble formation as a function of liquid type.

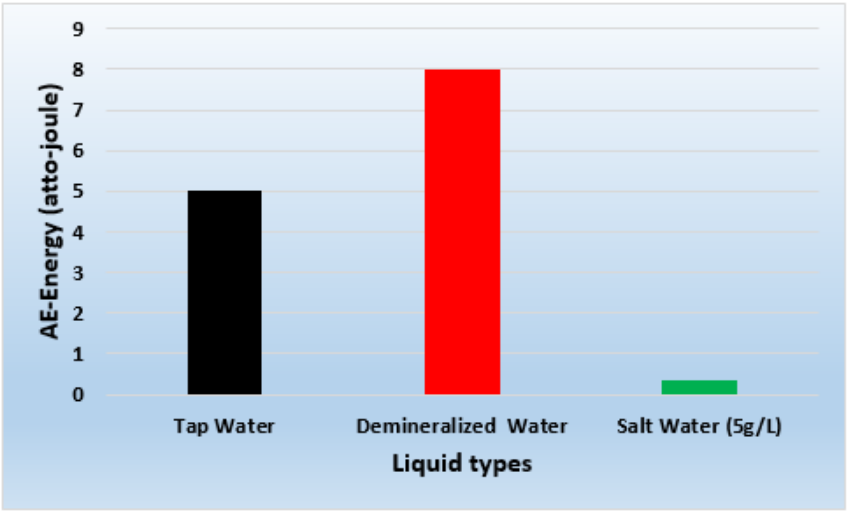

Figure 5-17: AE Energy for bubble formation as a function of liquid type.

Table 5-1 and Figures 5-15, 5-16, and 5-17, show the significant effect of liquid properties such as viscosity and surface tension on bubble activity and the AE Energy generated. The AE signal level increased as viscosity and surface tension decreased. These figures show that for demineralised water the count, energy level and rise time were consistently much the greatest, and for salt water were much the lowest. This is because of the bubble size in salt water is larger than for demineralised water.

Figure 5-18 shows the AE amplitude is not the same for all three liquids, it was 38 dB for both tap water and demineralized water but only 37 dB for salt water. This may be because both viscosity and surface tension were greatest for salt water.

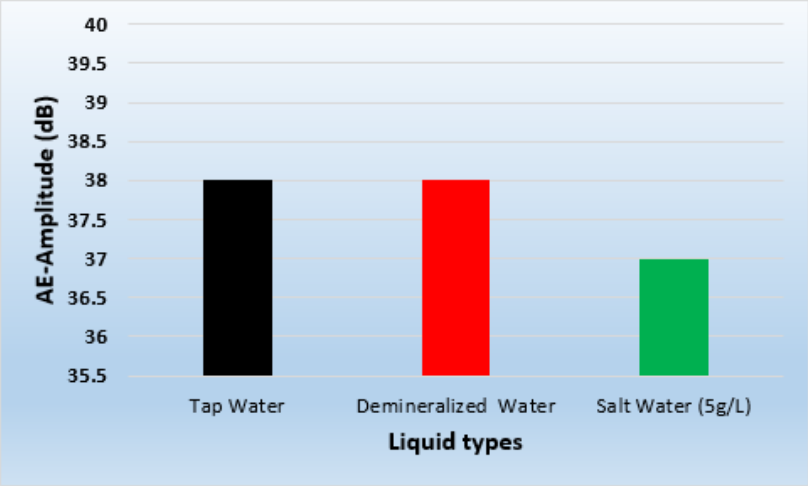

Figure 5-18: AE Amplitude from bubble formation as a function of liquid.

5.1.9 Observation of the effect of electric power-supply on AE signal using tap water

The next phase of the analysis was the use of the AE-RMS to identify bubble formation during the test period with different rates of power-supply to the plate heater. Figure 5-19 shows the plots of AE-RMS against measured water temperature for two rates of heat input, 3.0 kW and 2.5 kW.

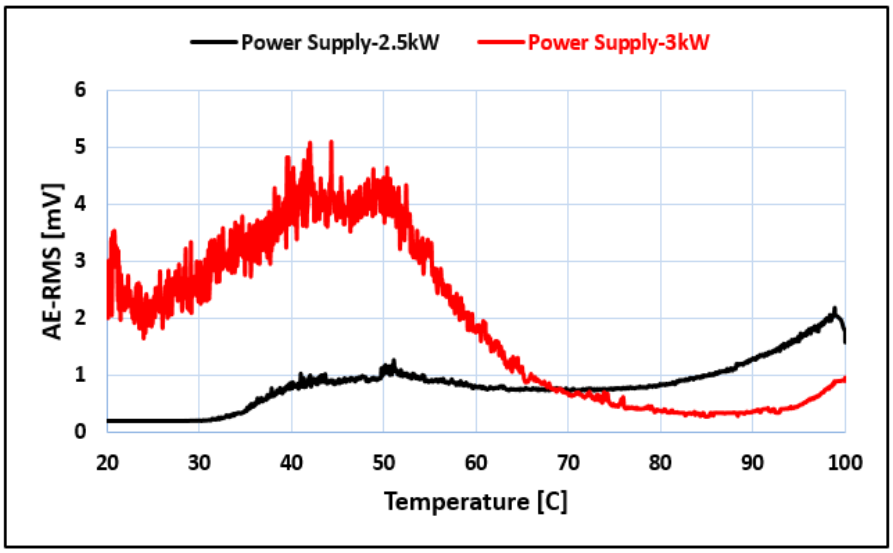

Figure 5-19: AE-RMS as a function of temperature for two rates of heat input. Signal from sensor 1 with tap water, depth of 200 mm.

For sensor 1, the AE-RMS plot in Figure 5-19 for heater of 2.5 kW power, follows very closely the Energy index plot presented in Appendix B, Figure (B-15). There is an increase in AE signal level with measured water temperatures. Bubbles started to detach from the heated surface to the surrounding water at about 35^0C with an electric power-supply of 2.5 kW. The value of the AE signal decreased slowly between 50 and 80^0C. In this period, attenuation occurs due to some bubbles sticking to the heated surface of the boiler, causing a reduction in the AE signal. In the last moments of the test (100^0C), large bubbles were bursting at the free surface, and the corresponding value of the AE-RMS at 2.5 kW was recorded as 2 mV.

With a power supply of 3 kW, the bubbles start to detach from the heated surface at the bottom of the boiler at around 22^0C with a substantial increase in the level of the AE-RMS between 22 and 50^0C. The AE signal level is much greater than for the 2.5 kW source, with the increased power supply generating a higher heat flux and causing more bubbles to form. The AE-RMS level for the 3 kW heater peaked at 5 mV between 40 and 50^0C, because in this period the bubbles formed at a faster rate, due to the increased heat flux and heated surface temperature. After that, there was a gradual decrease in the value of AE signal with increase in temperature from 50 to 100^0C. During this period, the water temperature and

bubble size increased, causing bubbles to burst near the free surface. It was observed that the electric power-supply has a significant effect on AE levels such that when the power supply increases, the trend of the AE signal changes as well.

5.1.10 Difference between rise times of AE-signals for bubble formation and bubble burst using tap water

In this test, two solid acoustic waveguides, made from stainless steel of square cross section 25 x 25 x 500 mm were used, see Appendix B Figure B-16. Figure 5-20 shows a schematic of the measurement positions for determining the difference between AE-signals associated with bubble formation and bubble burst. To measure the signals associated with bubble formation, acoustic waveguide 1 with a sensor attached was positioned with its end 5 mm from the bottom (heated) surface of the boiler. To monitor bubble burst at the surface, acoustic waveguide 2 was placed with its end 195 mm from the bottom heating surface. The AE signal rise times measured by waveguide 1 were greater than those for waveguide 2; 6494 µs compared to 1753 µs. This increase in rise time is because as the bubbles neared the surface their diameter increased, the bubbles became larger. The biggest bubbles burst on the surface of the water.

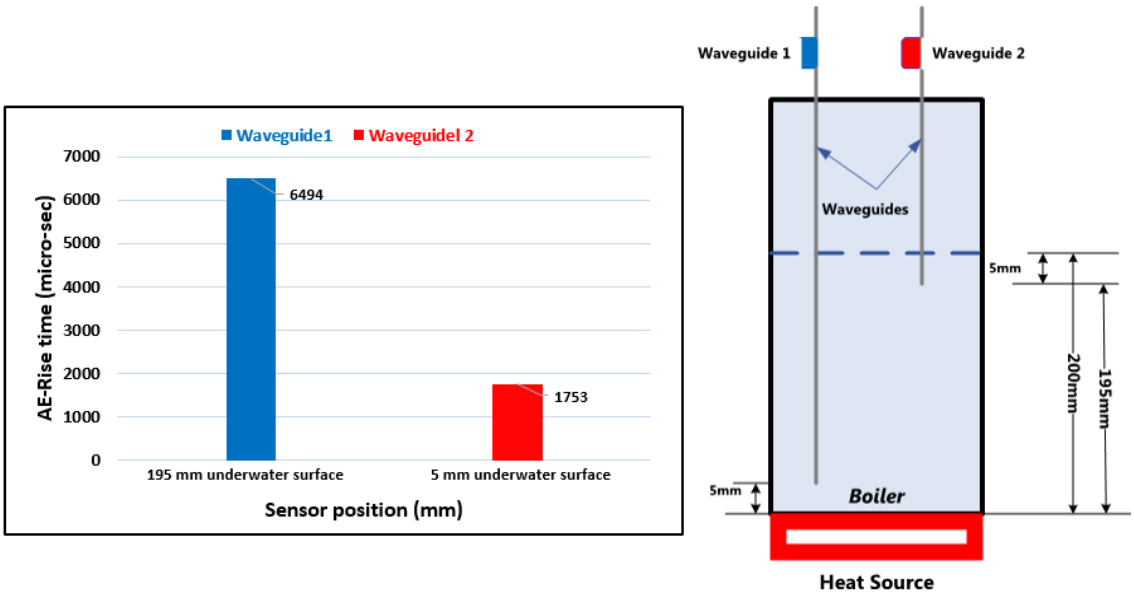

Figure 5-20: AE-rise times for both acoustic waveguides using tap water of depth 200 mm and 3 kW supply.

The identical setup was used to measure AE-RMS to identify characteristics of bubble activity such as bubble formation and burst, as shown in Figure 5-19. This analysis was performed to assess the ability of the RMS parameter to monitor bubble formation and burst during pool boiling. The results showed the AE signal for waveguide 1 was higher than that for waveguide 2; 3.5 mV and 0.7 mV respectively at 40^0C, see Figure 5-21. The peak values for waveguide 1, measuring activity 5 mm above the heated surface, was for the temperature range 30 to 50^0C, in the time period 300 to 700 s (see Figure 5-2). In this period, there was greater bubble formation on the heated surface with a few bubbles bursting on the water's free surface as bubbles started to detach from the heating surface of the boiler vessel into the surrounding water.

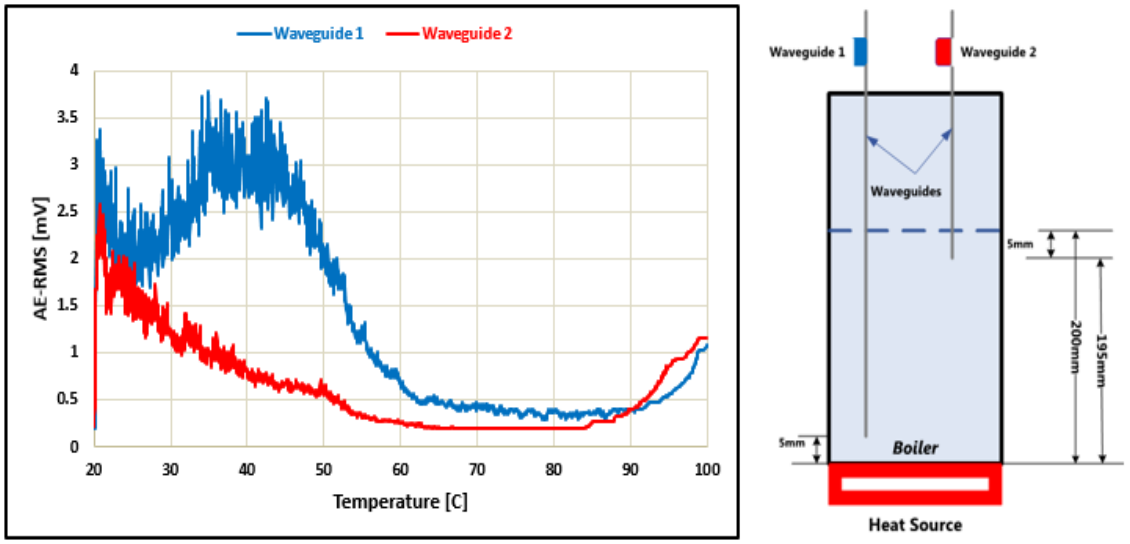

Figure 5-21: AE-RMS for different waveguide positions using tap water of depth 200 mm and 3 kW supply.

It was noted that the AE signal levels for waveguide 1 gradually decreased to approximately 0.4 mV between 55^0C and 80^0C but picking up slightly when the temperature rose above 95^0C. During this stage, some of the bubbles combined with adjacent bubbles and stuck to the heated surface of the boiler, causing attenuation of AE signals.

As the water approached the boiling phase between 95 and 100^0C, a gradual increase in AE signal levels to around 1 mV for both waveguides was observed, see Figure 5-21. This increase was attributed the heat gained by the water.

Furthermore, this heat caused a significant departure of the bubbles towards the top surface, and finally, large bubbles began to burst on the surface as both their size and internal energy increased. These results again lead to the hypothesis that the AE-signals of bubble formation are higher and more violent than those of bubble burst at the free surface. For temperature 90^0C and above the AE-RMS for Waveguide 1 is greater than for Waveguide 2 due to the bubbles bursting on the free surface.

Power spectral analysis identified frequency characteristics for bubble activity, such as bubble formation and burst in tap water, as shown in Figures 5-22, 5-23 and 5-24. This analysis was performed on the signals from sensors 1 and 2, to assess the ability of the power spectrum to monitor bubble formation and burst during pool boiling.

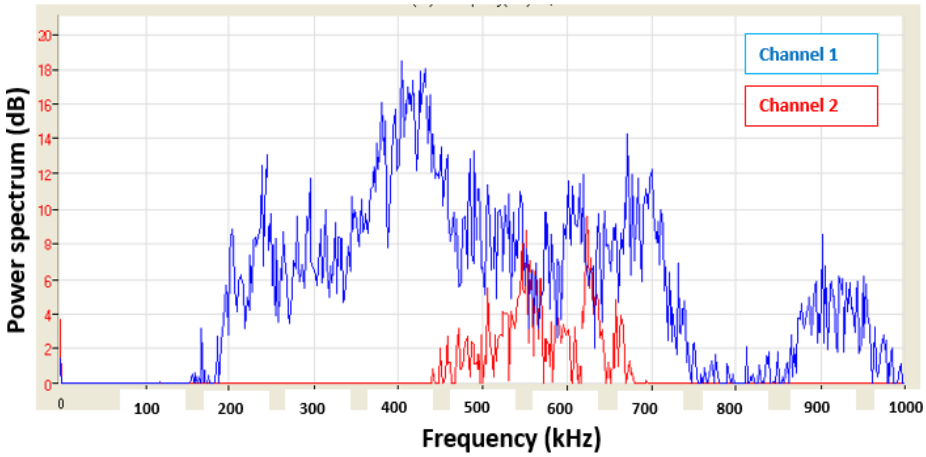

Figure 5-22: Plot of power spectrum for AE signal from sensors 1 and 2 for tap water at 40^0C with water level of 200 mm.

The results showed that at 40^0C, bubble formation generated a wide peak from about 200 kHz up to about 750 kHz for channel 1. For channel 2, some 100 mm above the surface of the water, a narrower peak extending from about 450 kHz to about 675 kHz can be seen. The peak levels of the power spectrums were 19 dB for channel 1 and 10 dB for channel 2. In this period, there was greater bubble formation on the heating elements, and then a few bubbles burst on the water free surface.

Figure 5-23 shows the power spectrum for AE signal from both channels obtained for tap water at 55^0C with water level of 200 mm. It can be seen that the AE signal peak levels gradually decreased to approximately 7 dB in channel 1, and for channel 2 were too small to be measured. During this stage, the bubbles started to detach from the heated surface of the boiler vessel into the surrounding water. Then, some of the bubbles combined with adjacent bubbles and stuck to the internal surface of the boiler, causing attenuation of AE signals.

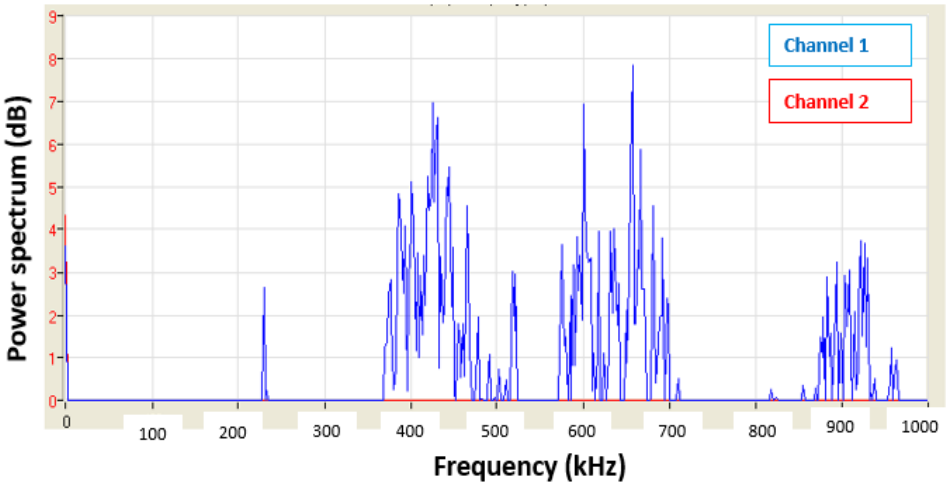

Figure 5-23: Plot of power spectrum for AE signal from sensors 1 and 2 for tap water at 55^0C with water level of 200 mm.

As the water approached the boiling phase between 90 and 100^0C for both channel 1 and channel 2, there was a gradual increase in AE signal peak levels to around 10 and 8 dB respectively, see Figure 5-24. This increase was attributed to the heat gained by the water causing a significant departure of the bubbles towards the top surface, and finally, at the termination of the test, large bubbles were bursting on the surface with increased size and internal energy.

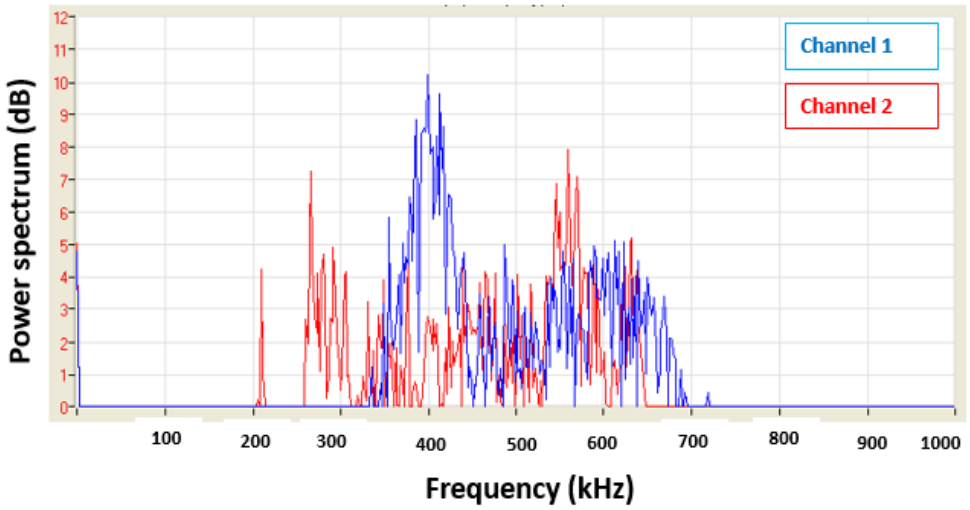

Figure 5-24: Plot of power spectrum for AE signal from sensors 1 and 2 for tap water at 90^0C with water level of 200 mm.

These results again lead to the hypothesis that the AE-signals due to bubble formation are higher than those due to bubble burst at the free surface.

5.1.11 Observation of the effect of threshold levels on AE signal levels using tap water

Figure 5-25 shows that there is a clear link between the number of hits for channel 2 and the level of the water in the container. This is obvious, because with the water level below the level of sensor 2 there is no direct transmission through the water to the sensor. At a threshold level of 36 dB the number of AE-Hits reached 160,000 hits for a water depth of 350 mm (water level above the sensor) compared with about 60,000 when the water level was below the sensor. As would be expected there was a slight increase in number of hits when the water level was increased from 100 mm to 200 mm due to the slight decrease in attenuation in the signal's path. Also, as would be expected, the number of hits decreased with increase in threshold level, as shown in Figure 5-25.

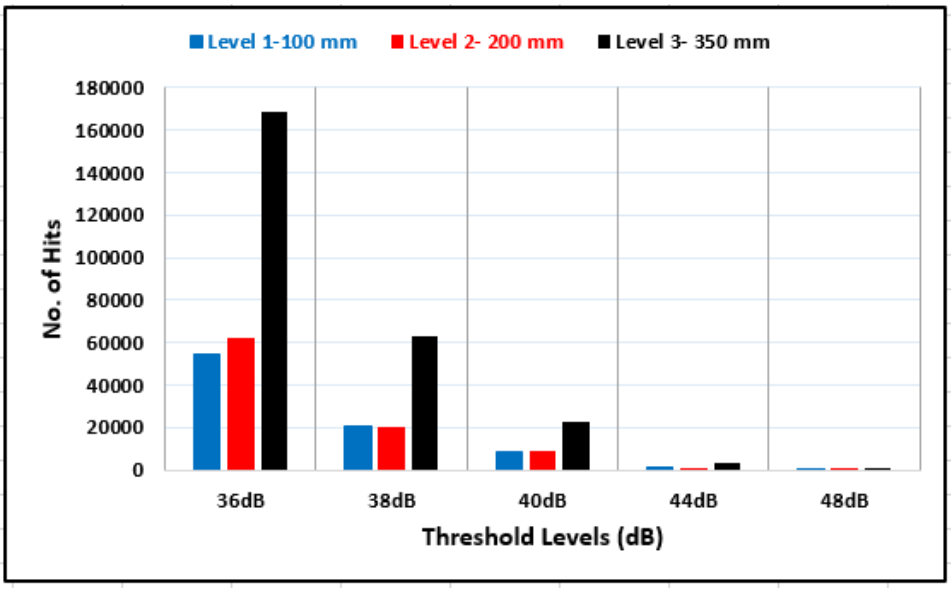

Figure 5-25: Effect of level of tap water and threshold levels on a number of AE-hits for channel 2.

Bubble formation phenomena during pool boiling can be used to provide a good source of information to control and vary the exact amount of power needed to complete the boiling processes in a more economical way. In addition, bubble occurrence can be used to predict the boiling process in industry by using the AE technique.

5.2 Conclusions

The results of the experiments on use of AE technique for the monitoring of bubble formation are encouraging. The results indicate the usefulness of AE technology for detection and monitoring of bubble occurrence in boiling processes. It has been shown that AE parameters, such as AE-RMS, AE-amplitude, AE-energy, AE-rise time and AE-count, are sensitive and reliable for the monitoring of bubble activity and the movement of bubbles towards the surface of the water.

It was observed that the presence of bubble formation in pool boiling is detectable by applying standard and commonly used analysis techniques, such as RMS, hits and threshold levels to the measured AE signals. It has been shown that there is a connection between bubble formation and water temperature during the boiling process. The monitoring of bubble formation using AE technology can

complement other condition monitoring methods, all of which are aimed at reducing energy losses and improving life cycle costs.

Importantly, the AE signals generated by the dynamic formation and bursting of bubbles and can differentiate between liquid types, in this case demineralised, tap and salt water. The chapter has also confirmed the well-known fact, that the signal from an AE sensor is able to monitor the level of liquid in a container with pool boiling. In addition, it has been found that the heater power supply has a significant effect on AE levels; as the electric power-supply increases, the levels of AE signals increase with increase in bubble formation.

The boiling process has offered a good opportunity to study bubble formation due to increase of liquid temperature. The next chapter will present results obtained from an experimental investigation of the capability of AE technique for monitoring bubble formation and collapse due to cavitation phenomena in flow through ball and globe valve.

Chapter 6 Results observations and discussions for valve experiments

This chapter assesses the feasibility of using AE techniques for detection and monitoring of bubble formation and collapse in ball and globe valves based on the experimental results obtained in the investigation. A discussion is presented on the statistical analysis of the AE output parameters: AE-Count, AE-Amplitude, AE-Abs Energy, AE-RMS, AE-Rise time, AE-Average signal level (AE-ASL), AE-Duration, AE-Frequency and AE-Energy. From these analyses, the best AE indicators will be determined. Results of signal processing of AE waveforms using FFT is also presented.

In the present work, pressure drop performance of BOSS^{TM} ball and globe valves is investigated respectively, and trends in the performance of these valves with increasing flow rate and different opening percentages identified.

An experimental investigation of cavitation occurrence will also be performed. Since cavitation causes severe damage to different components of the valves, the operating conditions which introduce cavitation must be identified. These conditions should be avoided or, if that is not possible, harder materials should be used to ensure cavitation does not shorten the life of valves. The cavitation investigations will compare the performance of different valves to better understand the important factors that characterise cavitation occurrence in a valve, with respect to the degree of opening of the valve.

Figures 6-1 and 6-2 provide the value of AE-Count signals for each of the two sensors through ball and globe when the opening percentages of the valves were 16.7% and 5.6 % respectively see Figures 4-9, 4-10 and 4-11. In Figures 6-1 and 6-2, it was noted that the value of AE signal in Channel 2 was higher than that of Channel 1 because it was closer to the bubble sources (downstream of the valve). In this chapter, the value of AE signal in Channel 2 will be used for all analyses.

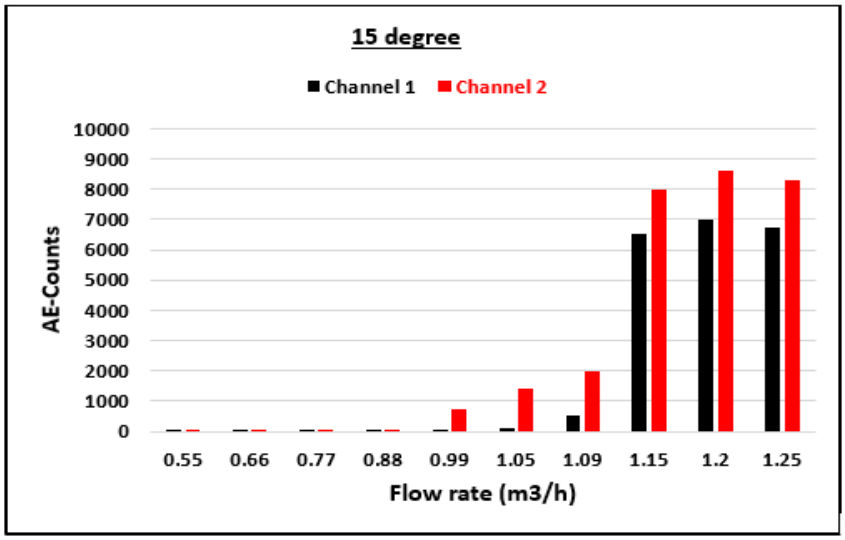

Figure 6-1: AE counts against flow rate for tap water for ball valve 15^0 open (16.7 % of fully open) at 20^0C.

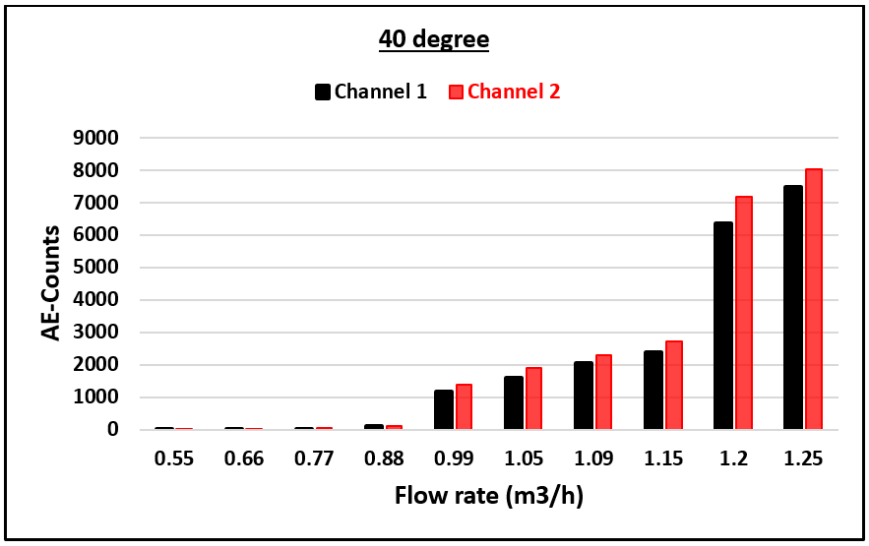

Figure 6-2: AE counts against flow rate for tap water for globe valve 40^0 open (5.6 % of fully open) at 20^0C.

6.1 Ball valve tests

6.1.1 Monitoring of bubble formation and collapse in ball valve

Ten different flow rates (0.55, 0.66, 0.77, 0.88, 0.99, 1.05, 1.09, 1.15, 1.2 and 1.25 m^3/h) were used for each percentage opening of the ball valve. The tests were undertaken for eight degrees of opening: 14^0, 15^0, 16^0, 17^0, 18^0, 20^0, 50^0 and 90^0 where 0^0 was fully closed and 90^0 was 100 % open, Preliminary test runs were undertaken for each degree of opening, with three tests for each run and

the average values of the AE signals calculated. For this study, in depth experimental studies are presented, for the case where the valve was opened to 15^0 (16.7% open). The plot of the trend for the AE counts against differential pressure ratio (K) and flow rate (m^3/h), for an opening of 15^0, is presented in Figure 6-3, as is the cavitation index (σ).

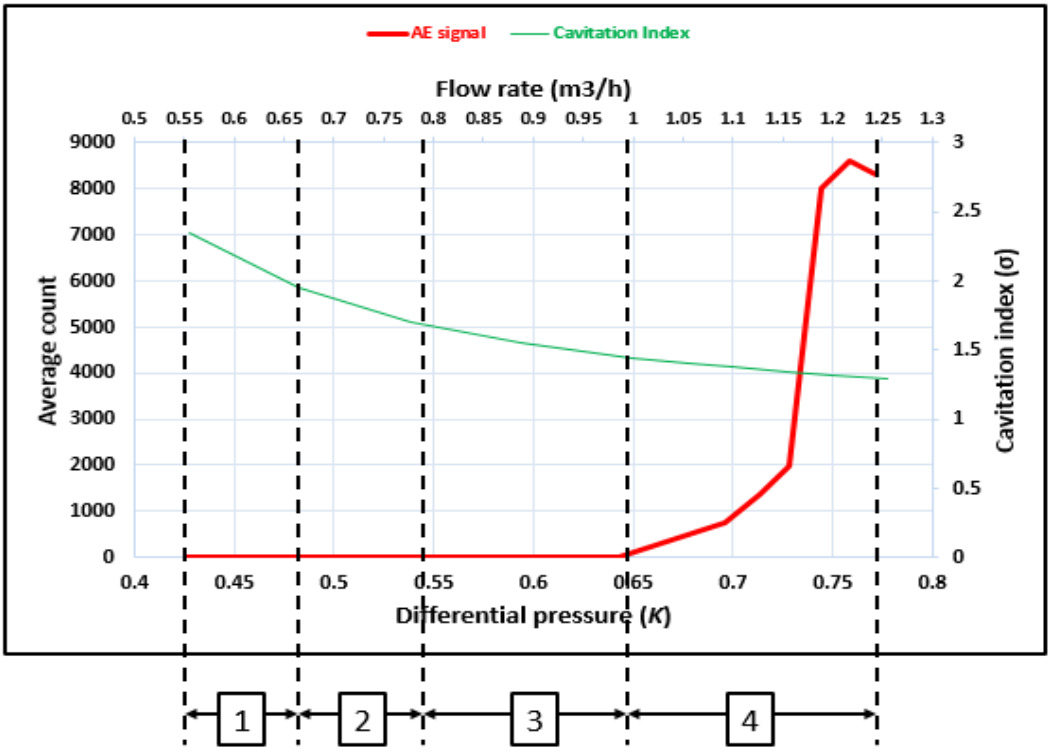

Figure 6-3: Plot of AE counts and cavitation index against K with flow rate for tap water for ball valve 15^0 open (16.7 % of fully open).

In Figure 6-3 the plot is divided into four different stages based on trend behaviour of the AE signal, and the AE-RMS values of the bubble activities as shown in Figure C-1 (see Appendix C), and Figure 6-4. The numbers in boxes at the bottom of the figure show the stage of the flow. During the first stage (< 0.66 m^3/h) bubbles do form but noise due to the flow is negligible which means there is no cavitation. In the second stage (0.66 – 0.79 m^3/h), with increasing flow rate and momentum, turbulence builds, bubbles form and noise increase, some cavitation might occur. In the third stage (0.79 - 1.00 m^3/h) bubble activity increases, cavitation begins and grows quickly to reach its fully developed stage, the accompanying vibration and noise increase rapidly. At the fourth stage (1.00 - 1.25 m^3/h), the downstream pressure continues to increase as shown in Table 6-

1, but some bubbles do not collapse and escape downstream with the flow. This persistence of the bubble is called the flashing phenomenon.

Table 6-1: P_1, P_2, K and σ associated with Figure 6-3.

Flow rate (m^3/h)	P_1 (bar)	P_2 (bar)	P_1-P_2	P_V at 20^{0}C	K	Cavitation Index (σ)	Appreciation of (σ)	Flow stages
0.55	1.727	1.002	0.725	0.023	0.42	2.34	No cavitation	Stage 1
0.66	2.055	1.016	1.039	0.023	0.51	1.95	Turbulence builds	
0.77	2.456	1.031	1.425	0.023	0.58	1.70	Bubble formation starts	Stage 2
0.88	2.894	1.050	1.844	0.023	0.64	1.55	Some cavitation might occur	Stage 3
0.99	3.462	1.071	2.391	0.023	0.69	1.43	Incipient cavitation	
1.05	3.729	1.083	2.646	0.023	0.71	1.40	Incipient cavitation	Stage 4
1.09	3.944	1.091	2.853	0.023	0.72	1.37	Cavitation occurs	
1.15	4.248	1.103	3.145	0.023	0.74	1.34	Cavitation occur	
1.20	4.518	1.112	3.406	0.023	0.75	1.31	Fully developed cavitation	
1.25	4.855	1.126	3.729	0.023	0.77	1.29	Flashing	

The relation between the flow rate (m^3/h) and AE-RMS of the ball valve for stages 1, 2 and 3 are shown in Figure 6-4. In stage 1, increasing the flow rate from 0.55 to 0.66 m^3/h gives to an approximately constant level of AE-RMS because there is no bubble activity. In stage 2 the value of AE-RMS slowly increases with increase in the flow rate to about 0.77 m^3/h, due to some bubbles forming. This is the stage in which some cavitation might occur. With incipient cavitation, the AE-RMS value continues to increase with flow rate until at a differential pressure ratio of about K= 0.69 when cavitation has reached the fully developed point, which is the maximum point of stage 3.

With incipient cavitation, the AE-RMS value continues to increases with flow rate until at about 1.0 m^3/h, K = 0.69 and the cavitation index approaches 1.43, when cavitation is likely to become severe, as shown in Figures 6-4 & 6-5. At a flow rate of 1.1 m^3/h, K = 0.7 and the cavitation index falls below 1.5, the cavitation will be severe. The sharp rise in the average count and the increasing gradient of the AE-RMS in Figures 6-4 and 6-5 confirm that cavitation becomes fully developed. Following this, with an increase in pressure difference (P_1-P_2) across

the ball valve, the cavitation index (σ) gradually decreases until it reaches a value at which some bubbles have a chance to travel downstream without collapsing, as shown in Table 6-1, this is the flashing phenomena.

The value of AE-RMS increased as the bubble activity increased, the AE-RMS reached a maximum of about 1 mV, which was due to bubble formation.

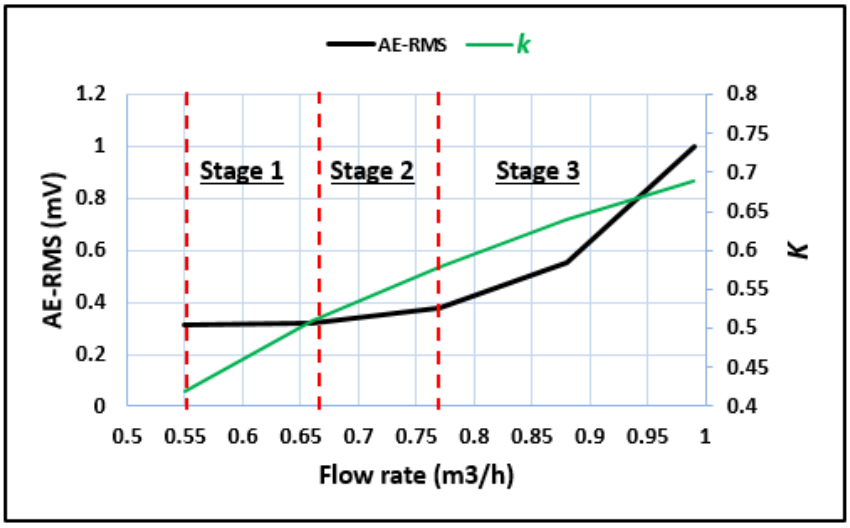

Figure 6-4: AE-RMS and differential pressure ratio as a function of flow rate of tap water during stages 1, 2 and 3 (channel 2).

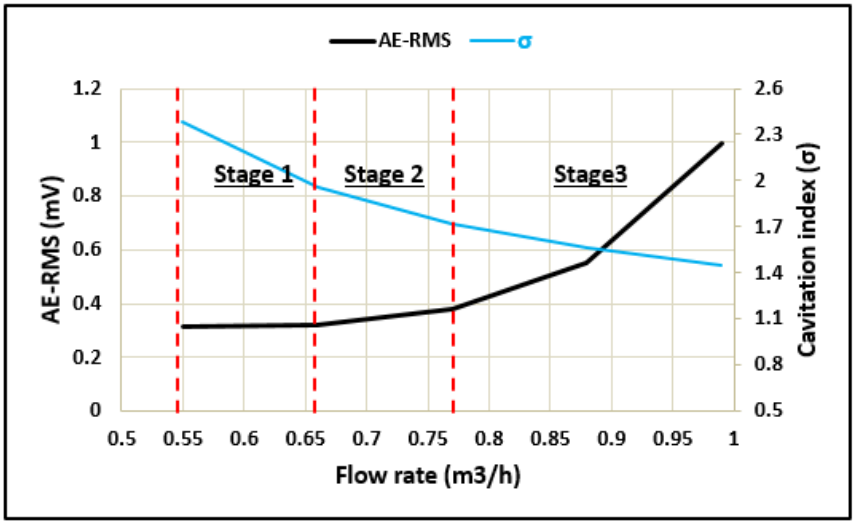

Figure 6-5: AE-RMS and cavitation index as a function of flow rate of tap water during stages 1, 2 and 3 (channel 2).

6.1.2 Statistical analysis of AE parameters with bubble activity in ball valve with different liquid types

Bubble activity and cavitation in the ball valve depend on flow rate, pressure difference and valve opening percentage. The bubble formation phenomena were statistically analysed to determine the AE parameter which is the best indicator to use for bubble occurrence detection. Tables (6-2), (6-3) and (6-4) show the ranges of values for comparison between the classical AE parameters as obtained directly from the AE system (AE-Rise Time, AE-Count, AE-Amplitude, AE-Abs. Energy and AE-Frequency) from sensor 2.

Table 6-2: AE parameters for bubble formation in ball valve for demineralized water at stages 1, 2 and 3.

Flow Rate (m^3/h)	Demineralized Water				
	AE Parameters				
	AE Rise Time (µs)	AE Count	AE Amplitude (dB)	AE Abs Energy (atto-joule)	AE Frequency (kHz)
0.55	41	21	31	20	144
0.66	148	45	30	31	212
0.77	160	56	31	75	160
0.88	678	67	32	81	138

Table 6-3: AE parameters for bubble formation in ball valve for tap water at stages 1, 2 and 3.

Flow rate (m^3/h)	Tap Water				
	AE Parameters				
	AE Rise Time (µs)	AE Count	AE Amplitude (dB)	AE Abs Energy (atto-joule)	AE Frequency (kHz)
0.55	15	4	29	2	225
0.66	17	6	29	3	223
0.77	149	15	30	26	181
0.88	586	12	31	31	143

Table 6-4: AE parameters for bubble formation in ball valve for salt water (5g/L) at stages 1, 2 and 3.

Flow rate (m^3/h)	Salt Water (5g/L)				
	AE Parameters				
	AE Rise Time (µs)	AE Count	AE Amplitude (dB)	AE Abs Energy (atto-joule)	AE Frequency (kHz)
0.55	20	5	29	3	226
0.66	25	6	29	4	218
0.77	135	15	30	25	167
0.88	239	20	30	28	156

The average values set out in Tables (6-2), (6-3) and (6-4) were taken for four different flow rates; 0.55 m^3/h, 0.66 m^3/h, 0.77 m^3/h and 0.88 m^3/h (stages 1, 2 and 3) with the ball valve open at 15^0. Figures 6-6, 6-7, 6-8, 6-9 and 6-10 respectively show the results for AE Rise time, AE count, AE Absolute Energy, AE Amplitude, and AE Frequency. The value of AE signal clearly changes with change in liquid properties, as shown in each of Figures 6-6, 6-7 and 6-8.

These figures suggest that for demineralized water, tap water and salt water (5g/L), only Figures 6-6 (rise time), 6-7 (count) and 6-8 (absolute energy) show any clearly discernible changes with flow rate, and then the changes are not uniform. In Figure 6-6 it can be seen that the AE rise time was more or less constant between 0.55 and 0.66 m^3/h, where this signal was caused by flow turbulence. The value of AE rise time gradually increases during stage 2, (0.66 to 0.77 m^3/h) which could be due to flow turbulence and some bubble formation. Following this, there was a sharp increase in the rise time to reach around 680 µs between 0.77-0.88 m^3/h during stage 3. The same pattern can be seen for all three liquids but is most pronounced for demineralized water and least for the salt water. The sudden increase in rise time is because bubbles start to form in this flow region.

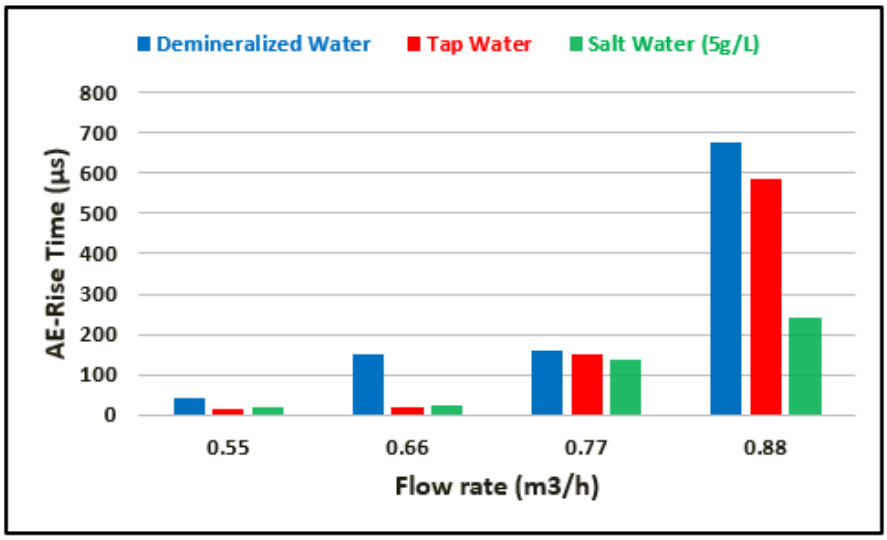

Figure 6-6: Rise time as a function of the flow rate for demineralised water, tap water and salt water (5 g/L).

In Figure 6-7, the value of AE-counts increases with increasing flow rate due to bubbles occurrence. Once again the AE signal for the demineralized water ranked the highest at 0.88 m^3/h. Viscosity, surface tension and density are least for demineralised water. Figure 6-8 shows a significant increase in the AE-absolute energy with increase in flow rate due to bubble activity.

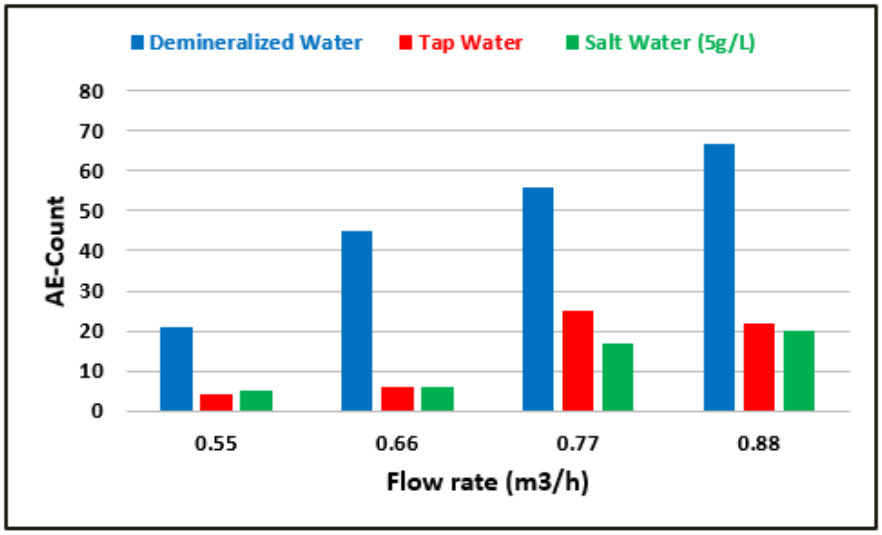

Figure 6-7: AE Count as a function of flow rate for demineralised water, tap water and salt water (5 g/L), ball valve open 15^0.

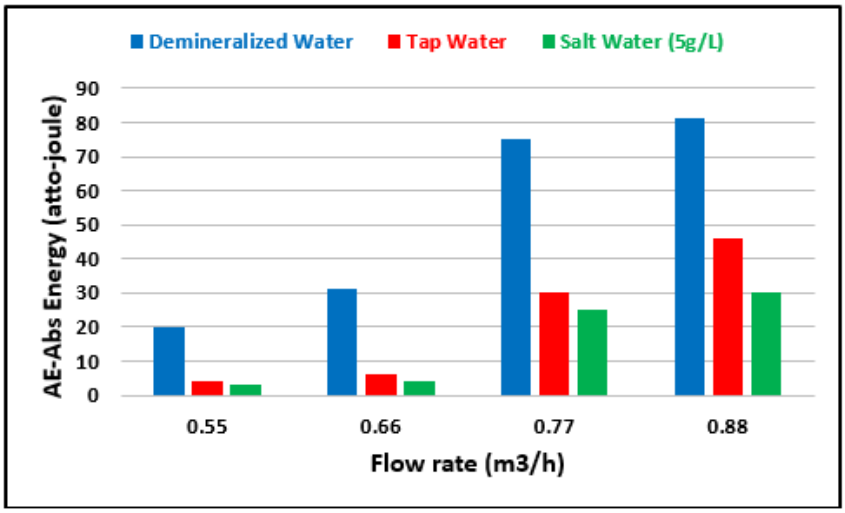

Figure 6-8: AE Absolute Energy as a function of flow rate for demineralised water, tap water and salt water (5 g/L), ball valve open 15^0.

The values of AE-Amplitude and AE-Frequency showed little change with flow rate, as shown in Figures 6-9 and 6-10, respectively. Figure 6-9 shows that value of AE amplitude was stable between 0.55 and 0.66 m^3/h in tap water and salt water (5g/L), because there is no bubble occurrence in this region. But for flow rates 0.66 m^3/h and above, a gradual increase in the value of the AE amplitude is observed for tap water and demineralised water, but not for salt water. Figure 6-10, on the other hand, shows that the AE peak frequency tends to decrease with increasing flow rate. This is because large bubbles start to form and large bubbles produce lower-frequency noise [43][44][116].

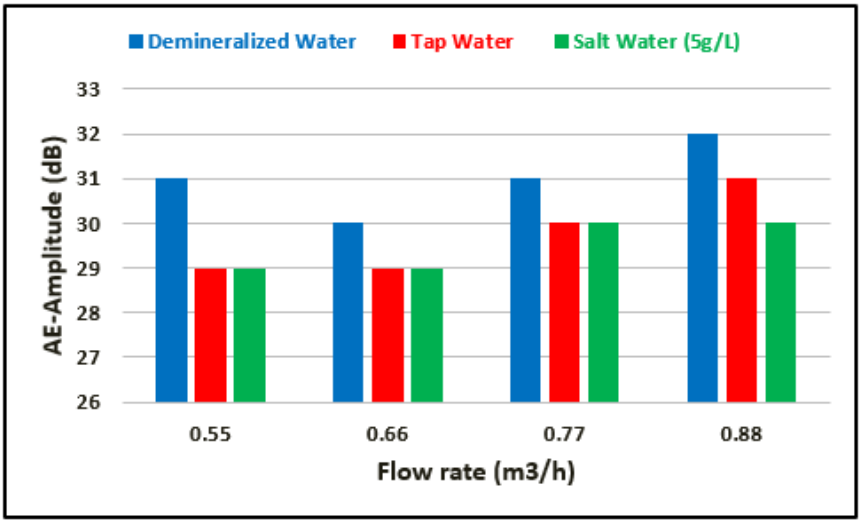

Figure 6-9: AE Amplitude (dB) as a function of flow rate for demineralised water, tap water and salt water (5 g/L), ball valve open 15^0.

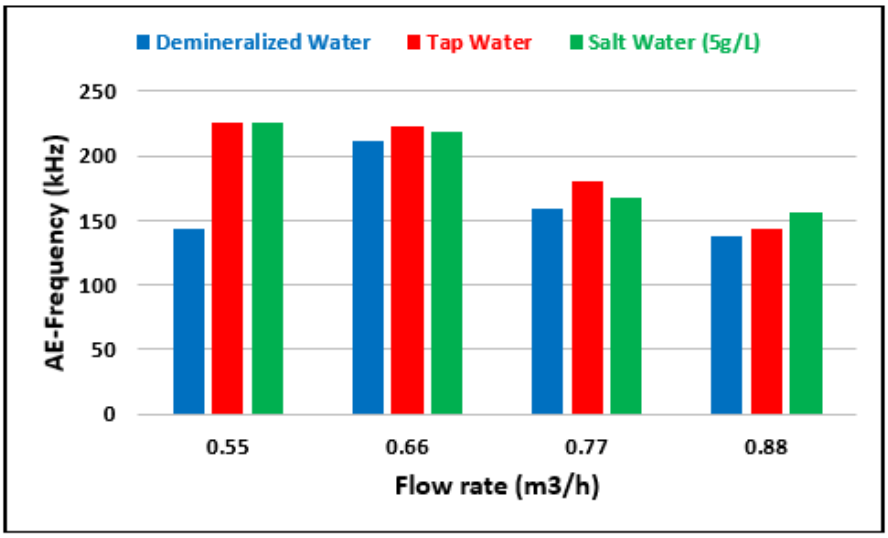

Figure 6-10: AE Frequency (kHz) as a function of flow rate for demineralised water, tap water and salt water (5 g/L), ball valve open 15^0.

6.1.3 Waveform analysis of AE amplitude through ball valves using tap water

Observations of the AE waveform, sampled at 5 MHz showed interesting changes in the signal characteristics as a function of flow rate stages, 1, 2, 3 and 4. Typical AE waveforms recorded after the system had time to reach equilibrium are presented in Figure 6-11. This shows AE transient events. At stage 1 (0.55 m^3/h), bubbles do not form (no cavitation is occurring) and the noise signal generated by the given turbulence in the flow is negligible; the peaks AE amplitude reached only 1.0 mV. Figures 6-12 and 6-13 confirm that the AE signal in stage 1 is due to turbulence flow, where it was noted that the AE amplitude in stage 1 is the same as that in Figure 6-13. Additionally, AE signal behaviour in Figure 6-12 is similar to that of Figure 6-3 (stage 1) with 1.0 mV.

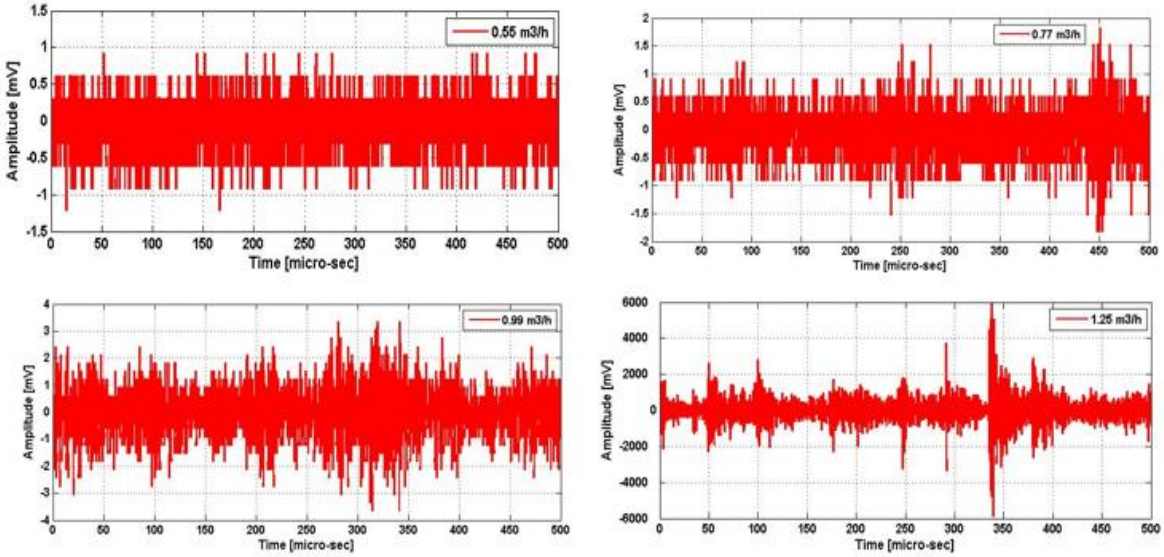

Figure 6-11: AE waveforms associated with the ball valve test results presented in Figure 6-3.

During stage 2 (0.66 - 0.77 m^3/h) with increase in flow rate there is greater noise due to flow turbulence, and peaks occur in the AE amplitude; some bubbles might form. It was noted that the value of AE amplitude gradually increased with increase in flow rate. In stage 3 (0.77 - 0.99 m^3/h), as the flow rate increases with increased pressure difference across the valve, bubbles start to form. The onset of cavitation occurs with subsequent bubble collapse.

In stage 4 (0.99 - 1.25 m^3/h) the AE amplitude was highest, with a magnitude of 600 mV, as shown in Figure 6-11. During this stage, the cavitation increased rapidly with increase in flow rate, and maximum noise also occurred. However, some bubbles did not collapse into micro-jets but escaped downstream. As stated above, this phenomenon is called flashing, and was observed for flow rates greater than about 1.2 m^3/h, the corresponding value of the cavitation index was around 1.3.

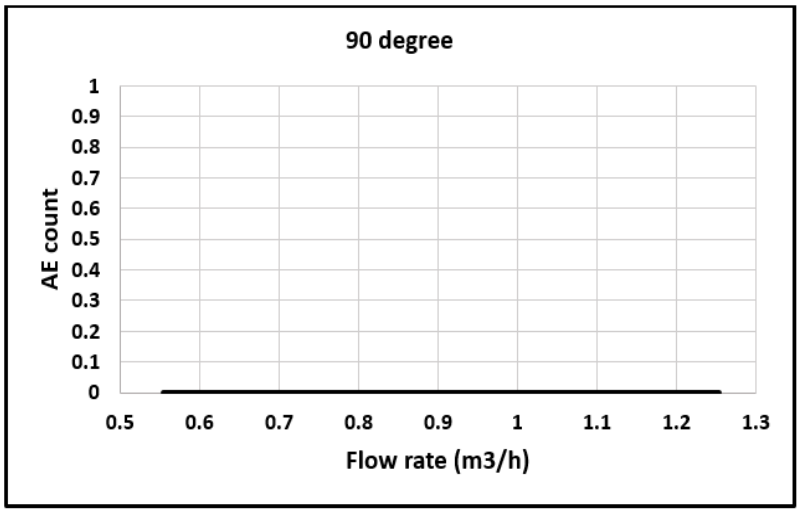

Figure 6-12: Plot of counts against flow rate for tap water for ball valve at 90^0 open (100 % of fully open), channel 2.

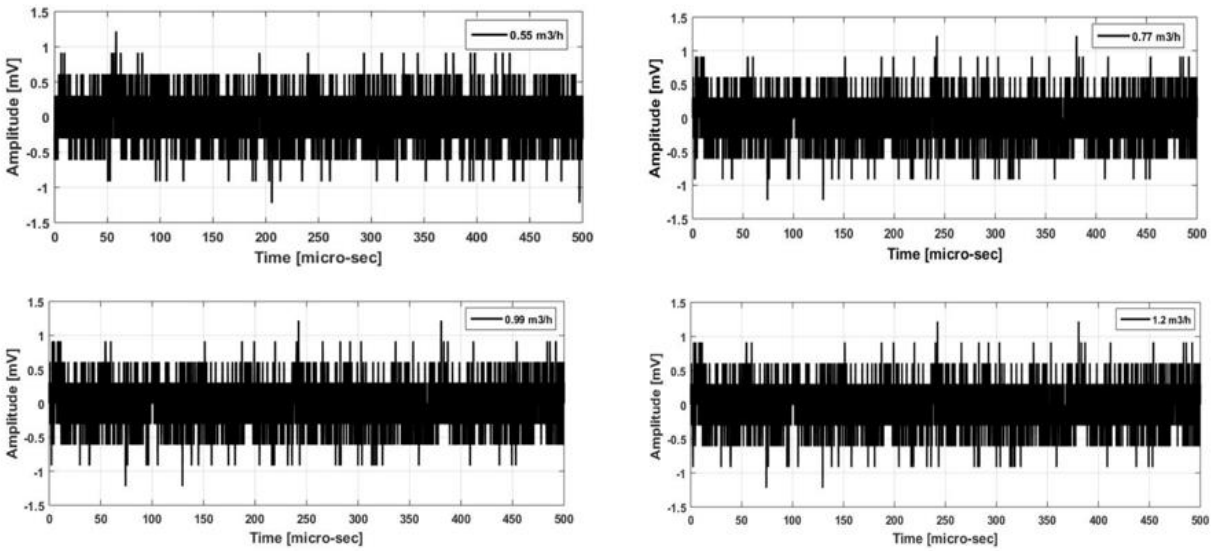

Figure 6-13: AE waveforms associated with the ball valve test presented with Figure 6-12.

6.1.4 Influence of AE sensor position on AE signal levels in ball valve

As the flow rate increases so does the pressure difference across the valve and Figure 6-14 shows that as a result there is more bubble formation in the downstream region. The magnitude of the AE signal for sensor 2 is higher than for sensor 1 because the position of sensor 2 was closer to the downstream region where the bubbles start to form and cavitation occurs, the position of sensor 1 is further from the area of bubble activity.

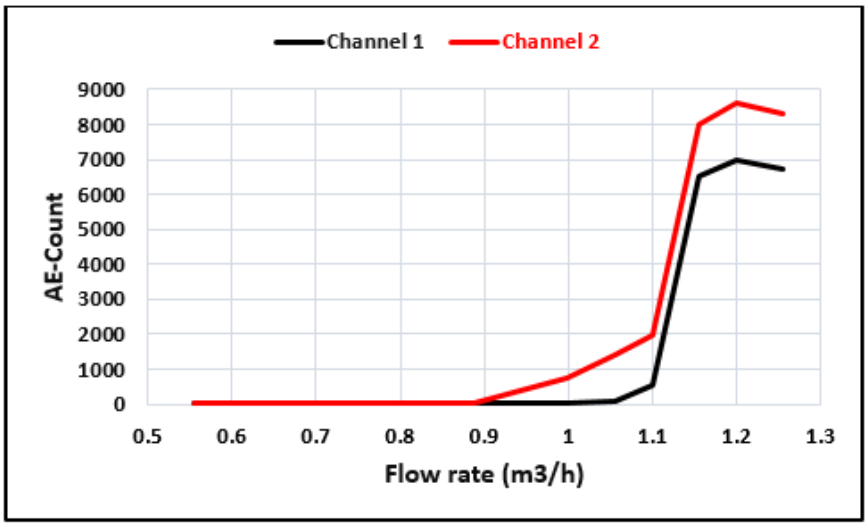

Figure 6-14: Average AE count with different flow rates with the ball valve 15^0 open for sensors 1 and 2.

The time domain of the AE signal recorded over a time window of 500 µs is shown in Figure 6-15. AE waveforms were measured by both sensors, when the valve opening was 15^0, showing different AE amplitudes depending on the flow rate. As previously noted, the value of AE signal from sensor 2 was higher than from sensor 1. It is confirmed that sensor location affects the level of the measured AE signal caused by bubble activity.

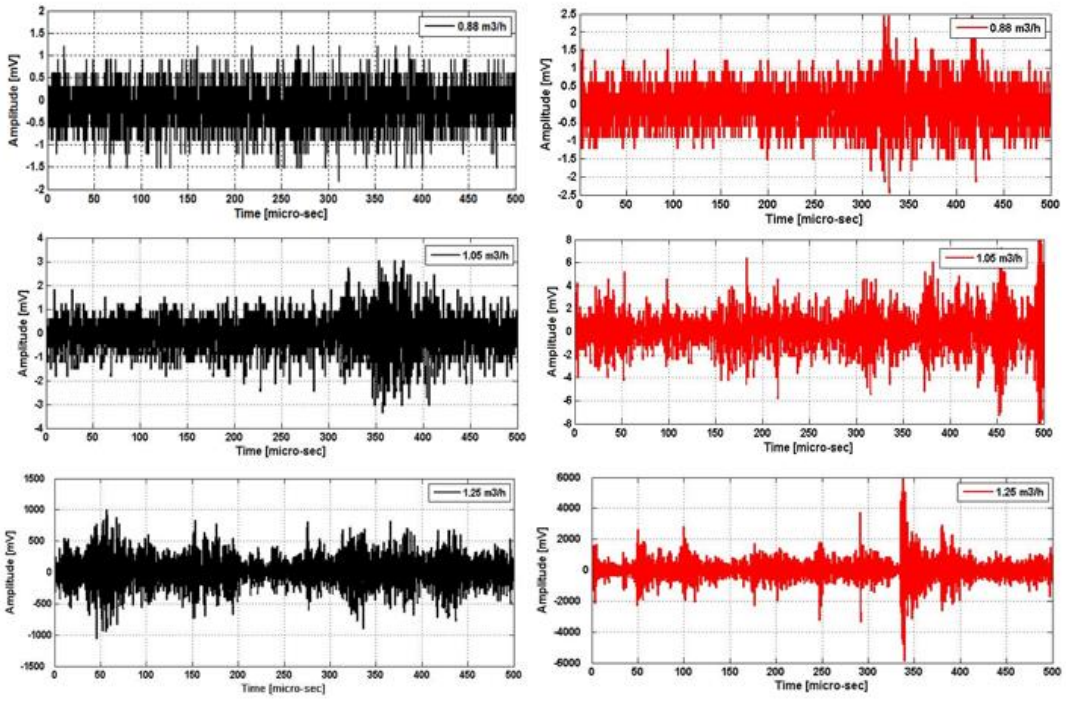

Figure 6-15: Time domain of AE waveforms from sensors 1 and 2 for three flow rates of tap water with the ball valve 15^0 open.

6.1.5 Influence of valve opening on AE signal levels using tap water

Figure 6-16 presents plots of AE-Frequency versus AE-Amplitude and flow rate for three degrees of ball valve opening. AE-Frequency levels for valve open at 16^0 and 20^0 show only some slight variation with AE-Amplitude. In particular the AE-Frequency for the 16^0 opening remains just under 100 kHz for all AE-Amplitude levels. For a flow rate of 0.88 m^3/h, the AE-Amplitude is about 31 dB, and the AE frquency is about 150 kHz. Following this, the value of the AE-Frequency signal increased sharply to a value of around 225 kHz for AE Amplitude levels above about 65 dB. This figure gives a good sense of bubble formation and collapse. For the 15^0 valve opening, when the flow rate generated an AE signal of amplitude 85 dB, the AE-Frequency increased to about 350 kHz. This means that for the same AE-amplitude, the higher flow rates generates a higher frequency of occurence of cavitation.

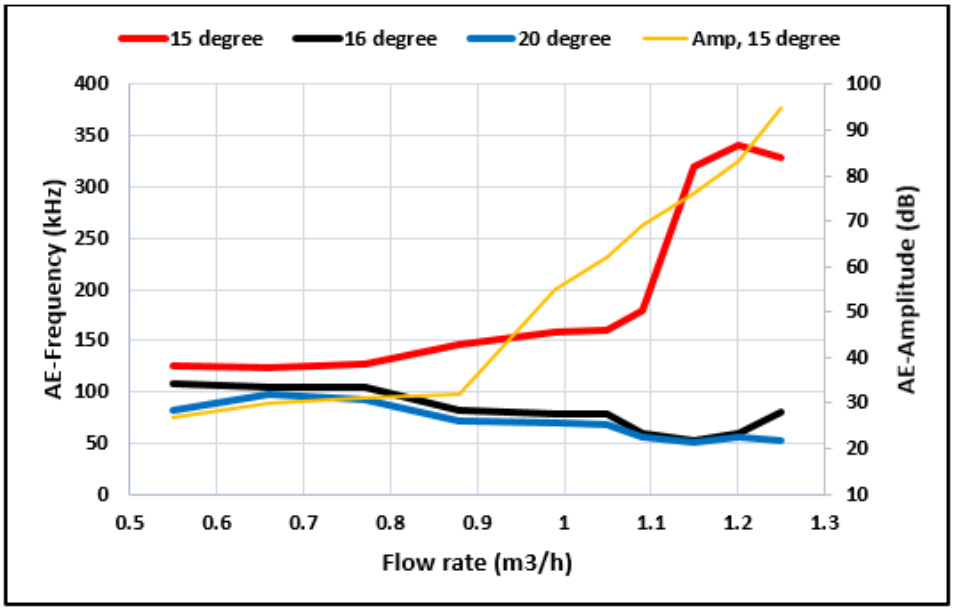

Figure 6-16: Relation between average AE-Frequency, AE-Amplitude and flow rate for three degrees of ball valve opening.

Figure 6-17 shows that when the ball valve is open by 15^0 or less, high-frequency vibration signals and noise are detected with flow rates above about 0.9 m^3/h. This indicates the presence of bubble collapse into micro-jets, generating pressure pulses that produce high-frequency vibration. It was observed that there is a difference in trend between 14^0, 15^0, 16^0, 17^0, 18^0 and 20^0, as shown in Figure

6-17. This is due to decrease in the pressure difference between upstream and downstream: it decreased when the percentage opening of the valve increased for the same flow rate, see Table 6-5. Furthermore, cavitation index increasing with increase in opening percentage of ball valves at the same flow rate, as shown in Appendix C in Tables C-1, C-2, C-3, C-4, C-5, C-6 and C-7.

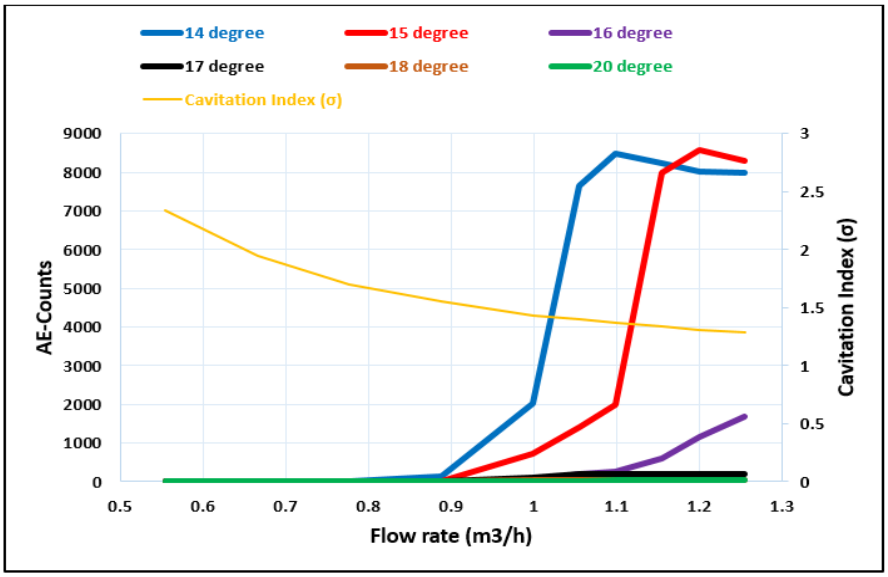

Figure 6-17: Plot of average AE-Count as measured by sensor 2, as a function of flow rate for different degrees of valve opening for tap water.

Table 6-5: Presents (P_1-P_2) for different opening percentage of ball valve associated with Figure 6-17.

Flow rate (m^3/h)	14 degree	15 degree	16 degree	17 degree	18 degree	20 degree
	(P_1-P_2), bar	(P_1-P_2), bar	(P_1-P_2), bar	(P_1-P_2), bar	(P_1-P_2), bar	(P_1-P_2), bar
0.55	0.877	0.728	0.484	0.431	0.225	0.128
0.66	1.223	1.039	0.707	0.685	0.318	0.173
0.77	1.639	1.425	0.929	0.918	0.414	0.233
0.88	2.151	1.844	1.011	0.827	0.534	0.299
0.99	2.797	2.391	1.017	1.022	0.667	0.38
1.05	3.096	2.646	1.102	1.048	0.755	0.419
1.09	3.237	2.853	1.887	1.057	0.835	0.456
1.15	3.597	3.145	1.934	1.105	0.919	0.498
1.20	3.966	3.406	2.060	1.108	0.975	0.545
1.25	4.240	3.729	2.227	1.115	1.061	0.580

6.1.6 Frequency domain analysis of bubble occurrence in ball valve using tap water

Fourier analysis of the measured AE data was used to estimate the power spectrum of the signal generated by bubble occurrence, see Figure 6-18. This analysis was performed to assess the ability of the FFT spectrum to determine bubble existence during ball valve operation. The results showed no bubble frequencies for flow rates 0.55, 0.66 and 0.77 m^3/h, when the ball valve was open at 15^0. However, the power spectrum shows increased turbulence flow activity and vortex shedding at the lower frequencies (0-200 kHz).

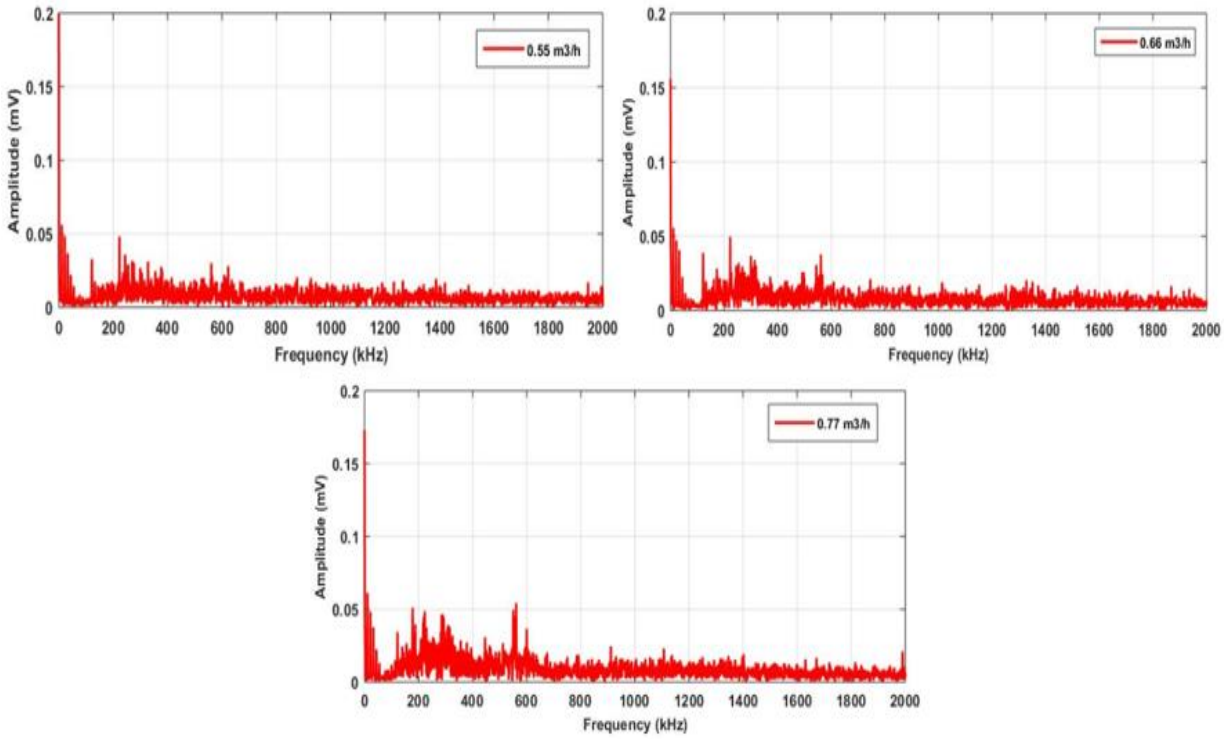

Figure 6-18: Power spectrums for turbulent flow at 0.55, 0.66 and 0.77 m^3/h (stages 1 and 2) tap water with the ball valve 15^0 open.

When, in stage 3, the flow rates increased to 0.88 - 0.99 m^3/h, bubbles started to form as do frequency peaks in the power spectrums, between 150 and 350 kHz. Figure 6-19 shows these peaks can reach 1 mV at 0.88 m^3/h, and over 2 mV at 0.99 m^3/h. The bubbles generated tend to have a size such that when they collapse they generate a signal with a peak at in the range 150 to 350 kHz. To a first estimate the peak frequency generated by the bubble would likely be

proportional to its radius, so if a higher flow velocity generated more but smaller bubbles then the peak would be expected to shift to a higher frequency.

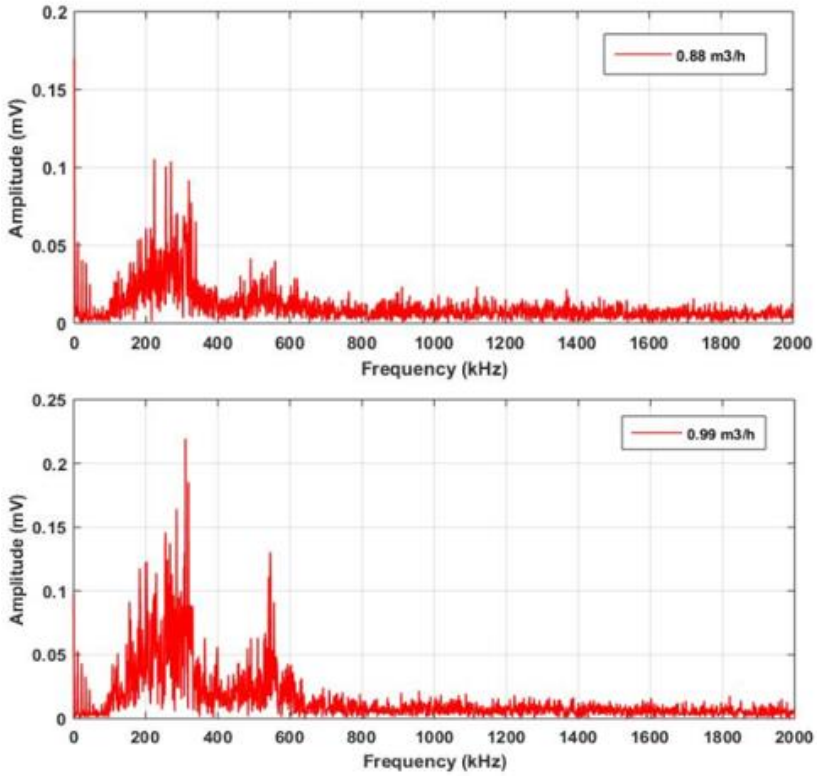

Figure 6-19: Power spectrums for turbulent flows of 0.88 and 0.99 m^3/h, (stage 3) tap water with the ball valve15^0 open.

Figure 6-20 shows power spectral plots for flow rates of 1.05, 1.09, 1.15, 1.20 and 1.25 m^3/h. (stage 4). The frequency spectrum for each flow rate shows AE events that are associated with different bubble sizes, and that any increase in AE amplitude depended on the level of bubble activity.

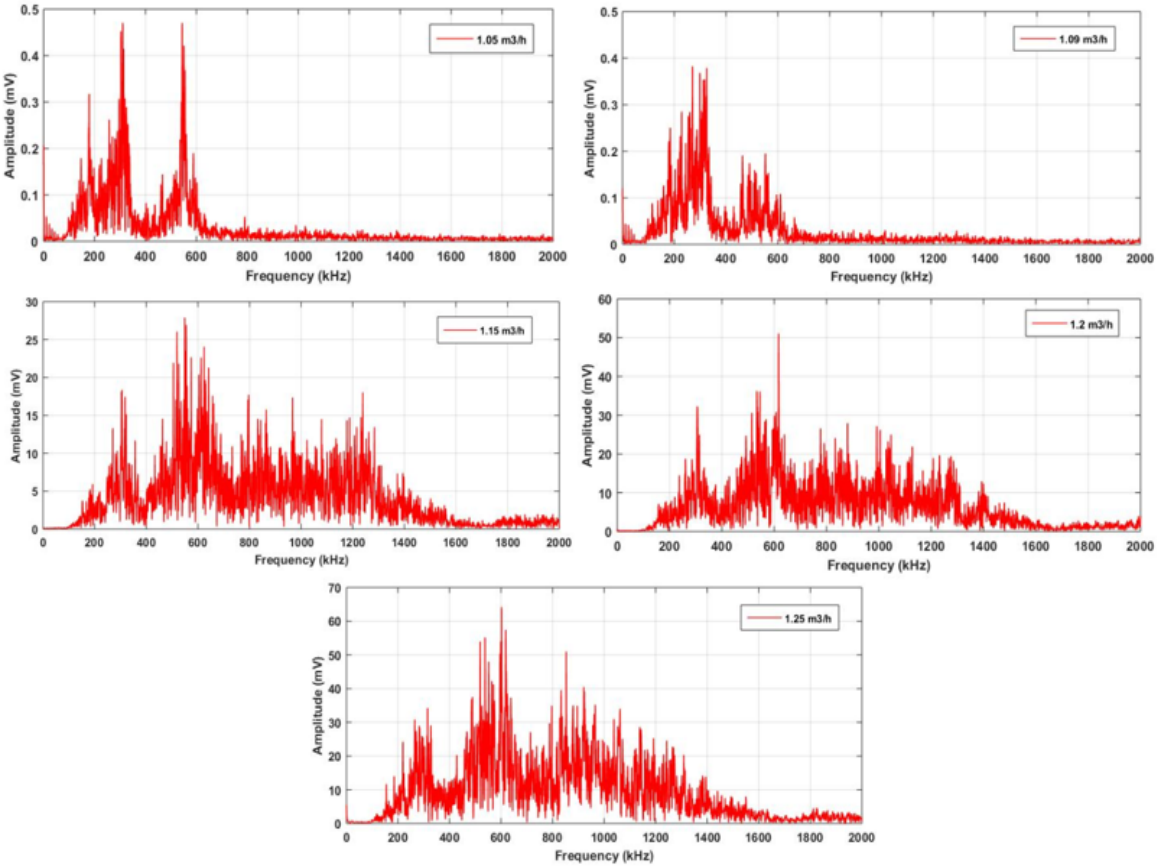

Figure 6-20: Power spectral plots for turbulent flows of 1.05, 1.09, 1.16, 1.20 and 1.25 m^3/h (stage 4) tap water with the ball valve 15^0 open.

The value of the amplitude of the primary frequency components in the region of about 150 - 350 kHz observed at 1.05 m^3/h increases with increasing flow rate, which suggests an increase in bubble activity, though there is also a shift of energy towards 350 KHz, which is due to cavitation. The amplitude of the AE signal between about 400 to 700 kHz increased not only absolutely but also relative to the peak at 350 kHz. Observation of the power spectrums shown in Figure 6-20, strongly suggest that the bubble occurrence frequency starts from around 200 kHz; increasing the flow rate increases both amplitude and peak frequency of the associated signal. That is, the increase in spectral activity above about 800 kHz is due to developing bubble activity and cavitation.

6.1.7 Influence of threshold levels on AE signal levels in ball valve

Figure 6-21 shows that there is a correlation between AE-Counts and flow rate. When the flow rate increases, AE-Counts increase due to the increase in number of bubbles formed. As would be expected, the value of AE-Counts ranked highest at a threshold level of 30 dB reaching 70 for 1.2 m^3/h. Obviously, the threshold levels have an effect on AE signal levels. When the threshold level increased, the AE-Counts decreased, as shown in Figure 6-21.

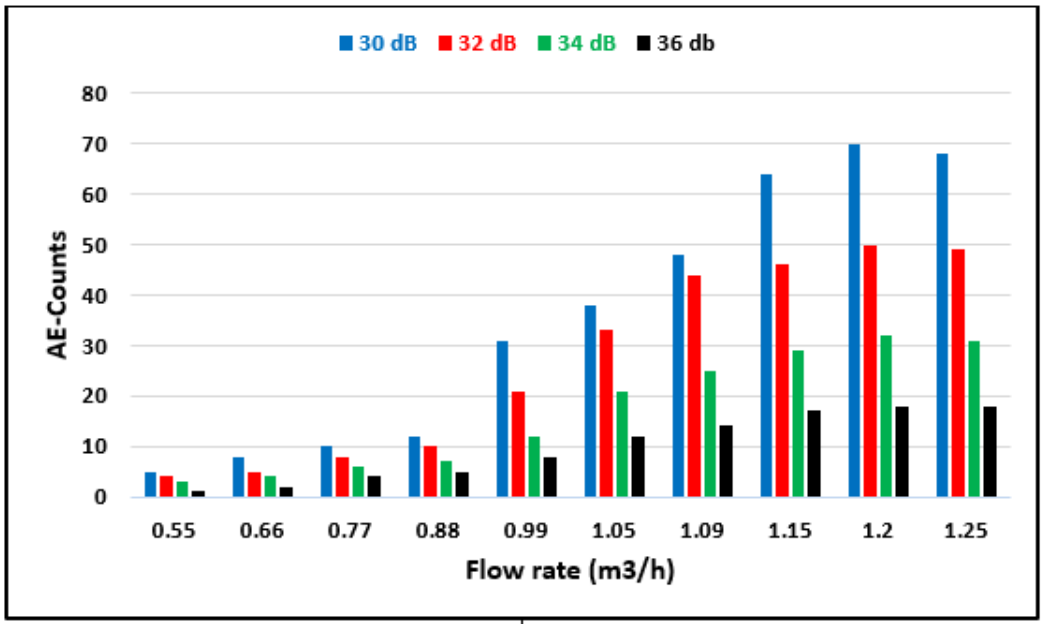

Figure 6-21: Effect of threshold levels on AE-Counts for channel 2, tap water with valve open at 15^0.

6.1.8 Influence of different liquids on AE signal levels for ball valve

A significant difference in the AE-Count occurs between demineralized water and tap water at 0.9 m^3/h for valve open 15^0, see Figure 6-22. This difference indicates earlier incipient cavitation commencing at a flow rate of about 0.9 m^3/h with demineralised water. In salt water (20g/litre), there was a more gradual increase in the AE level which did not commence until about 1 m^3/h. Not only was cavitation noticed earlier but the value of AE signal for demineralized water ranked the highest with 8500 counts at 1.1 m^3/h. It was concluded that the flow rate at which incipient cavitation occurs depends on the properties of the fluid. The greater the surface tension (and viscosity) the higher the flow rate before

cavitation occurs. Salt water (20g/litre) has a higher surface tension and viscosity than tap water and tap water a higher surface tension and viscosity than demineralised water.

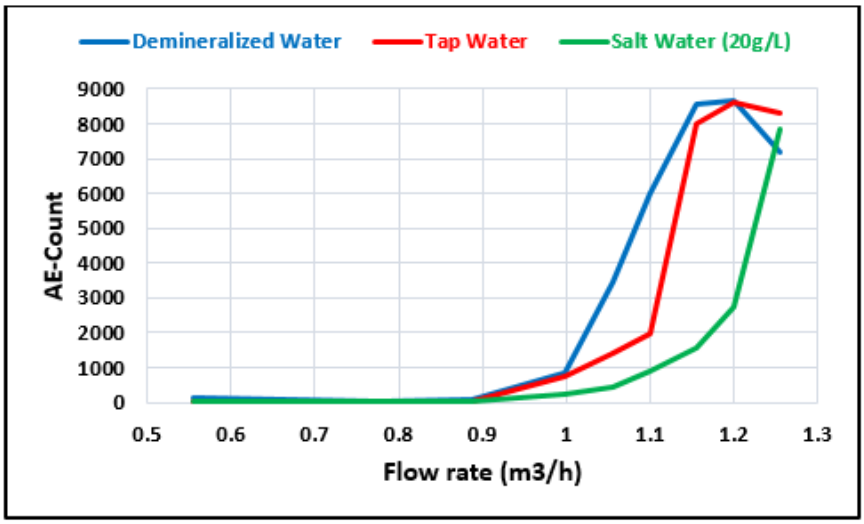

Figure 6-22: Plot of AE signal with flow rate for different liquid types, valve open 15^0, at 20^0C.

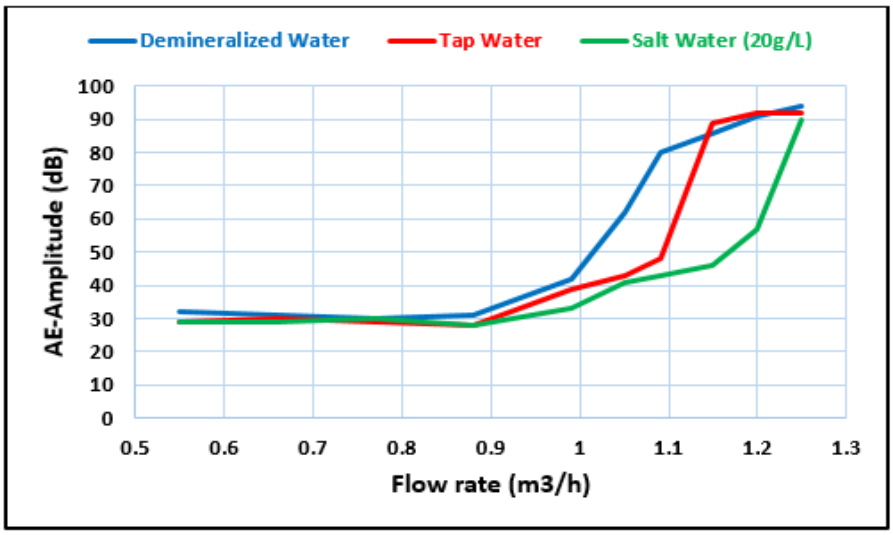

Figure 6-23: AE-Amplitude with flow rate for different liquid types, valve open 15^0, at 20^0C.

Observations of the AE waveforms, sampled at 5 MHz showed interesting characteristics as a function of time, as presented in Figure 6-24. This figure clearly shows AE transient events corresponding to cavitation in the different liquids. AE monitoring of bubble formation in the ball valve open 15^0, has shown different AE amplitude for different liquids.

At 0.99 m^3/h, in Figures 6-23 and 6-24, the AE-Amplitude in demineralized water ranked the highest with 10 mV and 35 dB, in tap water it ranked second with 4 mV and 31 dB, and in salt water (20g/L) ranked the lowest with 3 mV and around 29 dB. What this shows is that at this flow rate there are clear signs of bubble collapse with demineralised water, but not for tap water or salt water (20 g/L). This could be attributed to the surface tension and viscosity of demineralized water being lower than those for tap water and salt water (20g/L).

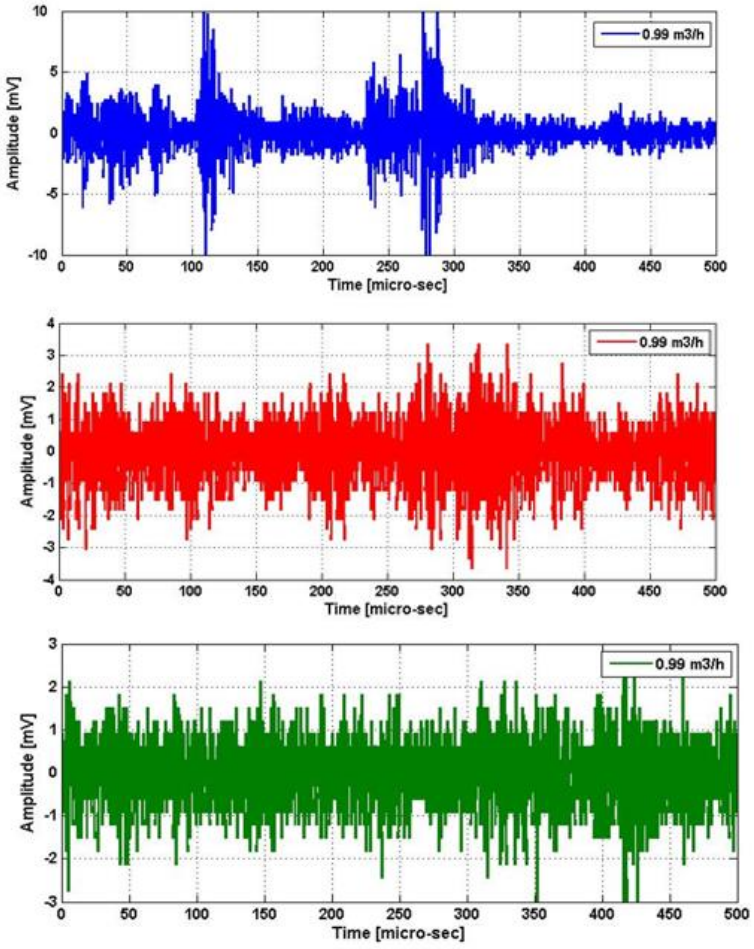

Figure 6-24: AE waveforms associated with demineralised water, tap water and salt water (20 g/L) for flow rate of 0.99 m^3/h and valve open 15^0. (Refer to Figure 6-24).

6.2 Globe valve tests

6.2.1 Monitoring of bubble formation and collapse in globe valve

Ten different tap water flow rates of 0.55, 0.66, 0.77, 0.88, 0.99, 1.05, 1.09, 1.15, 1.2 and 1.25 m^3/h were used for each percentage opening of the globe valve. The tests were undertaken for three degrees of opening: 40^0, 50^0, and 80^0, where 0^0 was fully closed and 720^0 was 100 % open. Three test runs were undertaken for each flow rate conditions, and the average values of the AE signals found. Here the results for one experimental case are presented in detail, the case where the valve was opened to 40^0 (5.6% of fully open). The plot of the trend for AE-Counts and cavitation index (σ) against differential pressure ratio (K), and flow rate (m^3/h), are presented in Figure 6-25.

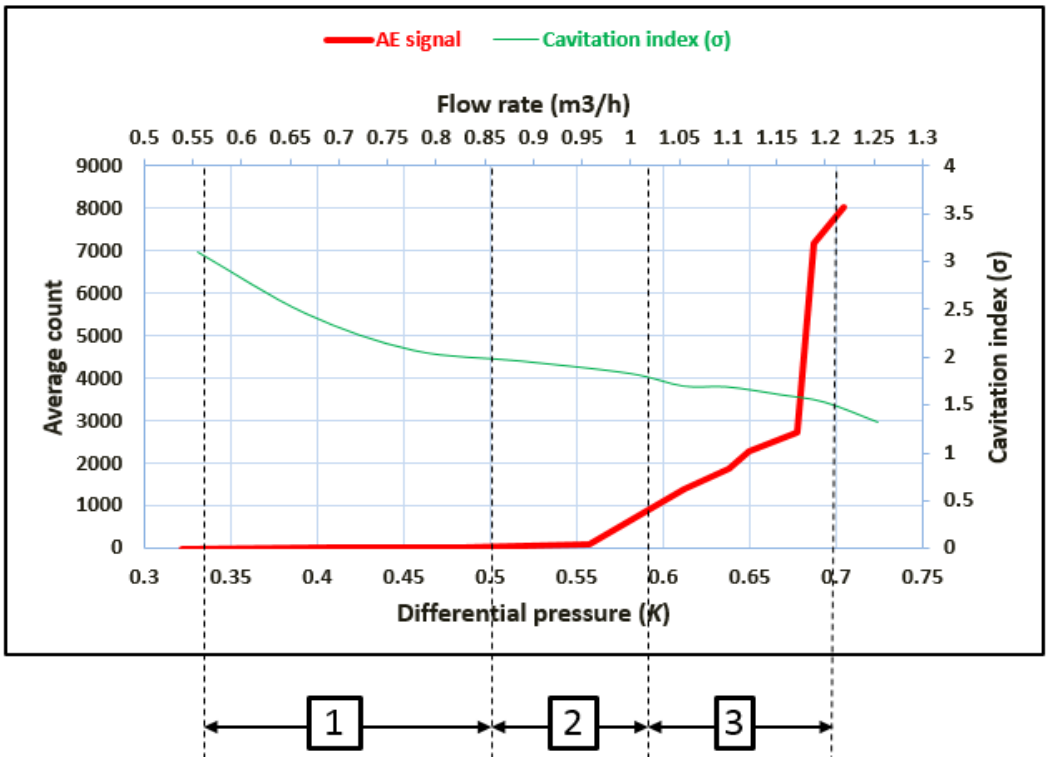

Figure 6-25: Plot of AE-Counts from sensor 2 and cavitation index against differential pressure and flow rate (m^3/h) for globe valve open 40^0 (5.6 % of fully open), for tap water at 20^0C.

In Figure 6-25 the plot is divided into three stages based on trend behaviour of the AE-Counts. The numbers in boxes at the bottom of the figure show the stage of the flow. During the first stage (< 0.85 m^3/h) bubbles do form but the noise due to the flow is negligible which means there is no cavitation. In the second stage

(0.85 – 1.02 m^3/h), with increasing flow rate bubbles start to form and noise increase, some cavitation may occur. In the third stage (1.02 – 1.2 m^3/h) bubble activity increases, cavitation starts and grows rapidly to reach its fully developed stage, the vibration and noise increase significantly. In addition, the downstream pressure continues to increase as shown in Table 6-6.

Table 6-6: Values of P_1, P_2, *K* and σ associated with Figure 6-25.

Flow rate (m^3/h)	P_1 (bar)	P_2 (bar)	P_1-P_2	P_V at 20°C	*K*	Cavitation Index (σ)	Appreciation of (σ)	Flow stages
0.55	1.503	1.027	0.476	0.023	0.32	3.10	No cavitation	Stage 1
0.66	1.741	1.044	0.697	0.023	0.41	2.46	No bubble activity	
0.77	2.028	1.063	0.965	0.023	0.48	2.07	Turbulence builds	
0.88	2.432	1.089	1.343	0.023	0.56	1.96	Some bubble forming	
0.99	2.839	1.115	1.724	0.023	0.61	1.83	Some cavitation might occur	Stage 2
1.05	3.082	1.131	1.951	0.023	0.64	1.70	Incipient cavitation	
1.09	3.212	1.140	2.072	0.023	0.65	1.69	Cavitation occurs	Stage 3
1.15	3.547	1.160	2.387	0.023	0.68	1.61	Cavitation occur	
1.20	3.694	1.170	2.524	0.023	0.69	1.53	Fully developed cavitation	
1.25	3.969	1.188	2.781	0.023	0.70	1.32	Flashing could occur	

The relation between the flow rate (m^3/h) and AE-Count of the globe valve for stages 1 and 2 are shown in Figure 6-26. In stage 1, increasing the flow rate from 0.55 to 0.75 m^3/h gives to an approximately constant low level of AE-Count value because there is no bubble activity. Between 0.75 and 0.87 m^3/h, the AE-Count slowly increases with increase in the flow rate to about 100, due to some bubbles forming. This is the stage in which some cavitation might occur.

For flows between 0.87 and 1.00 m^3/h there is a steep rise in the AE-Count due to the growth of cavitation. With increasing flow rate and increasing cavitation, the AE-Count continues to rise until about K= 0.64 when cavitation is fully developed. This is the maximum point of stage 3, as shown Figure 6-26. The AE-

Count increased as the bubble activity increased, reaching a maximum of about 1800 at stage 2, which is due to bubble formation.

With incipient cavitation, the AE-Count continues to increases with flow rate until at about 1.05 m^3/h, the cavitation index approaches 1.7 and at a flow rate of 1.15 m^3/h, the cavitation index falls to 1.61, where cavitation is likely to be fully developed stage. The sharp rise in the average count in Figure 6-26 confirm that cavitation becomes fully developed.

Following this, with an increase in pressure difference (P_1-P_2) across the globe valve, the cavitation index (σ) gradually decreases until it reaches a value at which some bubbles have a chance to travel downstream without collapsing, as shown in Table 6-6, and flashing could occur .

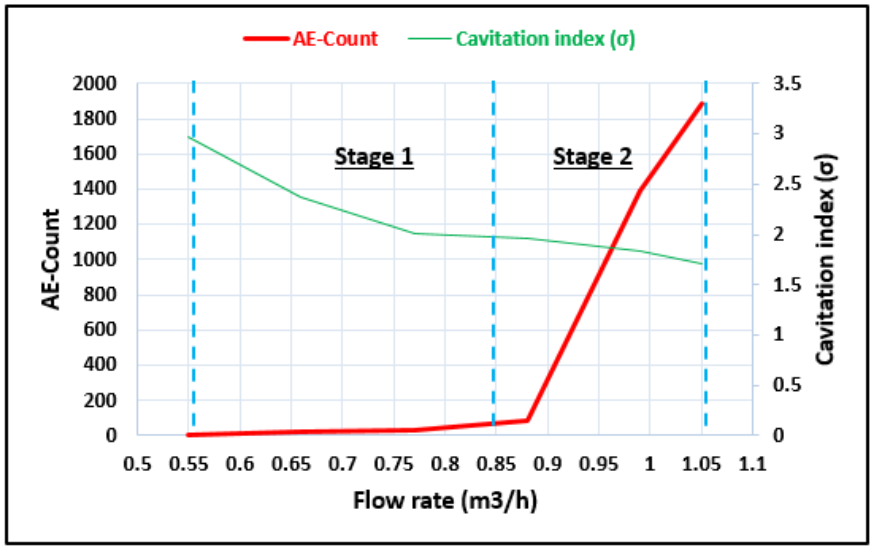

Figure 6-26: AE-Count as a function of flow rate for stages 1 and 2 (sensor 2), for tap water at 20^0C.

6.2.2 Statistical analysis of AE parameters for bubble activity in globe valve using tap water and demineralized water

The bubble formation in a globe valve depends on the liquid and flow rate. Thus the bubble formation events were statistically analysed to determine the critical AE parameter indicator for bubble activity detection. Tables (6-7) and (6-8), for comparison, show the average values of measured AE parameters; AE-Rise Time, AE-ASL, AE-Frequency and AE-RMS for tap water and demineralized

water respectively. Measurements made by sensor 2 for three stage 1 flow rates (0.55, 0.66 and 0.77 m^3/h). These statistical parameters were obtained directly from the AE system (AEWin). The average of values set out in Tables (6-7) and (6-8) were taken from three test samples.

Table 6-7: Comparison of AE parameter for tap water, globe valve open 40^0, for three stage 1 flow rates.

Flow rate (m^3/h)	Tap Water			
	AE Parameters			
	AE-Rise time (mμ)	AE-ASL (dB)	AE-Frequency (kHz)	AE-RMS (mV)
0.55	45	12	119	0.2
0.66	131	14	92	0.3
0.77	140	16	72	0.4

Table 6-8: Comparison of AE parameter for demineralised water, globe valve open 40^0, for three stage 1 flow rates.

Flow rate (m^3/h)	Demineralized Water			
	AE Parameters			
	AE-Rise time	AE-ASL (dB)	AE-Frequency (kHz)	AE-RMS (mV)
0.55	299	17	30	0.5
0.66	1375	19	18	0.6
0.77	8475	26	38	1.2

The results show that when the flow rate increases, AE-Rise time, AE-ASL, and AE-RMS all increase see Figures (6-27), (6-28) and (6-30) respectively. However the averaged value of AE-Frequency shows a steady decrease with increase in flow for tap water and an initial decrease for demineralised water, see Figure (6-29).

Figure 6-27 shows that for demineralized water, the AE-Rise time increases with flow rate. At a flow rate of 0.77 m^3/h the value of AE-Rise time increased to 8475

μs, indicating that some bubbles had started to form and flow turbulence was occurring. For tap water, the value of the AE-Rise time was stable during stage 1, because no bubbles occurred. This signal was caused by flow turbulence.

The value of AE-Rise time for demineralized water was higher than that for tap water, possibly reflecting its lower values of viscosity, surface tension and density.

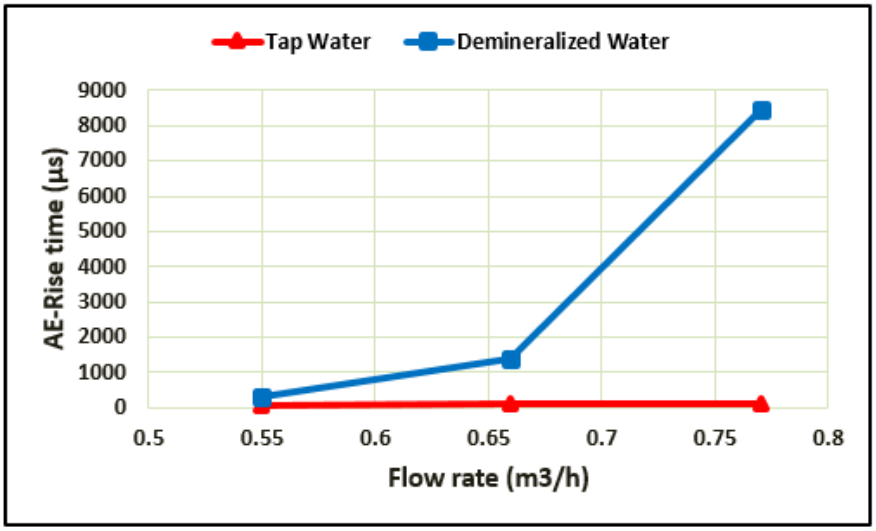

Figure 6-27: AE-Rise time as a function of the flow rate for tap water and demineralised water, globe valve open 40^0.

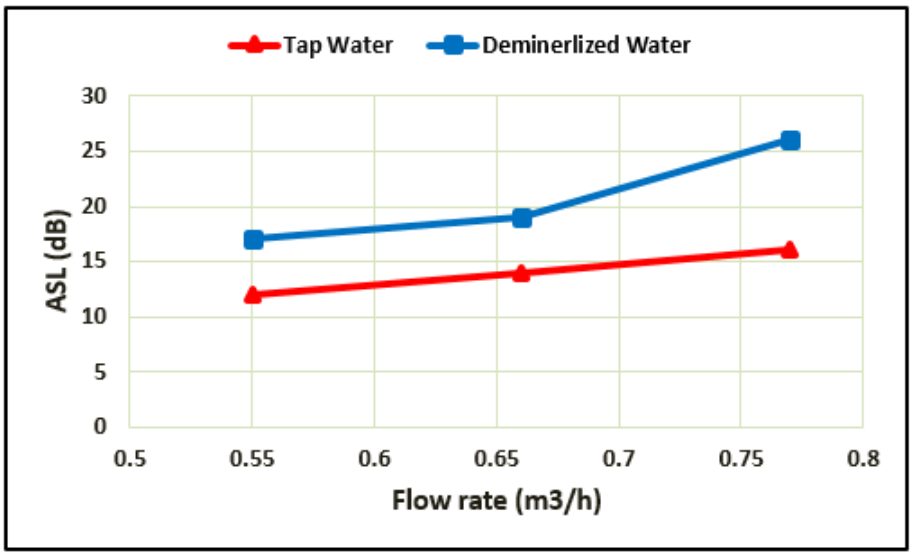

Figure 6-28: AE-ASL as a function of the flow rate for tap water and demineralised water, globe valve open 40^0.

In contrast, Figure 6-29 shows the AE-Frequency decreases with increasing flow rate and bubble activity. The frequency of cavitation bubble depends on the size of the bubble. Larger bubbles generate lower frequencies but release greater energy, and smaller bubbles produce a higher frequency and can form near to the surface [16][182].

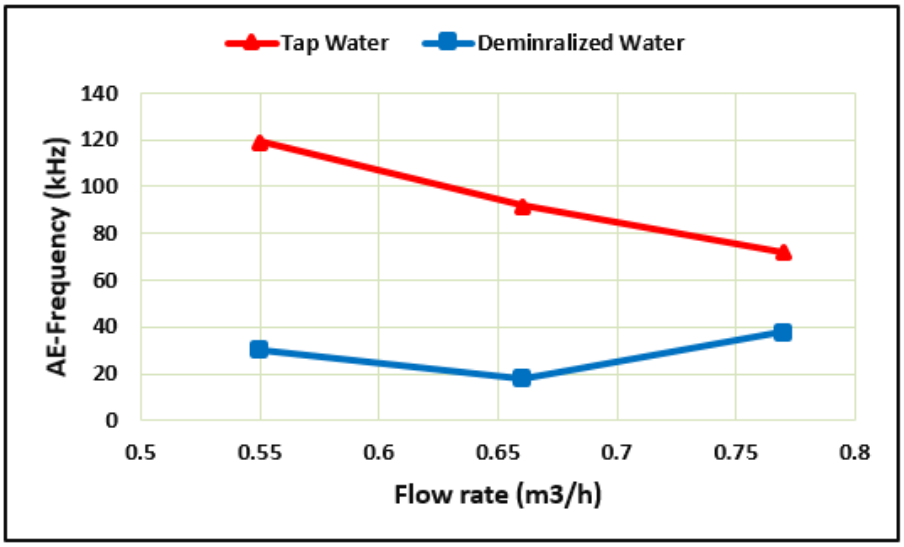

Figure 6-29: AE-Frequency as a function of the flow rate for tap water and demineralised water, globe valve open 40^0.

Figure 6-30 shows a clear and consistent increase in AE-RMS with flow rate with both demineralized water and tap water. The value of the AE-RMS was consistently higher for demineralised water than tap water. For flow rates above about 0.66 m^3/h the rate of increase of AE-RMS for demineralised water was much greater than for tap water. This is because of the differences in the relevant physical properties such as surface tension and viscosity. It has been suggested that the greater viscosity of the tap water might attenuate the signal more than for demineralised water and this could be a factor in the difference in the measured values [14][27].

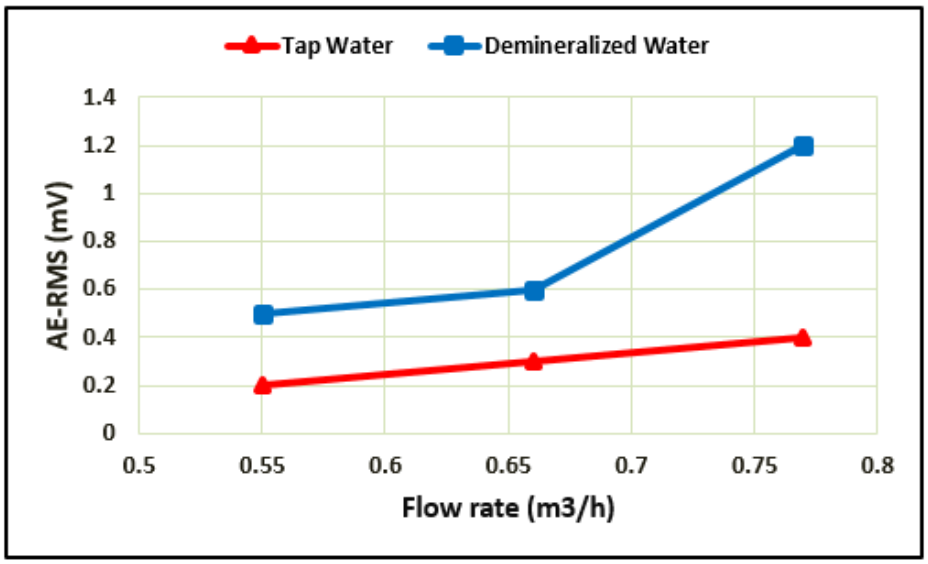

Figure 6-30: AE-RMS as a function of the flow rate for tap water and demineralised water, globe valve open 40^0.

6.2.3 Waveform analysis: AE duration and AE energy

Table 6-9 shows the values of AE-Duration and AE-Energy for tap water and demineralized water measured by sensor 2.

Table 6-9: Comparison of AE-Duration and AE-Energy for bubble formation in tap water and demineralized water globe valve open 40^0, for three stage 1 flow rates.

Flow rate (m3/h)	Tap Water		Demineralized Water	
	AE Parameters		AE Parameters	
	AE duration (µs)	AE energy (atto-joule)	AE duration (µs)	AE energy (atto-joule)
0.55	124	0.0233	617	0.22
0.66	433	0.4005	2919	1.88
0.77	445	0.5406	24989	31.00

The durations of AE transients were determined for three stage 1 flows and tabulated in Table 6-9. The AE-Duration is a measure of the average value of bubble occurrence duration. AE-Duration as measured by sensor 2 is plotted in Figure 6-31 for both liquids. The average AE-Duration increases with increasing

flow rate and bubble size in demineralized water, as shown in Figure 6-31. The average bubble formation duration in demineralized water was higher than in tap water: 24989 and 445 µs respectively, which implies that media properties such as viscosity, surface tension and density affect the wave propagation. The strength of the signal (from the potential energy of the bubble formation) increases as the flow rate increases in both liquids. Different liquid types, and their properties affect the AE signal [14][27][162].

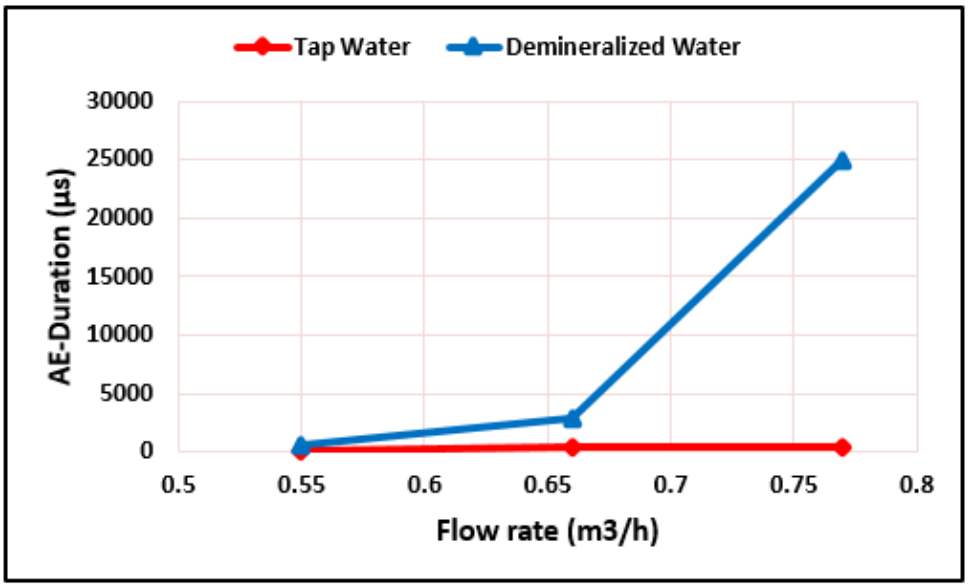

Figure 6-31: AE-Duration as a function of the flow rate for tap water and demineralised water, globe valve open 40^0.

The AE energy measured for bubble formation events associated with different flow rates and liquids is presented in Table 6-9. The AE-Energy increases with increasing flow rate, as shown in Figure 6-32. Differences in the overall AE signals between the tap water and demineralized water were attributed to differences in fluid properties that caused differences in the bubble event rate, bubble size and cavitation.

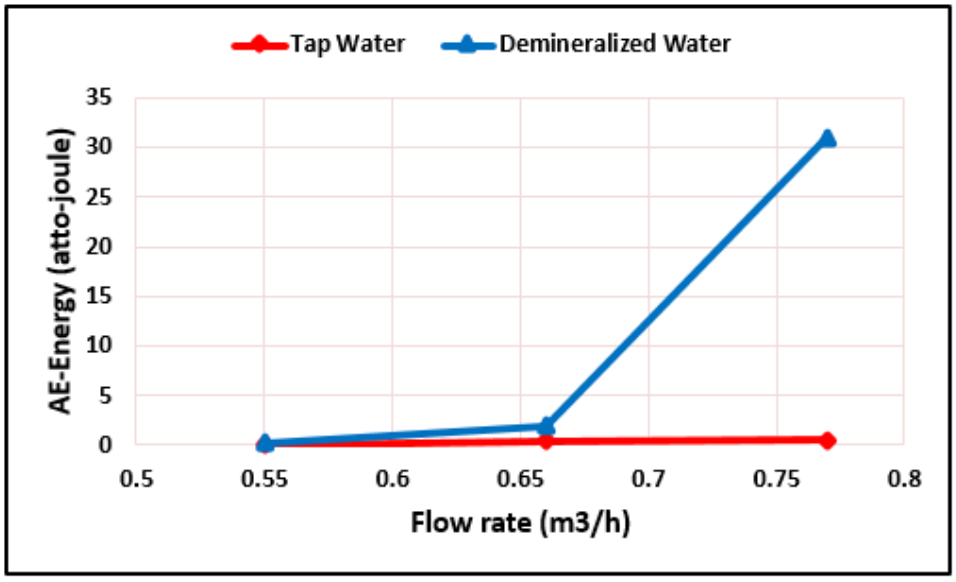

Figure 6-32: AE-Energy as a function of the flow rate for tap water and demineralised water, globe valve open 40^0.

6.2.4 Waveform analysis; AE amplitude for flow through globe valve using tap water

Observations of the AE waveform, sampled at 5 MHz showed interesting changes in the signal characteristics as a function of flow rate. Typical AE waveforms recorded after the system had time to reach equilibrium are presented in Figure 6-33. The three flow rates, 0.77 m^3/h, 0.99 m^3/h and 1.15 m^3/h represent the upper ends of stages 1, 2 and 3.

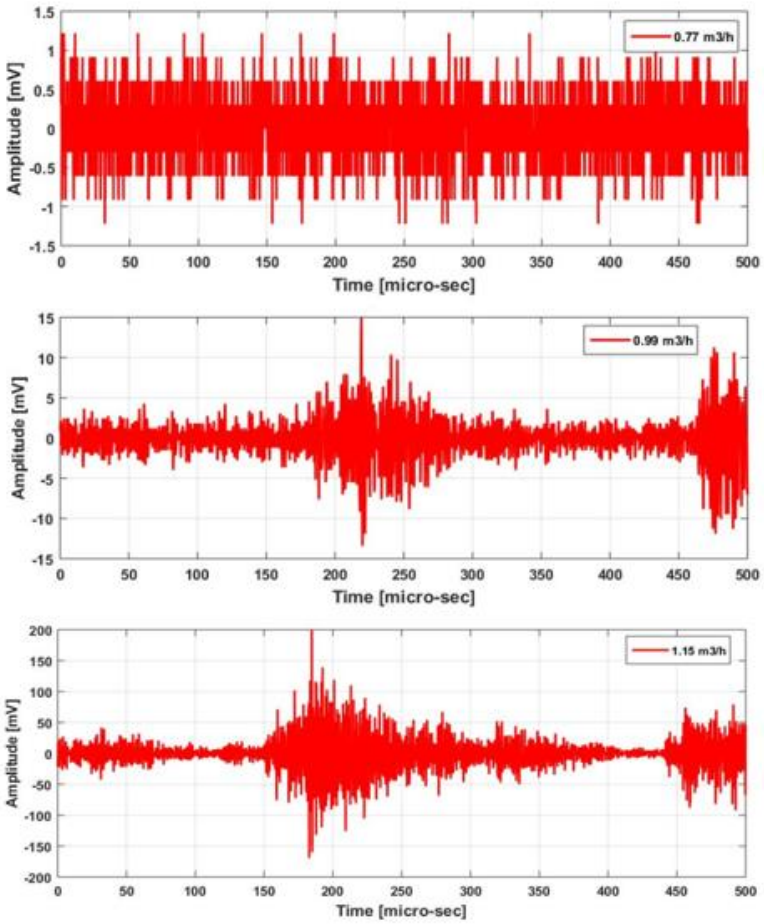

Figure 6-33: Time domain of AE waveforms for globe valve open 40^0, for tap water at three flow rates.

At stage 1 (0.77 m^3/h), bubbles do not form (no cavitation is occurring) and the vibration created by the turbulence in the flow is negligible; the peak AE amplitude reached only 1.0 mV. Increasing the flow rate to 0.99 m^3/h (stage 2) shows greater vibration due to flow turbulence and clear peaks occur in the AE amplitude. Bubbles start to form downstream of the valve. The onset of cavitation occurs with subsequent bubble collapse.

The magnitude of the peaks in the AE-Amplitude increased with increase in flow rate. At 1.15 m^3/h (stage 3), with the increased pressure difference across the valve more bubbles form. The onset of cavitation occurs with subsequent bubble collapse. The peak AE-Amplitude rose to 200 mV, as shown in Figure 6-33. The cavitation increased rapidly with increase in flow rate and a corresponding increase in vibration also occurred.

6.2.5 Effect of globe valve opening on AE signal using tap water

For AE signal analysis the first characteristic to be investigated was the AE-Count for each degree of valve opening with increasing flow rate. Figure 6-34 presents plots of AE-count against flow rate for three degrees of globe valve opening; 40^0, 50^0 and 80^0. It was observed that when globe valve opening was 40^0 the AE-Count remained close to zero until a flow rate of 0.9 m^3/h. Above 0.9 m^3/h high-frequency vibration and noise were noted, indicating the presence of bubble formation and collapse into micro-jets, generating pressure waves that produced the high-frequency vibration. From 0.9 m^3/h to about 1.15 m^3/h there was a steady increase in AE-Counts, from near zero to about 2700. For flows above 1.15 m^3/h the AE-Counts increased sharply to a value of 7300 at a flow rate of 1.20 m^3/h, after which the rate of increase was not so large reaching 8000 at 1.25 m^3/h. Figure 6-34 gives a good sense of bubble formation and collapse with different degrees of valve opening.

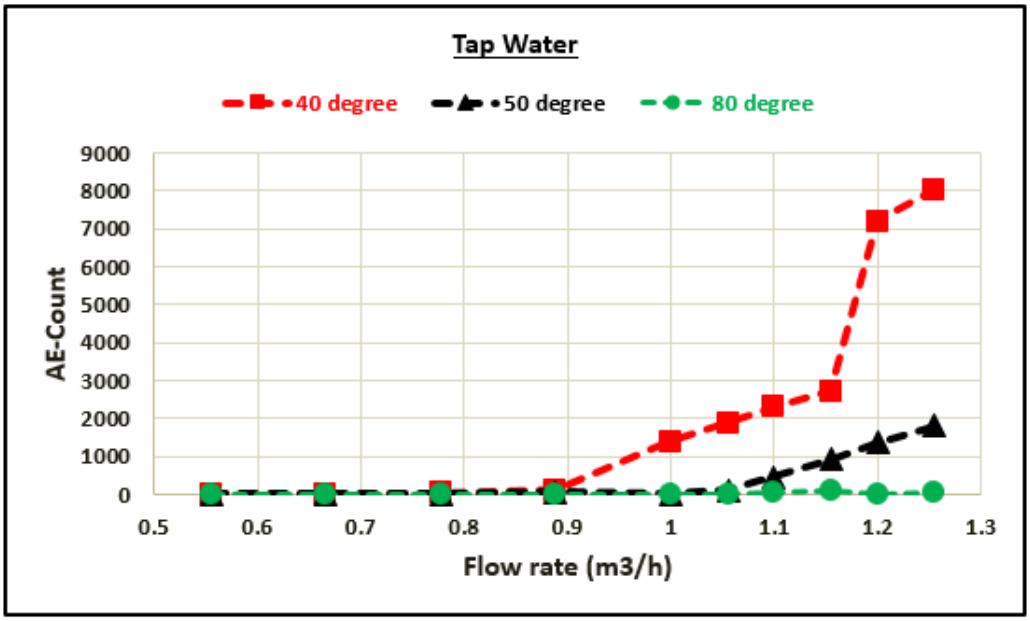

Figure 6-34: AE-Count measured by sensor 2, as a function of flow rate for three degrees of globe valve opening, for tap water at 20^0C.

AE-Counts fell substantially when the valve was opened first to 50^0 and then to 80^0. The AE-Count for the valve open at 50^0 remained close to zero until the flow rate was about 1.05 m^3/h. After which it rose steadily to just under 2000 at 1.25 m^3/h. For the valve open at 80^0 the AE-Count remained close to zero for all flow

rates. This means that for the same opening percentage, the higher flow rates generate higher AE-Counts, indicating the occurrence of cavitation.

6.2.6 Effect of different liquid types on AE-Count in globe valve

The valve opening was set at 40^0. A sharp transition in the AE-Count occurs for demineralized water at around 0.66 m^3/h, as shown in Figure 6-35. This change indicates the presence of incipient cavitation. With increase in flow more bubbles were formed and cavitation reached its fully developed stage for a flow rate of 1.15 m^3/h. In tap water, there was a gradual increase in the AE-Count from about 0.9 m^3/h and a steady increase in AE-Count until about 1.15 m^3/h (AE-Count = 2800) after which it rose sharply to about 7000 at 1.20 m^3/h. It followed that the chance of cavitation occurring in demineralized water is much larger than for tap water. This could be because viscosity, surface tension and density of tap water are higher than for demineralized water.

With a globe valve open at 40^0, and demineralised water with flow rate of 0.70 m^3/h, incipient cavitation may occur. On the other hand, under the same flow conditions with tap water there is no cavitation.

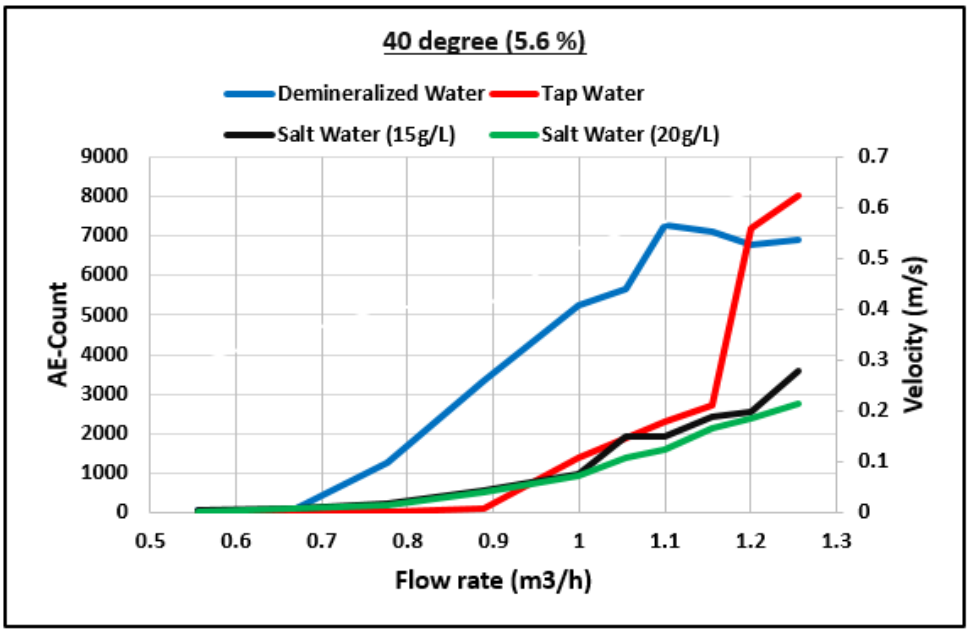

Figure 6-35: AE-Count against flow rate for demineralised water, tap water, and salt water, globe valve open at 40^0 (measurements made with sensor 2, at 20^0C).

Regarding salt water, for both concentrations, 15 g/L and 20 g/L, the AE-Count was much less than for the demineralised water, and less than for tap water above about 1.0 m^3/h. At a flow rate of 1.25 m^3/h the value of AE-Count for salt water (20g/L) ranked the lowest with 2800. It is confirmed that different liquid types have an effect on bubble occurrence for a given flow rate.

6.2.7 Frequency domain analysis of bubble activity with different liquids at 0.99 and 1.2 m^3/h.

Fourier analysis can help detect the frequency characteristics of bubble occurrence in different liquids, see Figure 6-36. The peak value of AE signal for the demineralized water ranked the highest with 0.5 mV, at 300 kHz.

The frequency domain analysis, as plotted in Figure 6-36, shows many peaks associated with bubble collapse. In this experiment, the peak frequency at 300 kHz which is the highest peak amongst the frequency components was chosen to show changes in amplitude with bubble activity. The averaged AE-Frequency spectra (averaged over 10 test-samples) showed an increase in amplitude with decreasing density, surface tension and viscosity for all four liquids.

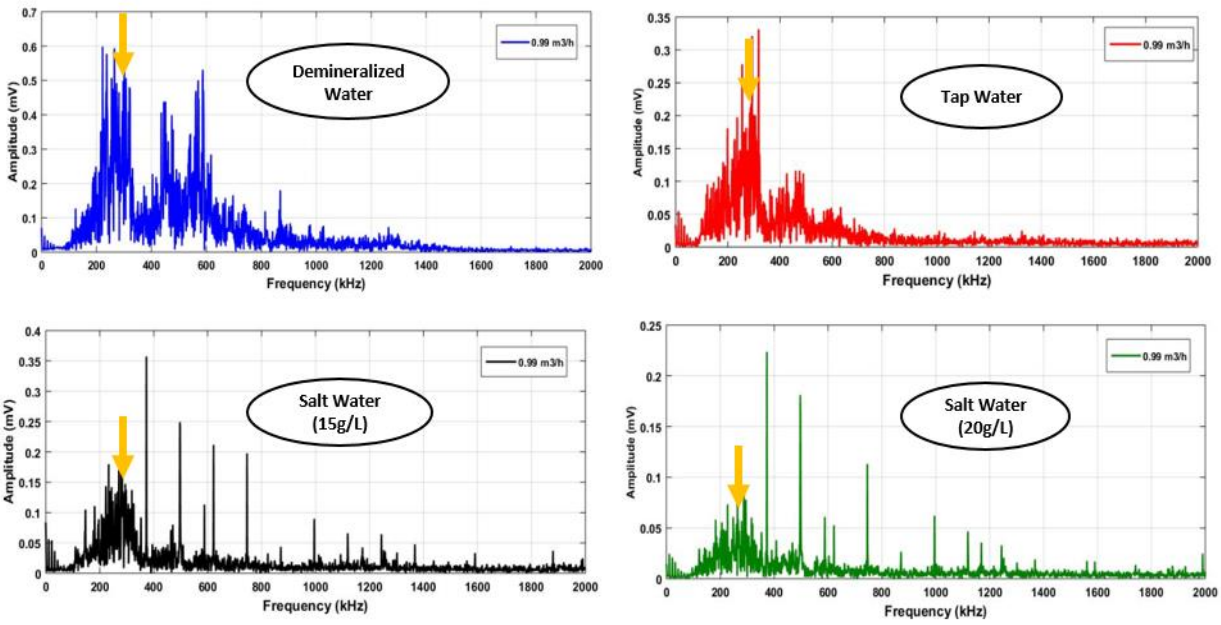

Figure 6-36: FFT frequency spectrum of bubble activity for four fluids with globe valve open 40^0, and flow rate 0.99 m^3/h (sensor 2).

Table 6-10 shows the comparison of peak amplitude at frequency 300 kHz for different liquids: demineralized water, tap water and salt water for two flow rates (0.99 and 1.2 m^3/h). It is clear that the amplitude of the peak for demineralised water is highest for both flow rates with 0.5 and 50 mV respectively.

Table 6-10: Comparison of amplitude of peak at 300 kHz for different liquids for two flow rates, 0.99 and 1.2 m^3/h.

Frequency	Demineralized water	Tap water	Salt water (15g/L)	Salt water (20g/L)
Peak amplitude at 300 kHz in 0.99 m^3/h	0.5 (mV)	0.22 (mV)	0.15 (mV)	0.07 (mV)
Peak amplitude at 300 kHz in 1.2 m^3/h	50 (mV)	12 (mV)	0.30 (mV)	0.15 (mV)

The peak for the 1.2 m^3/h flow rate is increased by a factor of 100 with respect to the peak for 0.99 m^3/h. This is a much larger relative increase than for any of the other liquids considered.

Figure 6-37 presents the AE-Spectra for the four liquids for a flow rate of 1.2 m^3/h. It was observed that the AE signal increased with decrease in the viscosity, surface tension and density of the liquid [27][162]. It is known that adding salt to water increases both the surface tension and the viscosity but, under the conditions of the experiments the two effects cannot be separated and so it is concluded that the lower the viscosity, surface tension and density, the higher the amplitude of the peak at 300 kHz.

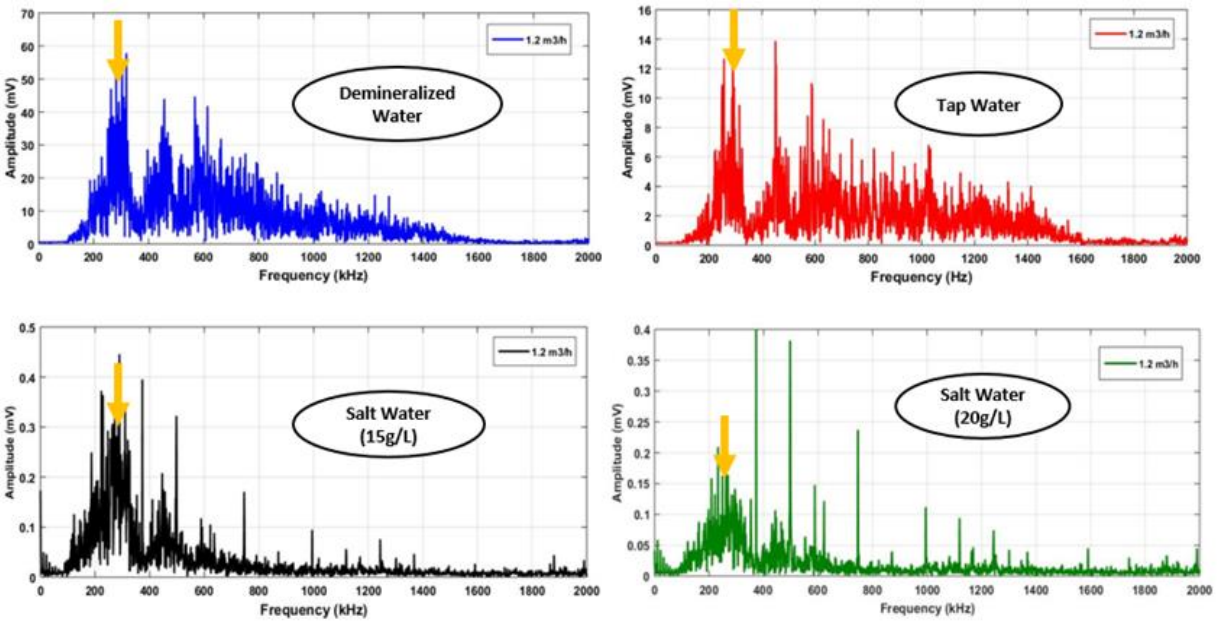

Figure 6-37: Average frequency spectrum for bubble activity at 5.6 % (Sensor 2), and 1.2 m^3/h.

6.2.8 Effect of temperature on AE signal levels in globe valve with tap water

Figure 6-38 shows how increasing the flow rate through the globe valve increases the AE-Count for a range of temperatures; 20, 35, 40, 45 and 50^0C. The figure provides a good sense of the development of cavitation. For the same flow rate, the AE-Count increases with increase in temperature due to changes in the physical properties of the fluids - viscosity, surface tension and density decrease with increase in temperature - so cavitation bubbles form more easily.

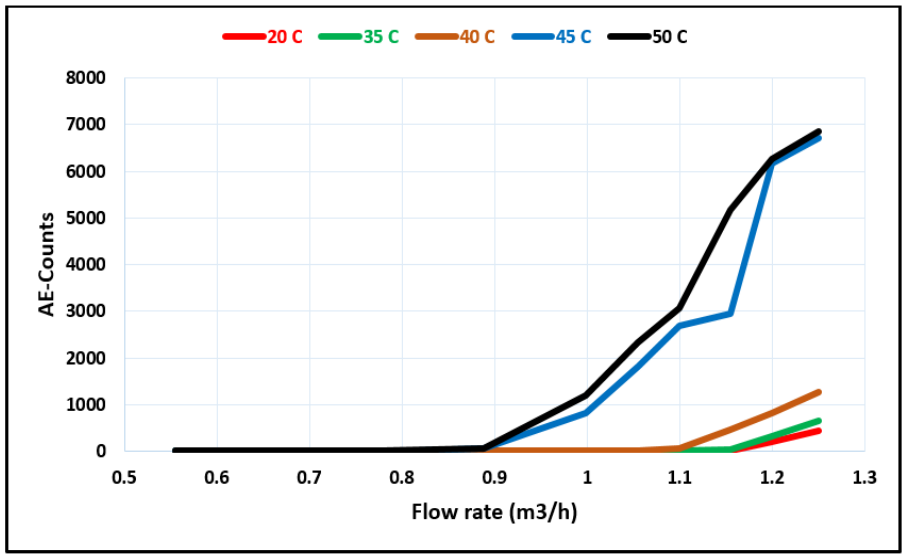

Figure 6-38: AE-Count with flow rate of tap water through globe valve open 55^0 (7.6%), for four temperatures: 20, 35, 40, 45 and 50^0C (sensor 2).

The difference between AE transient events with temperature of the tap water are presented in Figure 6-39 and are obvious. Here the flow rate was 1.15 m^3/h. It was found that the AE signal increased with tap water temperature as shown in Figure 6-39. In addition, it was found that the pressure difference across the globe valve increased as the water temperature increased. In these experiments, there is direct relation between pressure and temperature; when the temperature of the water increased in from 20 to 50^0C, the pressure difference increased in from 0.849 to 1.171 bar, with a corresponding increases in K from 0.42 to 0.53, and a corresponding decrease in the value of the cavitation index from 2.32 (no cavitation) to 1.87 (cavitation region). See Appendix D, Tables D-1 and D-5, pages (239-243).

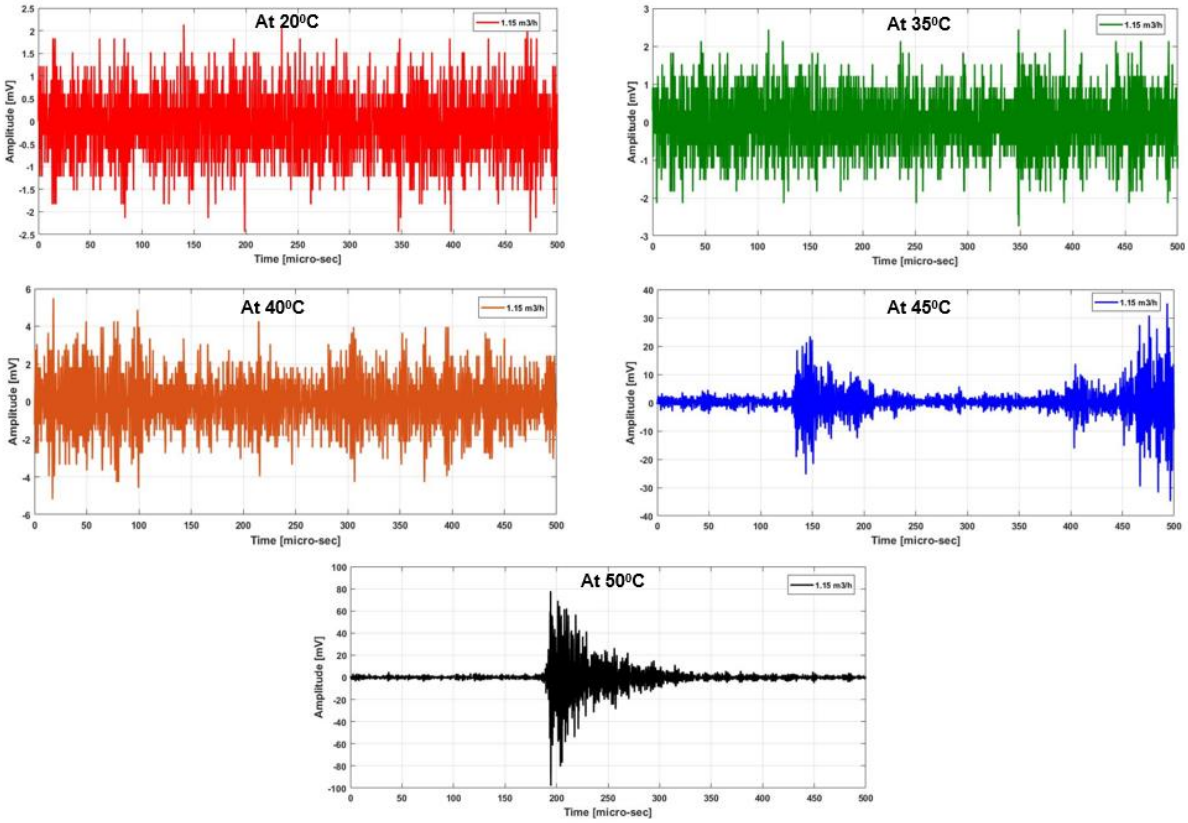

Figure 6-39: AE-Amplitude as a function in the time for tap water through globe valve open 55^0 (7.6%), for four temperatures: 20, 35, 40, 45 and 50^0C (sensor 2).

It was concluded that increasing the liquid temperature at the same flow rate and valve opening increased the AE-Count. For the range of temperatures investigated (20-50^0C) the AE-Energy levels, showed consistent but negligible changes see Figure 6-40. These observation suggest that it is generally permissible to neglect the effects of likely increases in fluid temperature generated by e.g. frictional forces in pipes and valves, or pumping effects, on the measured AE-Energy levels. It was observed that for a valve opening of 55^0 (7.6%), the increase in temperature resulted in increased AE-Energy. The value of AE signal is stable for temperatures of 35^0 and 40^0C for flow rates 0.55 and 0.66 m^3/h. This signal is generated by turbulent flow. Above 40^0C the AE-Energy gradually increases due to bubble generation. The value of AE-Energy increases with flow rate due to some bubbles inception at this stage.

It was noted that when the liquid temperature increased, the measured value of the AE signal increased except at the lowest flow rates.

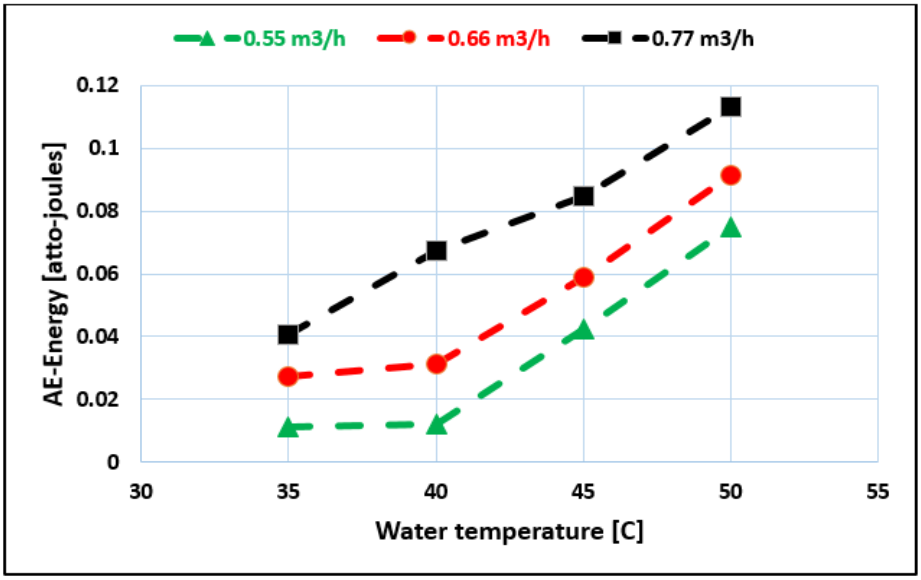

Figure 6-40: Temperature effect on the AE energy signal for globe valve open 55^0 (sensor 2), flow rates limited to stage 1.

6.2.9 Effect of pressure difference on AE signal levels in globe valve at 50^0C using tap water

The AE waveforms measured by sensor 2, when the tap water temperature was about 50^0C, showed different waveforms depending on pressure difference, as shown in Figure 6-41. For pressure difference (0.283 bar), at 0.55 m^3/h, the cavitation index approaches 4.20, there is virtually no AE signal caused by bubble activity, where the AE signal is generated by turbulent flow. For a flow rate 0.99 m^3/h, it was observed that the value of AE-Amplitude increased to as high as 2 mV, this was for a pressure difference 0.882 bar and a cavitation index of 2.11. At this stage, some bubbles were formed, as the pressure difference increased. At flow rate 1.15 m^3/h, cavitation index of 1.87, the AE-Amplitude reached to 40 mV, and AE-Counts to approximately 5500 due to greater bubble activity and incipient cavitation. At 1.25 m^3/h, cavitation index 1.78, the value of AE-Amplitude increased to about 400 mV; bubble activity increased, cavitation grew rapidly until it reached its fully developed stage, the vibration and noise increase substantially, as shown in Figure 6-41. If Tables D-1, as shown in Appendix D and 6-11 are compared it can be seen that when the temperature of the water is increased - in this case from 20^0C to 50^0C - the value of the cavitation index for a given flow rate will decrease substantially, depending on the flow rate, but typically by about

20%. This means, of course, that the likelihood of cavitation is significantly increased if the liquid is warmer rather than colder.

Table 6-11: P_1, P_2, *K* and σ at 55^0 associated with Figure 6-41, 50^0C.

Flow rate (m^3/h)	P_1 (bar)	P_2 (bar)	(P_1-P_2), (bar)	k	Cavitation Index (σ)
0.55	1.313	1.030	0.283	0.23	4.20
0.66	1.468	1.044	0.424	0.31	3.17
0.77	1.625	1.062	0.563	0.37	2.66
0.88	1.796	1.083	0.713	0.42	2.34
0.99	1.989	1.107	0.882	0.47	2.11
1.05	2.107	1.121	0.986	0.49	2.01
1.09	2.191	1.131	1.060	0.51	1.95
1.15	2.322	1.151	1.171	0.53	1.87
1.20	2.391	1.161	1.230	0.54	1.84
1.25	2.506	1.174	1.332	0.55	1.78

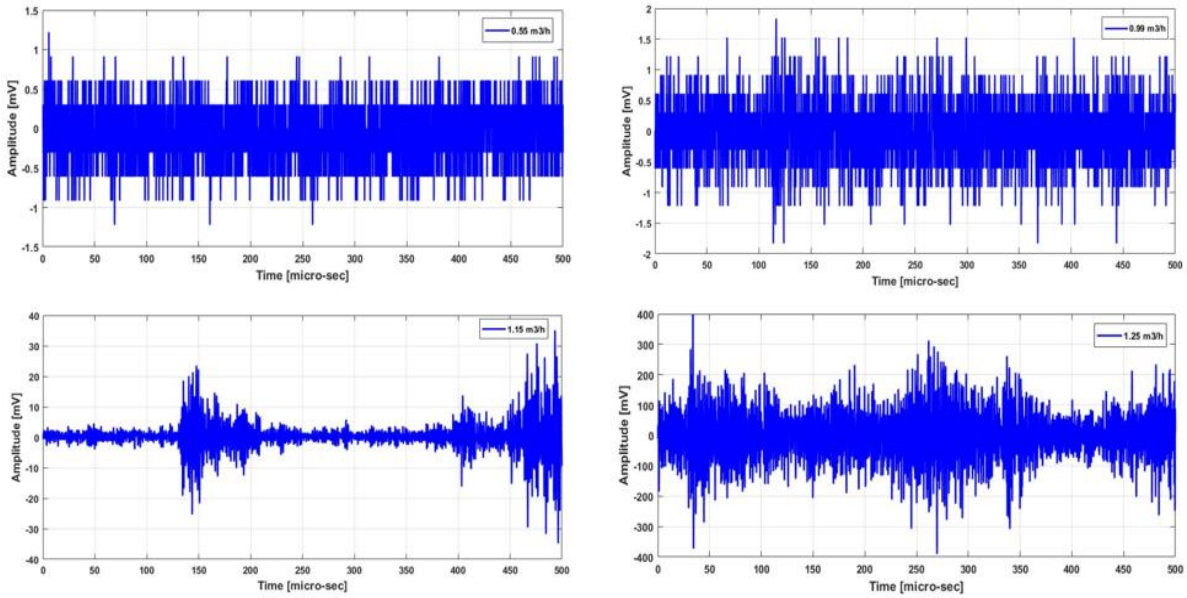

Figure 6-41: AE-Amplitude for tap water through globe valve open 55^0, for different inlet pressures, temperature 50^0C (sensor 2).

6.3 Effect of geometric shape of valves on AE signal levels using tap water

Figure 6-42 shows the plots of AE-Count vs flow rate for ball and globe valves for the same opening percentage (16.7%). For the ball valve a nonlinear relation is obvious.

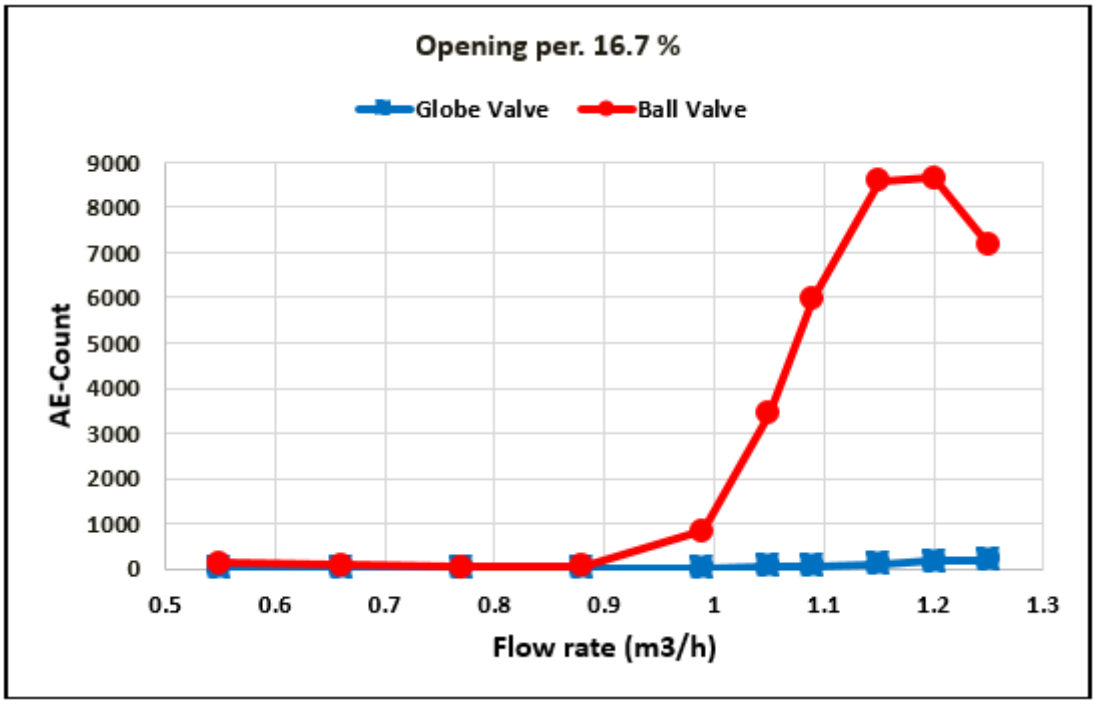

Figure 6-42: Influence of geometric on AE signal levels in both valves (ball & globe) for Sensor 2.

It can be seen that for the ball valve the AE-Count increased with flow rate, as shown in Figure 6-42 (see also Figure 6-3). For the ball valve, the point at which AE-Count begins to increase rapidly is close to the flow rate (0.9 m^3/h) at which incipient cavitation occurs. Before that vibration generated by turbulent flow and bubble formation is the source of the counts. The value of AE-Count peaked at about 8500 at 1.2 m^3/h due to cavitation.

For globe valve at the opening percentage (16.7 % fully open), the AE-Count remained close to zero, because there was no occurrence of bubbles (no cavitation). It was concluded that the geometric shape of valves has a major effect on AE signal levels.

The application of AE as a method for detection of bubble formation and collapse at the early stages in valves, provides an early warning of reduced efficiency, necessary maintenance, incipient failure and increased costs.

6.4 Conclusion

Experimental investigations have been conducted to relate pressure drop across and flow through ball and globe valves to resulting cavitation. The effect of open percentage of the valves, the water temperature and different fluids were investigated.

An AE technique was employed to monitor and detect bubble occurrence at an early stage. The AE technique used can detect and monitor bubble formation in ball and globe valves with a high degree of sensitivity. The results obtained have demonstrated the ability of AE to diagnose whether or not a ball and globe valve is being subjected to cavitation. The ball valve was opened at 15^0, and the globe valve opened at 40^0, it was found that cavitation from its inception to being fully developed can be detected by analysing the AE signals. A correlation between AE signals and threshold levels was noted; when the threshold levels increase, the value of AE signal decreases.

The present study concludes that undesired cavitation phenomenon can be attributed to flow geometry, upstream pressure and flow rate and that collapsing bubbles at higher flow rates generate higher amplitude AE signals. The results also demonstrate that incipient cavitation at lower flow rates can be detected using AE methods. This could enable reduction in erosion and pitting, and provision of safer working conditions. Finally, it can be said that the AE signals obtained using this technique can distinguish between different types of bubble formation and collapse. Additionally, and importantly, the AE signal were shown to be able to distinguish between different fluids and different liquid temperatures.

Chapter 7 Conclusions and recommendation for future work

7.1 Conclusions

This work has presented the application of Acoustic Emission to the diagnosis and monitoring of bubble formation and incipient cavitation in pool boiling and flow through ball and gate valves. It has been shown that the presence of bubble formation in both the boiling processes and valves is detectable using AE signals. AE parameters such as AE-RMS, AE-Energy, AE-Amplitude, AE-Rise time and AE-Count, are sensitive, robust and reliable measures for detection and monitoring of bubble activity in two-phase systems. The AE measured in this research covered the frequency range 100 kHz to 1 MHz for pool boiling, and 20 kHz to 1 MHz in the valve tests. It was demonstrated that an AE piezoelectric sensor can detect pressure pulses associated with bubble occurrence during pool boiling and cavitation in flow through valves.

The monitoring of bubble formation using AE technology can complement other condition monitoring methods, all of which are aimed at reducing energy losses and improving life cycle costs. AE technology is capable of detecting the dynamic formation, collapse and bursting of bubbles and could be used to predict the incidence of boiling in, say, nuclear reactors. This is also the case for monitoring of heat exchanger systems in industrial chemical processes, detecting bubble occurrence in the petrochemical industry, detecting gas layers in oil drilling, and monitoring and detection of cavitation phenomena in centrifugal pumps and valves.

This thesis has shown that the AE technique provides an efficient detection and monitoring method for bubble formation in two-phase flow systems and that these results contribute to the development of AE technology.

In summary, the conclusions are:

- The AE technique has been shown, experimentally, to be capable of detecting and monitoring bubble formation at an early stage in pool boiling.

- It was demonstrated that the liquid free surface level, liquid type, AE sensor position and rate of power supply to the heated surface have an effect on AE signal levels measured during the pool boiling process.
- It was established that bubble formation, burst, and collapse in both pool boiling and valves can be diagnosed and monitored using AE parameters measured in the time and frequency domains.
- It was established that signal threshold levels have an effect of on AE energy levels in pool boiling and valves, where AE signal levels decrease with increasing threshold levels.
- It was established that AE measurements can detect and diagnose bubble formation and collapse in valves.
- It was established from AE measurements that for flow control valves: the flow rate through the valve, liquid temperature, pressure difference across the valve, degree of valve opening and the characteristics of the fluid flowing all have an effect on bubble formation and collapse (cavitation development).

The successful detection of bubble occurrence in these experiments has provided a basis for the application of AE technique to measure flow parameters in two-phase systems such as boiling processes and valves. In addition, AE technology offers a simple non-invasive method which can be applied to metal pipes and opaque liquids. This technology could be instrumental in monitoring the flow of various multi-phase conditions as experienced in numerous industries.

7.2 Recommendation for future work

The results of the investigation into the use of AE techniques for monitoring of bubble formation during pool boiling and cavitation in valves were encouraging, and it is hoped that future researchers will further explore its potential. The AE signal emitted by bubble formation at the bottom during pool boiling and cavitation in valves clearly depends on the properties of the liquid. More investigation is

needed of the influence of these properties on the AE signal from bubble activity. It is known that both viscosity and surface tension are major factors in bubble formation and cavitation, but in the experiments carried out here the test conditions were such that when viscosity increased so did the surface tension, and vice versa.

To successfully develop the applications of AE technique to the monitoring of bubble formation and collapse under the influence of different flow conditions during pool boiling and through valves the following could be further investigated:

- Surface tension: develop a method to investigate the influence of surface tension on the AE signal levels generated by bubble occurrence during pool boiling and flow through valves. The effectiveness of such a method would be greatly enhanced if it allowed the viscosity to remain constant.
- Liquid viscosity: Tests to be carried out using fluids of different viscosities, possibly oils with different grades, on the AE signal levels generated by bubble occurrence during pool boiling and flow through valves. The effectiveness of such a method would be greatly enhanced if it allowed the surface tension to remain constant.
- Extend the investigation on surface tension and viscosity to attempt to determine if surface tension factors are more important for bubble formation and viscosity for bubble collapse.
- Pressure: to detect the effect of pressure parameters such as vacuum pressure and under-pressure on bubble formation and AE signal during boiling in vessels.
- Boiler wall thickness: effect of different wall thickness, surface quality, and variation in surface roughness on AE signal levels.
- Valve diameter: influence of different orifice diameters on AE signal levels. If the flow enters the valve smoothly does that produce less bubble formation, whereas a mismatch in inlet pipe diameter and valve could induce flow perturbations that enhanced bubble formation.

- Differentiate between AE-signals for bubble formation and bubble collapse in valves using AE technique.

REFERENCES

[1] M. Farhat, D., Obreschkow, P., Kobel, N., Dorsaz, and A., De Bosset, “Interaction of a cavitation bubble with a spherical free surface,” Sixth Int. Symp. On Cavitation, Wageningen, the Netherlands, September 2006.

[2] M. J. Petkovsek R, Mocnik G, “Measurements of the high pressure ultrasonic wave and the cavitation bubble by optodynamic method,” *Fluid Phase Equilibr*, no. 256, pp. 158–162, 2007.

[3] M. Szkodo, “Cavitation erosion behaviour of laser processed Fe-Cf-Mn and Fe-cr-Co alloys,” *J. Achiev. Mater. Manuf. Eng.*, no. 1–2, pp. 239–242, 2006.

[4] P. M. Neill, G.D., Reuben, and R., Sandford, “Detection of Incipient Cavitation in Pumps using Acoustic Emission.,” *J. Process Mech. Eng.*, vol. 211, no. 4, pp. 267–277, 1997.

[5] J. Yan *et al.*, “Nondestructive Detection of Valves Using Acoustic Emission Technique,” Advances in Materials Science and Engineering Volume 2015, 2015.

[6] E. Christopher, Brennen, *Cavitation and bubble dynamics*. Oxford: Oxford University Press, 1995.

[7] W. Lauterborn and C. D. Ohl, “Cavitation bubble dynamics,” *Basic Eng. Am. Soc. Mech. Eng.*, vol. 4, no. 2, pp. 65–75, 1997.

[8] A. J. Leighton, and T., Walton, “An experimental study of the sound emitted from gas bubbles in a liquid,” *Eur. J. Phys.*, vol. 8, pp. 98–104, 1987.

[9] M. S. Plesset, “Shockwaves from Cavity Collapse,” *R. Soc.*, vol. 260, pp. 241–244, 1966.

[10] C. Brennen, *Hydrodynamics of Pumps*, Oxford Uni. Cambridge University Press, 1994.

[11] M. Alssayh, “Slug Velocity Measurement and Flow Regime Recognition Using Acoustic Emission Technology,” PhD Thesis. Cranfield University, 2013.

[12] P. A. Corporation, “AE win PCI-2 Based AE System User’s Manual,” *Mistras Gr. Inc.*, vol. REV 3, no. April, pp. 1–312, 2007.

[13] P. Benes and M. Uher, “Identification of liquid boiling by acoustic emission,” *Fundam. Appl. Metrol.*, no. 1, pp. 1396–1401, 2009.

[14] Husin Shuib, “An experimental investigation into the correlation between Acoustic Emission (AE) and bubble dynamics,” PhD Thesis, Cranfield

University, 2011.

[15] T. Alhashan, M. Elforjani, A. Addali, and J. Teixeira, “Monitoring of Bubble Formation during the Boiling Process Using Acoustic Emission Signals,” *Int. J. Eng. Res. Sci.*, vol. 2, no. 4, pp. 66–72, 2016.

[16] A. I. and H. I. Carmi Rami , Bussiba Arie, “Detection of Transient Zones During Water Boiling by Acoustic Emission,” *Acoust. Emiss.*, vol. 29, pp. 89–97, 2011.

[17] T. Alhashan, A. Addali, and J. Amaral, “Experimental investigation of the influences of different liquid types on acoustic emission energy levels during the bubble formation process,” *Int. J. Energy Environ. Eng.*, 2017.

[18] M. Alssayh, A. Addali, D. Mba, and M. E. El-Alej, “Slug velocity measurement using acoustic emission technology,” *Proc. Inst. Mech. Eng. Part E J. Process Mech. Eng.*, vol. 230, no. 1, pp. 76–83, 2014.

[19] F. Elasha, M. Greaves, D. Mba, and D. Fang, “A comparative study of the effectiveness of vibration and acoustic emission in diagnosing a defective bearing in a planetry gearbox,” *Appl. Acoust.*, vol. 115, pp. 181–195, 2017.

[20] T. J. Fowler, “Chemical industry applications of acoustic emission,” *Mater. Eval.*, pp. 875–882, 1992.

[21] A. Addali, “Monitoring gas void fraction in two-phase flow with Acoustic Emission,” PhD Thesis. Cranfield University, 2010.

[22] W. M. Marto, and P., Rohsenow, “Effects of Surface Conditions on Nucleate Pool Boiling of Sodium,” *ASME J. Heat Transf.*, vol. 88, pp. 196–204, 1966.

[23] J. M. Mandhane, G. A. Gregory, and K. Aziz, “A flow pattern map for gas-liquid flow in horizontal pipes,” *Int. J. Multiph. Flow*, vol. 1, no. 4, pp. 537–553, 1974.

[24] A Addali, S. Al-lababidi, H. Yeung, D. Mba, and F. Khan, “Acoustic emission and gas-phase measurements in two-phase flow,” *Proc. Inst. Mech. Eng. Part E J. Process Mech. Eng.*, vol. 224, no. 4, pp. 281–290, 2010.

[25] T. Alhashan, A. Addali, J. Amaral Teixeira, and S. Elhashan, “Identifying bubble occurrence during pool boiling employing acoustic emission technique,” *Appl. Acoust.*, vol. 132, no. November 2017, pp. 191–201, 2018.

[26] N. Sinha, “Characterization of Liquids Using Gas Bubbles,” *United States Pat. No US 7,010,962 B2*, 2006.

[27] H. Shuib and D., Mba, “Acoustic emission of a single bubble activities,” in

Proceedings of the World Congress on Engineering 2010 Vol. II, 2010, vol. II, no. 0, pp. 0–5.

[28] M. S. Plesset, “Shockwaves from Cavity Collapse’,” *R. Soc. XXI*, p. pp 241-244, 1966.

[29] T. G. Leighton and A. J. Walton, “An experimental study of the sound emitted from gas bubbles in a liquid,” vol. 8, pp. 98–104, 1987.

[30] M. Minnaert, “On Musical Air-Bubbles and the Sounds of Running Water,” *Philos. Mag*, vol. 16, pp. 235–248, 1933.

[31] L. Pumphrey, and H., Crum, “Sources of ambient noise in the ocean and experimental investigation,” 1989.

[32] T. G. Leighton, “The acoustic bubble: Oceanic bubble acoustics and ultrasonic cleaning,” *Proc. Meet. Acoust.*, vol. 24, pp. 1–5, 2015.

[33] M. Strasberg, “Gas Bubbles as Sources of Sound in Liquids,” *J. Acoust. Soc. Am.*, vol. 28, no. 1, pp. 20–26, 1956.

[34] Deane G.B. and Czerski H.A., “Mechanism stimulating sound production from air bubbles released from a nozzle,” *ournal Acoust. Soc. Am.*, vol. 123, no. 126–132, 2008.

[35] R. Manasseh, R. F. LaFontaine, J. Davy, I. Shepherd, and Y. G. Zhu, “Passive acoustic bubble sizing in sparged systems,” *Exp. Fluids*, vol. 30, no. 6, pp. 672–682, 2001.

[36] M. S. Longuet-Higgins, “An analytic model of sound production by raindrops,” *J. Fluid Mech.*, vol. 214, pp. 395–410, 1990.

[37] M. S. Longuet-Higgins, “Monopole emission of sound by asymmetric bubble oscillations. Part 1. An initial-value problem,” *J. Fluid Mech.*, vol. 201, no. 1, p. 543, 1989.

[38] M. S. Longuet-Higgins, “Monopole emission of sound by asymmetric bubble oscillations, Part 2. An initial-value problem,” *J. Fluid Mech.*, vol. 201, pp. 543–565, 1989.

[39] M. Longuet-Higgins, “The release of air bubbles from an underwater nozzle,” *J. Acoust. Soc. Am.*, vol. 89, no. 4B, p. 2014, 1991.

[40] Y. Tomita, P. B. Robinson, R. P. Tong, and J. R. Blake, “Growth and collapse of cavitation bubbles near a curved rigid boundary,” *J. Fluid Mech.*, vol. 466, pp. 259–283, 2002.

[41] M. Hickling, and R. Plesset, “Collapse and rebound of a spherical bubble in water,” *Phys. Fluids,* vol. 4, pp. 7–14, 1964.

[42] F. G. Ivany, and R. Hammitt, “Cavitation bubble collapse in viscous, compressible liquids-numerical analysis.,” *ASME J. Basic Eng*, vol. 87, pp. 977--985, 1965.

[43] L. Alfayez, D. Mba, and G. Dyson, “The application of acoustic emission for detecting incipient cavitation and the best efficiency point of a 60 kW centrifugal pump: Case study,” *NDT E Int.*, vol. 38, no. 5, pp. 354–358, 2005.

[44] S. Ceccio, S. Gowing, and Y. Shen, “The Effects of Salt Water on Bubble Cavitation,” *J. Fluids Eng.*, vol. Vol. 119, pp. 155–163, 1997.

[45] J. R. Blake and D. C. Gibson, “Growth and collapse of a vapour cavity near a free surface,” *J. Fluid Mech.*, vol. 111, pp. 123–140, 1981.

[46] A. De Bosset and D. Obreschkow, “Direct effects of gravity on cavitation bubble collapse,” *58th Int. …*, pp. 1–5, 2007.

[47] Lord Rayleigh, “On the pressure developed during the collapse of a spherical cavity,” *Philos. Mag.*, vol. 34(199), pp. 94–98, 1917.

[48] D. Ross, *Mechanics of underwater noise. Chapter 7: Cavitation*, Pergamon P. 1976.

[49] H. Shangguan, L. W. Casperson, and S. Prahl, “Pressure impulses during microsecond laser ablation.,” *Appl. Opt.*, vol. 36, no. 34, pp. 9034–9041, 1997.

[50] A. B. Pandit, J. Varley, R. B. Thorpe, and J. F. Davidson, “Measurement of bubble size distribution: an acoustic technique,” *Chem. Eng. Sci.*, vol. 47, no. 5, pp. 1079–1089, 1992.

[51] R. Manasseh, G. Riboux, and F. Risso, “Sound generation on bubble coalescence following detachment,” *Int. J. Multiph. Flow*, vol. 34, no. 10, pp. 938–949, 2008.

[52] R. Manasseh, G. Riboux, A. Bui, and F. Risso, “Sound emission on bubble coalescence: imaging, acoustic and numerical experiments,” *16th Australas. Fluid Mech. Conf.*, no. December, pp. 167–173, 2007.

[53] T. G. Leighton, K. J. Fagan, and J. E. Field, “Acoustic and photographic studies of injected bubbles,” *Eur. J. Phys.*, vol. 12, no. 2, pp. 77–85, 1991.

[54] J. Hinze, “Fundamentals of the Hydrodynamic Mechanism of Splitting in Dispersion Processes,” *AIChE J.*, vol. 1, no. 3, pp. 289–295, 1955.

[55] J. F. Walter and H. W. Blanch, “Bubble break-up in gas-liquid bioreactors: Break-up in turbulent flows,” *Chem. Eng. J.*, vol. 32, no. 1, 1986.

[56] H. K. Nahra and Y. Kamotani, “Prediction of bubble diameter at detachment

from a wall orifice in liquid cross-flow under reduced and normal gravity conditions," *Chem. Eng. Sci.*, vol. 58, no. 1, pp. 55–69, 2003.

[57] S. Di Bari and A. J. Robinson, "Experimental study of gas injected bubble growth from submerged orifices," *Exp. Therm. Fluid Sci.*, vol. 44, pp. 124–137, 2013.

[58] W. Zhang and R. B. H. Tan, "A model for bubble formation and weeping at a submerged oriÿce with liquid cross- flow," *Chem. Eng. Sci.*, vol. 58, pp. 287–295, 2003.

[59] S. Gowing, "Dissolving of Bubble in a Liquid," *DTNSRDC Rep.*, vol. 6, p. 87, 1987.

[60] A. H. Blanchard, D. C., and D., Woodcock, "Bubble Formation in Modification in the Sea and its Meteorological Signifcance," *Tellus*, vol. vol.9, NO., pp. 145–158, 1957.

[61] T. Abe, "On the Stable Formation of Sea Water in Seas," *J. Oceanogr. Soc. Japan*, vol. 20, pp. 242–250, 1962.

[62] G. I. Kushinov, "Effect of Surface Tension on the Collapse of a Cavitation Bubble," *J. Eng. Phys.*, vol. 60, no. 1, pp. 34–37, 1991.

[63] L. A. Crum, J. B. Gallemore, and D. A. Nordling, "Effect of Surface Tension on the Cavitation Threshold of Water Published by the Acoustical Society of America and Oscillation," vol. 151, no. 1972, 1972.

[64] Y. Cengel, *Heat Transfer: A Practical Approach*, vol. Second EDI. 2003.

[65] A. Ferreira, A. Egas, A. Domingues, C. Fernandes, and L. Lobo, "Vapor Pressure and Boiling Point Elevation of Eucalyptus Kraft Black Liquors," vol. 19, no. 1, pp. 13–22, 2011.

[66] A. M. Jazi and H. Rahimzadeh, "Detecting cavitation in globe valves by two methods: Characteristic diagrams and acoustic analysis," *Appl. Acoust.*, vol. 70, no. 11–12, pp. 1440–1445, 2009.

[67] S. Roper, *Roper's Engineer's Handy Book*. Philadelphia: David McKay, 1899.

[68] T. C. E. Company, "Locomotive Boilers," 1900. [Online]. Available: https://en.wikipedia.org/wiki/Boiler_explosion#cite_ref-1. [Accessed: 20-May-2016].

[69] C. H. Hewison, "Locomotive Boiler Explosions," no. ISBN 0-7153-8305 1, 1983.

[70] A. McEwen, "Historic Steam Boiler Explosions," *Sledgehammer Eng. Press*, no. ISBN 978-0-9532725-2-5, 2009.

[71] S. Nukiyama, “The maximum and minimum values of heat transmitted from metal surface to boiling water under atmospheric pressure.,” *J. Japan Soc. Mech. Eng.*, vol. 367–364, 1937.

[72] J. R. H. Warren and M. Rohsenow, *Hand Book of Heat Transfer*. New York San Francisco Washington, D.C. Auckland Bogot6: Library of Congress Cataloging-in-Publication Data, 1998.

[73] N. X. Zhao R, Xu RQ, Shen ZH, Lu J, “Experimental investigation of the collapse of laser generated cavitation bubbles near a solid boundary,” *Opt Laser Technol*, vol. 39, pp. 968–972, 2007.

[74] D. F. Gaitan, “An experimental investigation of acoustic cavitation in gaseous liquids,” University of Southwestern Louisiana. USA., 1990.

[75] K. E. Rydberg, “Energy efficient water hydraulic systems,” *Fifth Int. Conf. Fluid Power Transm. Control. HangZhou, Chinahe*, pp. 44–46, 2001.

[76] K. Vorkurka, “Amplitudes of free bubble oscillations in liquids,” in *Journal of Sound and Vibration*, 1990, vol. 141(2), pp. 259–275.

[77] P. Skousen, *Valve Handbook*, Second edi. New York: McGraw-Hill., 1998.

[78] S. J. Weninger, K.R., Camara, and C., Putterman, “Energy focusing in a converging fluid flow: implications for sonoluminescence,” *Phys. Rev. Lett.*, vol. 83(10), pp. 2081–2084, 1999.

[79] N. Naveen and N. Sinha, Los Alamos, “Characterization of liquids using gas bubbles,” *United States (12), Pat. Appl. Publ.*, vol. 1, no. 19, 2004.

[80] W. J. Rahmeyer, “Cavitation noise from butterfly valves,” *Nucl. Eng. Des.*, vol. 72, no. 3, pp. 297–301, 1982.

[81] R. M. Meland E. , Henriksen V., and Hennie E., “Spectral analysis of internally leaking shut-down valves,” *Measurement*, vol. 44, pp. 1059–1072, 2011.

[82] J. Rajtar, and R. Muthiah, “Pipeline leak detection system for oil and gas flowlines,” *J. Manuf. Sci. Eng.*, vol. 119, pp. 105–109, 1997.

[83] W. C. F. Han, B. Song, and T. Yu, “Present state and prospects for valve reliability technique study,” *Mach. Tool Hydraul.*, vol. (9), p. 48, 2008.

[84] Thompson G. and Zolkiewski G., “An experimental investigation into the detection of internal leakage of gases through valves by vibration analysis,” *Proc. Inst. Mech. Eng.*, vol. 211, 1997.

[85] T. Alhashan, A. Addali, and J. Teixeira, “Exploration of the Possibility of Acoustic Emission Technique in Detection and Diagnosis of Bubble Formation and Collapse in Valves,” vol. 13, no. 4, pp. 1–9, 2016.

[86] A. M. Jazi and H. Rahimzadeh, “Waveform analysis of cavitation in a globe valve,” *Ultrasonics*, vol. 49, no. 6–7, pp. 577–582, 2009.

[87] Flowserve, “Flowserve Cavitation Control,” pp. 1–20, 2006.

[88] J. P. Tullis, *Choking and supercavitation valves*, Vol. 97. Proc. ASCE, 1971.

[89] T. Excel, “Local pressure loss calculation,” *ThermExcel - All Rights Reserved*, 2014. [Online]. Available: https://www.thermexcel.com. [Accessed: 01-Dec-2016].

[90] J. Askew, “Centrifugal pumps: Avoiding cavitation,” *World Pumps*, vol. 2011, no. August, pp. 34–39, 2011.

[91] J. P. Michel and M. Michel, *Fundamentals of Cavitation*. NewYork, London, 2005.

[92] D. Obreschkow, P. Kobel, N. Dorsaz, A. De Bosset, C. Nicollier, and M. Farhat, “Cavitation bubble dynamics inside liquid drops in microgravity,” *Phys. Rev. Lett.*, vol. 97, no. 9, pp. 1–5, 2006.

[93] E. A. Neppiras, “Acoustic cavitation,” *Phys. Rep.*, vol. 61, no. 3, pp. 159–251, 1980.

[94] S. Husin, A. Addali, and D. Mba, “Study of the application of Acoustic Emission technology for on-line monitoring of bubble phenomena and flow patterns in two-phase gas-liquid flow,” Trans. on Engineering Sciences, vol. 74, pp. 403–414, 2012.

[95] M. Lindel, “Valve & pipeline cavitation ©,” *Erhard Valves*, 2008.

[96] J. C. P., “More on What is Cavitation?,” *lightmypump*, no. February, pp. 1–13, 2003.

[97] J. Monsen, “Liquid Flow in Control Valves,” 2015. [Online]. Available: http://www.valin.com/resources/blog/liquid-flow-control-valves. [Accessed: 02-Jun-2015].

[98] Thomas A. Hughes. *Measurement and Control Basics*, Fifth Edit. Copyright © 2015 International Society of Automation (ISA).

[99] E. Summary, “To Flashing and Cavitation Subject:,” pp. 1–6, 2015.

[100] S. C. Li, *Cavitation of Hydraulic Machinery*, Vol. 1. university of warwick, UK: 2000 by Imperial college press, 2000.

[101] J. Van der Meulen, “Incipient and desinent cavitation on hemispherical nosed bodies,” *Mar. Eng.*, vol. 19 (209), pp. 218–220, 1972.

[102] R. and K. Gorla, *Turbomachinery: Design and Theory*. USA: Marcel Dekker

Inc., 2003.

[103] J. Herbich, *Handbook Of Dredging Engineering*. McGraw Hill: USA, 2000.

[104] V. Shah, Y. Pandit, and A. Moholkar, *Cavitation Reaction Engineering*. Kluwer Academic, Spinger Verlag, USA, 1999.

[105] I. J. Karassik, J. P. Messina, P. Cooper, and C. HealdW, “Pump Handbook,” *AIChE J.*, vol. 22, no. 6, pp. 1156–1156, 1976.

[106] I. Karassik, and C. Heald, ''*Pump handbook''*, Second edi. McGraw-Hill, 2001.

[107] R. K. Iyer, “The Cavitation Phenomenon,” 2006. [Online]. Available: http://www.executiveship.com/newslett-jul062.htm. [Accessed: 25-Jul-2015].

[108] S. A. Alhashmi, “Detection and diagnosis of cavitation in centrifugal pumps,” PhD thesis, University of Manchester, 2005.

[109] M. S. Plesset and R. B. Chapman, “Collapse of an initially spherical Vapor Cavity in the Neighborhood of a solid Boundary,” *J. Fluid Mech.*, vol. 47, no. 2, pp. 283–290, 1971.

[110] W. Lauterborn and H. Bolle, “Experimental investigations of cavitation-bubble collapse in the neighbourhood of a solid boundary,” *J. Fluid Mech.*, vol. 72, no. 2, p. 391, 1975.

[111] A. T. Plesset, and M. Ellis, “On the mechanism of cavitation damage,” *Trans. ASME,* pp. 1055-- 1064, 1955.

[112] Tullis, *Hydroulic of pipelines : pumps, valves, cavitation*. New York, Toronto: Copyright 1989 by John Wiley and Sons. Inc., 1989.

[113] I. Engineering360, “Valve Applications,” *2015 IHS*, 2015. [Online]. Available: http://www.globalspec.com/pfdetail/valves/applications. [Accessed: 20-Oct-2015].

[114] VAG, “Dams / Hydropower,” *VAG Germany*, 2015. [Online]. Available: http://www.vag-armaturen.com/en/application-fields/dams-hydropower.html. [Accessed: 01-Oct-2015].

[115] M. Company, “World Industrial Valve Market,” *Copyright 1997 - 2015*, 2011. [Online]. Available: http://impeller.net/magazine/news_en/doc5719x.asp. [Accessed: 01-Dec-2015].

[116] L. Alfayez, D. Mba, and G. Dyson, “Detection of incipient cavitation and the best efficiency point of a centrifugal pump using Acoustic Emission,” J. Acoustic Emission, 22, 2004.

[117] I. Howard, “A review of rolling element bearing vibration:detection, diagnosis and prognosis,” *Journal of Mechanical Science and Technology*, vol. 29, no. 1. pp. 35–41, 1994.

[118] M. Vishwakarma, R. Purohit, V. Harshlata, and P. Rajput, “Vibration Analysis & Condition Monitoring for Rotating Machines: A Review,” *Mater. Today Proc.*, vol. 4, no. 2, pp. 2659–2664, 2017.

[119] P. J. Shull, *Non-destructive Evaluation, Theory, Technique and Applications*. 2002.

[120] M. P. Miller RK, *Non-destructive Testing Handbook*. 1987.

[121] T. Verbruggen, “Wind turbine operation and maintenance based on condition monitoring WT-Ω,” *Tech. Report,ECN-C–03-047,* no. April, 2003.

[122] M. A. Elforjani, “Condition Monitoring of Slow Speed Rotating Machinery Using Acoustic Emission Technology,” PhD Thesis, Cranfield Univesity, 2010.

[123] D. P. Walsh, “Oil Analysis 101,” *Orbit*, vol. 25, no. 2, pp. 0–5, 2005.

[124] K. V. Jenderka and C. Koch, “Investigation of spatial distribution of sound field parameters in ultrasound cleaning baths under the influence of cavitation,” *Ultrasonics*, vol. 44, no. SUPPL., pp. 401–406, 2006.

[125] M. H. and B. Zeqiri, “A detector for monitoring the onset of cavitation during therapy-measurements of ultrasonic power,” *J. Phys. Conf. Ser.*, pp. 112–117, 2004.

[126] P. J. Wolff, R. K. Jones, and P. March, “Evaluation of Results from Acoustic Emissions-Based Cavitation Monitor , Grand Coulee Unit G-24,” no. October, pp. 1–15, 2005.

[127] FDIS ISO, *International Standards Organization Documents 22096*. Condition monitoring and diagnosis of machines – J. Acoustic Emission, 2007.

[128] D. Breysse, *Non-Destructive Assessment of Concrete Structures: Reliability and Limits of Single and Combined Techniques*, no. 978-94-7-2735–9. Springer, 2012.

[129] M. E. El-Alej, “Monitoring Sand Particle Concentration in Multiphase Flow Using Acoustic Emission Technology,” PhD Thesis, Cranfield University, 2014.

[130] G. R. Staszewski, W. J., Boller, and C. Tomlinson, *Health Monitoring of Aerospace Structures: Smart Sensor Technologies and Signal Processing*. John Wiley & sons Ltd, UK, 2004.

[131] G. R. Lihui W, *Condition Monitoringand Control for Intelligent Manufacturing*. USA: University of Michigan, 2006.

[132] V. S. Gmbh, “Acoustic Emission Sensors - Specification,” *Vallen Syst.*, p. 24, 2012.

[133] V. S. Gmbh, “Acoustic Emission Sensors - Specification,” *Vallen Syst.*, p. 24, 2012.

[134] B. Muravin, “Acoustic emission science and technology,” *J. Build. Infrastucture Eng. Isr. Assoc. Eng. Archit.*, no. Figure 1, pp. 1–12, 2009.

[135] C. J. Hellier, *Handbook of Nondestructive Evaluation*, vol. 69. 2012.

[136] R. Miller, *Nondestructive Testing Handbook*. Amer Society for Nondestructive, 1987.

[137] M. S. A. Abouelwafa and E. J. M. Kendall, “The measurement of component ratios in multiphase systems using alpha -ray attenuation,” *J. Phys. E.*, vol. 13, no. 3, pp. 341–345, 1980.

[138] W. Merilo, and R. Dechene, “Void Fraction Measurement with a Rotating Electric Field Conductance Gauge,” *ASME J. Heat Transf.*, vol. 99 (2), pp. 330–332, 1977.

[139] T. G. Leighton, *The acoustic bubble*. London: Academic Press, 1994.

[140] D. Mba and R. B. Rao “Development of Acoustic Emission Technology for Condition Monitoring and Diagnosis of Rotating Machines: Bearings, Pumps, Gearboxes, Engines, and Rotating Structures,” *Shock Vib. Dig.*, vol. 38, no. 1, pp. 3–16, 2006.

[141] J. W. R. Boyd and J Varley, “The uses of passive measurement of acoustic emissions from chemical engineering processes,” *Chem. Eng. Sci.*, vol. 56, no. 5, pp. 1749–1767, 2001.

[142] P. J. McNulty, “Pump Hydraulic Noise: Its uses and cures,” *Marine Engineers Review.*, pp. 22-23, 1985.

[143] H. N. Oguz and A. Prosperetti, “Bubble entrainment by the impact of drops on liquid surfaces,” *J. Fluid Mech.*, vol. 219, no. 1, p. 143, 1990.

[144] M. R. Lee and J. H. Lee, “A Study on Characteristics of Leak Signals of Pipeline Using Acoustic Emission Technique,” *Solid State Phenom.*, vol. 110, pp. 79–88, 2006.

[145] J. Van Ooijen, J. A. C., van Tooren, and E. Reedijk, “Acoustic emission during the preparation of dichloro (pyrazine) zinc(II),” *J. Am. Chem. Soc.*, vol. 100(17), no. 5569–5570, 1978.

[146] S. D. Lubetkin, “Measurement of bubble nucleation rates by an acoustic method,” *J. Appl. Electrochem.*, vol. 19, no. 5, pp. 668–676, 1989.

[147] G. B. Deane, “Sound generation and air entrainment by breaking waves in the surf zone,” *J. Acoust. Soc. Am.*, vol. 102, no. 5, pp. 2671–2689, 1997.

[148] S. Vergniolle, G. Brandeis, and J. C. Mareschal, “Strombolian explosions 2. Eruption dynamics determined from acoustic measurements,” *J. Geophys. Res.*, vol. 101, pp. 20449–20466, 1996.

[149] G. Street, “Non-invasive measurement techniques to monitor acoustic cavitation activity Kornpatsitt Promasa Submitted in May 2014 for the degree of Doctor of Philosophy University of Strathclyde,” no. May, 2014.

[150] “Electrowave Ultrasonics Corporation,” 2015. [Online]. Available: http://www.electrowave.org/Cavitation.html. [Accessed: 15-Aug-2015].

[151] H. Lamb, *Hydrodynamics*, 6th ed. New York, 1945.

[152] Steven F., *Encyclopedia of Mathematics and Its Applications*. Cambridge-UK: The Press Syndicate of the University of Cambridge, 2003.

[153] S. Prabhakar, A. R. Mohanty, and A. S. Sekhar, “Application of discrete wavelet transform for detection of ball bearing race faults,” *Tribol. Int.*, vol. 35, no. 12, pp. 793–800, 2002.

[154] S. A. Niknam, V. Songmene, and Y. H. J. Au, “The use of acoustic emission information to distinguish between dry and lubricated rolling element bearings in low-speed rotating machines,” *Int. J. Adv. Manuf. Technol.*, vol. 69, no. 9–12, pp. 2679–2689, 2013.

[155] K. R. Al-Balushi, A. Addali, B. Charnley, and D. Mba, “Energy index technique for detection of acoustic emissions associated with incipient bearing failures,” *Appl. Acoust.*, vol. 71, no. 9, pp. 812–821, 2010.

[156] J. O. Smith III, *Mathematics of the Discrete Fourier Transform (DFT)*. 2002.

[157] N. Tondon and A. Choudhury, “A review of vibration and acoustics measurement methods for the detection of defects in rolling element bearing,” *Tribol. Int.*, vol. 32, no. 8, pp. 469–480, 1999.

[158] S. M. Kay and S. L. Marple, “Spectrum analysis - A modern perspective,” *Proc. IEEE*, vol. 69, no. 11, pp. 1380–1419, 1981.

[159] S. H. Baek, K. Wu, H. S. Shim, D. H. Lee, J. G. Kim, and D. H. Hur, “Acoustic emission monitoring of water boiling on fuel cladding surface at 1 bar and 130 bar,” *Meas. J. Int. Meas. Confed.*, vol. 109, pp. 18–26, 2017.

[160] J. Derakhshan J. Houghton, R. Jones and P. March, “Cavitation monitoring of hydro turbines with RMS acoustic emission measurements,” *Proc. world*

Meet. onacousticemission, vol. 15, p. p.305, 1989.

[161] S. Husin, A. Addali, and D. Mba, “Observation of acoustic emission from gas bubble inception and burst,” *Proc. Inst. Mech. Eng. Part E J. Process Mech. Eng.*, vol. 226, no. 1, pp. 79–88, 2012.

[162] T. Alhashan and A. Addali, “The Effect of Salt Water on Bubble Formation during Pool Boiling Using Acoustic Emission Technique,” vol. 13, no. 5, pp. 51–56, 2016.

[163] S. Husin, A. Addali, and D. Mba, “Feasibility study on the use of the Acoustic Emission technology for monitoring flow patterns in two phase flow,” *Flow Meas. Instrum.*, vol. 33, pp. 251–256, 2013.

[164] S. Al Lababidi, A. Addali, H. Yeung, D. Mba, and F. Khan, “Gas Void Fraction Measurement in Two-Phase Gas/Liquid Slug Flow Using Acoustic Emission Technology,” *J. Vib. Acoust.*, vol. 131, no. 6, p. 064501+, 2009.

[165] J. E. Kloeppel, “Scientists measure energy dissipation in a single cavitating bubble,” *Phys. Sci.*, vol. 217, pp. 244–1073, 2002.

[166] L. Jaubert, S. Maillard, and V. Sulis, “Monitoring of Fluidic Systems By Acoustic Emission,” in *European conf. AE Testing*, 2008, pp. 334–339.

[167] A.E.G. Benz, “Use of Acoustic Emission Techniques for Detection of Discontinuities,” *Mater. Eval.*, vol. 5, NO. 10, pp. 1215–1222, 1998.

[168] J. Lee, M. Lee, J. Kim, and J. Kim, “Analysis of acoustic emission signals for condition monitoring of check valve at nuclear power plants,” *Key Eng. Mater.*, vol. 270–273, pp. 531–536, 2004.

[169] Osterman Aljaž, M. Hočevar, B. Širok, and M. Dular, “Characterization of incipient cavitation in axial valve by hydrophone and visualization,” *Exp. Therm. Fluid Sci.*, vol. 33, no. 4, pp. 620–629, 2009.

[170] W. Kaewwaewnoi, A. Prateepasen, and P. Kaewtrakulpong, “Measurement of Valve Leakage Rate using Acoustic Emission,” in *Proceedings of the 2nd International Conference on Electrical Engineering/Electronics, Computer, Telecommunications and Information Technology*, 2005, pp. 3–6.

[171] W. K. Chan, “Detection of cavitation erosion in centrifugal pumps,” *Int. J. Heat Fluid Flow*, vol. 9, no. 1, pp. 74–77, 1988.

[172] L. Tan, B. Zhu, S. Cao, and Y. Wang, “Cavitation flow simulation for a centrifugal pump at a low flow rate,” *Chinese Sci. Bull.*, vol. 58, no. 8, pp. 949–952, 2013.

[173] S. Lee, K. Jung, J. Kim, and S. Kang, “Cavitation Mode Analysis of Pump Inducer,” vol. 16, 2002.

[174] IEC 60534-8-1, “Industrial-process control valves - Part 8-1: Noise considerations - Laboratory measurement of noise generated by aerodynamic flow through control valves,” 2005. .

[175] IEC 60534-8-4 Ed, “Industrial-process control valves - Part 8-4: Noise considerations - Prediction of noise generated by hydrodynamic flow,” 2005. .

[176] L. Trefethen, “Surface tension in fluid mechanics,” *Natl. Comm. Fluid Mech. Film notes*, no. 21610, 1969.

[177] J. H. L. Nayar, K. G., D. Panchanathan, G. H. McKinley, “Surface Tension of Seawater,” *J. Phys. Chem.*, 2014.

[178] BS EN 13554:2002, “Non-destructive testing –Acoustic Emission – General principle.” 2002.

[179] T. Boczar and M. Lorenc, “Determinig the repeatability of acoustic emission generated by the Hsu-Nielsen calibrating source,” *Mol. Quantum Acoust.*, vol. 25, pp. 177–192, 2004.

[180] L. Alfayez, “Detection of Incipient Cavitation and the Best Efficiency Point for Centrifugal Pumps Using Acoustic Emission,” vol. 22, pp. 77–82, 2004.

[181] K. L. Mitta, *Advances in Contact Angle, Wettability and Adhesion*. Canada: Scrivener Publishing LLC. All rights reserved, 1983.

[182] T. Leighton, *The Acoustic Bubble*. Cambridge University Press, 1994.

[183] S. Swarup. Fluid Dynamics. 1976; (1): 2-11. India. ISBN NO: 81-85842-92-2.

[184] Khurana a. K, Kumar R. Studies in bubble formation - III. Chemical Engineering Science. 1969; 24(11): 1711–1723. Available at: DOI:10.1016/0009-2509(69)87036-3.

[185] W. Siemes and J. F. Kaufmas. Die periodische Entstehung von Gasblasen an Dusen. Chrmiral Enginwriny Scicnrc. 2008; 5: 127.

[186] Everything About Education. What’s the Difference Between Salt Water vs. Fresh Water? 2016. (Accessed: 20 September 2016).

[187] Bates, Roger G. Determination of pH: theory and practice. Wiley, 1973.

[188] Lim, Kieran F. "Negative pH does exist". Journal of Chemical Education. 83 (10): 2006.

APPENDICES

Appendix A

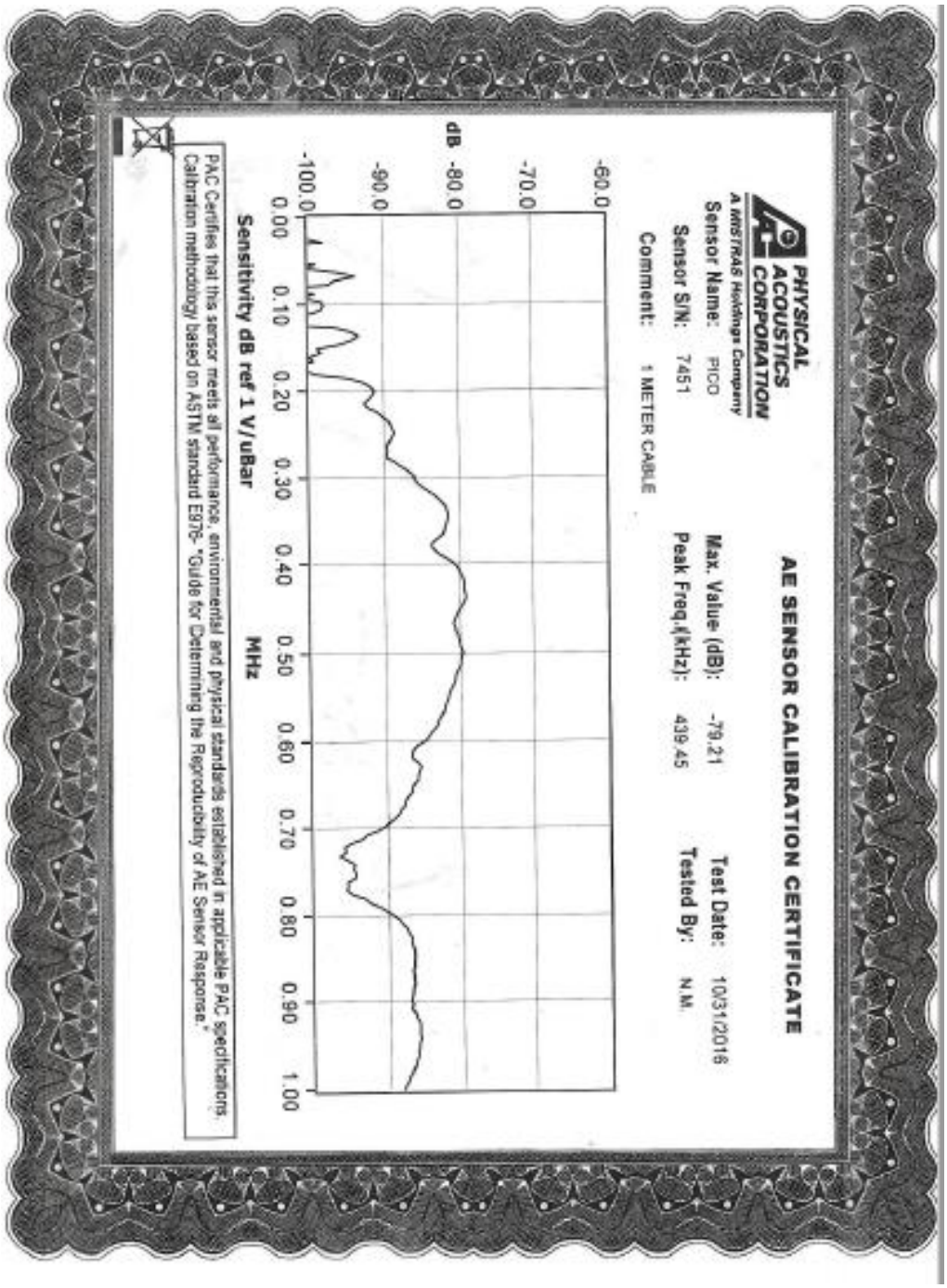

Figure A-1: Calibration certificate for PICO type sensor (Sensor 1).

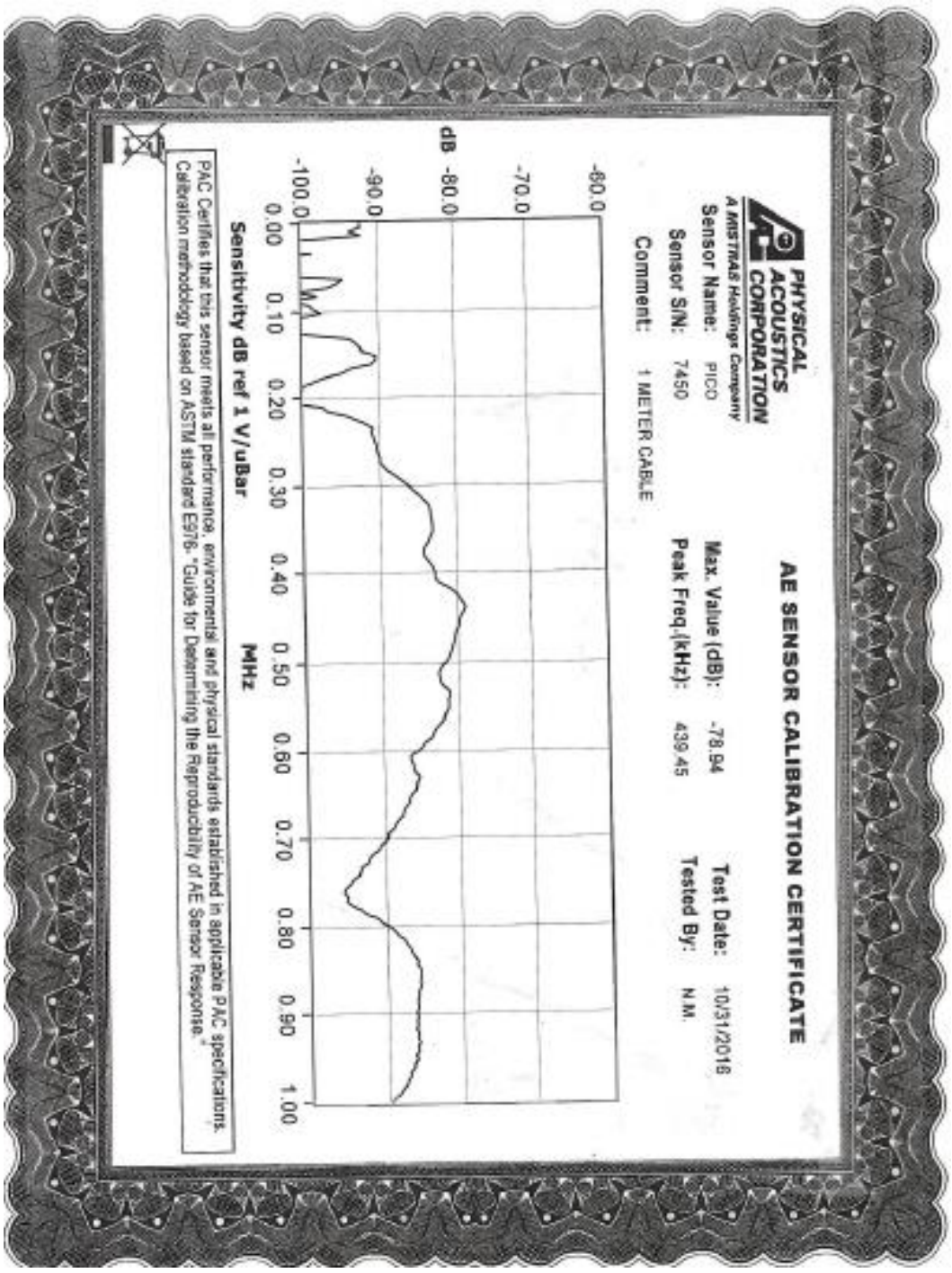

Figure A-2: Calibration certificate for PICO type sensor (Sensor 2).

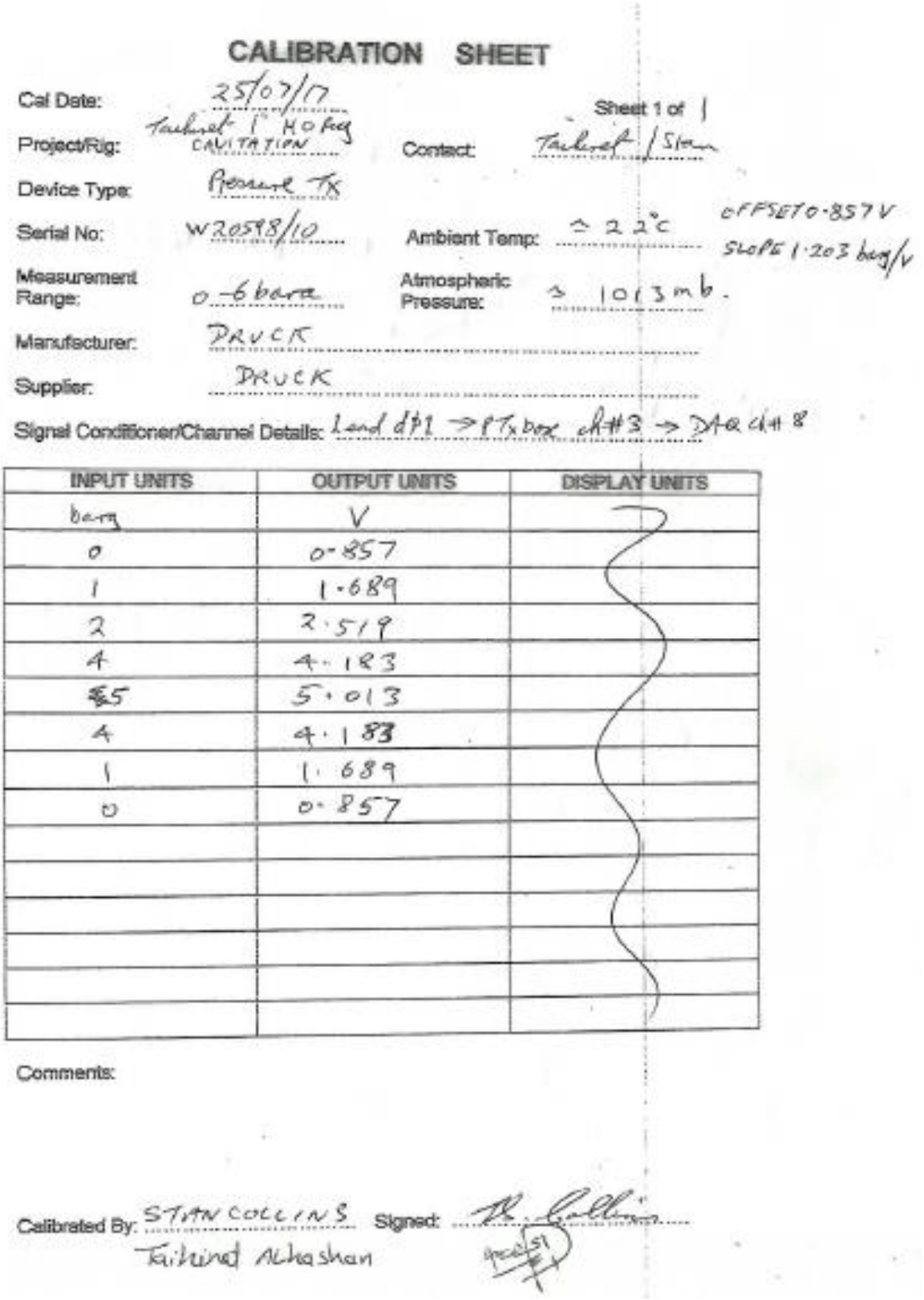

CALIBRATION SHEET

Cal Date: 25/07/17 Sheet 1 of 1

Project/Rig: Tailored 1" HO Proj CAVITATION Contact: Tailored / Stan

Device Type: Pressure Tx

Serial No: W20598/10 Ambient Temp: ≈ 22°C OFFSET 0·857 V SLOPE 1·203 barg/V

Measurement Range: 0-6 barg Atmospheric Pressure: ≈ 1013 mb.

Manufacturer: DRUCK

Supplier: DRUCK

Signal Conditioner/Channel Details: Lead dP1 → PTx box ch#3 → DAQ ch# 8

INPUT UNITS	OUTPUT UNITS	DISPLAY UNITS
barg	V	
0	0·857	
1	1·689	
2	2·519	
4	4·183	
5	5·013	
4	4·183	
1	1·689	
0	0·857	

Comments:

Calibrated By: STAN COLLINS Signed:

Tailwind Alhashan

Figure A-3: Calibration certificate for pressure transducer (PMP 1400).

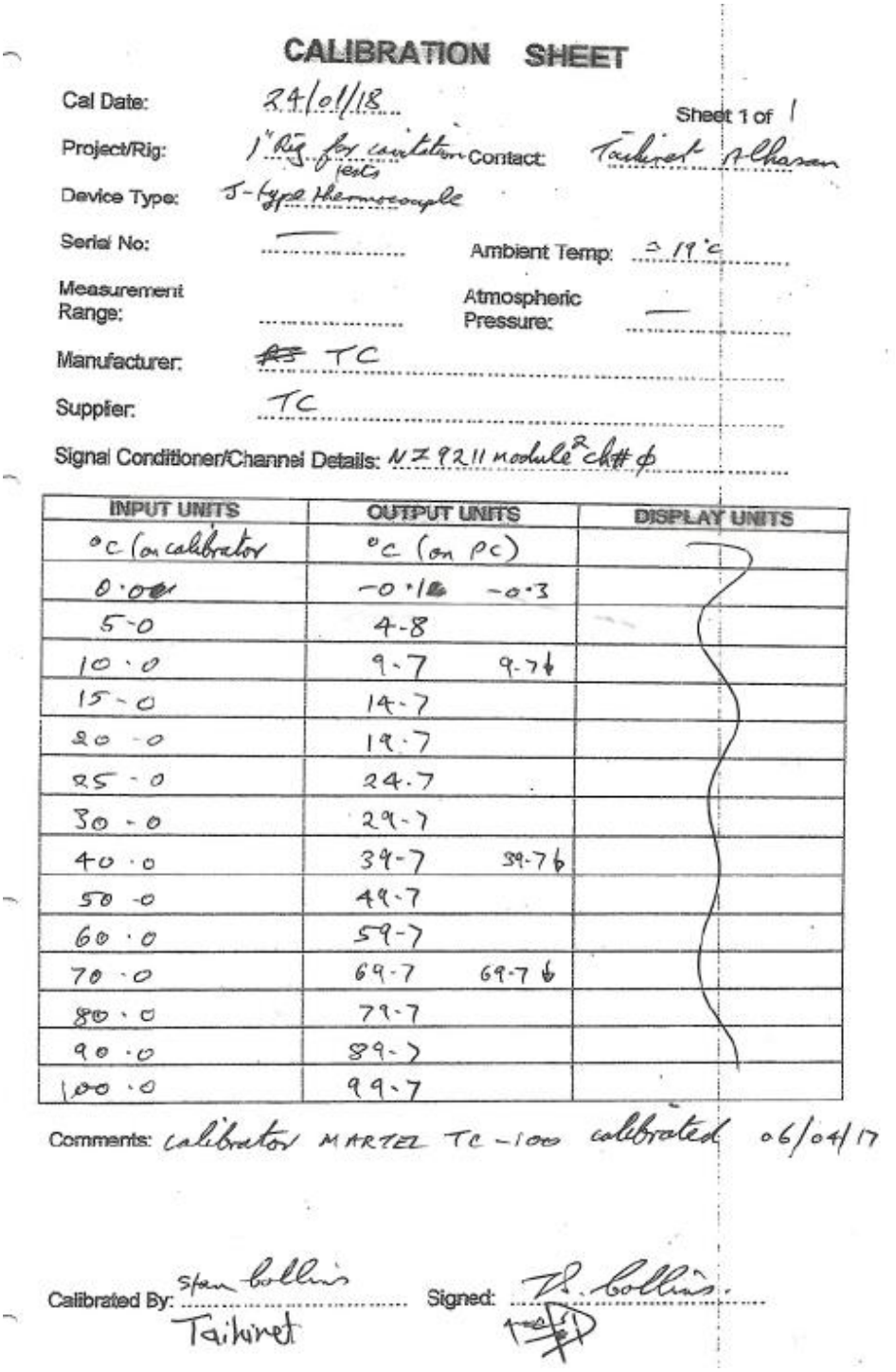

CALIBRATION SHEET

Cal Date: 24/01/18

Sheet 1 of 1

Project/Rig: 1" Rig for cavitation tests Contact: Taihirat Alhassan

Device Type: J-type thermocouple

Serial No: —

Ambient Temp: ≈ 19°c

Measurement Range:

Atmospheric Pressure: —

Manufacturer: ~~RS~~ TC

Supplier: TC

Signal Conditioner/Channel Details: NI 9211 module 2 ch# 0

INPUT UNITS	OUTPUT UNITS	DISPLAY UNITS
°C (on calibrator	°C (on PC)	
0.0	-0.1 -0.3	
5.0	4.8	
10.0	9.7 9.7	
15.0	14.7	
20.0	19.7	
25.0	24.7	
30.0	29.7	
40.0	39.7 39.7	
50.0	49.7	
60.0	59.7	
70.0	69.7 69.7	
80.0	79.7	
90.0	89.7	
100.0	99.7	

Comments: calibrator MARTEL TC-100 calibrated 06/04/17

Calibrated By: Stan Collins Taihirat Signed: S. Collins

Figure A-4: Calibration sheet for T-type thermocouple (TC-100) .

Pressure transducers calibration

The calibration of pressure transducers has been conducted against standard pressure gauge with an accuracy of ±0.04 bar. Each pressure transducers was connected to a pressure calibration device to measure air pressure as shown in Figures A-5. An output voltage of the pressure transducer was compared to the corresponding standard gauge pressure reading, as shown in Figure A-6. (See calibration sheet in Appendix A, Figure A-3).

Figure A-5: Pressure transducer calibration (PMP 1400).

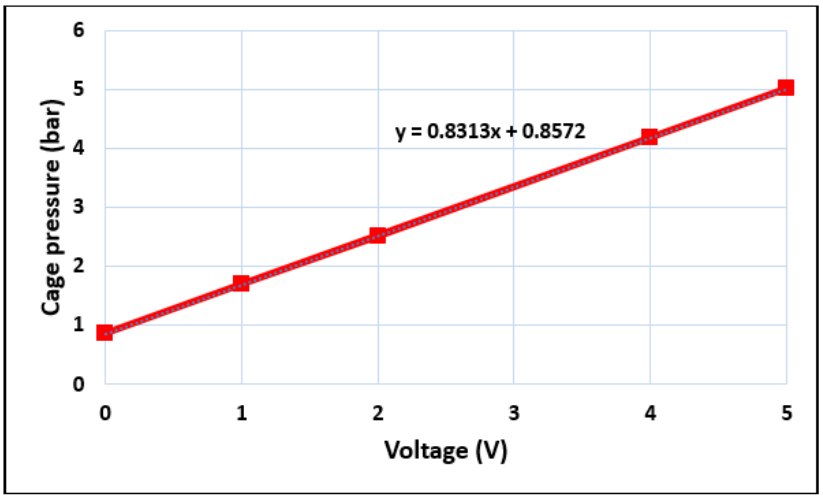

Figure A-6: Pressure transducer calibration curve.

Thermocouple calibration

A T-type thermocouple was installed to measure the liquid temperature at both boiler vessel and valve test-rig. This thermocouple was calibrated against calibrator MARTEL TC-100 type, as shown in Figure A-7. The T-type thermocouple and the calibrator MARTEL TC-100 were fitted in the water vessel to measure water temperature. The water was heated, and the thermocouple was connected to the TC-100 data logger and PC to display the temperature readings. Figure A-8 shows the calibration results of the T-type thermocouple against the calibrator MARTEL TC-100 thermocouple readings. (See calibration sheet for temperature in Appendix A, Figure A-4).

Figure A-7: Thermocouple calibration MARTEL TC-100.

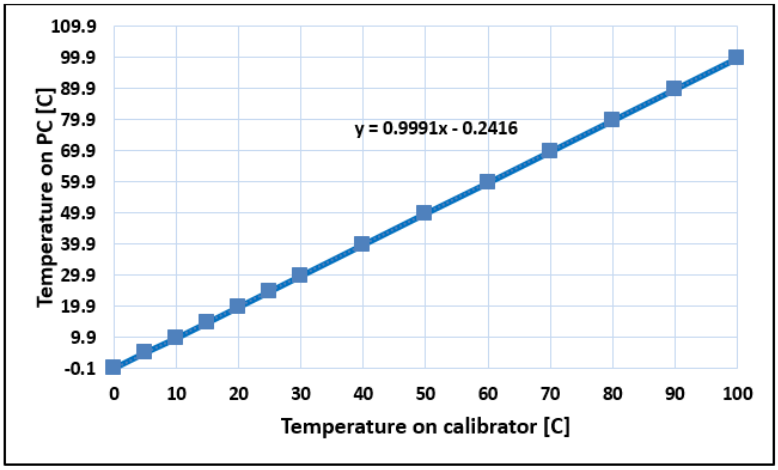

Figure A-8: Temperature calibration curve.

Figure A-9: Measurement device of density.

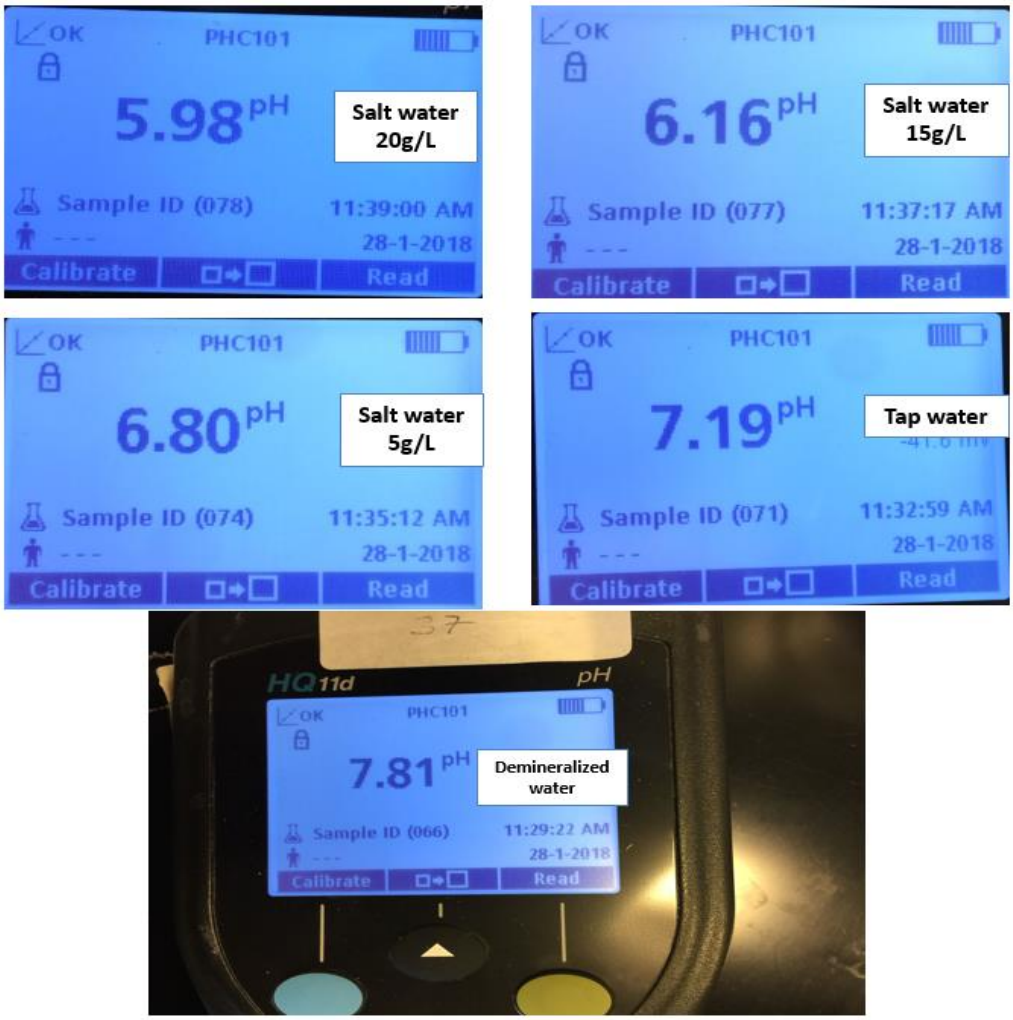

Figure A-10: Measurement device of pH (HQ11d).

A-1 Liquid properties

A-1-1 Viscosity Effect

Viscosity is a measure of a fluids resistance to flow; this means that some fluids will be faster than others. Also, it is called dynamic viscosity or absolute viscosity. When the oil temperature increases, its molecules moved faster and the distance between them increases, causing thus viscosity decreased [183].

$$\mu = \frac{\tau_w}{d_u / d_y} \qquad \text{(A-1)}$$

Where:

μ **:** Viscosity, $\frac{N.\sec}{m^2} = P_a.\sec$

τ_w **:** Shear stress, *N/m²*

$\frac{d_u}{d_y}$ **:** d_u is velocity, m/s and d_y is distance, *m.*

Bubbles size are independent of the liquid viscosity, when the liquid viscosity increases, the size of bubbles increase [184]. Siemes and Kaufmann [185] found that the high liquid viscosity causes an increase in bubble size, but at a small flow rate.

A-1-2 Density:

Density is defined as mass per unit volume. The density of salt water is higher than that of fresh water. Furthermore, when salt is dissolved in water, as it is in ocean water, that dissolved salt adds to the mass of the water and makes the water denser than it would be without salt. Because objects float better on a dense surface, they float better on salt water than fresh water. Fresh water has a density of 1.0 *kg/m³* while salt water has a density of 1.025 *Kg/m³* [186].

$$\rho = \frac{M}{V} \qquad \text{(A-2)}$$

Where:

ρ : Density, *Kg/m³*

M : Mass, *Kg*

V : Volume, *V*

A-1-3 Potential of hydrogen (PH):

PH is a numeric scale used to specify the acidity or basicity of a water solution. It is measured in units of moles per liter, of hydrogen ions. It is the negative of the base 10 logarithm of the activity of the hydrogen ion [187]. Solutions with a pH less than 7 are acidic and solutions with a pH greater than 7 are basic. Pure water is neutral, at pH 7 (25 °C), being neither an acid nor a base [188].

Appendix B

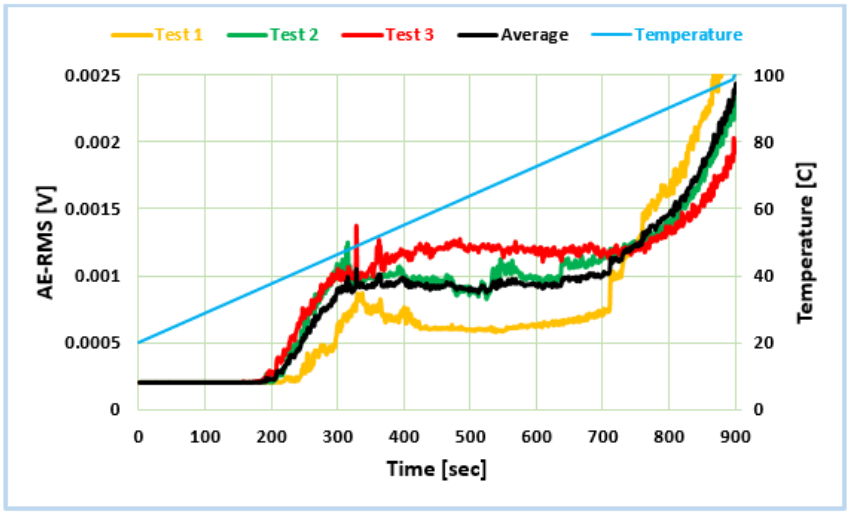

Figure B-1: Test average of pool boiling with tap water level of 100 mm for sensor 1.

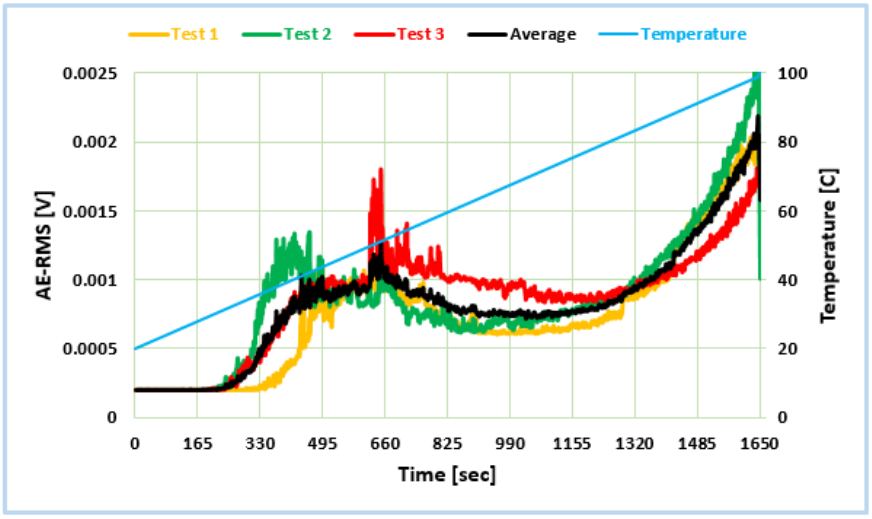

Figure B-2: Test average of pool boiling with tap water level of 200 mm for sensor 1.

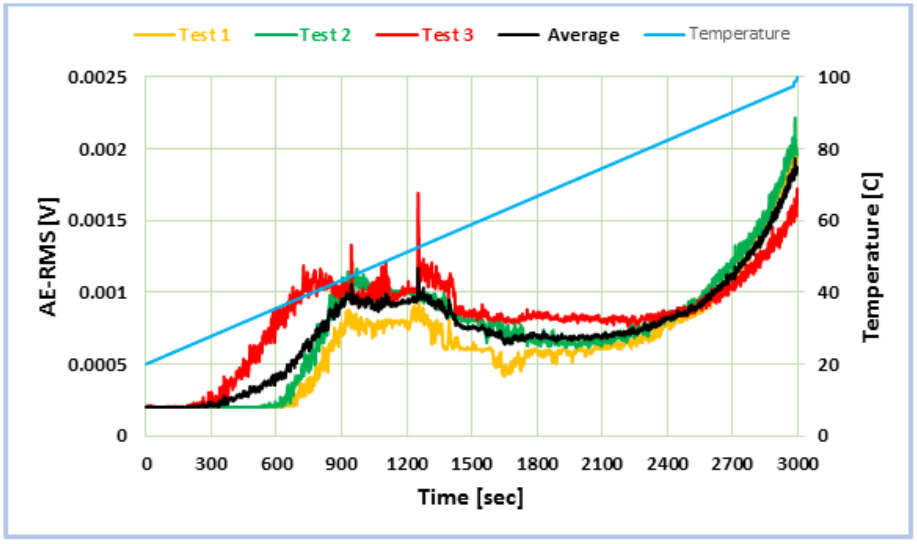

Figure B-3: Test average of pool boiling with tap water level of 350 mm for sensor 1.

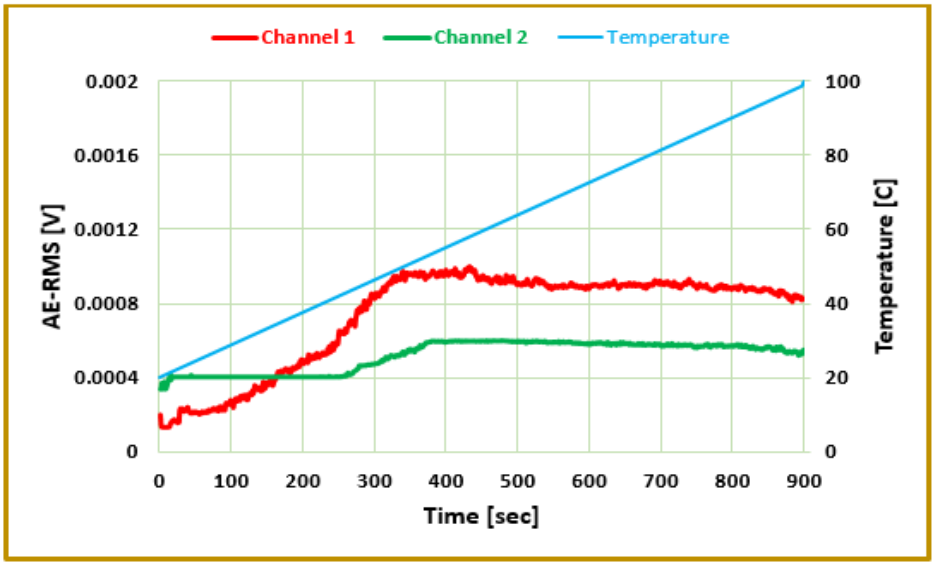

Figure B-4: Observation of boiling test for salt water (5g/L) at the water level of 100 mm.

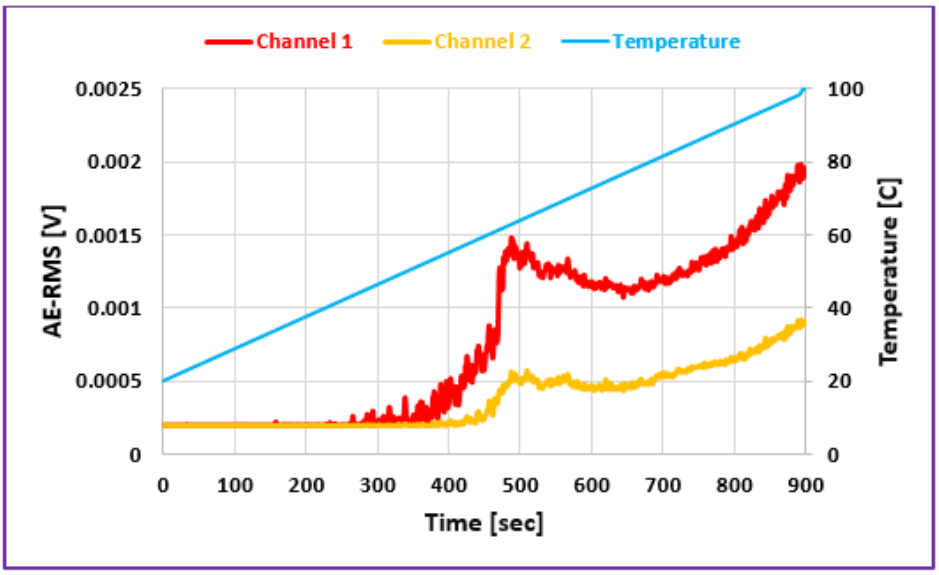

Figure B-5: Observation of boiling test for demineralized water (water level of 100 mm).

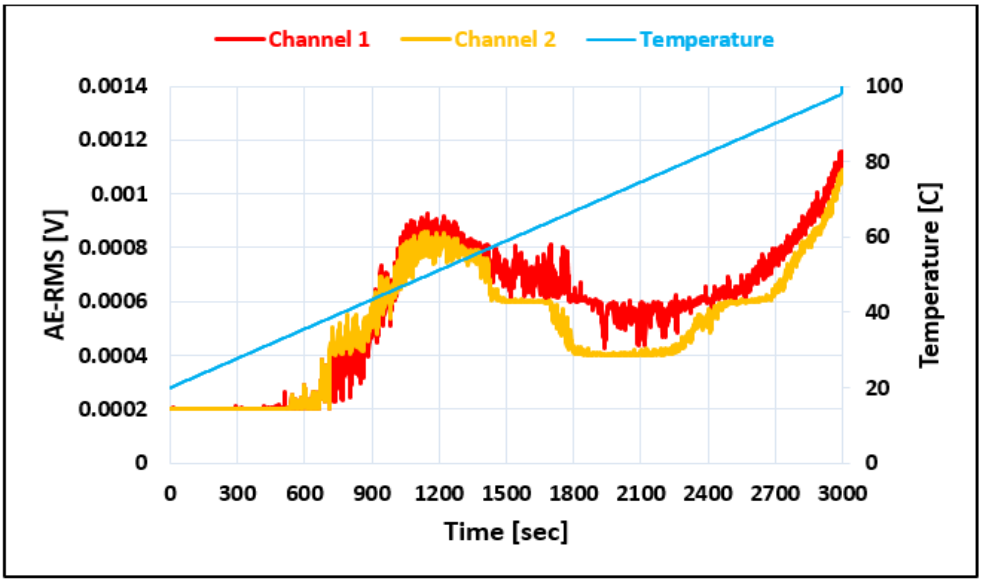

Figure B-6: Observation of boiling test for demineralized water (water level of 350 mm).

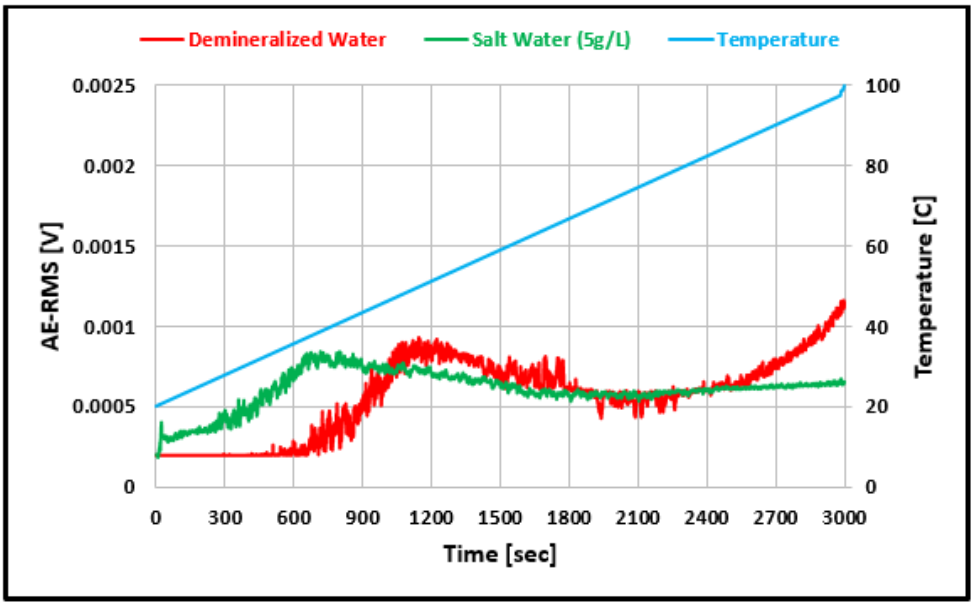

Figure B-7: Comparison between salt water (5g/L) and demineralized water for water level of 350 mm (channel 1).

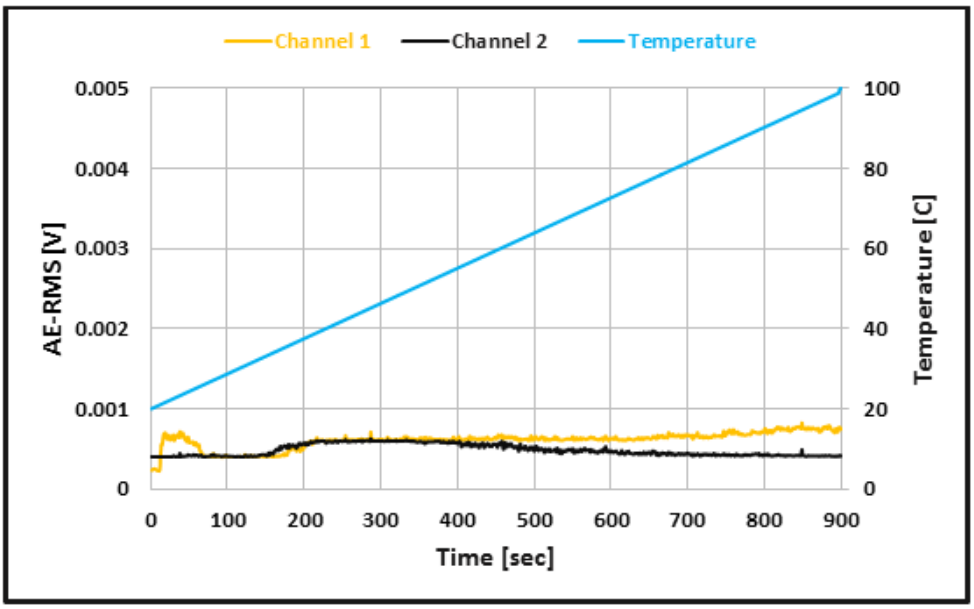

Figure B-8: Observation of boiling test for salt water (30g/L) for water level of 100 mm.

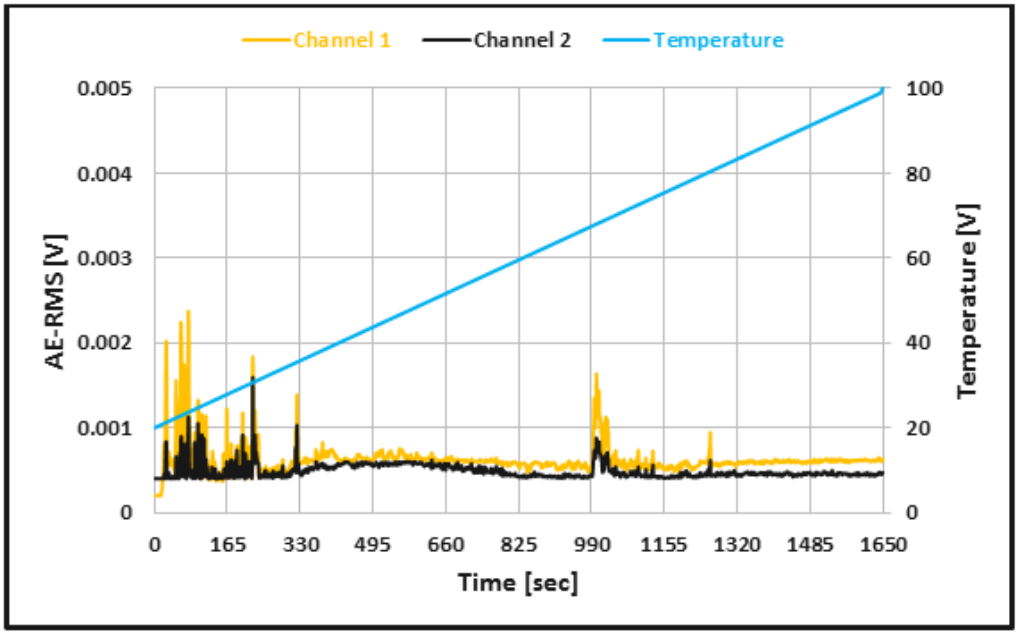

Figure B-9: Observation of boiling test for salt water (30g/L) for water level of 200 mm.

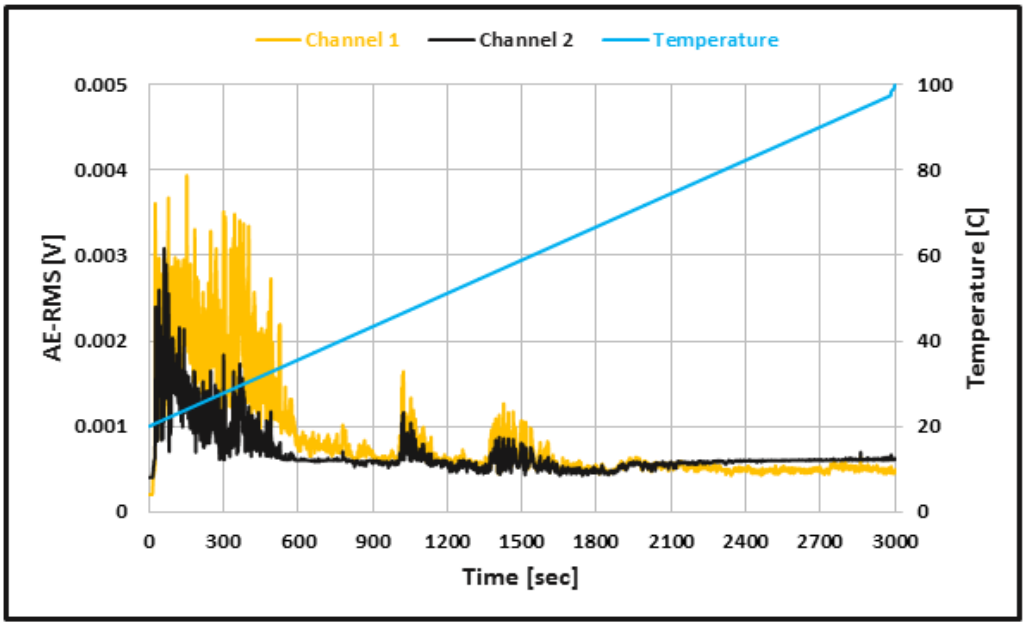

Figure B-10: Observation of boiling test for salt water (30g/L) for water level of 350 mm.

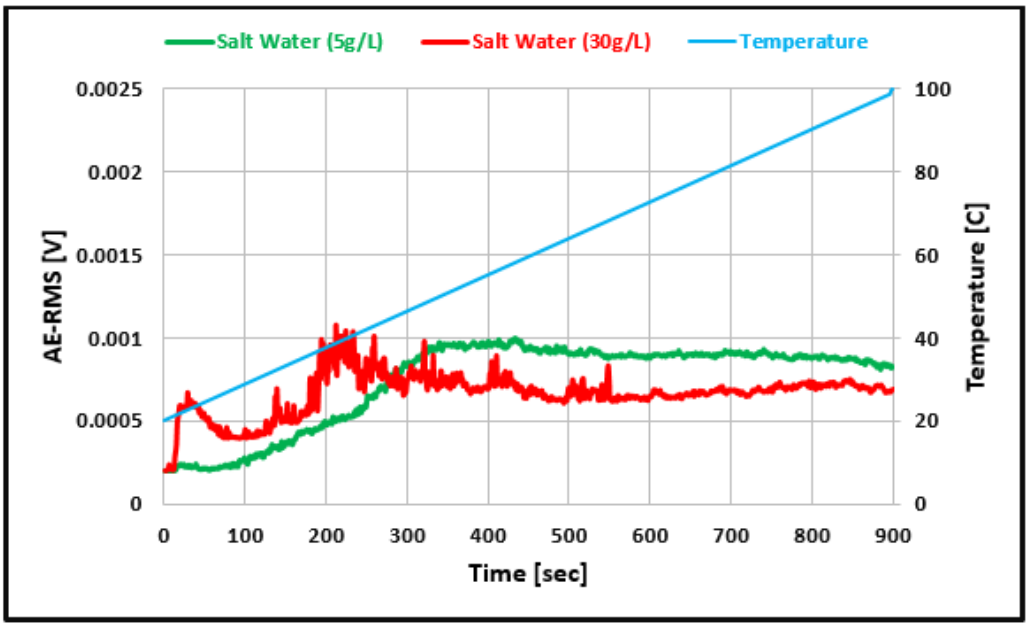

Figure B-11: Observation of boiling test with salt water concentration (5g/L) and (30 g/L) water of 100 mm.

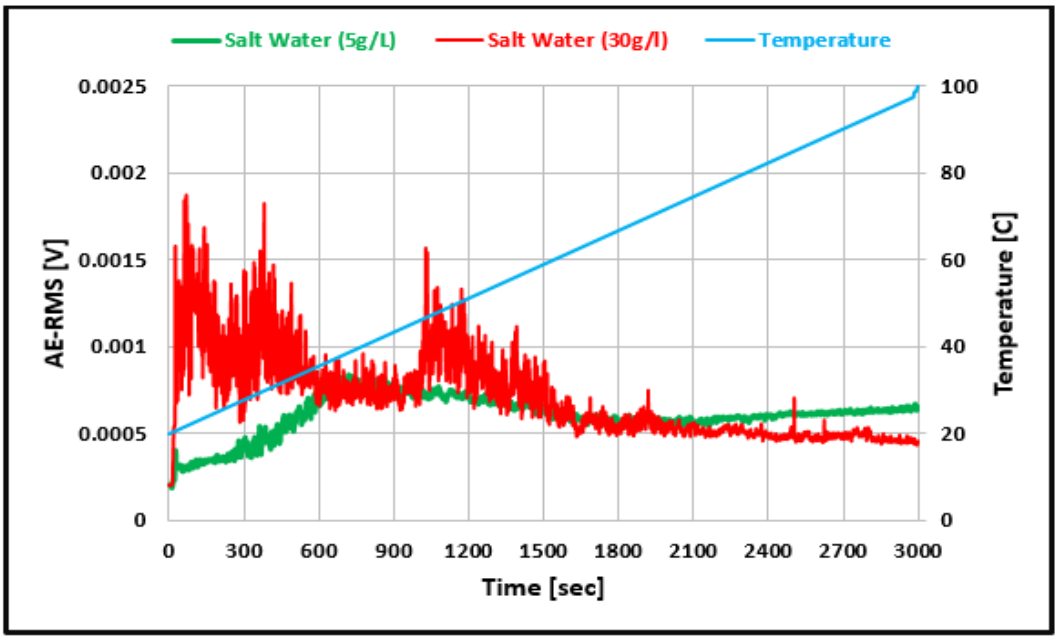

Figure B-12: Observation of boiling test with salt water concentration (5g/L) and (30 g/L) water level of 350 mm.

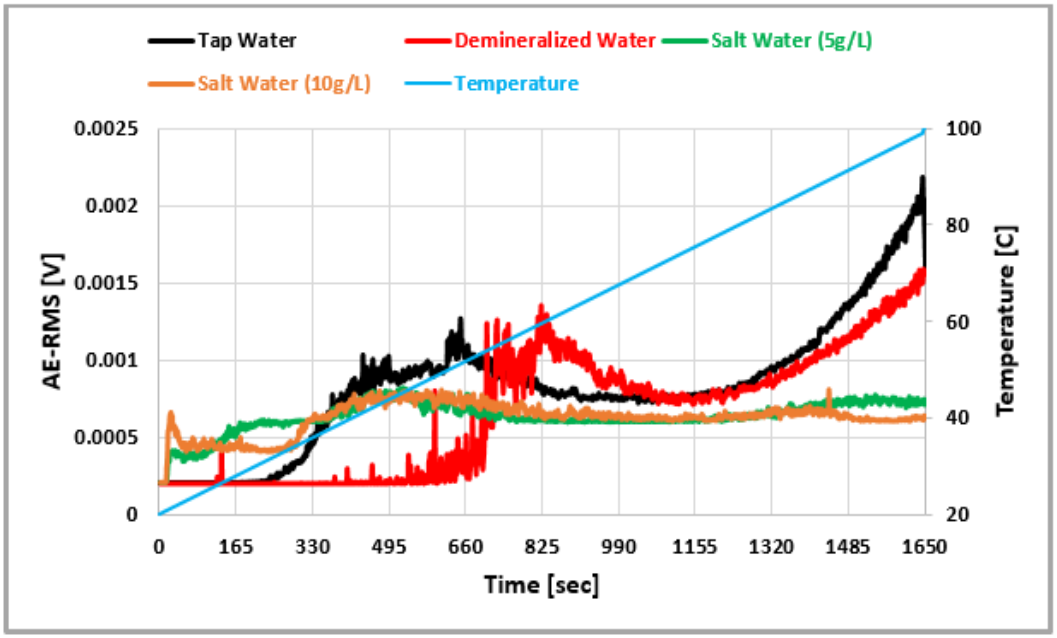

Figure B-13: Comparison of boiling test with tap water, demineralized water, salt water (5g/L) and salt water (10g/L) water level of 200 mm; sensor 1.

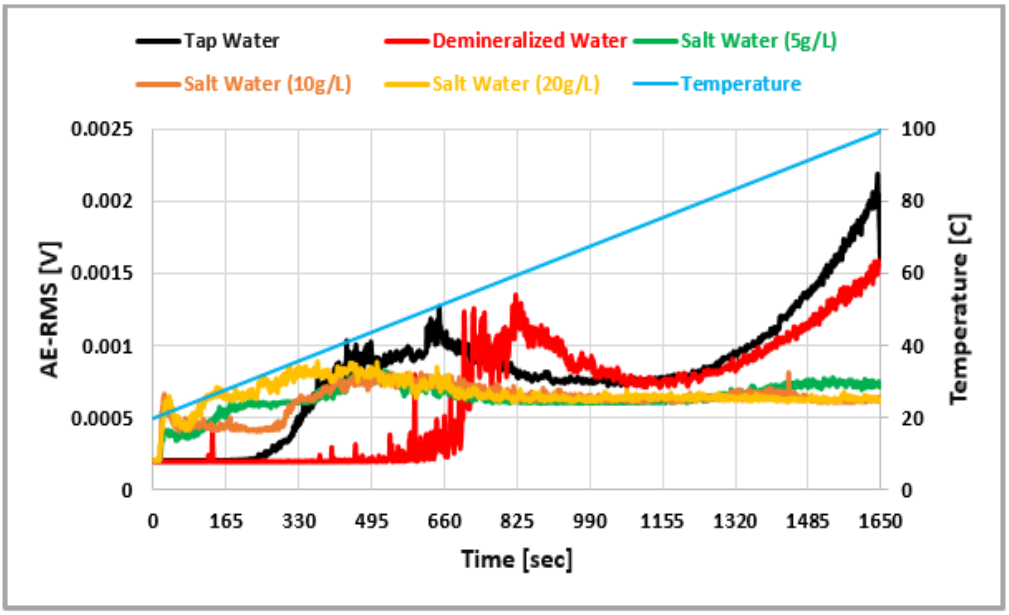

Figure B-14: Comparison of boiling test with tap water, demineralized water, salt water (5g/L), salt water (10g/L) and salt water (20g/L) water level of 200 mm, sensor 1.

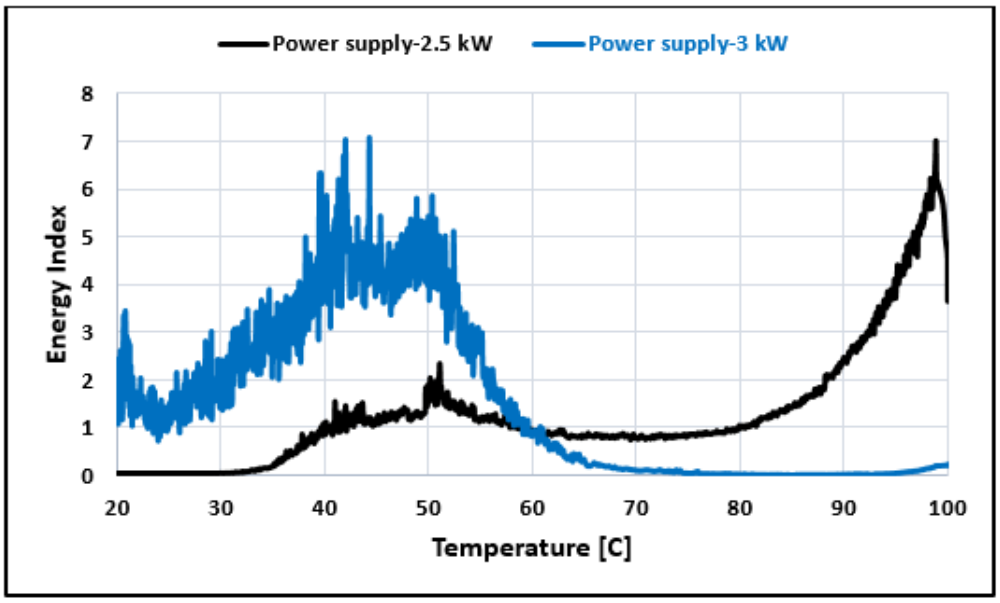

Figure B-15: AE Energy Index as a function of temperature for two rates of heat input. Signal from sensor 1 with tap water, depth of 200 mm.

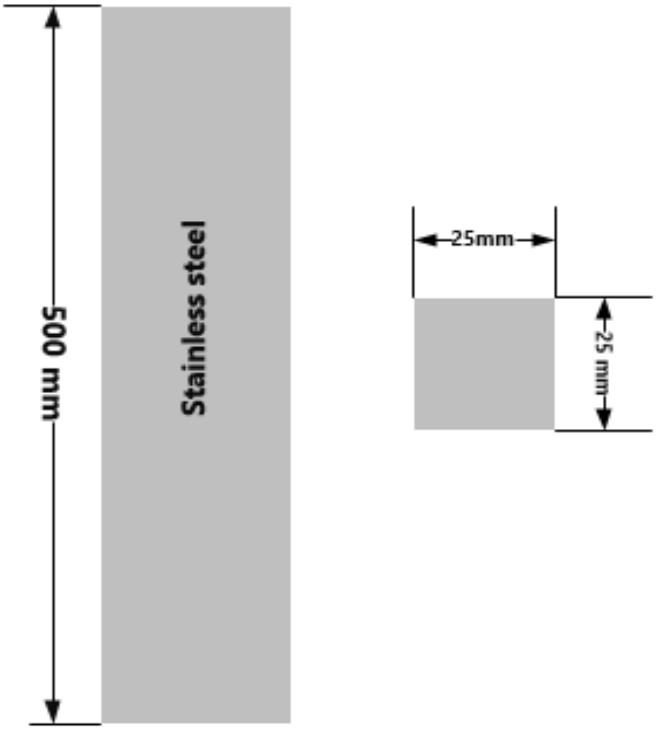

Figure B-16: Dimension of waveguides 1&2.

Appendix C

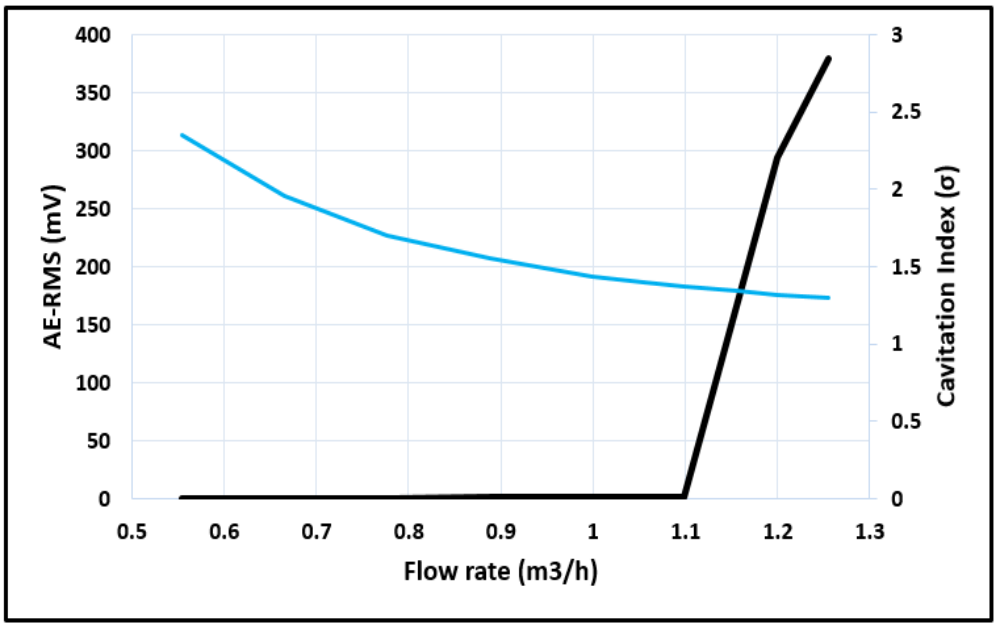

Figure C-1: Plot of AE-RMS and cavitation index against flow rate for tap water for ball valve 15^0 open (16.7 % of fully open).

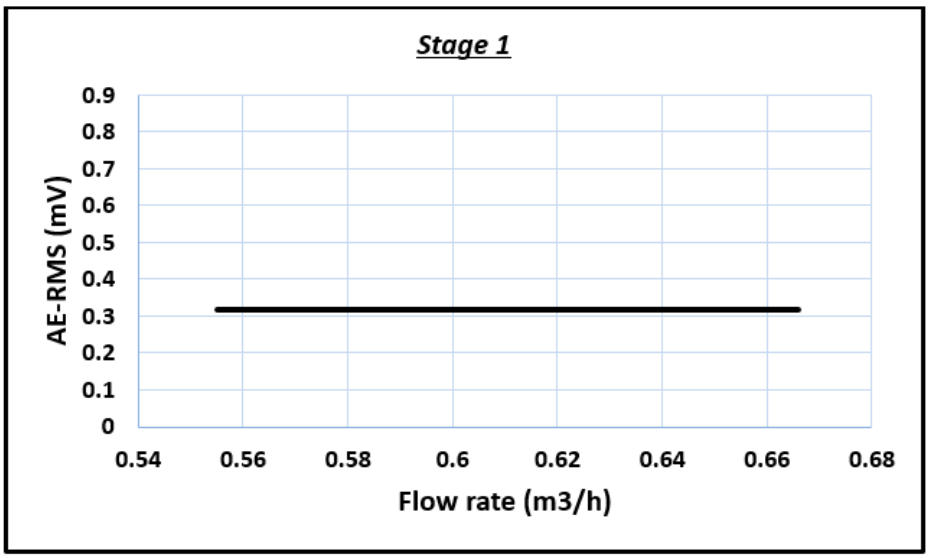

Figure C-2: RMS-flow rate diagram during stages 1 (channel 2), associated with Figure C-1.

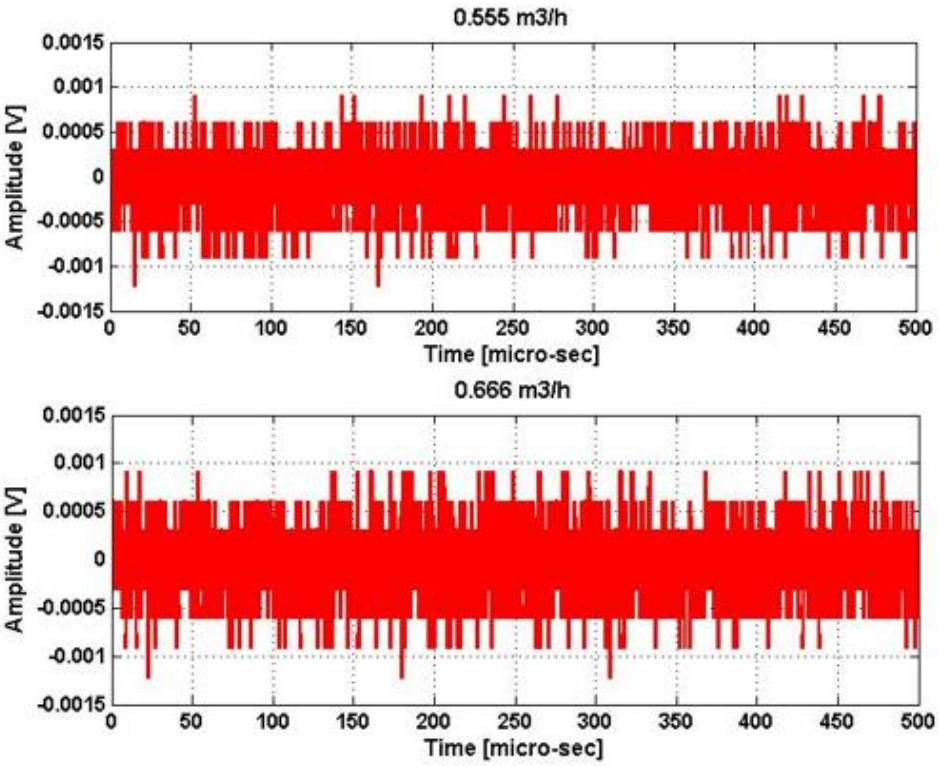

Figure C-3: AE waveforms associated with the ball valve test presented with Figure C-2.

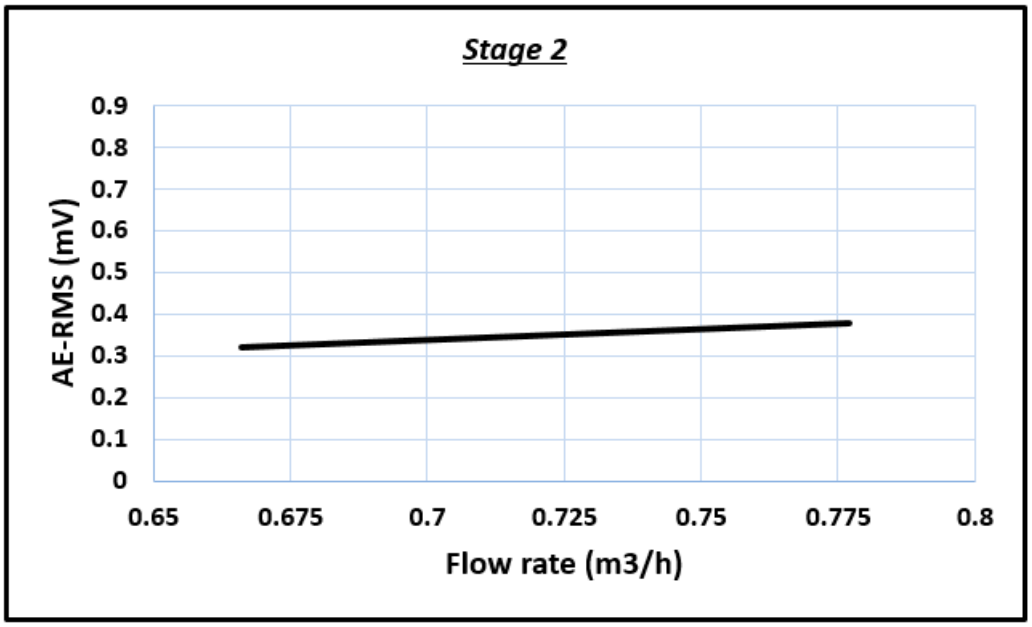

Figure C-4: AE- RMS vs flow rate during stage 2 (sensor 2) associated with Figure C-1.

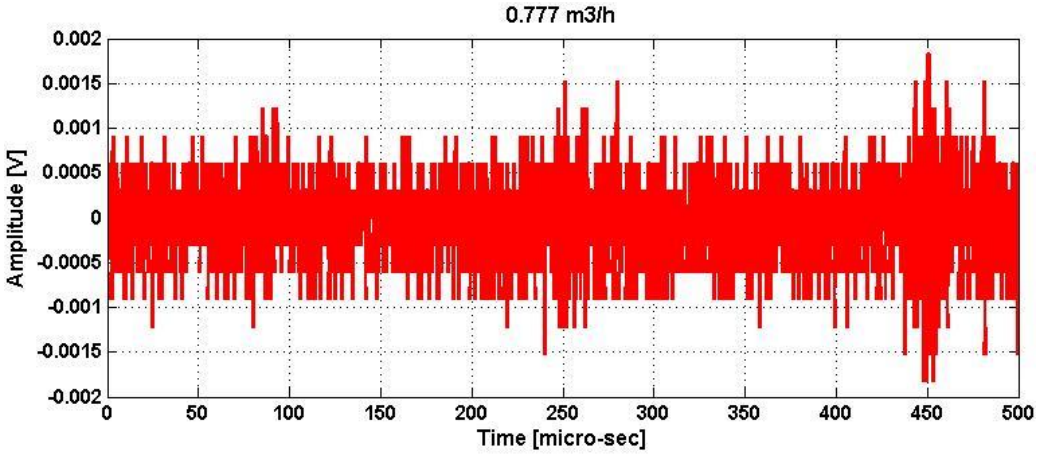

Figure C-5: AE waveform associated with the ball valve test presented with Figure C-4.

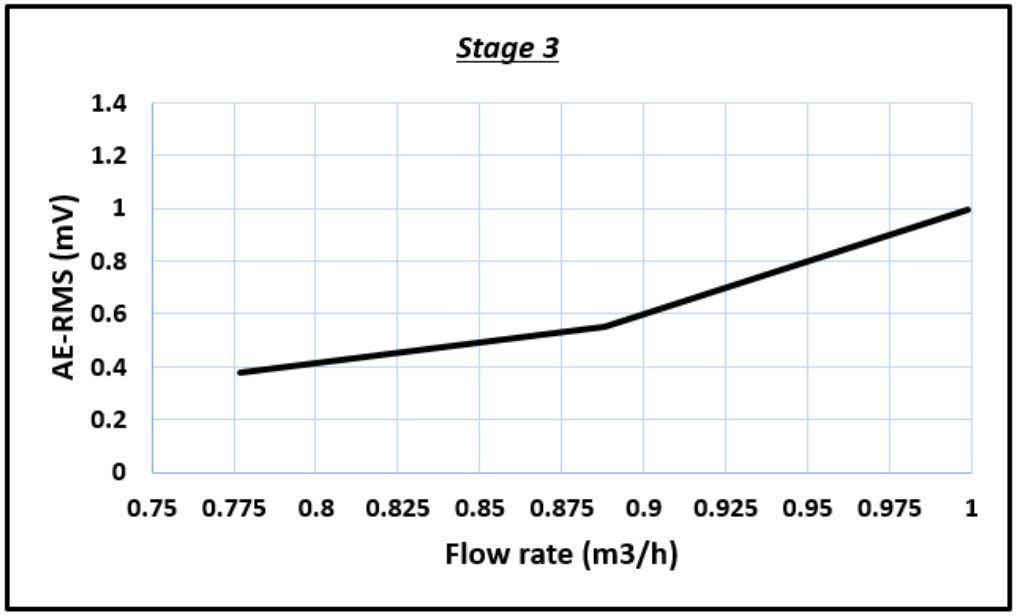

Figure C-6: AE-RMS vs flow rate diagram during stage 3 (sensor 2) associated with Figure C-1.

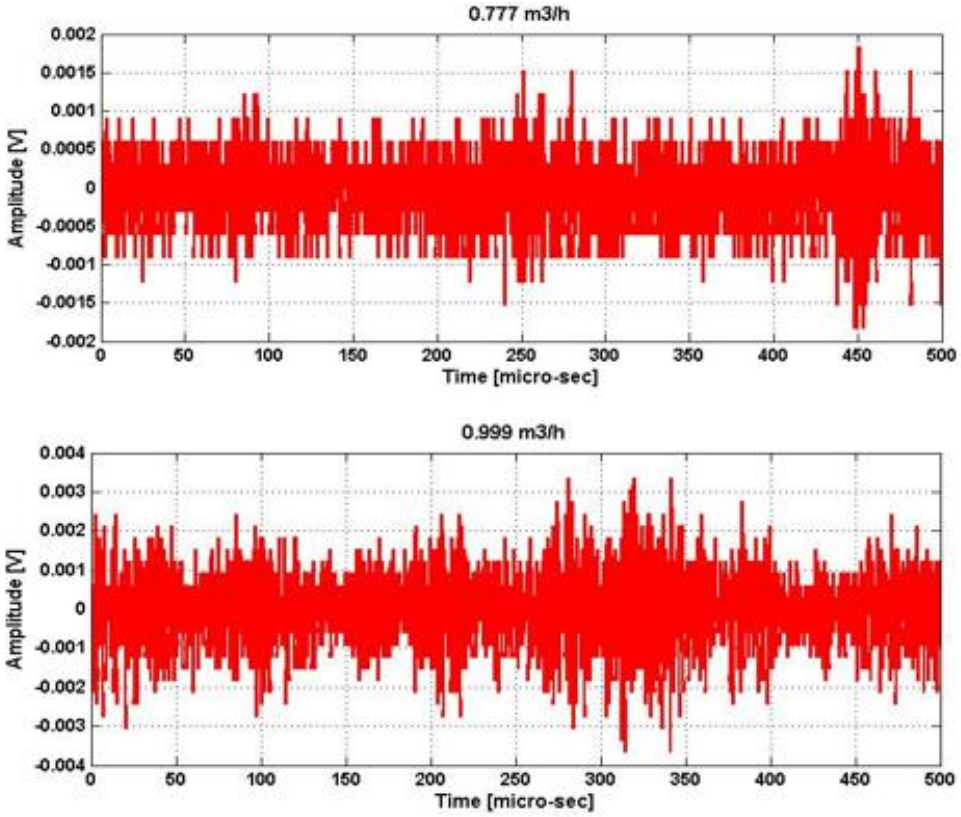

Figure C-7: AE waveforms associated with the ball valve test presented with Figure C-6.

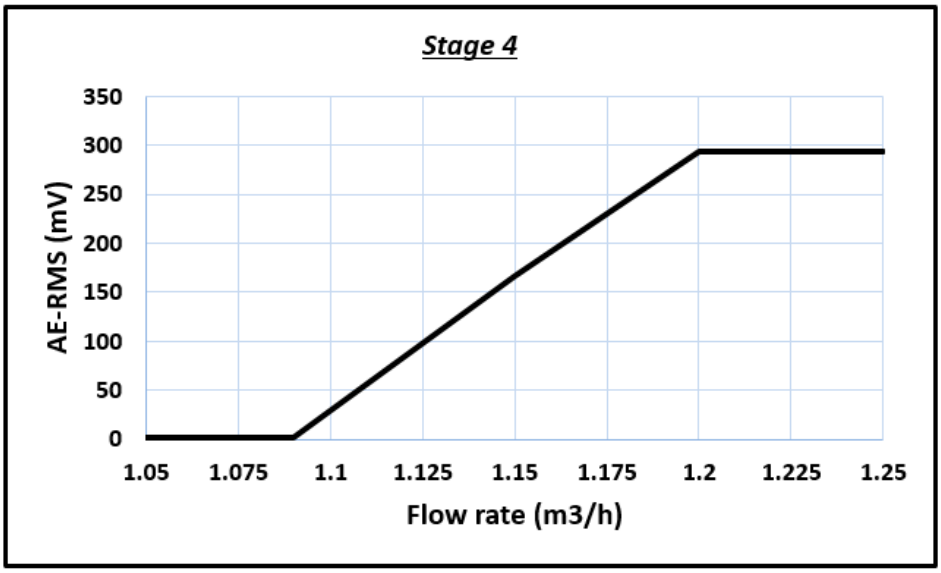

Figure C-8: AE-RMS vs flow rate diagram during stage 3 (sensor 2) associated with Figure C-1.

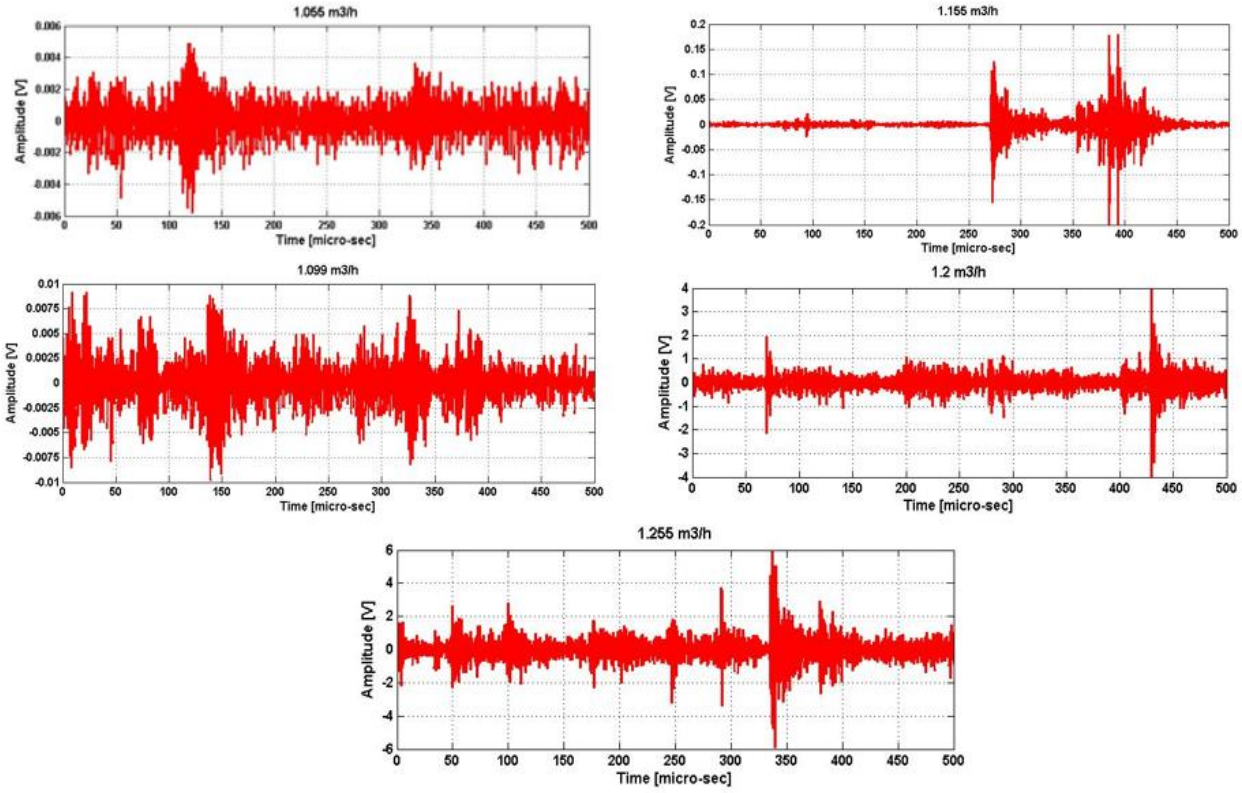

Figure C-9: AE waveforms associated with the ball valve test presented with Figure C-8.

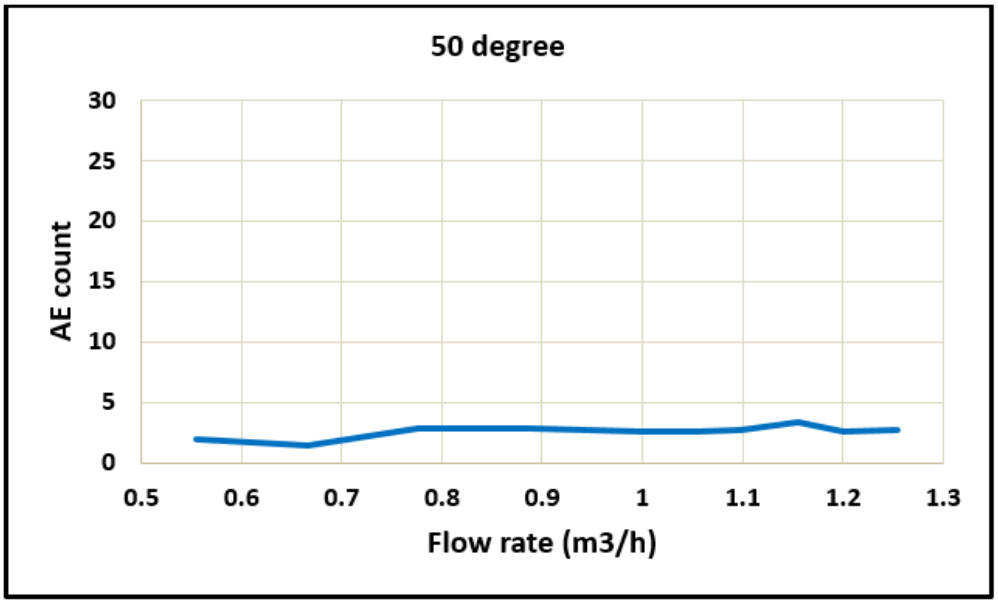

Figure C-10: Plot of counts against flow rate for ball valve at 50^0 open; sensor 2 (55.6 % of fully open).

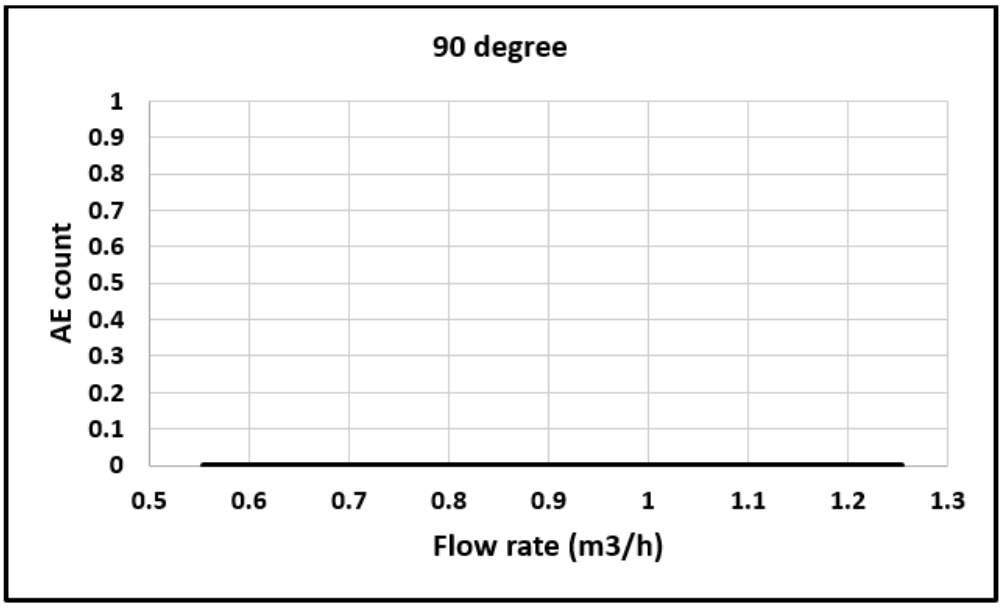

Figure C-11: Plot of counts against flow rate for ball valve 90^0 open; sensor 2 (100 % of fully open).

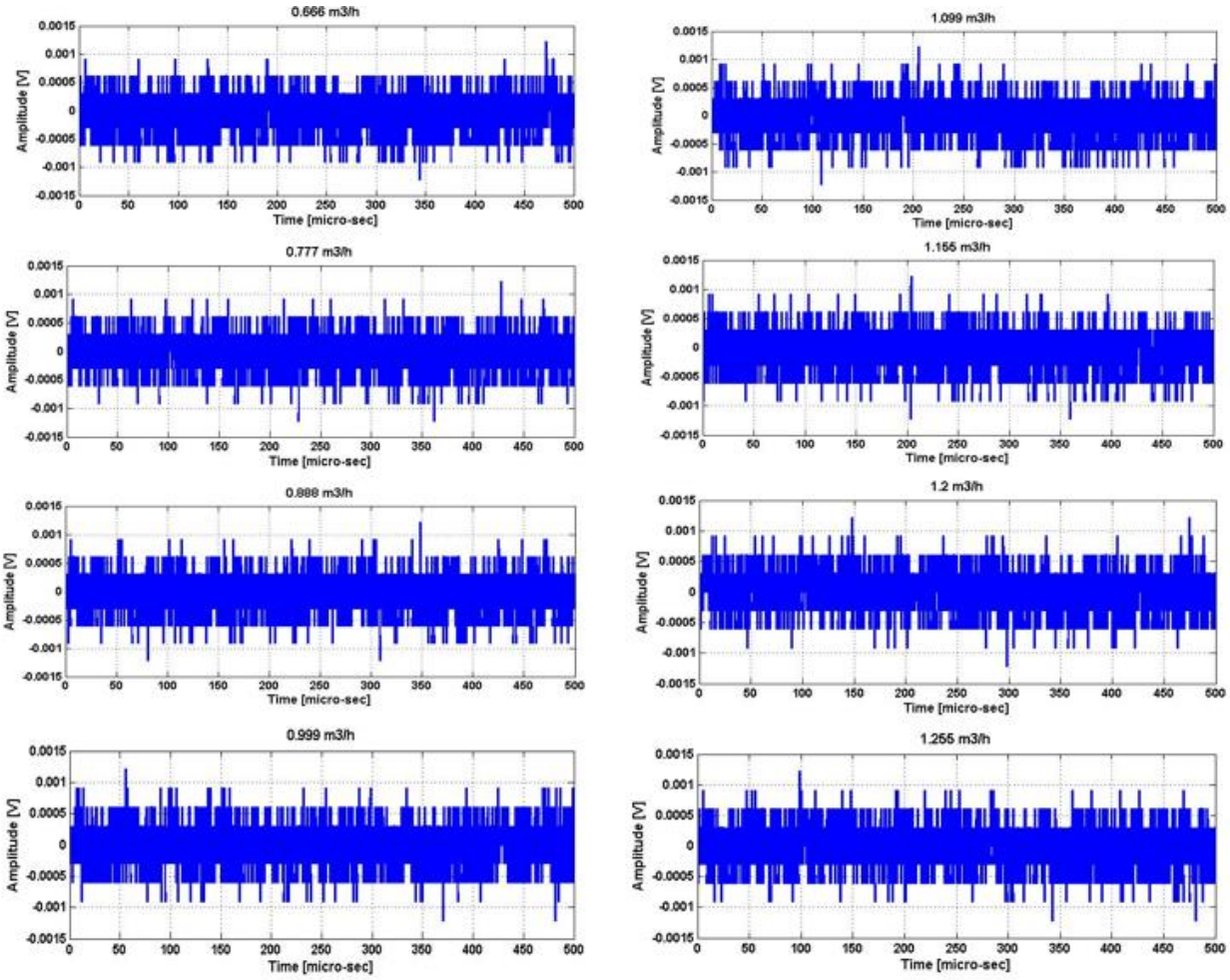

Figure C-12: AE waveforms associated with the ball valve test presented with Figure C-10.

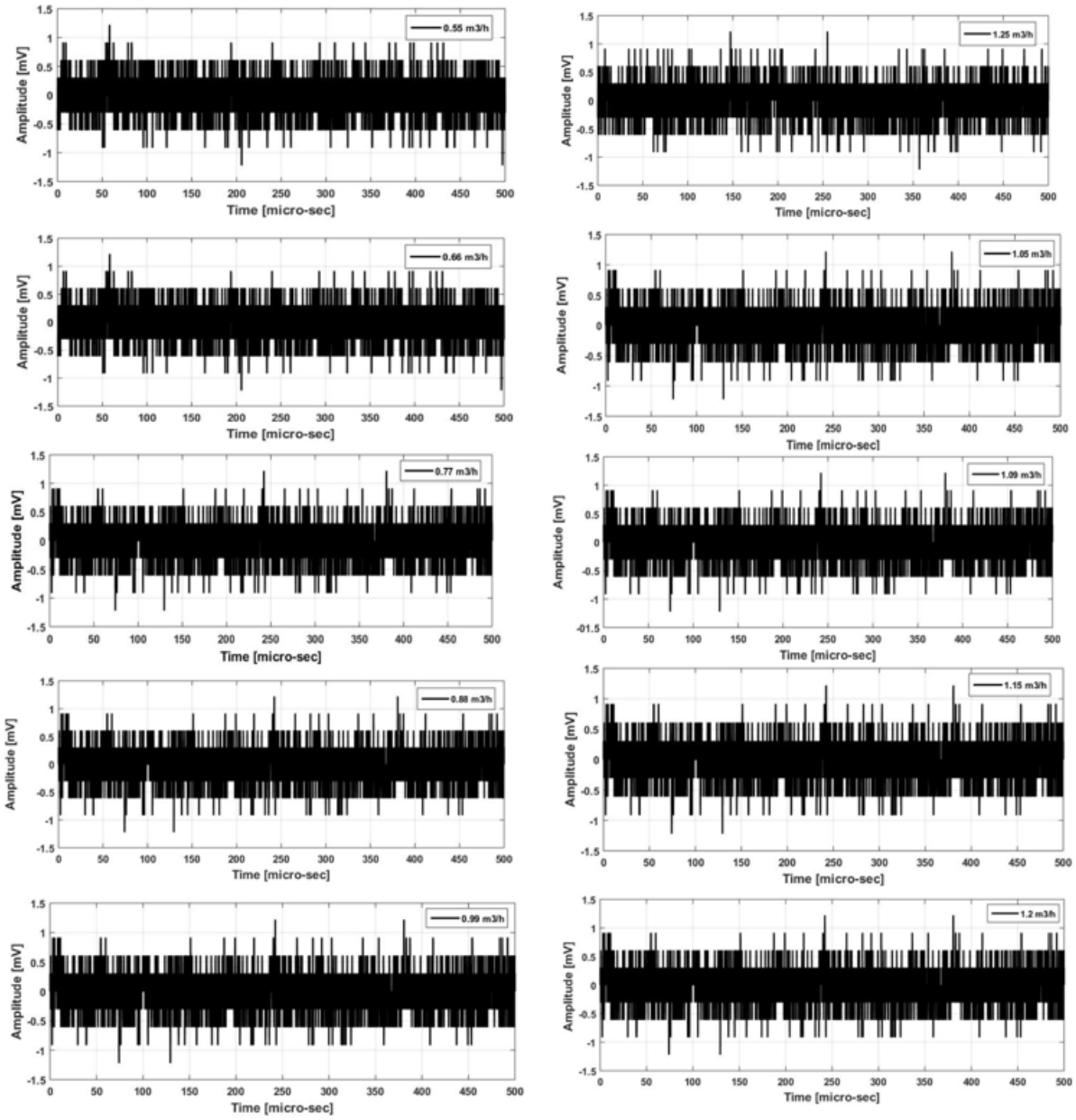

Figure C-13: AE waveforms associated with the ball valve test presented with Figure C-11.

Table C-1: P_1, P_2, K and σ at 14^0 associated with Figure C-14.

Flow rate (m^3/h)	P_1 (bar)	P_2 (bar)	P_1-P_2	P_V at 20^0C	K	Cavitation Index (σ)
0.55	1.905	1.028	0.877	0.023	0.46	2.14
0.66	2.268	1.045	1.223	0.023	0.54	1.80
0.77	2.705	1.066	1.639	0.023	0.61	1.63
0.88	3.242	1.091	2.151	0.023	0.66	1.49
0.99	3.809	1.0117	2.797	0.023	0.73	1.35
1.05	4.233	1.137	3.096	0.023	0.73	1.35
1.09	4.381	1.144	3.237	0.023	0.74	1.34
1.15	4.758	1.161	3.597	0.023	0.75	1.31
1.2	5.145	1.179	3.966	0.023	0.77	1.29
1.25	5.433	1.193	4.240	0.023	0.78	1.27

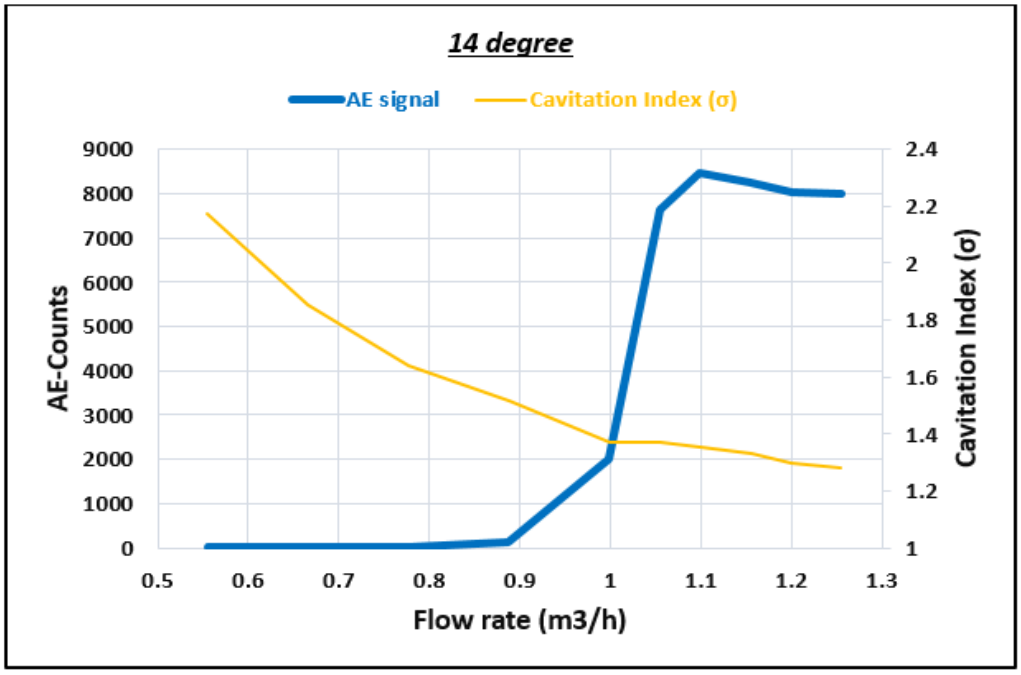

Figure C-14: Plot of counts against flow rate, cavitation index for ball valve 14^0 open; sensor 2 (15.6 % of fully open).

Table C-2: P_1, P_2, K and σ at 16^0 associated with Figure C-15.

Flow rate (m^3/h)	P_1 (bar)	P_2 (bar)	P_1-P_2	P_V at 20^0C	K	Cavitation Index (σ)
0.55	1.511	1.027	0.484	0.023	0.32	3.07
0.66	1.754	1.047	0.707	0.023	0.40	2.44
0.77	1.995	1.066	0.929	0.023	0.47	2.12
0.88	2.102	1.091	1.011	0.023	0.48	2.05
0.99	2.133	1.116	1.017	0.023	0.48	2.07
1.05	2.234	1.132	1.102	0.023	0.49	2.00
1.09	3.035	1.148	1.887	0.023	0.62	1.59
1.15	3.093	1.159	1.934	0.023	0.63	1.58
1.2	3.227	1.167	2.060	0.023	0.64	1.55
1.25	3.419	1.192	2.227	0.023	0.65	1.52

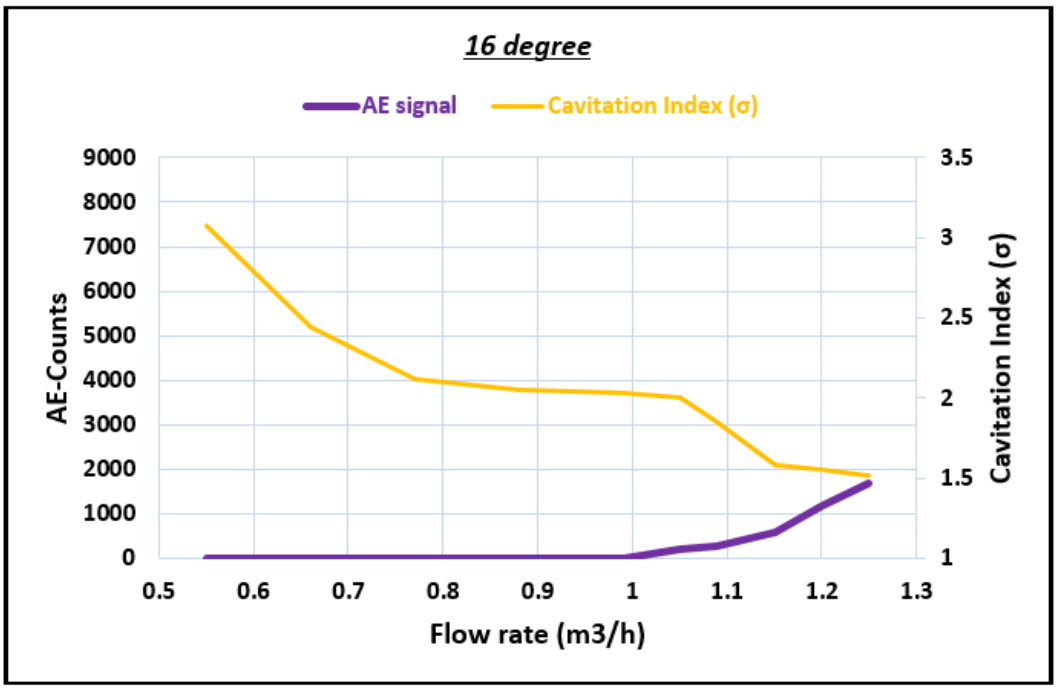

Figure C-15: Plot of counts against flow rate, cavitation index for ball valve 16^0 open; sensor (17.8 % of fully open).

Table C-3: P_1, P_2, K and σ at 17^0 associated with Figure C-16.

Flow rate (m^3/h)	P_1 (bar)	P_2 (bar)	P_1-P_2	P_V at 20^0C	K	Cavitation Index (σ)
0.55	1.366	1.026	0.431	0.023	0.25	3.94
0.66	1.523	1.045	0.685	0.023	0.31	3.13
0.77	1.704	1.066	0.918	0.023	0.37	2.63
0.88	1.916	1.089	0.827	0.023	0.43	2.28
0.99	2.137	1.115	1.022	0.023	0.45	2.21
1.05	2.179	1.147	1.048	0.023	0.46	2.15
1.09	2.302	1.239	1.057	0.023	0.46	2.15
1.15	2.347	1.242	1.105	0.023	0.47	2.10
1.2	2.357	1.249	1.108	0.023	0.48	2.07
1.25	2.366	1.251	1.115	0.023	0.49	2.03

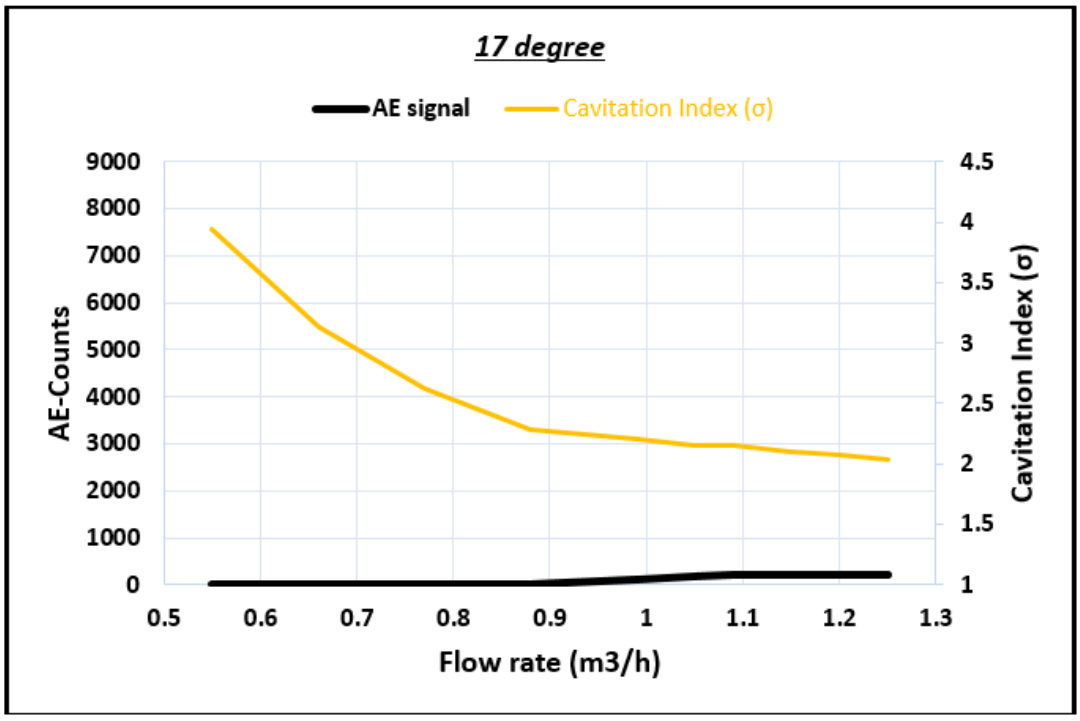

Figure C-16: Plot of counts against flow rate, cavitation index for ball valve 17^0 open; sensor 2 (18.9 % of fully open).

Table C-4: P_1, P_2, K and σ at 18^0 associated with Figure C-17.

Flow rate (m^3/h)	P_1 (bar)	P_2 (bar)	P_1-P_2	P_V at 20^0C	K	Cavitation Index (σ)
0.55	1.25	1.025	0.225	0.023	0.183419	5.45
0.66	1.362	1.044	0.318	0.023	0.237544	4.20
0.77	1.476	1.062	0.414	0.023	0.284987	3.50
0.88	1.62	1.086	0.534	0.023	0.33444	2.99
0.99	1.777	1.110	0.667	0.023	0.380339	2.62
1.05	1.876	1.121	0.755	0.023	0.407513	2.45
1.09	1.975	1.140	0.835	0.023	0.427832	2.33
1.15	2.077	1.158	0.919	0.023	0.447485	2.23
1.2	2.145	1.170	0.975	0.023	0.459537	2.17
1.25	2.247	1.186	1.061	0.023	0.477133	2.09

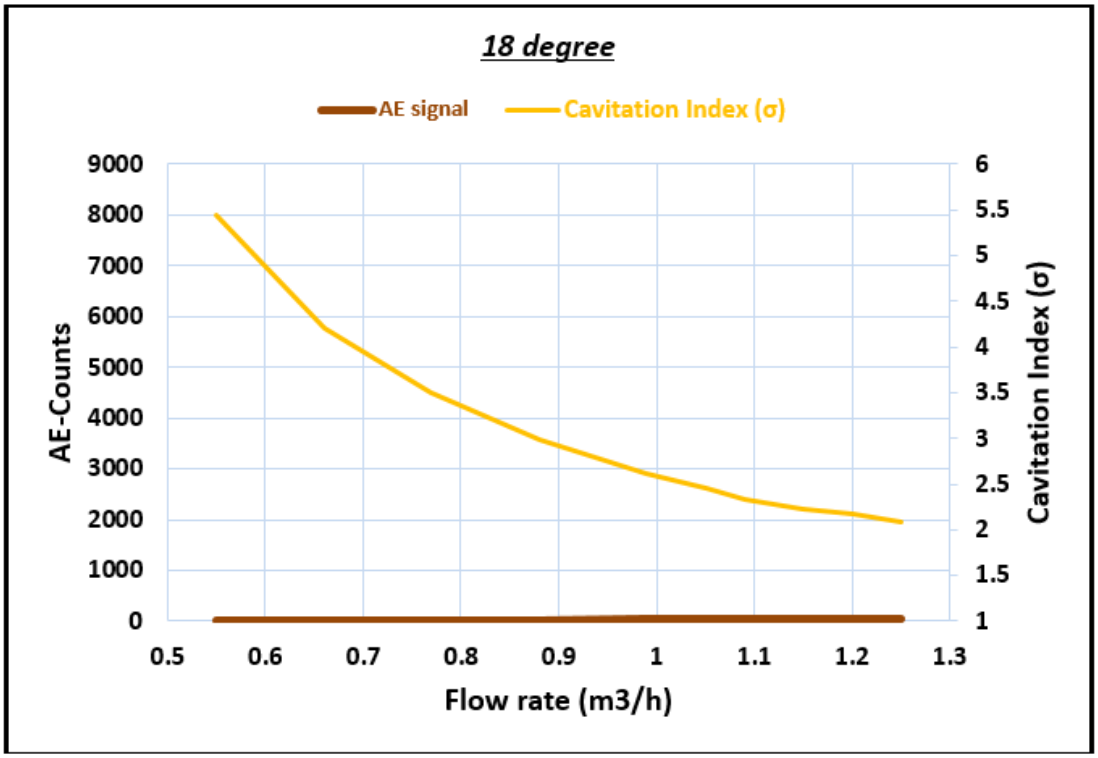

Figure C-17: Plot of counts against flow rate, cavitation index for ball valve 18^0 open; sensor 2 (20 % of fully open).

Table C-5: P_1, P_2, K and σ at 20^0 associated with Figure C-18.

Flow rate (m^3/h)	P_1 (bar)	P_2 (bar)	P_1-P_2	P_V at 20^0C	K	Cavitation Index (σ)
0.55	1.152	1.024	0.128	0.023	0.11	8.81
0.66	1.214	1.041	0.173	0.023	0.14	6.88
0.77	1.296	1.063	0.233	0.023	0.18	5.46
0.88	1.386	1.087	0.299	0.023	0.21	4.55
0.99	1.493	1.113	0.38	0.023	0.25	3.86
1.05	1.547	1.128	0.419	0.023	0.27	3.63
1.09	1.596	1.140	0.456	0.023	0.28	3.44
1.15	1.652	1.154	0.498	0.023	0.30	3.27
1.2	1.716	1.171	0.545	0.023	0.32	3.10
1.25	1.763	1.183	0.580	0.023	0.33	2.99

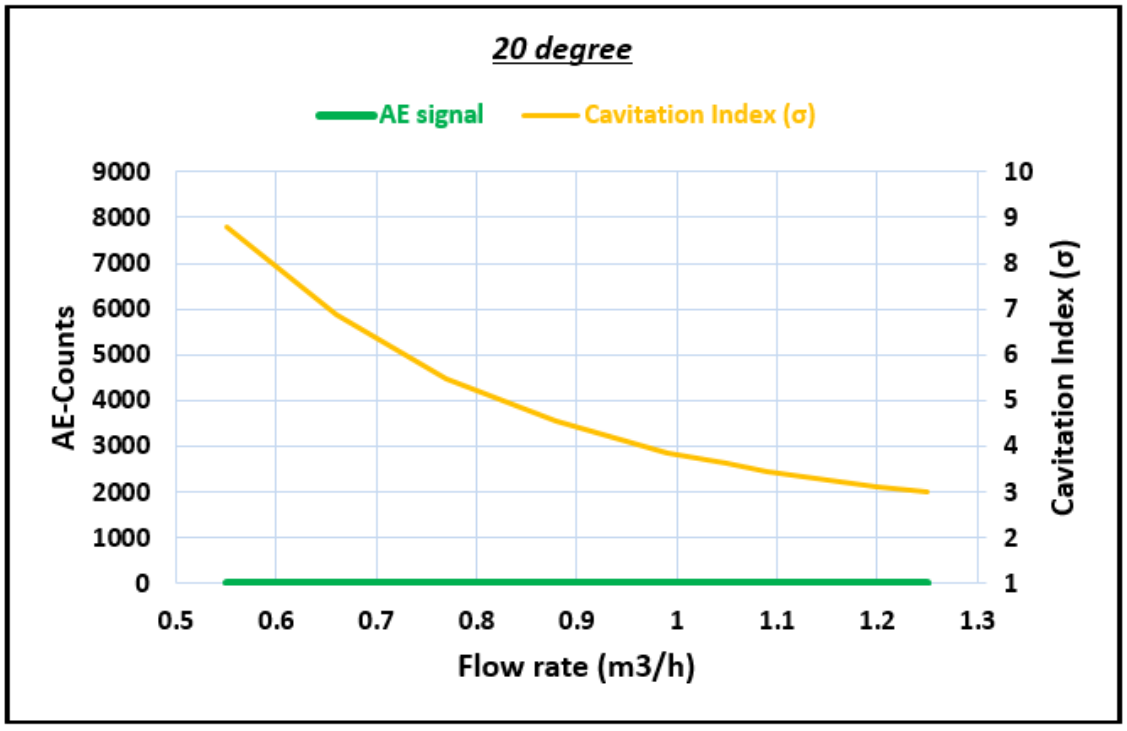

Figure C-18: Plot of counts against flow rate, cavitation index for ball valve 20^0 open; sensor 2 (22.2 % of fully open).

Table C-6: P_1, P_2, *K* and σ at 50^0 associated with Figure C-10.

Flow rate (m^3/h)	P_1 (bar)	P_2 (bar)	P_1-P_2	P_V at 20^0C	*K*	Cavitation Index (σ)
0.55	1.047	1.026	0.021	0.023	0.02	50
0.66	1.066	1.042	0.024	0.023	0.02	50
0.77	1.094	1.066	0.028	0.023	0.02	50
0.88	1.119	1.087	0.032	0.023	0.03	33.33
0.99	1.15	1.113	0.037	0.023	0.03	33.33
1.05	1.167	1.126	0.041	0.023	0.03	33.33
1.09	1.178	1.137	0.041	0.023	0.03	33.33
1.15	1.196	1.152	0.044	0.023	0.03	33.33
1.2	1.213	1.166	0.047	0.023	0.04	25
1.25	1.229	1.18	0.049	0.023	0.04	25

Table C-7: P_1, P_2, *K* and σ at 90^0 associated with Figure C-11.

Flow rate (m^3/h)	P_1 (bar)	P_2 (bar)	P_1-P_2	P_V at 20^0C	*K*	Cavitation Index (σ)
0.55	1.039	1.025	0.014	0.023	0.013	76.92
0.66	1.056	1.042	0.014	0.023	0.013	76.92
0.77	1.076	1.062	0.014	0.023	0.013	76.92
0.88	1.098	1.083	0.015	0.023	0.013	76.92
0.99	1.123	1.108	0.015	0.023	0.013	76.92
1.05	1.139	1.125	0.014	0.023	0.012	83.34
1.09	1.146	1.132	0.014	0.023	0.012	83.34
1.15	1.165	1.15	0.015	0.023	0.012	83.34
1.2	1.177	1.164	0.013	0.023	0.011	90.91
1.25	1.195	1.180	0.015	0.023	0.011	90.91

Table C-8: Shows AE Counts for different salt water concentration at 15^0 associated with Figure C-19.

Flow rate (m3/h)	Salt water (5 g/L)	Salt water (15 g/L)	Salt water (20 g/L)
0.55	5	5	5
0.66	6	7	5
0.77	15	13	8
0.88	20	17	10
0.99	187	94	77
1.05	771	694	420
1.09	1614	1369	876
1.15	5868	3322	1540
1.2	7936	4921	2742
1.25	7633	5960	4866

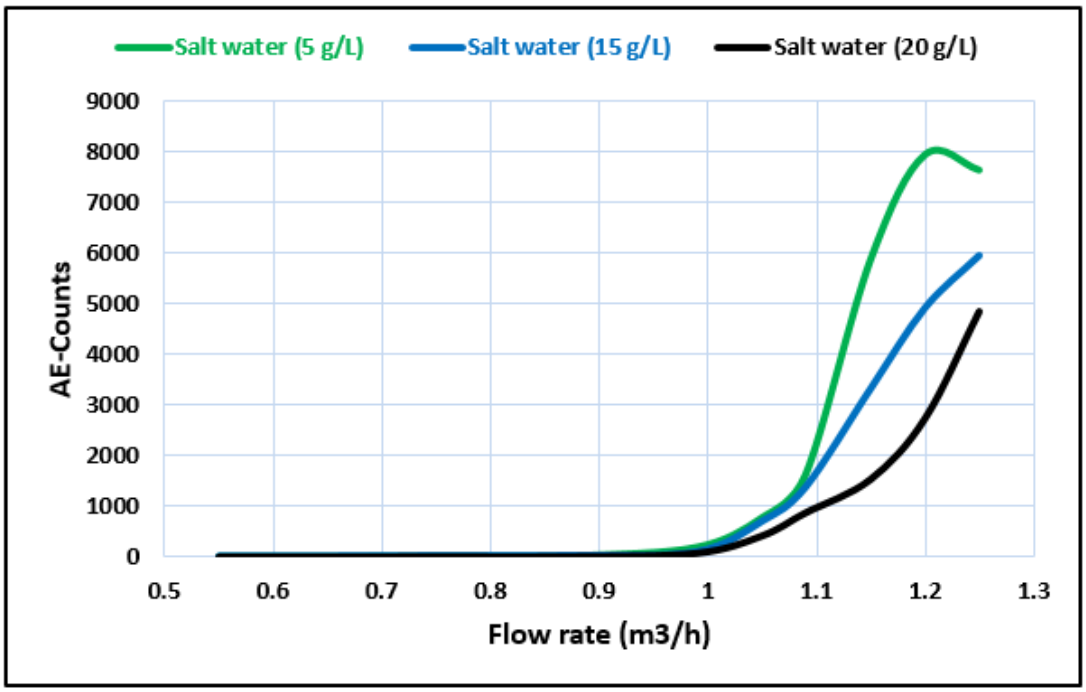

Figure C-19: Plot of AE signal for different salt water concentration during ball valve at 16.6 % (15^0) - sensor 2.

Table C-9: AE parameters for bubble formation in ball valve for salt water (5g/L) at stages 1, 2 and 3.

Flow rate (m^3/h)	Salt Water (5g/L)				
	AE Parameters				
	AE Rise Time (µs)	AE Count	AE Amplitude (dB)	AE Abs Energy (atto-joule)	AE Frequency (kHz)
0.55	20	5	29	3	226
0.66	25	6	29	4	218
0.77	135	15	30	25	167
0.88	239	20	30	28	156

Table C-10: AE parameters for bubble formation in ball valve for salt water (15g/L) at stages 1, 2 and 3.

Flow rate (m^3/h)	Salt Water (15g/L)				
	AE Parameters				
	AE Rise Time (µs)	AE Count	AE Amplitude (dB)	AE Abs Energy (atto-joule)	AE Frequency (kHz)
0.55	25	5	29	6	163
0.66	17	7	29	9	161
0.77	91	13	30	10	147
0.88	234	17	30	22	77

Table C-11: AE parameters for bubble formation in ball valve for salt water (20g/L) at stages 1, 2 and 3.

Flow rate (m^3/h)	Salt Water (20g/L)				
	AE Parameters				
	AE Rise Time (µs)	AE Count	AE Amplitude (dB)	AE Abs Energy (atto-joule)	AE Frequency (kHz)
0.55	15	5	29	3	180
0.66	19	5	29	4	170
0.77	162	8	30	7	140
0.88	232	10	28	20	64

Table C-12: Liquid properties for different concentration of salt at 20^0C [14][176][177].

Properties / Liquids	Salt water (5g/L)	Salt water (15g/L)	Salt water (20g/L)
Viscosity	1.019 mm^2/s	1.068 mm^2/s	1.175 mm^2/s
Density	1.025 g/cm^3	1.078 g/cm^3	1.195 g/cm^3
Surface tension	75 mN/m (Literature)	76 mN/m (Literature)	78 mN/m (Literature)

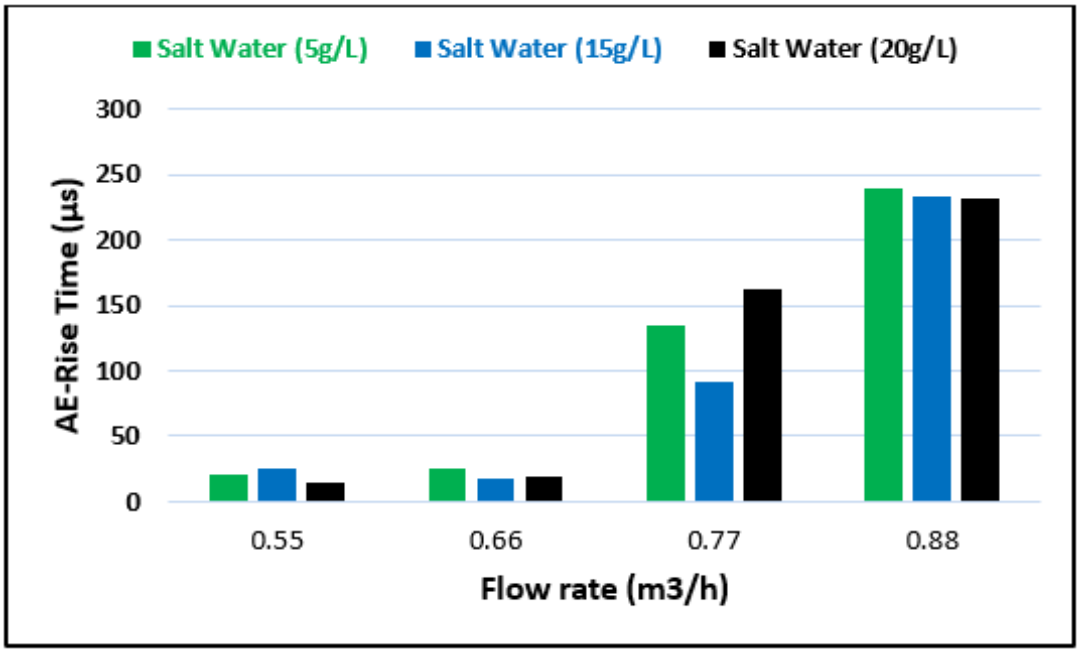

Figure C-20: Rise time as a function of the flow rate for salt water (5 g/L), salt water (15 g/L) and salt water (20 g/L), ball valve open 15^0.

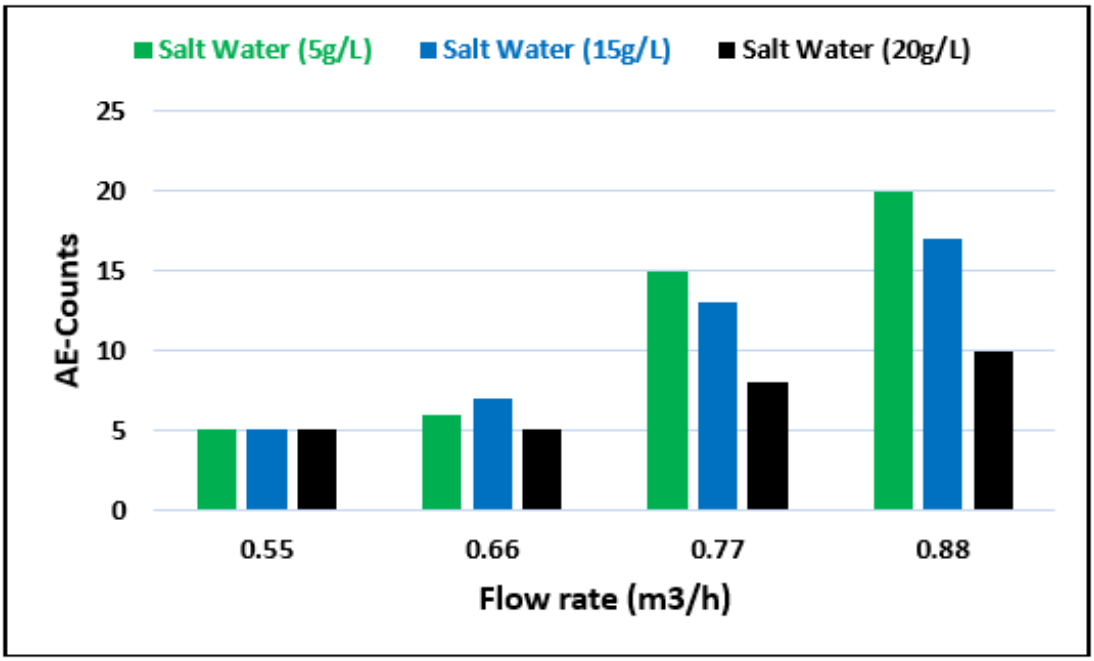

Figure C-21: AE Count as a function of flow rate for salt water (5 g/L), salt water (15 g/L) and salt water (20 g/L), ball valve open 15^0.

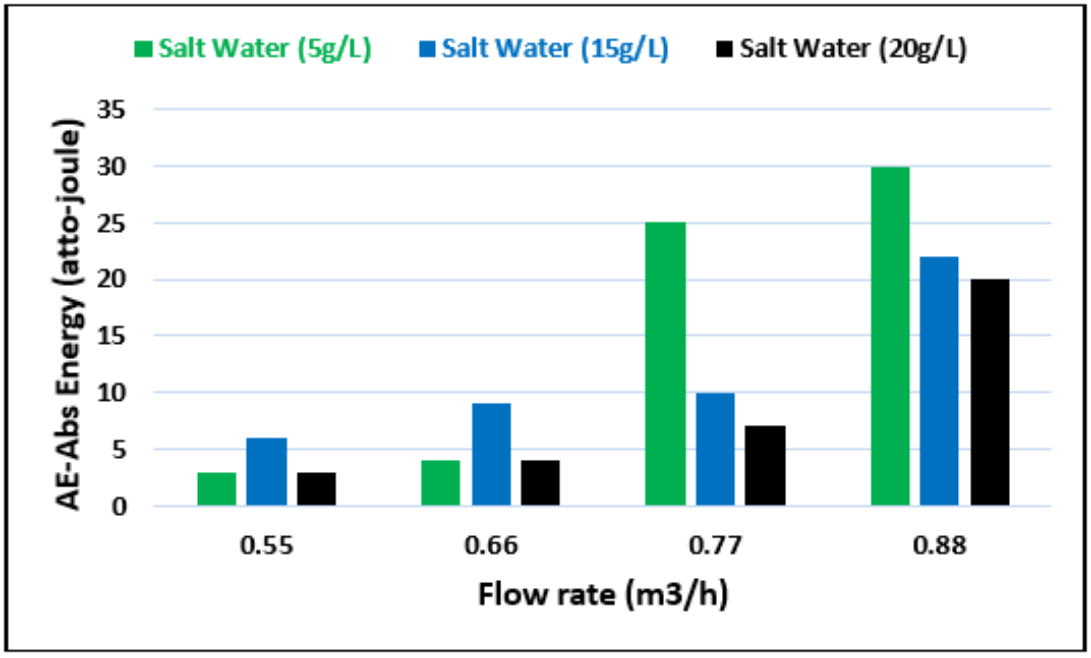

Figure C-22: AE Absolute Energy as a function of flow rate for salt water (5 g/L), salt water (15 g/L) and salt water (20 g/L), ball valve open 15^0.

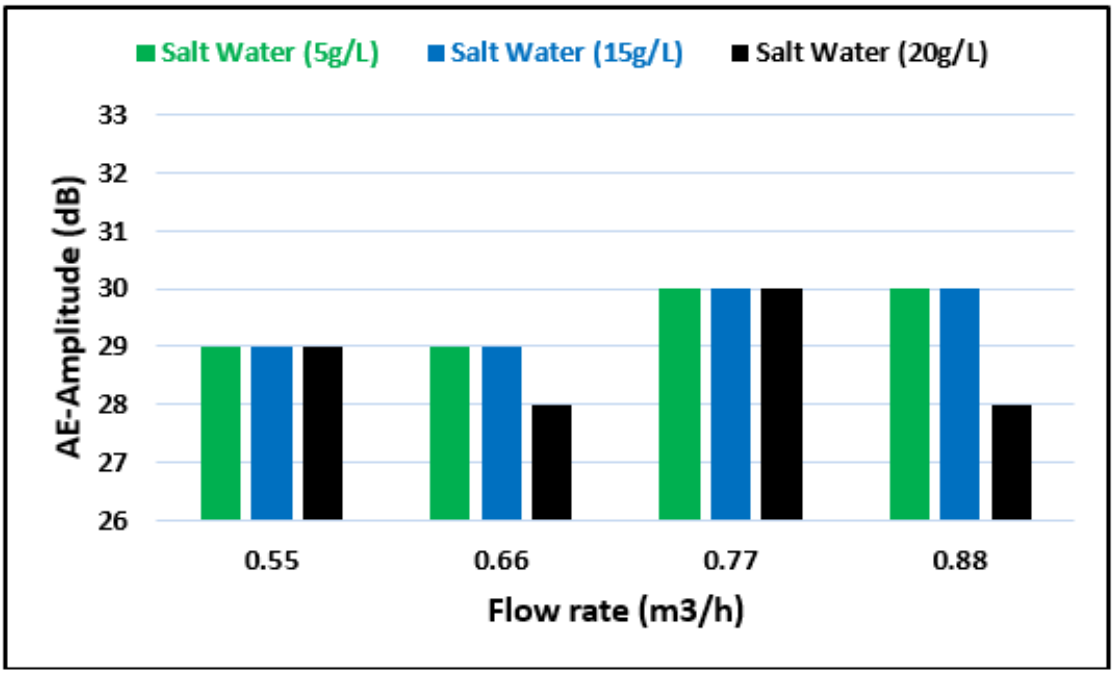

Figure C-23: AE Amplitude (dB) as a function of flow rate for salt water (5 g/L), salt water (15 g/L) and salt water (20 g/L), ball valve open 15^0.

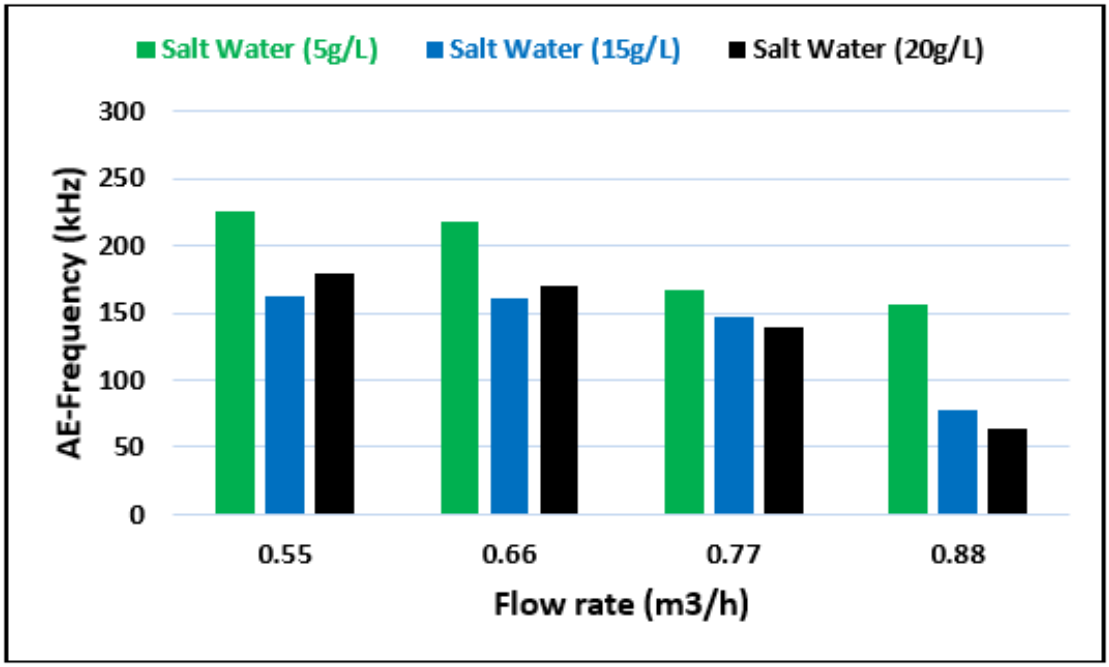

Figure C-24: AE Frequency (kHz) as a function of flow rate for salt water (5 g/L), salt water (15 g/L) and salt water (20 g/L), ball valve open 15^0.

Difference between rise times of AE-signals for bubble formation and bubble collapse in ball valves using tap water

Figure C-25 presents a typical example of an AE waveform obtained from the formation and collapse of bubbles in tap water at a flow rate of 1.15 m^3/h as detected by sensor 2. As expected, there were significant differences between AE rise time of signals generated by bubble formation and bubble collapse. The AE signal increased sharply for both bubble formation and collapse, about 30 – 60 µs respectively. Following this, the AE signals gradually decreased, the AE amplitude value of bubble collapse is higher than that of bubble formation with 150 and 100 mV respectively, as shown in Figure C-25. Figure (2-1), in Chapter 2, confirms that the sound signal caused by bubble generation and detachment from nozzle can increase suddenly [33]. It was observed that the value of AE rise time in bubble formation is less than that of bubble collapse. During the collapse process into micro-jets, a small bubble is capable of causing high pressure in the liquid, which in turn causes high fluid velocity and the micro-jetting phenomena. That creates the cavitation effect that produces high local temperatures, and extremely high pressure [149]. Furthermore, collapsing bubbles will oscillate before they subsequently collapse and produce a shock-wave [90][112]. For this reason, the AE-signals for bubble collapse are higher and more violent than those for bubble formation. These results lead to the conclusion that the AE-signals of bubble collapse are higher and more violent than those of bubble formation at 1.15 m^3/h. This result will need more investigation as mentioned in future work in chapter 7, section (7.2).

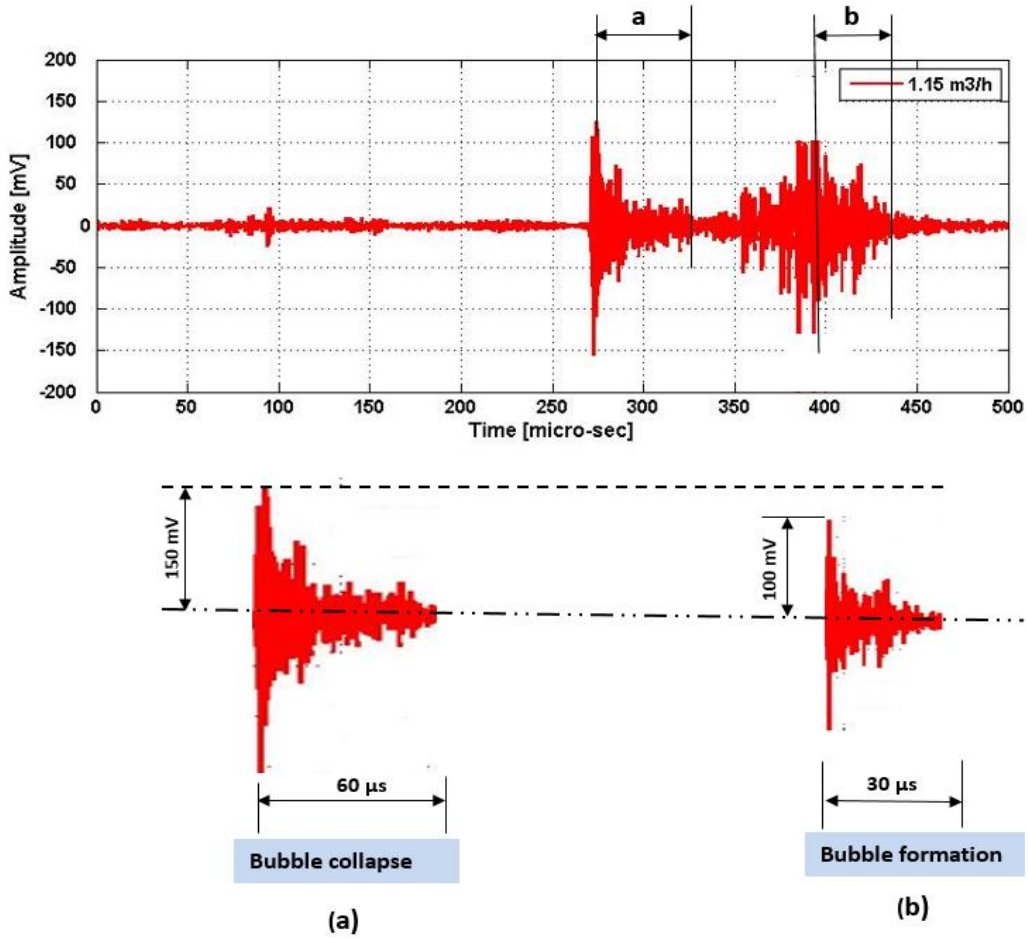

Figure C-25: AE amplitude for bubble formation and collapse at a flow rate 1.15 m^3/h for tap water, valve open 15^0, sensor 2.

Appendix D

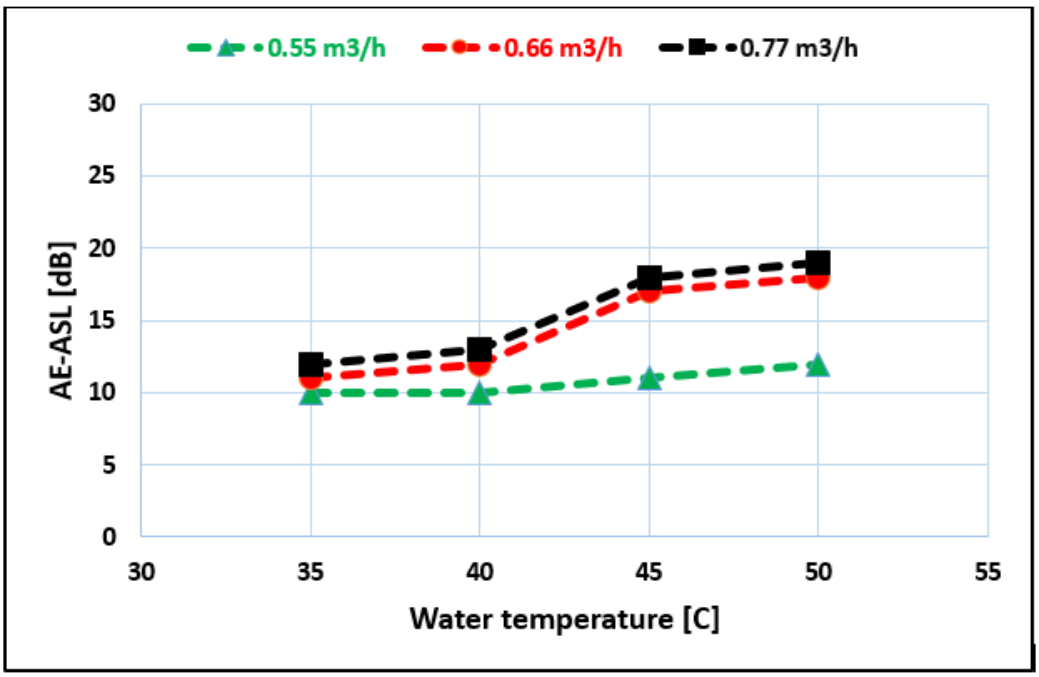

Figure D-1: Effect of different fluid temperatures on the AE-ASL signal at 40^0 in globe during stage 1 (Sensor 2).

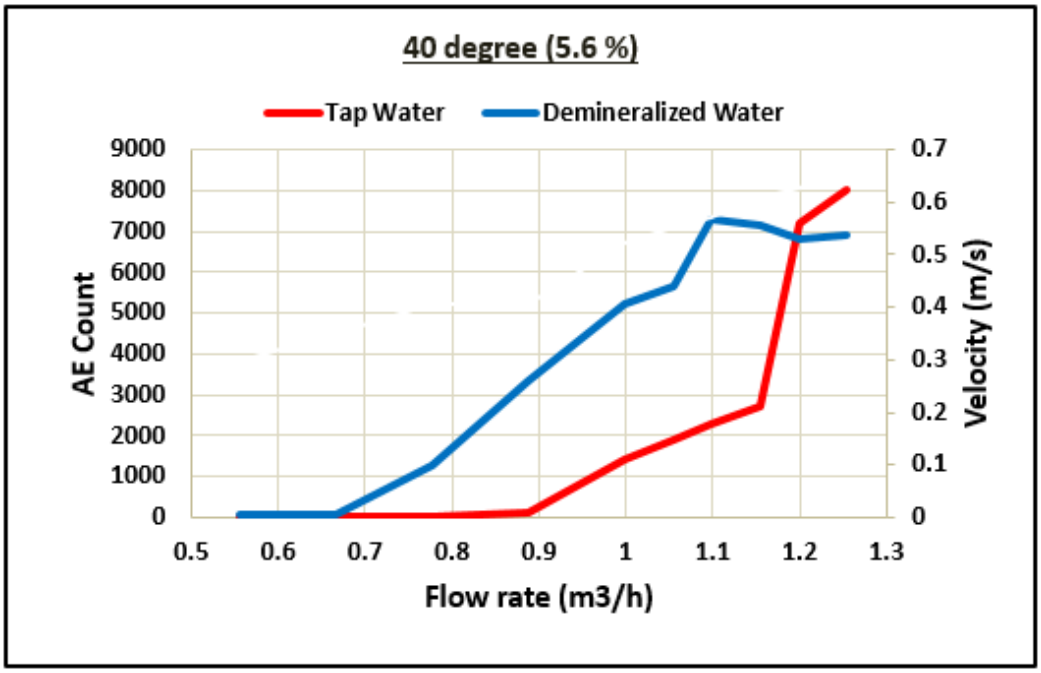

Figure D-2: Comparison of AE-Count of bubble occurrence in demineralized water and tap water at opening percentage 5.6 %. (Sensor 2).

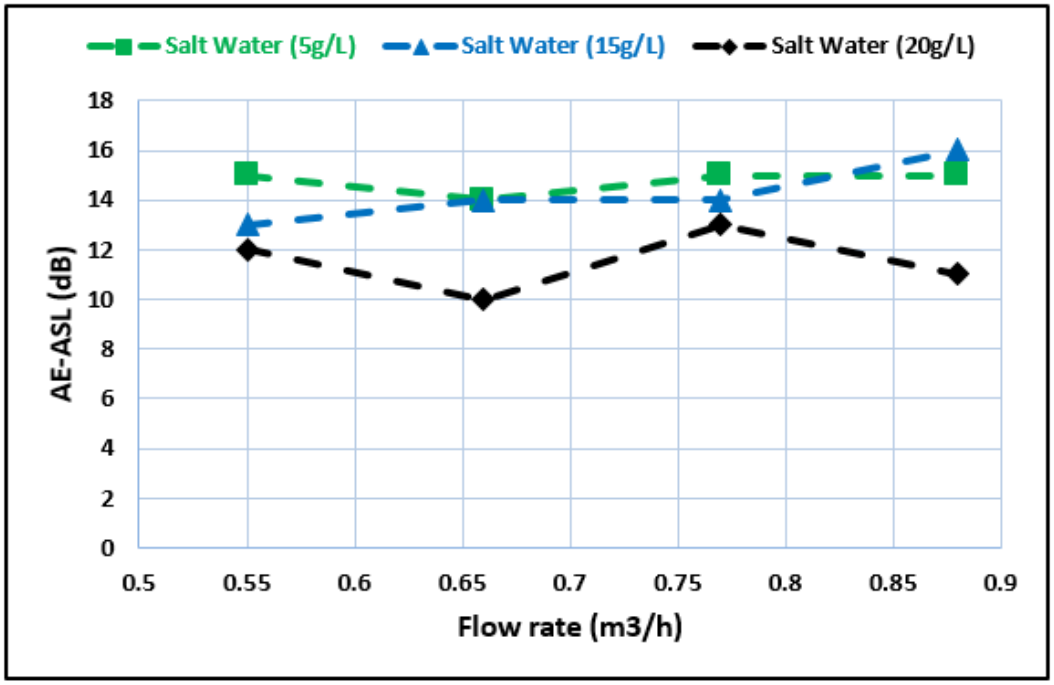

Figure D-3 : Effect of different salt water concentration on AE-ASL level, globe valve 40^0 open during stage 1 (Sensor 2).

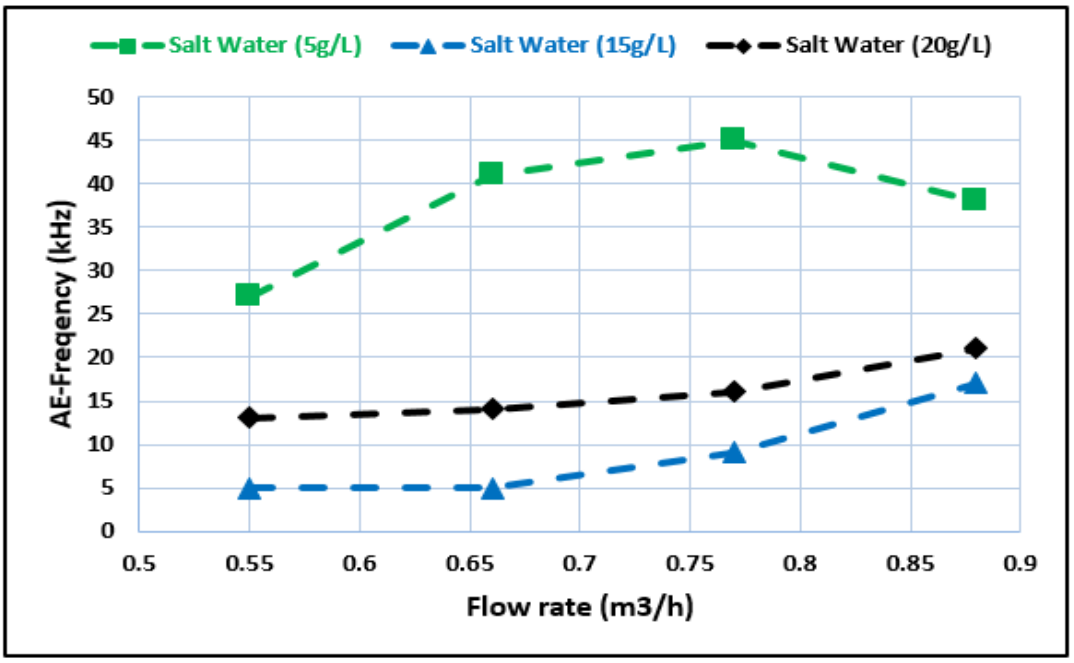

Figure D-4: Effect of different salt water concentration on AE-Frequency signal globe valve 40^0 open during stage 1. (Sensor 2).

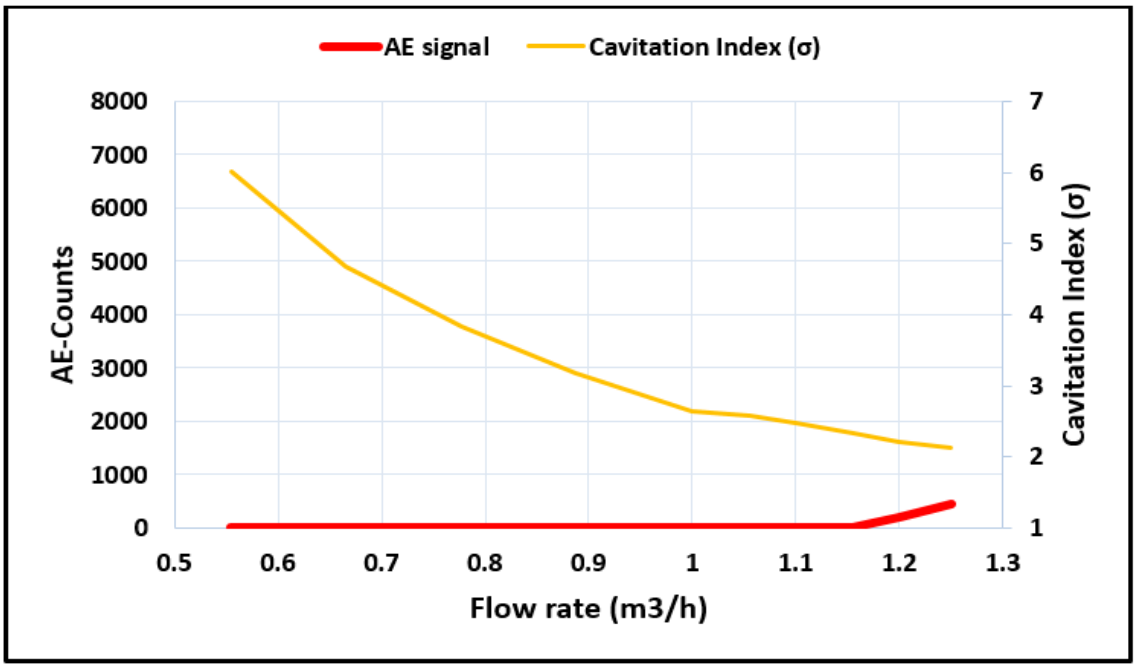

Figure D-5: Plot of counts against flow rate, cavitation index for globe valve 55^0 open, sensor 2, at 20^0C (7.6 % of fully open).

Table D-1: P_1, P_2, K, σ and P_v= (0.023) at 55^0 associated with Figure D-5, 20^0C.

Flow rate (m^3/h)	P_1 (bar)	P_2 (bar)	(P_1-P_2), bar	k	Cavitation Index (σ)
0.55	1.226	1.026	0.200	0.16	6.01
0.66	1.319	1.042	0.277	0.21	4.67
0.77	1.426	1.061	0.365	0.26	3.84
0.88	1.573	1.085	0.488	0.31	3.17
0.99	1.774	1.112	0.662	0.37	2.64
1.05	1.829	1.127	0.702	0.38	2.57
1.09	1.882	1.134	0.748	0.40	2.48
1.15	2.001	1.152	0.849	0.42	2.32
1.20	2.112	1.17	0.942	0.45	2.21
1.25	2.214	1.186	1.028	0.47	2.13

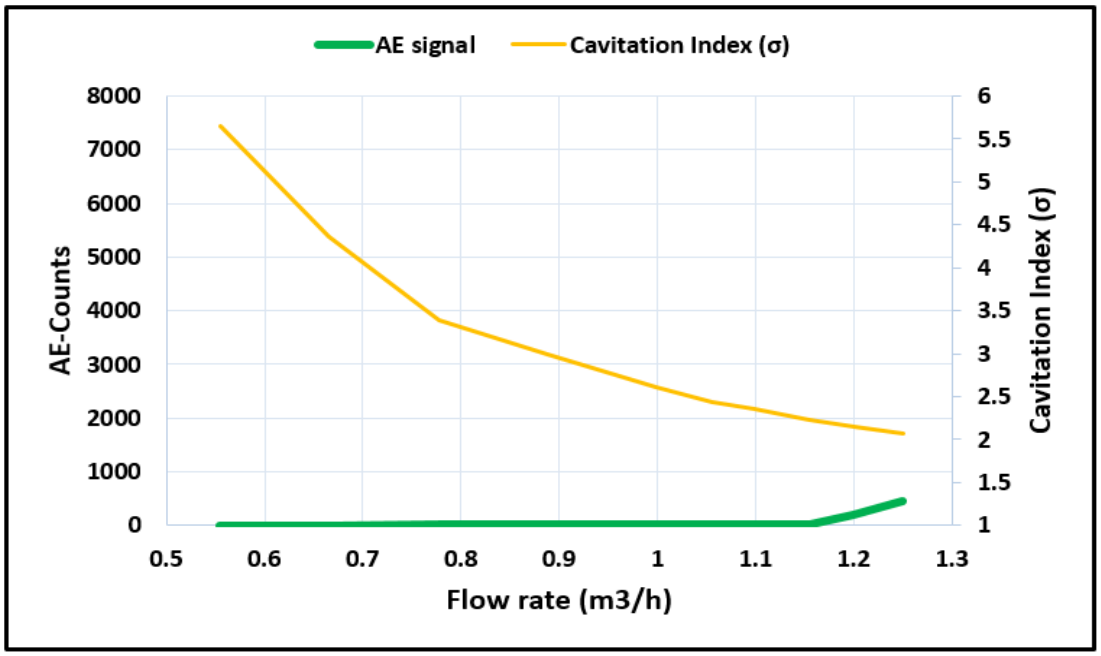

Figure D-6: Plot of counts against flow rate, cavitation index for globe valve 55^0 open, sensor 2, at 35^0C (7.6 % of fully open).

Table D-2: P_1, P_2, K, σ and P_v= (0.056) at 55^0 associated with Figure D-6, 35^0C.

Flow rate (m^3/h)	P_1 (bar)	P_2 (bar)	(P_1-P_2), bar	k	Cavitation Index (σ)
0.55	1.238	1.029	0.209	0.17	5.65
0.66	1.341	1.046	0.295	0.22	4.35
0.77	1.494	1.069	0.425	0.29	3.38
0.88	1.607	1.088	0.519	0.33	2.98
0.99	1.767	1.113	0.654	0.38	2.61
1.05	1.873	1.129	0.744	0.40	2.44
1.09	1.932	1.138	0.794	0.42	2.36
1.15	2.049	1.156	0.893	0.44	2.23
1.20	2.138	1.171	0.967	0.46	2.15
1.25	2.247	1.185	1.062	0.48	2.06

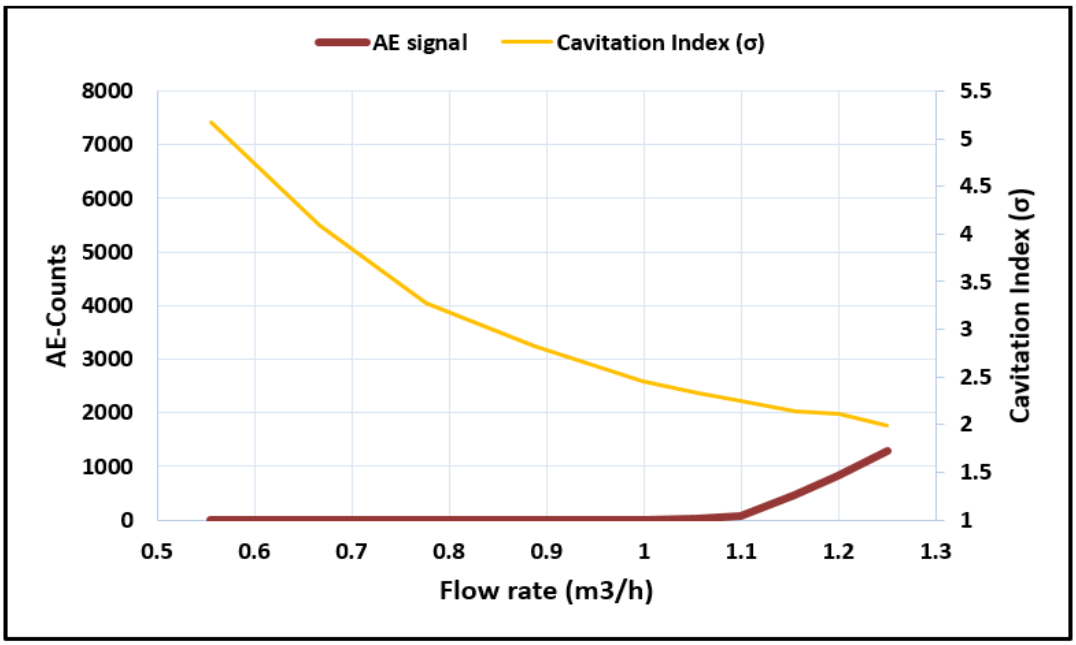

Figure D-7: Plot of counts against flow rate, cavitation index for globe valve 55^0 open, sensor 2, at 40^0C (7.64 % of fully open).

Table D-3: P_1, P_2, K, σ and P_v= (0.074) at 55^0 associated with Figure D-7, 40^0C.

Flow rate (m^3/h)	P_1 (bar)	P_2 (bar)	(P_1-P_2), bar	k	Cavitation Index (σ)
0.55	1.259	1.03	0.229	0.19	5.17
0.66	1.36	1.046	0.314	0.24	4.09
0.77	1.503	1.067	0.436	0.30	3.27
0.88	1.646	1.088	0.558	0.35	2.81
0.99	1.831	1.116	0.715	0.40	2.45
1.05	1.924	1.131	0.793	0.42	2.33
1.09	1.997	1.141	0.856	0.44	2.24
1.15	2.105	1.156	0.949	0.46	2.14
1.20	2.154	1.169	0.985	0.47	2.11
1.25	2.303	1.183	1.12	0.50	1.99

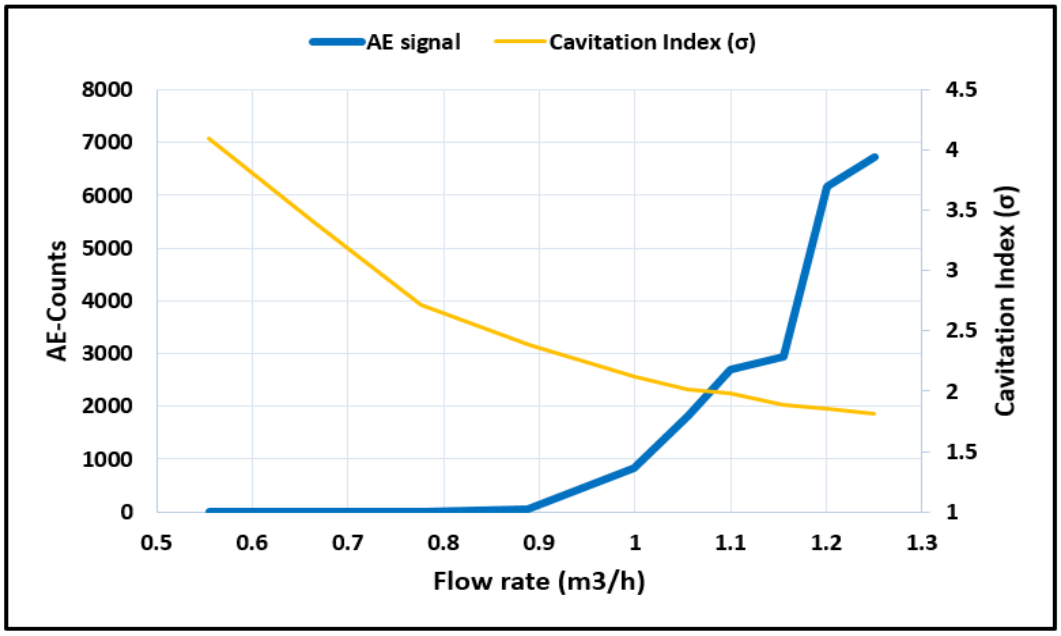

Figure D-8: Plot of counts against flow rate, cavitation index for globe valve 55^{0} open, sensor 2, at 45^{0}C (7.64 % of fully open).

Table D-4: P_1, P_2, K, σ and P_v= (0.096) at 55^{0} associated with Figure D-8, 45^{0}C.

Flow rate (m^3/h)	P_1 (bar)	P_2 (bar)	(P_1-P_2), (bar)	k	Cavitation Index (σ)
0.55	1.324	1.024	0.300	0.24	4.09
0.66	1.436	1.041	0.395	0.29	3.39
0.77	1.623	1.061	0.562	0.36	2.71
0.88	1.787	1.079	0.708	0.41	2.38
0.99	2.011	1.106	0.905	0.47	2.11
1.05	2.132	1.123	1.009	0.49	2.01
1.09	2.179	1.127	1.052	0.50	1.98
1.15	2.322	1.146	1.176	0.52	1.89
1.20	2.398	1.156	1.242	0.53	1.85
1.25	2.506	1.174	1.332	0.55	1.80

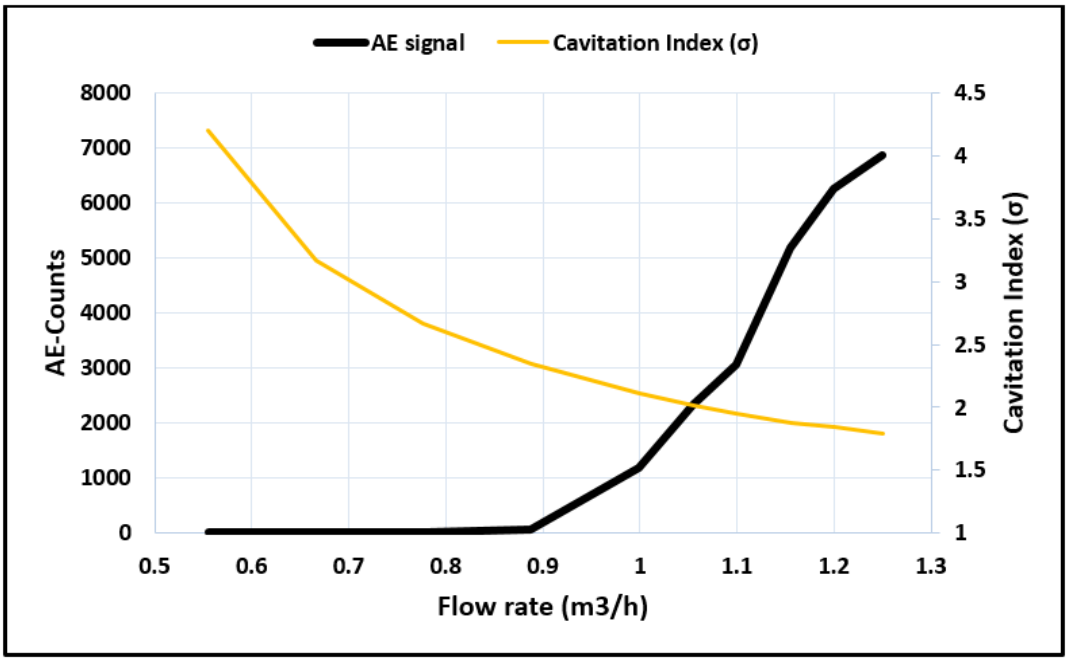

Figure D-9: Plot of counts against flow rate, cavitation index for globe valve 55^0 open, sensor 2, at 50^0C (7.64 % of fully open).

Table D-5: P_1, P_2, K, σ and P_v= (0.123) at 55^0 associated with Figure D-9, 50^0C.

Flow rate (m^3/h)	P_1 (bar)	P_2 (bar)	(P_1-P_2), (bar)	k	Cavitation Index (σ)
0.55	1.313	1.030	0.283	0.23	4.20
0.66	1.468	1.044	0.424	0.31	3.17
0.77	1.625	1.062	0.563	0.37	2.66
0.88	1.796	1.083	0.713	0.42	2.34
0.99	1.989	1.107	0.882	0.47	2.11
1.05	2.107	1.121	0.986	0.49	2.01
1.09	2.191	1.131	1.060	0.51	1.95
1.15	2.322	1.151	1.171	0.53	1.87
1.20	2.391	1.161	1.230	0.54	1.84
1.25	2.506	1.174	1.332	0.55	1.78